MOMS
Multi Optical Mine Detection System
-Initial Report

S. Sjökvist, S. Abrahamson, P. Andersson, T. Chevalier, G. Forssell, C. Grönvall, H. Larsson, D. Letalick, A. Linderhed, D. Menning, S. Nyberg, I. Renhorn, M. Severin, O. Steinvall, G. Tolt, M. Uppsäll

FOI-R-- 1721 --SE
ISSN 1650-1942

Sensor Technology
Base data report

September 2005

FOI is an assignment-based authority under the Ministry of Defence. The core activities are research, method and technology development, as well as studies for the use of defence and security. The organization employs around 1350 people of whom around 950 are researchers. This makes FOI the largest research institute in Sweden. FOI provides its customers with leading expertise in a large number of fields such as security-policy studies and analyses in defence and security, assessment of different types of threats, systems for control and management of crises, protection against and management of hazardous substances, IT-security and the potential of new sensors.

FOI
Defence Research Agency
Sensor Technology
P.O. Box 1165
SE-581 11 Linköping

Phone: +46 13 37 80 00
Fax: +46 13 37 81 00

www.foi.se

MOMS

Multi Optical Mine Detection System

-Initial Report

FOI-R--1721--SE
ISSN 1650-1942

Sensor Technology
Base data report

September 2005

Issuing organization	Report number, ISRN	Report type
FOI – Swedish Defence Research Agency Sensor Technology P.O. Box 1165 SE-581 11 Linköping	FOI-R--1721--SE	Base data report
	Research area code 4. C4ISTAR	
	Month year September 2005	**Project no.** E3084
	Sub area code 42 Above water Surveillance, Target acquistion and Reconnaissance	
	Sub area code 2	

Author/s (editor/s)		Project manager
S. Sjökvist	A. Linderhed	Stefan Sjökvist
S. Abrahamson	D. Menning	**Approved by**
P. Andersson	S. Nyberg	Mattias Severin
T. Chevalier	I. Renhorn	**Sponsoring agency**
G. Forssell	M. Severin	Swedish Armed Forces
C. Grönvall	O. Steinvall	**Scientifically and technically responsible**
H. Larsson	G. Tolt	Stefan Sjökvist
D. Letalick	M. Uppsäll	

Report title

MOMS Multi Optical Mine Detection System - Initial Report

Abstract

This report shows the first year of research and investigations carried out within the project "Multi Optical Mine Detection System", MOMS. Activities have mainly been focused on basic principles, phenomena, acquisition of knowledge and literature studies. The report introduces the reader with the aim of the project and the interpretations of the task. This report will serve as a common base for the evolution of the project.

A survey of relevant mines and UXO has been performed, considering the functionality, geometry, size and colour. A field test with passive and active electro optical sensors was carried out in close cooperation with SWEDEC. The purpose was to collect data from surface laid mines, UXO, submunitions, and environmental background. Laboratory experiments have been made. Initial results are shown.

An initial evaluation of sensor candidates and their detection phenomenology is discussed. Considered sensor phenomenologies are: 3-D shape, retro reflection, spectral characteristics, angular reflection characteristics, temporal characteristics, spatial characteristics, polarization and fluorescence.

Modelling and simulation (MoS) as well as signal and image processing methods are reported for buried and surface laid objects. A survey of in house software and methods and their capacity and are reported.
System approaches suitable for MOMS are discussed.

Keywords

Landmine, UXO, EO, Optical, Infrared, Laser, Multisensor, Signal, Modelling, Detection, Concept, Phenomenology

Further bibliographic information	Language English
ISSN 1650-1942	**Pages** 210 p.
	Price acc. to pricelist

Utgivare	Rapportnummer, ISRN	Klassificering
FOI - Totalförsvarets forskningsinstitut Sensorteknik Box 1165 581 11 Linköping	FOI-R--1721--SE	Underlagsrapport
	Forskningsområde 4. Ledning, informationsteknik och sensorer	
	Månad, år September 2005	**Projektnummer** E3084
	Delområde 42 Spaningssensorer	
	Delområde 2	

Författare/redaktör		Projektledare
S. Sjökvist	A. Linderhed	Stefan Sjökvist
S. Abrahamson	D. Menning	**Godkänd av**
P. Andersson	S. Nyberg	Mattias Severin
T. Chevalier	I. Renhorn	**Uppdragsgivare/kundbeteckning**
G. Forssell	M. Severin	Försvarsmakten
C. Grönvall	O. Steinvall	**Tekniskt och/eller vetenskapligt ansvarig**
H. Larsson	G. Tolt	Stefan Sjökvist
D. Letalick	M. Uppsäll	

Rapportens titel

MOMS Multioptisk Minspaning - Inledande Rapport

Sammanfattning

Den här rapporten redovisar verksamheten det första året i projektet ”Mult Optisk Minspaning ”, MOMS. Verksamheten har huvudsakligen fokuserats mot grundläggande principer, fenomenologi, kunskapsuppbyggande och omvärldsbevakning genom litteraturstudier. Rapporten introducerar läsaren till projektets mål, syfte och avgränsningar. Denna rapport kommer utgöra en gemensam grund för utvecklingen inom projektet.

En överblick av relevanta minor och OXA med avseende på funktion, geometri, storlek och färg redovisas. Ett fältförsök med både passiva och aktiva optiska system har utförts i samarbete med SWEDEC. Syftet var att registrera signaturdata av ytlagda minor, OXA, substridsdelar och bakgrund. Några preliminära resultat visas.

Inledande utvärdering av sensorkandidater och deras detektionsfenomenologi diskuteras. Fenomenologier som betraktats är: 3D struktur, retro- och vinkelberoende reflektion, polarisation, fluorescens, spektral-, temporal-, spatiell och reflektions karakteristik.

Metoder för modellering, simulering och bild- signalbehandling för ytlagda och nedgrävda minor samt OXA presenteras. En genomgång av egna mjukvaror och metoder samt deras kapacitet görs. Systemkoncept lämpliga för MOMS diskuteras.

Nyckelord

Landminor, OXA, EO, Optisk, Infraröd, Laser, Multisensor, Signal, Modellering, Detektion, Koncept, Fenomenologi

Övriga bibliografiska uppgifter	Språk Engelska
ISSN 1650-1942	**Antal sidor:** 210 s.
Distribution enligt missiv	**Pris: Enligt prislista**

ABBREVIATIONS AND ACRONYMS

AHM	Anti-helicopter mine
ALRT	Airborne Littoral Reconnaissance Technologies
AP	Anti-personnel
APD	Avalanche Photo Diode
AT	Anti-tank
AV	Anti-vehicular
CEM	Combined Effects Munition
CMT	Mercury-Cadmium-Telluride, HgCdTe
COBRA	Coastal Battlefield Reconnaissance and Analysis
DoLP	Degree of Linear Polarization
DPICM	Dual-purpose Improved Conventional Munitions
IED	Improvised Explosive Device
EO	Electro-optical
EOCM	Electro-optical Countermeasures
EOD	Explosive Device
FM	Swedish Armed Forces
FPA	Focal Plane Array
GPR	Ground Penetrating Radar
IR	Infrared
LADAR	Laser Radar
LAMD	Lightweight Airborne Multispectral Minefield Dtection
LIDAR	Light Detection and Ranging
LIF	Laser Induced Fluorescence
LWIR	Long Wave Infrared
LOCAAS	Low Cost Autonomous Attack System
MOMS	Multi Optical Mine detection System
PCA	Principal Component Analysis
ROC	Receiver Operating Characteristics
ROIC	Read-out Integrated Circuit
SFM	Sensor Fused Munition
SNR	Signal-to-noise Ratio
STIL	Streak-tube Imaging Lidar
SWEDEC	Swedish EOD and Demining Centre
SWIR	Short Wave Infrared
UXO	Unexploded Ordnance
UV	Ultra-violet
VIS	Visible
VNIR	Visible/Near Infrared
WAM	Wide Area Munition

CONTENTS

1 Introduction

1.1 Aim of this report

This report shows the first year of research carried out within the project “Multi Optical Mine Detection System”,MOMS.

The first year of research has mainly been focused on basic principles, phenomena, acquisition of knowledge and literature studies. A first field test with a large number of passive and active electro optical (EO) sensors was carried out in close connection with SWEDEC with the purpose to gather data for initial and further use. The initial work and some conclusions from this field trial are presented in the report.

This report presents methods, results and analysis based on ongoing and previous research work carried out at FOI and through studies of international presented work. This report will serve as a common base for the evolution of the project.

This report is divided into 11 chapters. Each of the chapters treats specific and important parts of the research direction and future system development. The report concludes with a summary. Also a short summary concludes all individual chapters.

1.2 Background

According to document HKV bet 21 100:71047 the Swedish Armed Forces (FM) have, in connection with FMV and FOI, analyzed the ongoing and the planned research within ammunitions and mine clearance activities with the aim to submit a proposal about future R&D in this area. In June 2004, a decision was taken to initialize and launch a new research project based on electro optical (EO) sensors where the multi sensor approach is a necessity, the Multi Optical Mine detection System (MOMS). The project was started at FOI in March 2005.

1.3 Overall objectives of the project

The overall objective for MOMS is to provide knowledge and competence for fast detection of mines, especially surface laid mines, and thereby increase the FM manoeuvrability in international as well as national operations.

The first phase, with duration 2005-2009, the research phase, is essentially a feasibility study and will focus on the possibilities and limitations of a multi-sensor system with both active and passive EO-sensors. The requirements for detection due to crieterias and phenomena will be investigated. Sensor concepts in different combinations or single used are, for example, 3-D imaging, gated viewing, retro reflection detection, multispectral imaging, thermal imaging, polarization and fluorescence. The MOMS project is directed to a Level 2 of demonstrator projects until 2009, see Table 1-1.

In a second phase, primarily after 2009, the research results will support the realization of a demonstrator.

Level	Type	Objective/Goal
1	Principle demonstration Demonstration of technological and/or scientific principles	Aimed at (through experiment) showing if a theory or method is feasible. Can be conducted as computer simulation or arrangement in a laboratory. **Goal:** Basic data as regard to threats and opportunities for use in studies of an idea nature. Playing card of a conceptual nature.
2	Operations demonstration Demonstration of technical functions in a realistic test environment	Aimed at showing that a concept, often consisting of different components, provides the expected outcome of operations. **Goal:** Basic data for studies before decisions on PDF. Playing card type A (collaboration with research activities).
3	Technical demonstration Demonstration of function, performance and feasibility (Upgrading existing objects using partially new technology)	Aimed at showing that an object's or concept's performance and feasibility provide the expected outcome. Can be compared with hardware that has no or little similarity with the intended finished product. Used in PDF. **Goal:** Basic data for studies before decisions on unit development. Playing card type B.
4	Field demonstration Demonstration of technical performance and manageability in field environment and/or tactical use.	Aimed at using field experience as the basis for development of combat techniques and for prospective development of demonstrators. The demonstrator resembles the conceived finished product concerning handling and function. **Goal:** Basic data for studies supporting decisions on procurement. Playing card type C.
5	Systems demonstration Demonstration of a series-like technical solution in its system environment in field-like conditions.	Aimed at verifying that requirement specifications are fulfilled. Conducted in a systems environment in field-like conditions. **Goal:** Basic data for studies supporting procurement decisions. Playing card type C.

Table 1-1 Level division of demonstration projects. Types 1-3 can occur within R&T activities. Types 3-5 can occur within unit and material development, from [1].

The project will also focus and search for technical solutions to meet requirements on fast processing of data, high capacity of area scanning, high accuracy of positioning and day and night capacity. The initial research will also include advanced sensor concepts by utilizing both ground-based and airborne platforms, integrated signal processing, laboratory tests and initial field tests, survey of national and international literature and experiences from own relevant research.

A relevant system concept will be taken into consideration.

1.4 Interpretation of the task

This subchapter is an interpretation of the task, given by FM and its annexes, in order to primarily clarify the order's objectives and thereby to decrease the risk for missinterpretations.

MOMS will give answers to the question: How should an optical mine detection system be designed, based on laser and EO/IR sensors, in order to detect land mines and UXO in accordance with the scenarios defined by FM.

The main documents which are governing the project are shown in Table 1-2. The hierarchical order in which the documents are interpreted is as follows:

1. Document no 2 ”Forskningsinriktning för området ammunitions- och minröjning”
2. Document no 3 ”Redovisning av studien FramFoT”
3. Document no 7 ”Redovisning av projektförslag”

Doc No.	Original name	New FOI name
1	Inriktning för FM ammunitions- och minröjningsverksamhet, 2003-06-13 HKV bet 13 301:67952	FM inriktning am- och minröjning
2	Forskningsinriktning för området ammunitions- och minröjning, 2004-06-23 HKV bet 21 100:71047	HKV_beslut_forskningsinriktning
3	Redovisning av studien FramFoT FMV bet VO FoT 23 321:27926/4	FramFoT Studien 2004-06-21
4	Bilaga 1; Beskrivning av Försvarsmaktens behov FMV bet VO FoT 23 321:27926/4	FramFoT Bil 1 FM behov
5	Bilaga 2; Beskrivning av värderade alternativ FMV bet VO FoT 23 321:27926/4	FramFoT Bil 2 Alternativ
6	Bilaga 3; Beskrivning av utredningens genomförande FMV bet VO FoT 23 321:27926/4	FramFoT Bil 3 om studien
7	Bilaga 4; Redovisning av projektförslag FMV bet VO FoT 23 321:27926/4	FramFoT Bil 4 Proj input
8	Regeringens samlade syn på minhantering Fö2002/350/MIL	Regeringens syn på minhantering

Table 1-2. Governing documents (In Swedish)

1.5 Priorities and readjustments

In June 2005 a readjustment of the priorities of the scenarios was decided by FM according to document HKV 21 100:71581.

The new priorities for the scenarios are:

1. Increase Swedish Armed Forces's international capacity/ability to check roads
2. Mine detection for battalion's offensive against recently landed airborne enemy
3. Contribute to development of mine detection within humanitarian mine clearance (Describe the possibilities in this scenario)
4. Mine detection in order to open roads and paths for own forces
5. Mine detection for battalion crossing watercourses

For this first year this new priority of scenarios has a minor influence, but for forthcoming years this will have effects.

1.6 Traceability against FM tasks

A request from FM FoT-8 on how MOMS is connected to the FM main tasks was initiated and studied during 2005. The result is shown in Figure 1-1. The stars indicate where MOMS are in accordance with the predefined blocks.

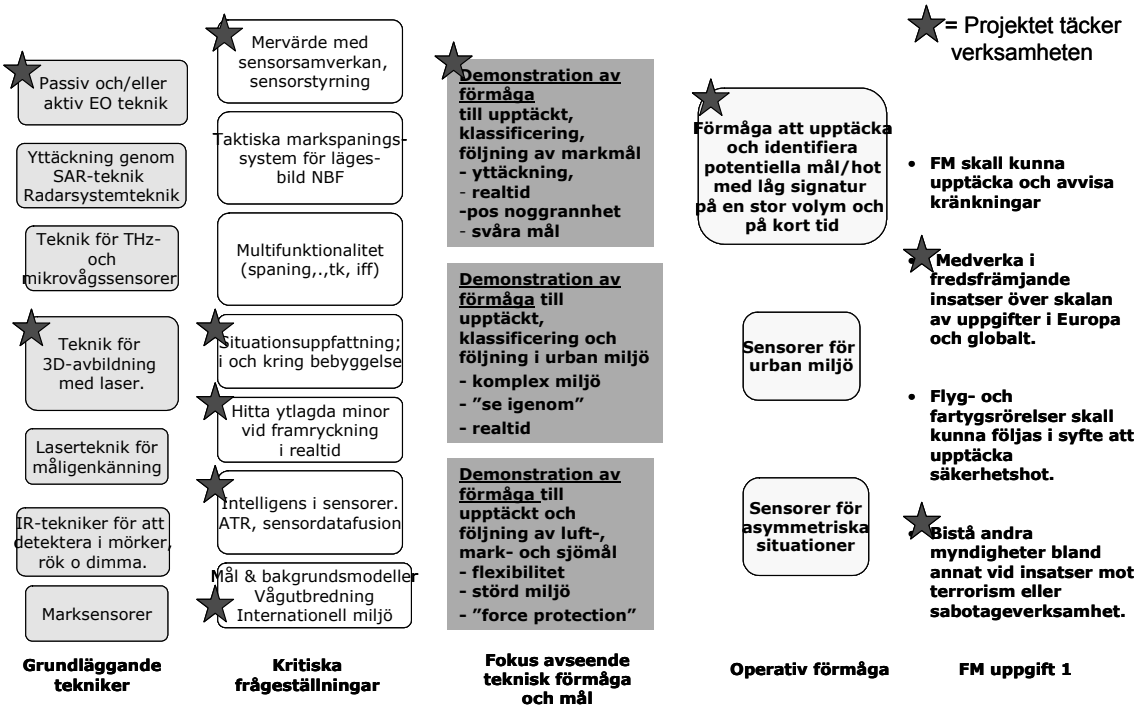

Fig 1-1. This figure (in Swedish) is from a request from FoT-8 on the traceability against FM main tasks. The stars indicate resemblance with the predefined blocks.

2 Mines and UXO aspects

In this chapter we discuss some of the characteristic features of mines and UXO. Geometry, size and colour are discussed in section 2.1, and in section 2.2, a selection of mines are described in more detail. Data and images of mines, in this chapter, are to a great extent from [2] and [3]

There are about 2000 different types of mines for which catalogues exist. Typical mines are shown in Figure 2-1. Generally mines are classified in 3 categories:

- Anti-tank mines usually react on pressures of 150-300 kg. They may also be initiated by a tilt rod (so called full width AT mines), or by induction. These types of mines are not the main focus of humanitarian mine clearance operations, because they are designed for operation against vehicles and are normally not triggered by the weight of humans. Therefore, civilians are less prone to exposure of these types of mines.
- Anti-personnel mines with fragmentation can be completely or partially buried into the ground (bounding fragmentation mines), but they may also be placed above ground level (stake mines, off-route mines etc.). Fragmentation mines are often triggered by wire and are lethal within a radius of about 30 m.
- Blast anti-personnel mines often include less than 100 g of explosive. This is the most common type of mine. It has a simple construction and diameters of about 10 cm. Blast mines are triggered by a pressure of about 10 kg/dm^2, exceptionally by trip wire. These mines are mainly designed to badly maim, not to kill, but there are exceptions.

The last category represents the biggest problem. AP mines are very cheap (down to a few US dollars a piece) and are very hard to locate. For these reasons they are extremely widespread. A useful catalogue of mines is found in[2]. Figure 2-1 and Figure 2-16 show examples of images of “operational” mines and those under development. Mine types under development include multiple charge mines, and mines with new types of triggering mechanisms, such as acoustic, seismic and electro-optical sensors.

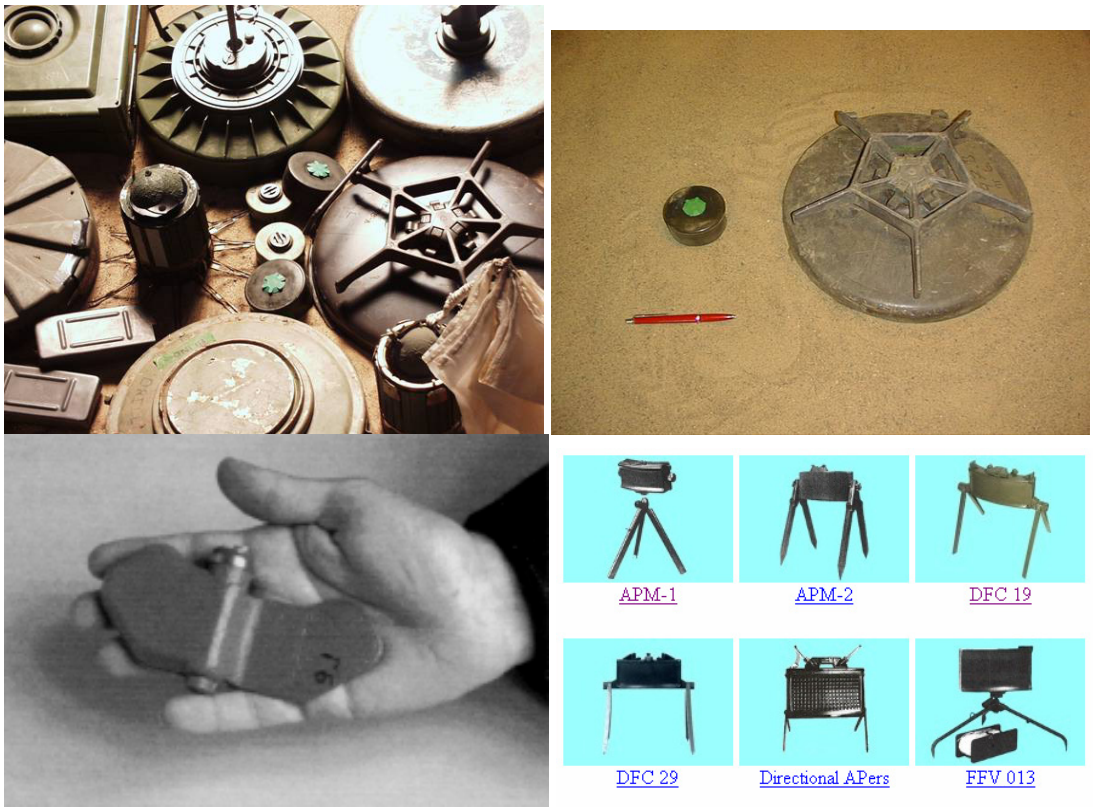

Figure 2-1. Examples of AP and AT mines including side hitting AP and AT mines. FFV013 is an example of an anti-vehicle mine (below right)

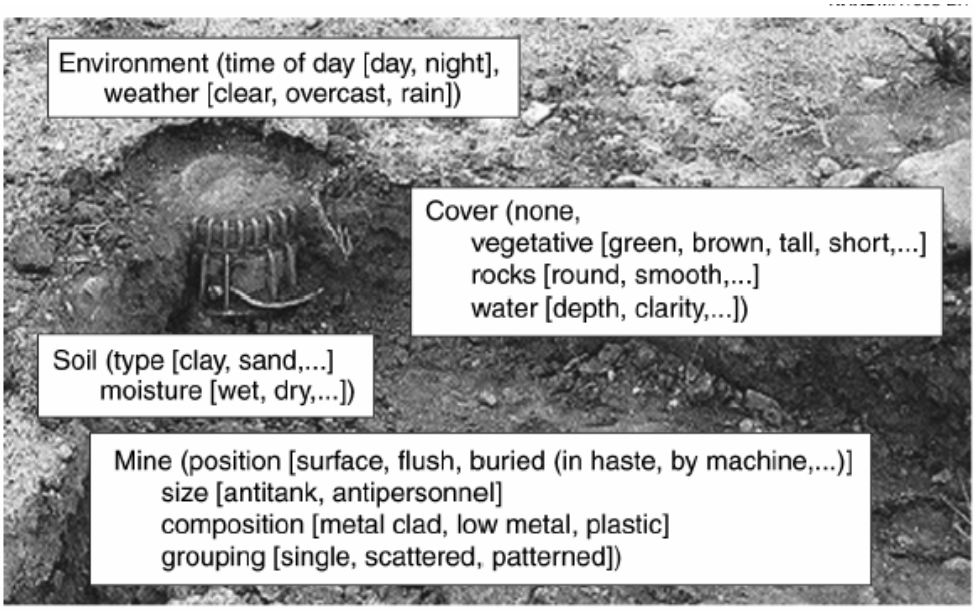

Figure 2-2. The mine and its environment relevant for optical detection[4].

The mine will always have to be detected in a cluttered environment so the task of mine detection is not only a matter of adapting to the mine signatures only but also to distinguish the mine or rather mine-like object from the background. Figure 2-2 shows many of the parameters relevant for optical mine detection [4]. The great manifold of mine types and their appearances in various backgrounds point out the importance to set realistic performance

specifications concerning detection probability and false alarm rate as represented by the Receiver Operating Characteristics (ROC) curve.

2.1 Mine geometry, material and colour

Based on data from the catalogue of mines [2] we have plotted some statistics which will be of interest for setting system parameters etc. Note that the figures do not take into account the number of mines actually deployed or estimated to be deployed in a real situation. In the diagrams, we have assigned a "new mine" for each colour. This typically means that the absolute numbers for features other than colour are 2-3 times larger than the number of types.

2.1.1 Anti-personnel (AP) mines

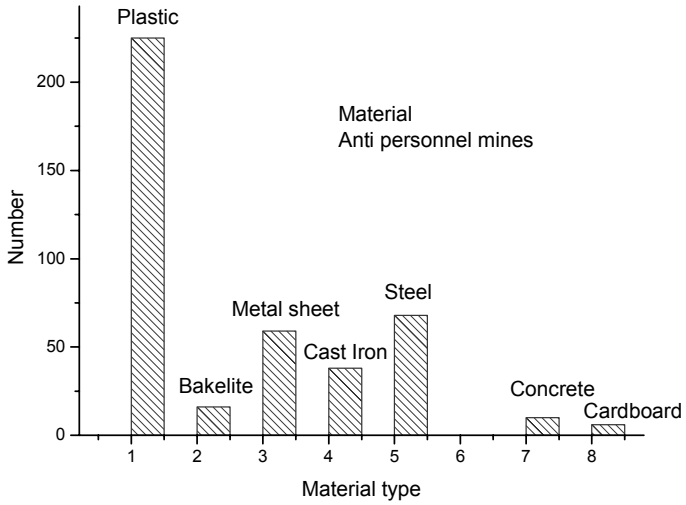

Figure 2-3. Relative distribution of material of AP mines.

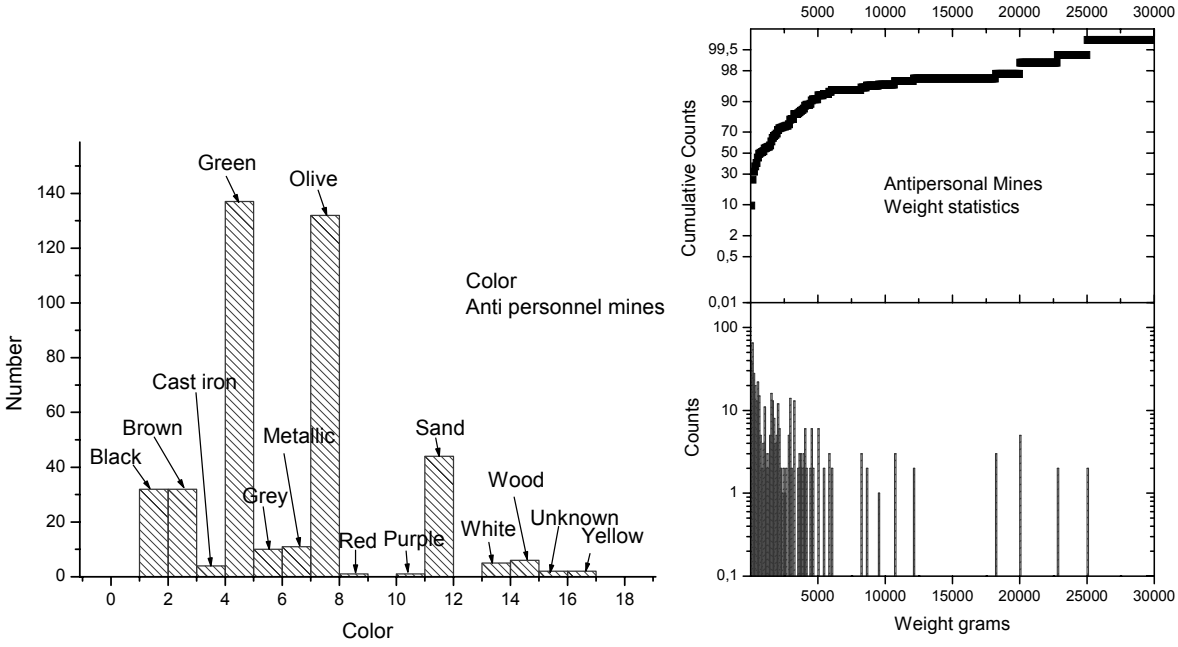

Figure 2-4. Left the distribution of colours and right the weight distribution for AP mines.

In Figure 2-3 we have plotted the distribution of material for AP mines. The total number of plastic mines is somewhat larger than that of metal mine. Some “odd” materials, such as concrete and cardboard, are also found. The colour (Figure 2-4) is dominated by green and olive but other like sand and white are also present. One may expect that a detection discrimination based on colour only, will not be robust as mines easily may be painted in new colour even in the field. The weight (Figure 2-4 right part) is dominantly less than 1 kg with 30 % below 200 g. The dominating shapes (Figure 2-5) for AP mines are cylindrical or circular (flat cylinders) and rectangular. The side hitting claymore type is also rather frequent while other types are in smaller numbers.

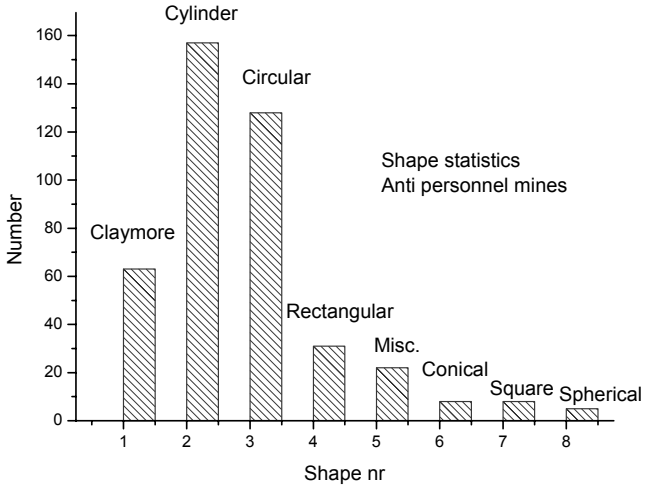

Figure 2-5. The shape statistics for AP mines.

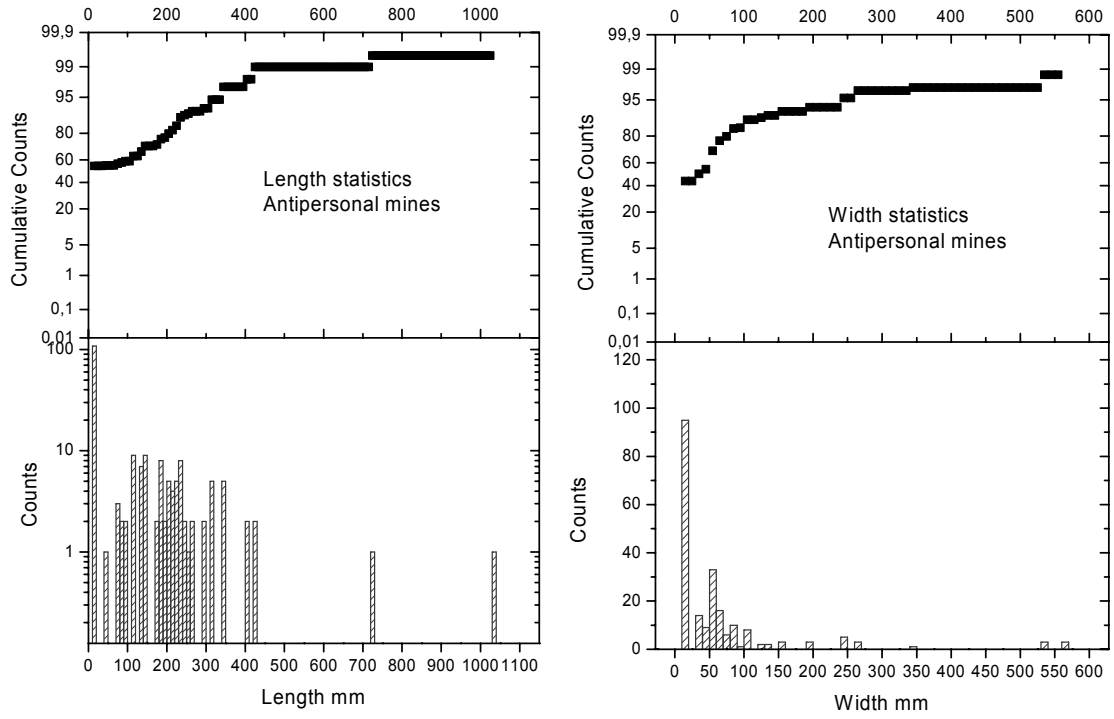

Figure 2-6. Length and width statistics for AP mines.

Figure 2-6 shows the length and width statistics for AP mines. The larger sizes, typically for claymore mines are about 25×15×5 cm^3. The height and diameter distributions are shown in Figure 2-7.

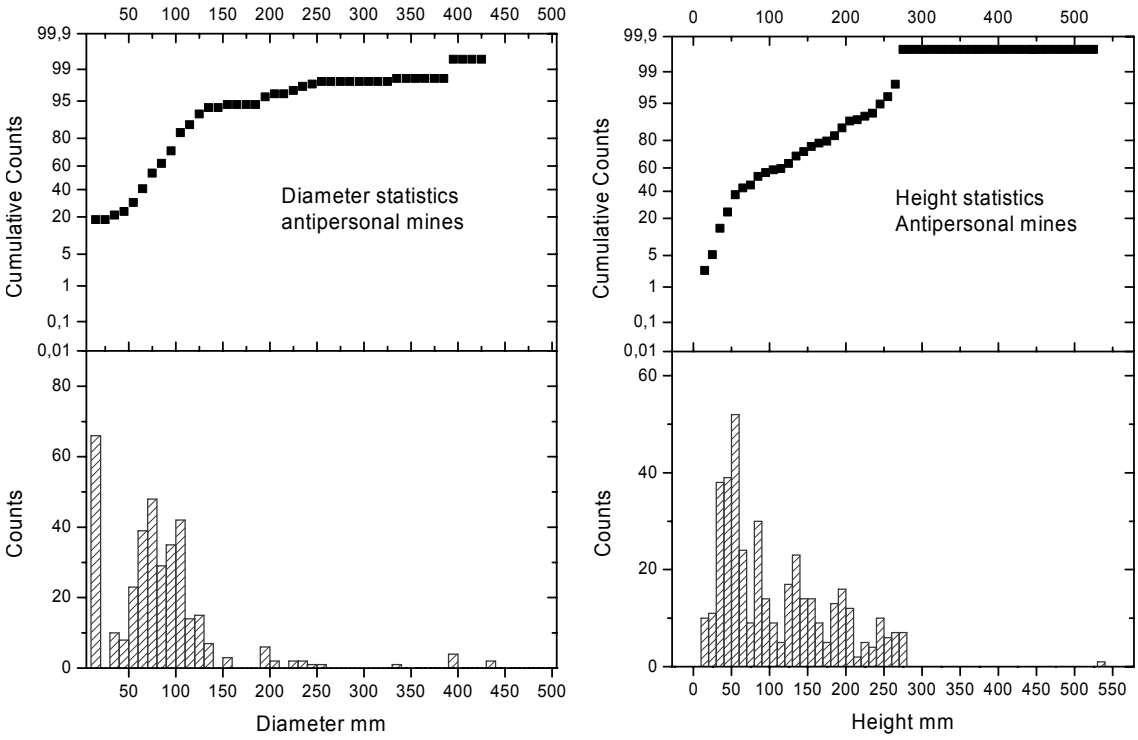

Figure 2-7. Diameter and height statistics for AP mines.

2.1.2 Anti-tank (AT) mines

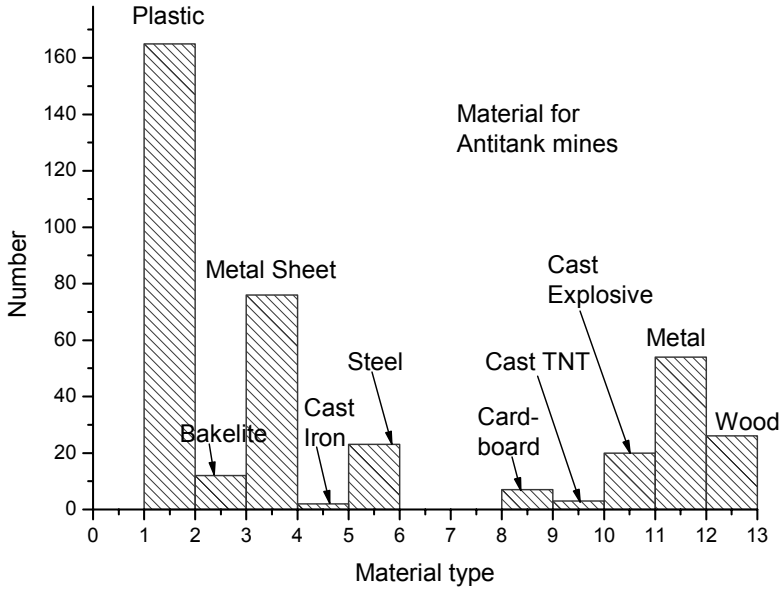

Figure 2-8. Relative distribution for material of AT mines.

Figure 2-8 shows the materials for AT mines. The mines with metallic cases are marginally the largest class when compared with the plastic mines. Also note that other materials like wood, cardboard and bakelite are used. Figure 2-9 shows colour and weight statistics for AT mines. The colour distribution for AT mines is similar to that for AP while the weight is several kg.

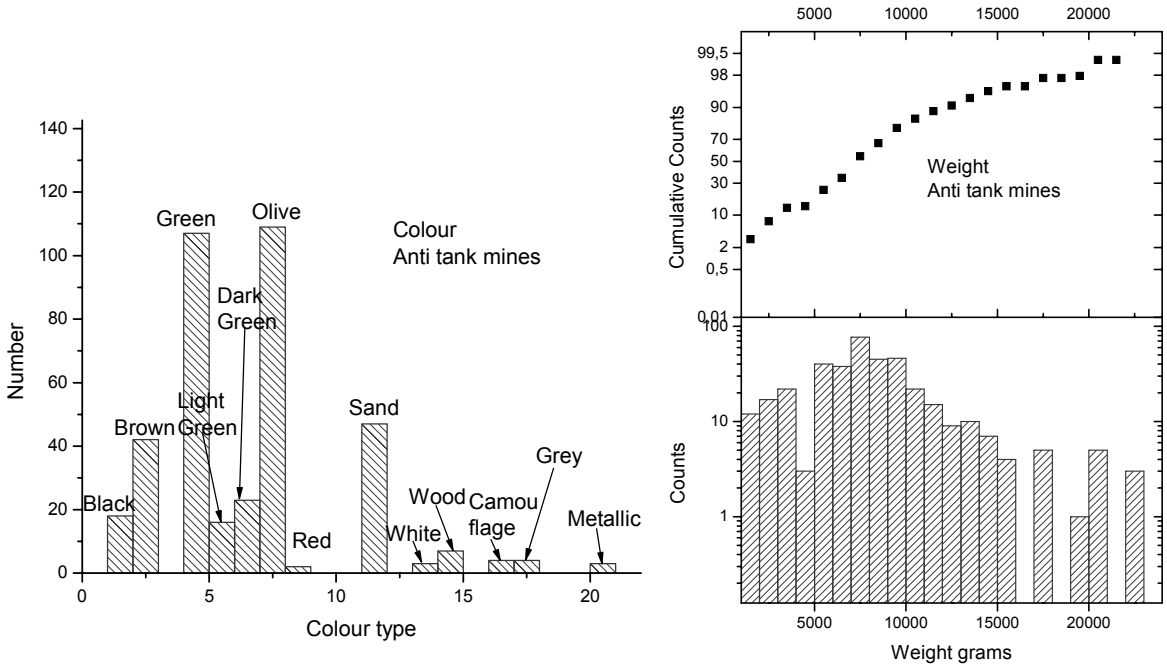

Figure 2-9. Colour (left) and weight distributions (right) for AT mines.

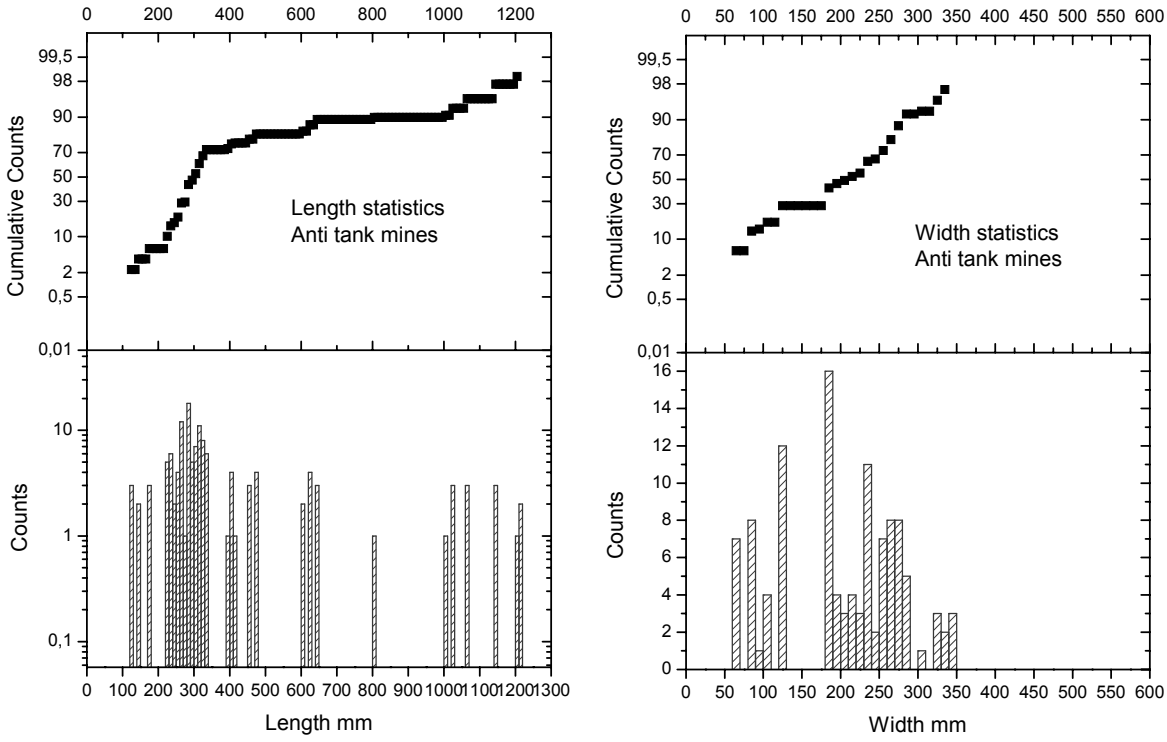

Figure 2-10. Length and width statistics for AT mines.

In Figure 2-10 and Figure 2-11 we show the size statistics for AT mines. While the largest linear dimension of an AP mine generally is less than 10 cm, the anti-tank mines often have a largest dimension of about 30-40 cm.

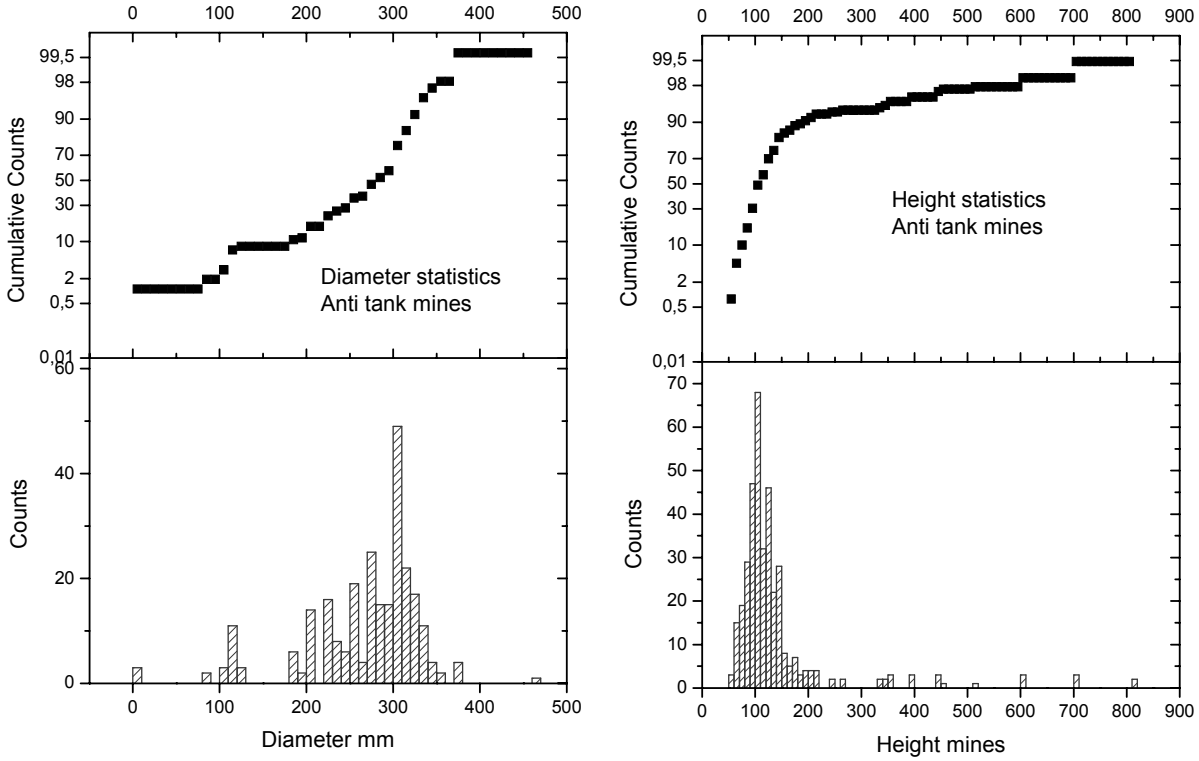

Figure 2-11. Diameter and height statistics for AT mines.

2.1.3 Surf/Beach zone mines

Many of the land mines can be used in shallow waters. On the beach, ordinary AP and AT mines are laid, but in the shallow waters other types are found. Some examples are shown in Figure 2-12Figure 2-14.

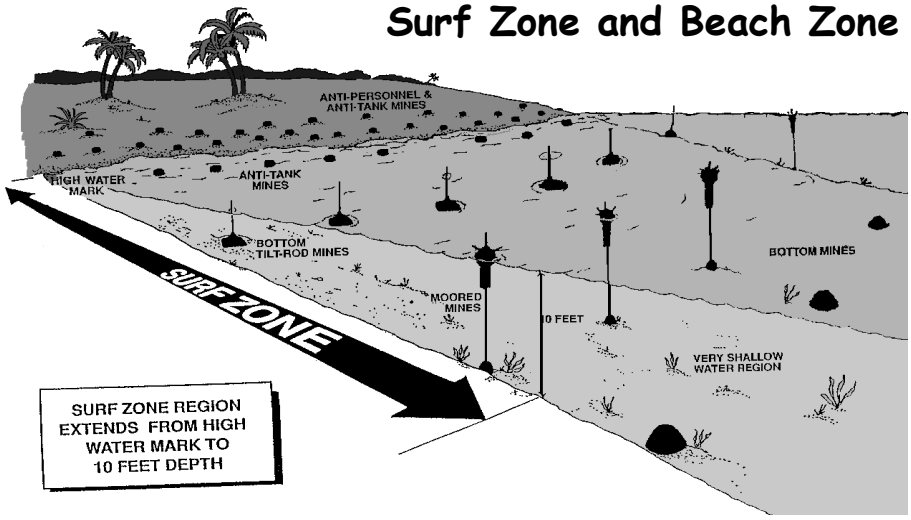

Figure 2-12. Mines on the beach and in the surf zone [5].

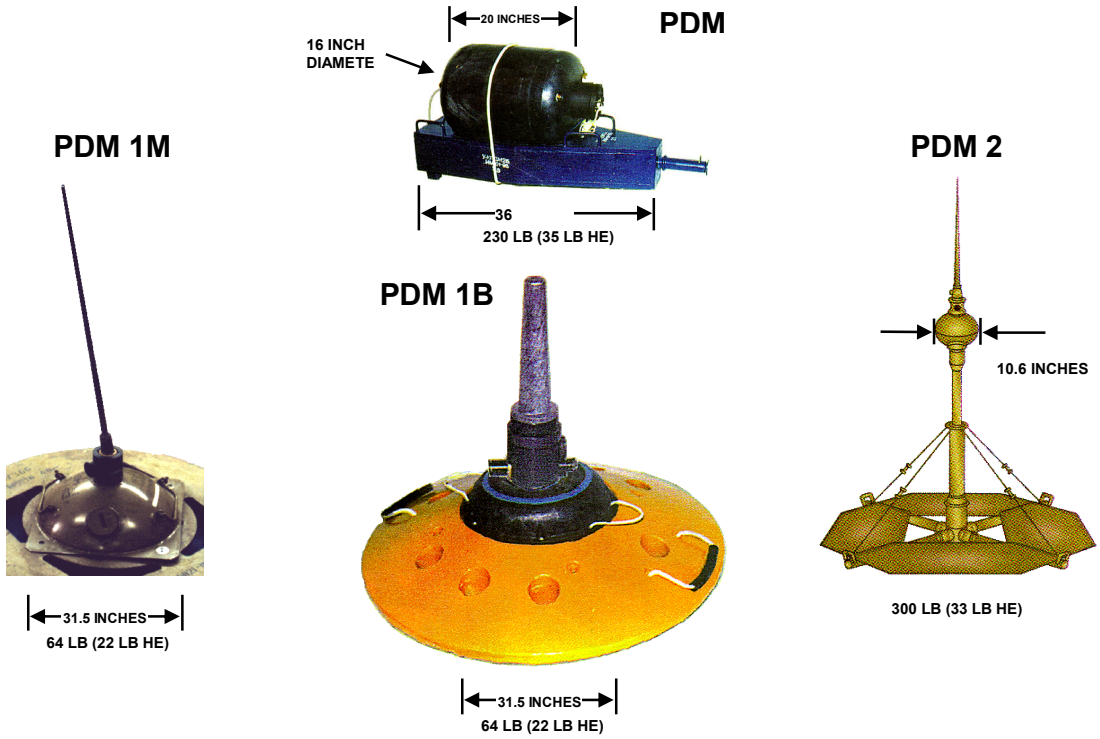

Figure 2-13. Size, weight and appearance of some shallow water (surf zone) mines[5].

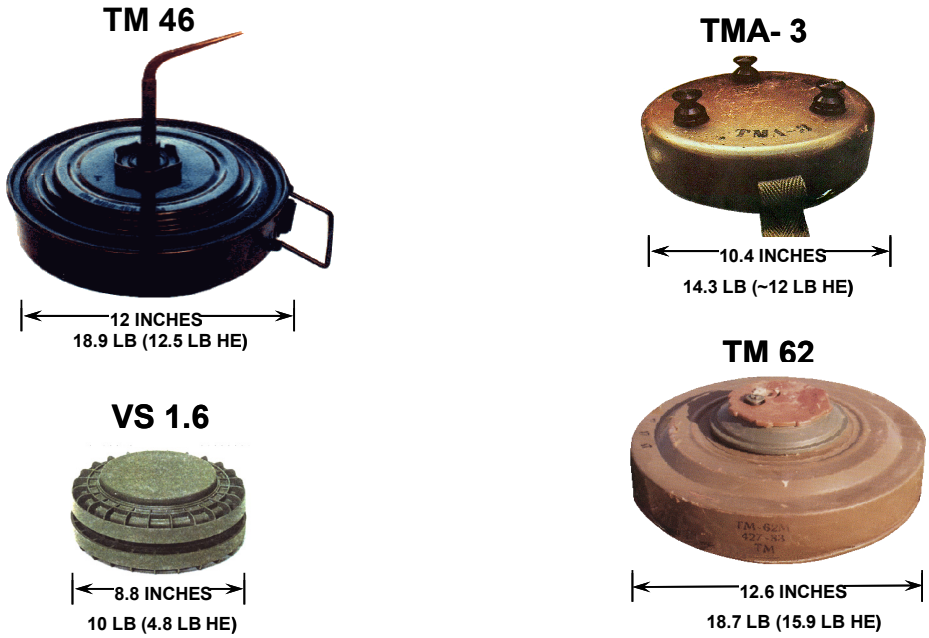

Figure 2-14. Example of beach zone mines (Russian, Yugoslavian and Italian) [5]

2.1.4 Improvised Explosive Devices (IED's)

A NATO definition of IED's is "(DOD, NATO) "A device placed or fabricated in an improvised manner incorporating destructive, lethal, noxious, pyrotechnic, or incendiary chemicals and designed to destroy, incapacitate, harass, or distract. It may incorporate military stores, but is normally devised from nonmilitary components [6]

The information below, on Improvised Explosive Devices (IED's) was found in [7].

> *An IED can be almost anything with any type of material and initiator. It is a "homemade" device that is designed to cause death or injury by using explosives alone or in combination with toxic chemicals, biological toxins, or radiological material. IEDs can be produced in varying sizes, functioning methods, containers, and delivery methods. IEDs can utilize commercial or military explosives, homemade explosives, or military ordnance and ordnance components.*
>
> *They are unique in nature because the IED builder has had to improvise with the materials at hand. Designed to defeat a specific target or type of target, they generally become more difficult to detect and protect against as they become more sophisticated.*
>
> *IEDs fall into three types of categories:*
>
> - *Package Type IED*
> - *Vehicle-Borne IEDs (VBIEDs)*
> - *Suicide Bomb IED*
>
> *Though they can var widely in shape and form, IEDs share a common set of components and consist of the following:*
>
> - *An initiation system or fuze;*
> - *Explosive fill;*
> - *A detonator;*
> - *A power supply for the detonator; and*
> - *A container.*
>
> *Improvised devices are characterized by varying employment techniques. In most of the techniques shown below, an unexploded ordnance (UXO) can easily be engineered to replace a mine or explosive device using one of the several following techniques:*
>
> - *Coupling is a method of linking one mine or explosive device to another, usually with detonating cord. When the first device is detonated, it also detonates the linked explosive. This technique is often used to defeat countermine equipment, such as mine rollers*
> - *Rolling. The roller will pass over the initial, unfuzed device and set off the second fuzed device. This in turn detonates the overpassed device underneath the clearing vehicle. When the linked devices are directional fragmentation mines, they can create a large, lethal engagement area.*
> - *Boosting. Buried mines, UXOs, or other explosive devices are stacked on top of one another. The device buried deepest from the*

surface is fuzed. Fuzing only the deepest ordnance helps mask no- and low-metal explosive hazards placed near the surface. This reduces the probability of detection by metal detectors, and it increases the force of the blast.

- *Sensitizing antitank (AT) mines. On some nonmetallic AT mines, the pressure plate is cracked and the spring is removed to reduce the pressure required to initiate the mine. Similarly, the pressure plate can be removed from metallic AT mines to create the same effect. A pressurefuzed AP mine can be placed on the top of an AT mine, thus creating a very large AP mine as an alternative method.*
- *Daisy chaining. AP mines may be used in daisy chains linked with other explosive hazards. Enemy forces may link the mines together with trip wire or detonating cord. When the initial mine is detonated, the other mines may detonate. This may also create large, lethal engagement areas. .*

2.1.5 Trip wires

Trip wires come in different materials and are very difficult to detect, see Figure 2-15.

Figure 2-15. Small AP mine in foliage with tripwire. Even though not heavily obscured by vegetation, the tripwire is extremely difficult to detect against background clutter with the unaided eye. From [8].

Some types of trip wires are much thinner than usual trip wires and are even more difficult to detect than ordinary ones. These are implemented in AP mine system such as the U.S. ADAM, the Russian POM-2S.

2.2 Selection of typical mines and other explosive devices

A selection of objects has been made. The characteristics and specific data for each object is not classified information, nor new (there are numerous references readily available), but the list is compiled in order to be useful for the evaluation of EO and active sensors performance that is to be done the coming years. Initial evaluations of the objects have been made in preliminary field tests in the project. Of course, the selection of objects will change over time, due to the dynamic threat that mines, UXO, and submunitions pose.

2.2.1 Anti-Personnel (AP) mines

Some AP mines are listed in Table 2-1 and further described in the text below.

AP Mine	Shape	Size [mm]				Material	Colour/-s	Texture
		L	W	H	D			
PMA-1	Rectangular	140	70	30		Plastic (bakelite)	Dark Green, Light Green, Olive	
PMA-2	Circular			61	68	Plastic	Dark Green, Light Green, Olive	
PMA-3	Circular			36	103	Plastic/rubber	Black, Dark Green, Light Green, Olive	
VS-50	Circular			45	90	Plastic	Brown, Grey, Green, Olive, White, Sand	
OZM-72	Cylindrical			172	106	Steel	Olive	
M14	Cylindrical			40	56	Plastic	Green, Olive	
PFM-1	Irregular	119	64	20		Plastic (LDPE)	Brown, Green, White, Sand	
PGMDM/PTM-1S	Triangular bar	320	65	75		Plastic	Light Green, Brown, White	
M18A1	Convex, rectangular	216	35	82.5		Plastic (PS)	Olive	
MON-100	Convex, circular			83	236	Steel	Olive Drab	

PROM-1	Cylindrical			260	75	Steel	Olive, Dark Green, Light Green
PMR-2A	Cylindrical			140	60	Cast iron	Olive, Dark Green, Light Green
ADAM	Circle sector, wedge		57	82.5		Metal	
BLU-92/B Gator	Cylindrical/ rectangular	146	127	66		Steel/plastic	Olive
MI AP DV 59	Cylindrical			55	62	Plastic	Olive
Gravel mines, (XM22-XM65)	Quadrant, Rectangular, Square	25-76	25-70		64-89	Cloth	Olive, straw coloured, brown
Type 72	Cylindrical			38	78.5	Plastic	Light Green

Table 2-1. Parameters and project-relevant information for the different types of AP mines described below.

2.2.1.1 PMA-1

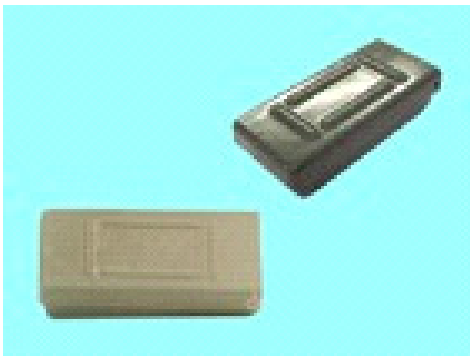

The former Yugoslavian PMA-1A is a rectangular shaped, plastic bodied AP mine which is designed to wound or kill by blast effect. The mine body is green and consists of two rectangular plastic parts, which are hinged clamshell style. The upper surface has 4 distinct strengthening ridges in a rectangular pattern. The mine body is not watertight and the 200 g explosive charge is very hygroscopic, after prolonged periods in the ground the performance of the charge would be severely degraded. Therefore the mine should only be used in dry areas where water does not accumulate (well drained soil). The PMA-1A uses the UPMAH-1 chemical action fuse and a No 8 detonator as its initiator; the main charge is a 200 g block of Trotyl or TNT. The UPMAH-1 fuse assembly consists of a small Bakelite casing: one end is sealed and contains a friction-sensitive composition; the other is open and accepts a No 8 detonator. The PMA-1A is not detectable under most field conditions although a mine detector can detect the metal in the detonator in some cases. The mine is rapidly defeated by explosive breaching systems such as the Giant Viper and MICLIC. In Croatia this mine is nicknamed the “Fishbox” because it resembles a sardine can.

2.2.1.2 PMA-2

The former Yugoslavian PMA-2 is a small, circular, plastic bodied AP mine which is designed to wound or kill by blast effect. The mine body is moulded from bright green plastic, it has a smooth appearance with a lip along the top edge where the top is glued to the bottom part. The mine is hermetically sealed and can be laid underwater or in snow as well as surface laid or buried. The PMA-2 contains 70g of TNT and a Tetryl booster pellet. Tests have also shown presence of RDX in PMA-2 boosters. The fuse body is made of dark brown bakelite, it contains a friction sensitive flash compound and a detonator, the fuse body supports a small star shaped pressure plate which comes in 3 colours; green, black and white. The fuse is screwed into the top centre of the mine body with four right hand threads. The mine is unarmed if the wire safety pin is secured through a hole in the fuse body. The PMA-2 cannot be located using metal detectors under most field conditions.

2.2.1.3 PMA-3

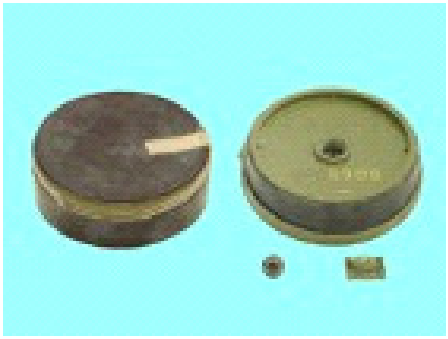

The former Yugoslavian PMA-3 is a small, circular, plastic bodied AP mine which is designed to wound or kill by blast effect. The mine is moulded from bright green plastic and consists of an upper and lower section connected by a black rubber protective cover. The upper section is able to pivot inside the lower section when pressure is applied to the top edges of the mine. The mine has a knurled fuse cavity cap centred on the bottom and the word PMA-3 is prominently embossed on the bottom as well. The upper section of the mine contains a 35 g charge of Tetryl. The PMA-3 is hermetically sealed and can be laid in wet ground for periods up to 6 months, after this time the black rubber cover will begin to deteriorate. The mine can function in temperatures from -20' to +50' C. The only metal in the mine is the thin aluminium shell of the detonator which causes the PMA-3 to be undetectable using metal detectors in most field conditions. Serbian and Croatian forces will rarely lift this mine once it has been laid.

2.2.1.4 VS-50

The Italian VS-50 is a circular, plastic bodied, AP mine which is designed to wound or kill by blast action. It can be scatter laid from a helicopter or a vehicle and hand laid to a depth of 2cm. The VS-50 comes in a variety of colours including sand, olive and light green. The mine has twelve prominent strengthening ribs around its circumference, a black rubber pressure pad on the top and a green slotted detonator well centred on the bottom. The VS-50 is waterproof and non-buoyant, staying effective after prolonged periods under water. It is designed to function in temperatures from -32 to +70' C. The mine is actuated by pressure of 10 kg and the blast will penetrate 5mm of mild steel leaving a 80mm diameter hole. A special variant of the mine called the VS-50A is equipped with an electronic anti-handling/self destruct mechanism. The VS-50 is very difficult to locate using metal detectors under most field conditions. The mine is also produced in Singapore as the SPM-1.

2.2.1.5 OZM-72

A Russian AP mine developed from earlier versions of the same type in order to achieve greater efficiency. The OZM-72 is the successor to the OZM-4 mine. Other than size, the primary difference found in the OZM-72 is a pre-fragmented sleeve contained in an outer body. Detonation is normally accomplished from a tripwire fuse, but command-detonated, tension-release, or simple pressure fuses could also be used. Height of burst is determined by a lanyard packed in the base of the mine as in the OZM-4, but a secondary initiation system using a delay charge has been added. The ensuing fragmentation of the mine body results in the lethal radius of 25 meters – a former Soviet design standard. This mine is considerably larger than the M16A1 which has a clamed lethal radius of 27 meters.

2.2.1.6 M14

The small US M14 is a cylindrical plastic bodied AP mine which is designed to wound or kill by blast effect. The top of the mine is a combination pressure plate and arming dial with a yellow arrow moulded into it. A horseshoe shaped metal safety clip holds the pressure plate in the up position during storage (it must be removed during the arming process). The upper edge of the mine body has a "S" to indicate safe and an "A" to indicate armed when the yellow arrow is pointing at it. The bottom of the mine has a cavity to insert the M46 detonator assembly. The mine is actuated by pressure of 9 kg and it can function in temperatures from -40 to +50 C, it has an emplaced life expectancy (70% chance of functioning as designed) of 7 months in a tropical environment and up to 20 years in temperate zones with clay soil. The M14 has low metal content and is very difficult to locate using metal detectors under most field conditions.

2.2.1.7 PFM-1

The Russian PFM-1 is a plastic bodied scatterable AP mine which is designed to wound by blast effect. It is an oddly shaped mine which resembles a seed from a maple tree, one end is bulbous and contains the explosive while the other end is thin and acts as a stabilizer when the mine is scattered from the air. The MVDM fusing mechanism is in the centre of the mine body. It is delay armed after release from its canister which allows it to impact with the ground unarmed. It is actuated by a cumulative pressure of 5 kg, either one full pressure such as stepping on it, or many light pressures such as handling it. The mine has a low/medium metal content and it can be located visually or with metal detectors under most field conditions. A special variant called the PFM-1S has a 24 hour self destruct time and is distinguished by a red band around the top of the fuse. The PFM-1 can be defeated by blast overpressure from explosive breaching systems such as the Giant Viper or MICLIC. The delivery system on the Mi-8 "Hip" helicopter holds 2 x containers of 144 mines; the PFM-1 can also be delivered by a 220 mm rocket which holds 312 mines or a 240 mm mortar round which hold 20 mines. In Afghanistan the PFM-1 is known as the “Green Parrot”.

The PFM-1 is packaged in a long kidney shaped metal container which holds 20 mines. The container will normally be found in the same area as the mines.

2.2.1.8 PGMDM

Russian AP mine. This scatterable anti-vehicular blast mine, complements the PFM-1 (and PFM-1S) AP mine. The mine is OD green.

2.2.1.9 M18A1

U.S. AP mine, also known as “Claymore”. Directional fragmentation mine. The M68 practice mine is similar to the M18A1 mine except that the inert loaded M33 mine body replaces the high explosive loaded M18A1 mine body, and the empty practice blasting cap M10 replaces the loaded blasting cap. These are directional, fragmentation, high explosive (HE) AP landmines which may be electrically or non-electrically initiated. They may be used as controlled fired mines in offensive or defensive situations. The M18A1 mine is olive drab.

2.2.1.10 MON-100

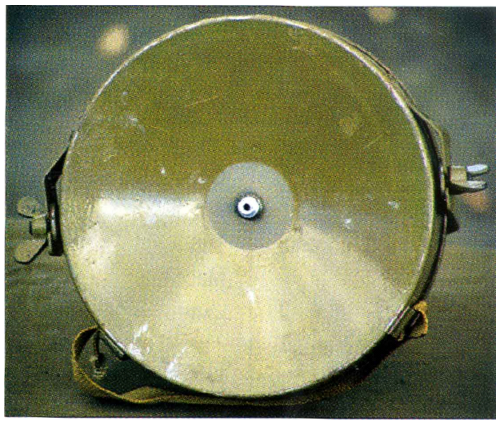

The MON-100 is a cylindrical directional fragmentation mine designed by the former Soviet Union. It consists of a metallic case containing an explosive charge, steel fragments, and a metal stand. The 400 cylindrical steel fragments (10 mm×10 mm) are embedded in a plastic matrix in front of the explosive. The mine can be attached to any fixed object or mounted on its own metal stake. The MON-100 can be functioned by a tripwire, a break-wire or command detonated (including by a variety of minefield control devices) and has a lethal range of 100 meters. At 100 m, 50% of the fragments will strike within 5 m of the mines aiming point. The MON-100 can be used singly or as part of an integrated explosive barrier. The mine is not only effective against dismounted infantry, but also lightly armoured vehicles. The mine is OD green.

2.2.1.11 PROM-1

The former Yugoslavian PROM-1 is a cylindrical, steel bodied, bounding AP mine which is designed to wound or kill by fragmentation. The mine is similar in shape and size to a half litre beer bottle. The casing has a smooth finish and is connected to a rough base with five brass shear screws. The PROM-1 uses the UPROM-1 combination pull/pressure fuse which is similar to the UMPR-3 used on the PMR-3 AP mine. When the mine is set for tripwire actuation about 10 cm of the fuse is exposed above the ground. When set for pressure the whole mine is buried and only the fuse prongs may be exposed. The PROM-1 can be used in snow and shallow water for short periods and in Croatia it has been observed taped in trees at head height with the tripwires running perpendicular to the ground. It can have up to 6×16 meter long trip wires attached to the fuse. The PROM-1 contains 425 g of TNT and when actuated it bounds to a height of 70-80 cm, explodes and propels fragmentation to a lethal radius of 40 meters. The mine can be located visually and with metal detectors under most field conditions and it can be defeated by blast overpressure from explosive breaching systems like the Giant Viper and MICLIC.

2.2.1.12 PMR-2A

The PMR-2A is Former Yugoslavian stake mine. It is a cylindrical, cast iron bodied, stake mounted AP mine which is designed to wound or kill by fragmentation. The mine body is green and has 9 rows pre-notched on its exterior aid its fragmentation. The mine stake is normally natural wood but a metal stake which is meant to be used with the training version of the mine has also been encountered. The PMR-2A is made from separate components which are assembled on site. The mine is actuated when 3 kg or more of pull is applied to a tripwire. The PMR-2A has a lethal radius of 10 meters and a hazard radius of 25 meters. The explosive charge is 100g of Trotyl in a cardboard tube. The PMR-2A can be located visually as well as with metal detectors under most field conditions. A choice of standard (UPMR-2A) or flare (UPMR-2AS) fuses is available; the UPMR-2AS has two strikers (one for the mine and one for the flare).

The PMR-2A comes loaded in a green wooden box which is hinged at the top. The box contains 8 sets of mine components complete with charges and a small metal box which contains 6 x UPMR-2A and 2 x UPMR-2AS fuses plus 8 M67 non-electric detonators. The wood box is marked with the name PMR-2A/AS as well as the lot number.

2.2.1.13 ADAM

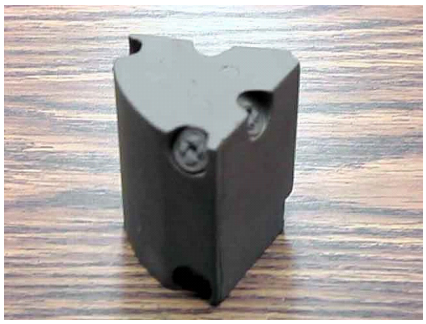

Area Denial Artillery Munition. These are scatterable, antidisturbance or self-destruct fired, bounding AP mines. The ADAM mines are ejected from a 155 mm (M731 or M692) projectile. They are used for area denial and are designed to self-destruct at 4 hours or at 48 hours after deployment. The mine with the long self-destruct time is ejected from the M692 projectile and the mine with the short self-destruct time is ejected from the M731 projectile. Each projectile contains 36 mines. The ADAM mines are olive drab and do not have any markings. The mine nomenclature and lot number are stenciled in black on the two sides of

the mine body. The arming strap and nose guard are green. A yellow stenciled warning notice is on the arming strap.

2.2.1.14 BLU-91 Gator

A U.S. mine system delivered by aircraft in Cluster Bomb Units (CBUs). The BLU-91 is a type of submunition. This is an air-delivered, free-fall, bi-directional-ballistic-disk (Misznay-Schardin), electromechanically armed, magnetic influence- or self-destruct fired, antitank/anti-vehicular (AT/AV) landmine. It is used, along with its companion AP mine, for rapid, large-scale mining, with the potential of being delivered deep behind enemy lines. The aero ballistic adapter, the mine case, and a thin circumferential ring on the mines covers are olive drab.

2.2.1.15 MI AP DV 59

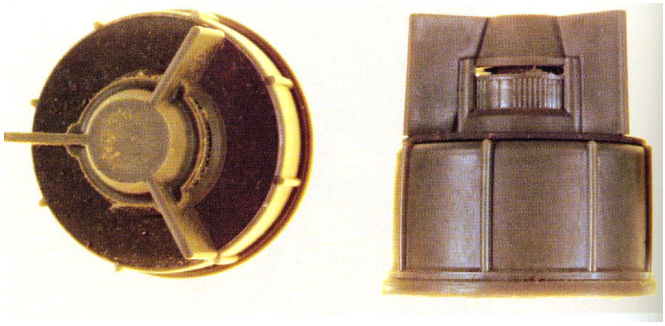

The French MI AP DV 59, or “inkstand mine”, was developed as the replacement to the Model 1951 antipersonnel mine. The mine is plastic bodied with a non-detectable pressure friction fuse. The mine has a removable metal detector plate, which is normally removed prior to emplacing the mine. A practical version of this mine is produced for training purposes. The mine case is OD green with yellow markings.

2.2.1.16 Gravel mines

Mines in the shape of a cloth bag, used extensively in South East Asia, during the 1960s. More than 37 million gravel mines were produced during 1967-68.[9]

2.2.1.17 Type 72

The Type 72 AP mine is a small, plastic-bodied device that has seen widespread use in Afghanistan, Cambodia, Kuwait, and increasingly throughout Africa. While not expected to be encountered, there are two anti disturbance variants of the Type 72. The Type 72B uses a ball-in-cage mechanism to function solely as an antipersonnel mine and a booby trap device. There have been reports that the Type 72C is very sensitive and can be detonated in the presents of magnetic mine detectors. The South African Non-Metallic Antipersonnel Mine, indigenously produced, is a direct copy of the Chinese Type 72. The case colour is green.

2.2.2 Anti Tank (AT) mines

In this category of mines, vehicle mines are included. Some relevant AT mines are listed in Table 2-2 and further described below.

AT Mine	Shape	Size [mm]				Material	Colour/-s	Texture
		L	W	H	D			
TM-62D	rectangular	340				Wood	Olive drab green, brown,khaki/sand	
FFV 013		250	420			Plastic	camouflage	
MON-200	circular				431	Metallic	Olive drab green	
TMM-1	Circular			100	310	Sheet metal	dark green, light green, olive	
TMA-1	Circular			100	315	Plastic	dark green, light green, olive	
AT-2	Cylindrical			128	103.5	Plastic	Black, green, olive	
TMA-5	Square	312	275	113		Plastic	dark green, light green, olive	
TMRP-6	circular			132	290	Plastic	dark green, light green, olive	
Strvmina 5	Circular			77	332	Plastic	Dark olive drab	
M15	Circular			125	334	Metallic	Olive drab	
TC-6	cylindrical			179	273	Plastic	buff	

Table 2-2 Parameters and information on the AT mines described below.

2.2.2.1 Remote Anti-Armour Mine (RAAM)

Remote Anti-Armour Mine (RAAM). A U.S. AT mine deployed in artillery shells. It is also included in the Remote Area Denial Artillery Munition (RADAM) system, which was under development and ceased in the year 2002 [10]. These are projectile-dispensed, setback-, centrifugally and flight-armed, ferromagnetic influence-fired mines used to cause delay or denial of a specific area. The mines incorporate either a 4-hour or a 48-hour self-destruct (SD) delay. Some mines incorporate an anti-disturbance feature. The mines are painted green with no external markings.

2.2.2.2 TM-62D

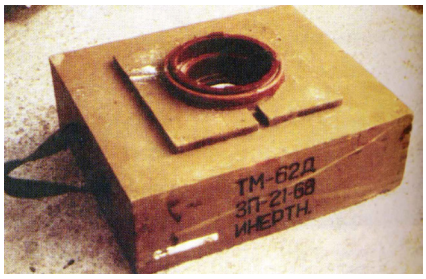

Rectangular wooden casing AT mine of Russian origin. The TM-62 series are high-explosive, blast, AT mines used against track and wheeled vehicles. These mines can be planted in the open (above grade), covered (below grade), and in shallow water. Mines are emplaced manually, by mechanical mine-laying equipment, or dispensed from a helicopter-carried dispenser. Some of the TM-62 series mines also have secondary fuse wells. The mines may be olive drab, green, brown, or khaki/sand coloured. Painting and markings for the TM-62D landmine are unknown. Service fuses are green or green with a brown bakelite plastic pressure plate. These fuses may also be light brown or khaki/sand coloured.

2.2.2.3 FFV 013 (Fordonsmina 13)

Anti-vehicle mine placed on tripod and directed horizontally towards a selected aim point. A directional fragmentation mine. The landmine contains 1,200 (5 grams) balls. The landmine is painted camouflage.

2.2.2.4 MON-200

Russian, directional, side-hitting fragmentation mine. Can also be used as an AP mine. The MON-200 is a larger version of the MON-100 mine. It consists of a metallic case containing the explosive charge and 900 steel fragments (12 mm×12 mm) and a metal stand. Like the MON-100, the cylindrical steel fragments are embedded in a plastic matrix in front of the explosive. The mine can be attached to any fixed object or mounted on its own metal stand. It can be functioned by tripwire, a break-wire or command detonated and has a lethal range of 200 m. The MON-200 can be used singly or as part of an integrated explosive barrier. The mine is not only effective against dismounted infantry but also against personnel in lightly armoured vehicles. The mine is OD green.

2.2.2.5 AT-2

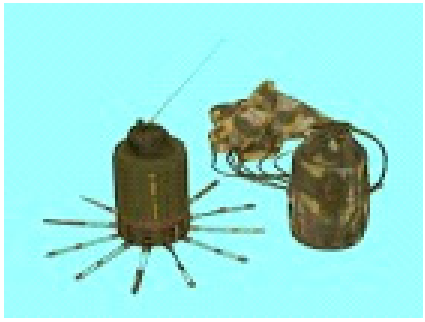

The AT2 is a cylindrical, plastic bodied AT mine which is designed to damage or destroy vehicles by a penetrating effect. The AT2 is a scatterable mine which can be launched from the German LARS or multi-national MLRS rocket systems or the German Skorpion tracked mine layer. The body has small indentations around its circumference and spring loaded erection legs around the bottom edge; these orient the mine properly when it hits the ground. The mine has a protective rubber dome which protects the standoff and a thin wire antenna which acts as the target sensor on top. Rocket launched mines may be found with a small parachute attached to the top edges. The mine's safe & arm unit is in the bottom and it contains the mechanical components as well as the electronics and battery. The electronics process and evaluate signals from the sensor antennae and actuate the mine when a target meets the parameters. The AT2 has a self-destruct mechanism which can be set between 4 and 96 hours, and it has integral anti-disturbance to prevent hand or mechanical clearance. The AT2 can be detected visually as well as with metal detectors under most field conditions.

2.2.2.6 TMM-1

The TMM-1 is a circular, sheet metal bodied AT mine which is designed to damage or destroy a vehicle by blast effect. It is a former Yugoslavian mine and is a copy of the German Tellermine 42 from World War 2. It is a low profile mine and has two parts; the mine body which contains the charge and the screw on pressure plate which covers the fuse cavity. The fuse is a simple spring loaded shear pin design. The TMM-1 has a steel carrying handle spot welded to the side and two anti-disturbance fuse cavities, one in the bottom off centre and one beside the carrying handle. The anti-disturbance fuse cavities are threaded for any 10mm anti-disturbance fuse but the most common is the UMP-1 mechanical pull fuse. The TMM-1 is easily located with metal detectors under most field conditions.

2.2.2.7 TMA-1

The TMA-1 is a circular, plastic bodied AT mine which is designed to damage or destroy a vehicle by blast effect. The TMA-1 is a two part mine; it has a distinct corrugated design on the top which radiates out from the fuse cavity. The fuse cavity is threaded for the UTMAH-1 chemical pressure fuse and is covered by a plastic screw on cap. The mine body is a dark green colour with a rough texture. The lower half of the mine contains the explosives and the upper half, which acts as a pressure plate, is secured with 4 plastic shear pins. The TMA-1 has a plastic carrying handle which slides into a recess in the bottom, as well as one anti-disturbance fuse cavity also located on the bottom of the mine. The TMA-1 cannot be located using metal detectors under most field conditions.

2.2.2.8 TMA-5

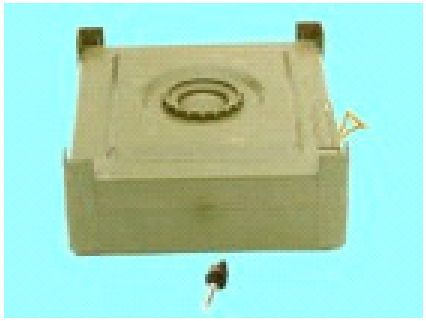

The TMA-5 is a square, plastic bodied AT mine which is designed to damage or destroy vehicles by blast effect. It is former Yugoslavian. The fuse cavity is threaded for the UTMAH-1 chemical pressure fuse and is covered by a simple plastic screw on cap. The mine body is a light green colour with a smooth texture. The TMA-5 has distinct stacking guides on each corner; they are used for stacking the mine during transport. In Bosnia they have been used to stack 2 or 3 mines in one hole. The interior of the mine holds two x 2.7 kg blocks of cast Trotyl and a 150 g Tetryl booster for a total of 5.55 kg of explosive. The mine has a rope carrying handle attached to the side and a fuse shipping cavity on the top. It has no anti-disturbance fuse cavity although it has been reported booby-trapped with a UMNOP-1 multi function fuse. The TMA-5 cannot be located using metal detectors under most field conditions.

2.2.2.9 TMRP-6

The TMRP-6 is a former Yugoslavian AT mine with a shaped charge. It is a circular, plastic bodied mine, designed to destroy vehicles by a penetrating effect. The mine body has a ribbed upper surface with an integral fuse centered on the top and a plastic handle which folds into a recess in the body. The TMRP-6 contains 5.1 kg of cast TNT and it is actuated by pressure of 150 kg or lateral force on the tilt-rod of 1.3 kg. The fuse is mechanical with a clockwork arming delay system (1 to 4 minutes).The TMRP-6 comes packed in a natural or green painted wooden box with black markings. The box contains 4 x TMRP-6's, 4 x tilt-rods, and 2 x brass clock set keys.

2.2.2.10 M15

U.S. AT blast mine. The M15 is a high explosive (HE), heavy AT landmine. The mines have manually armed pressure actuated primary internal fuses. These mines are painted olive drab (OD) with identifying markings stencilled in yellow on the bottom of the mine. The tactical fuses are OD with yellow markings. The tilt rod fuse has yellow identifying markings on the bottom of the fuse. These markings cannot be seen when the fuse is screwed into the mine. The adapter is anodized black with yellow marking.

2.2.2.11 Strvmina 5

Swedish AT blast mine designated M5 (STRIDSVAGNSMINA 5) by the Swedish army. These are nonmetallic, caseless, antitank (AT) landmines with pressure fuzes. The mines are painted dark olive drab and may be marked with a yellow ring or yellow square. The mine body is cast explosive, reinforced with fiberglass. The handle is plastic rope. The fuse is plastic. The fuse well, booby trap fuse well(s), and shipping plug are plastic. A rubber gasket seals the fuse well.

2.2.2.12 TC/6

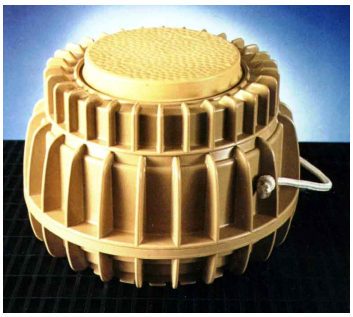

Italian pressure fired AT mine with a very small metal content. Plastic casing

2.2.2.13 BLU-92 Gator

U.S. AT mine delivered by CBUs. The BLU-92/B (Gator) is an air-delivered, free-fall, bi-directional electromechanically armed AP mine. It is fired by trip line sensors or self-destruct timers. However, some units have an additional anti-disturbance feature. This mine is used for

rapid large-scale mining, with the potential of being delivered deep behind enemy lines. It is designed to disrupt and disorganize troops, deny utilization of key areas, and thwart mine clearance operations. The aero ballistic adapter and mine case are olive drab. Each cover has a 51 mm yellow dot at its centre.

2.2.3 UXO

Initially this section is very limited and is perhaps the most complex part of trying to make a classification due to the enormous variety of objects that is included in the definition of Unexploded Ordnance (UXO). At present time, the focus is a few objects in a couple of different categories of UXOs. Some examples are listed in Table 2-3.

Ordnance
Bomb
Artillery shell
Mortar round
<105 mm amm.
AA ammunition
Rocket
Missile
RPG
Hand grenade
Rifle grenade
Grenade, 40mm
Cluster Bomb Unit

Table 2-3 Some typical UXOs.

2.2.4 UXO (Submunitions)

A selection of different objects in the submunition category is somewhat easier than for mines, due to the limited number of different types of submunitions being produced in the world until present time. The difference is that the limited number of submunition types have been, and are being, produced in huge series. Some examples of submunitions are listed in Table 2-4 and further described below.

Submunition (UXO)	Shape	Size [mm]				Material	Colour/-s	Texture
		L	W	H	D			
BLU-61A/B	Sphere				99	Steel	Black	
BLU-63	Sphere				76	Steel	Black	
BLU-97	Cylinder/ballute			169	64	Steel casing	Yellow/white	
BL-755	Hemisphere/spring			149/ 630	68	Steel casing	Metallic	
KB-1	Cylinder/cord			80	40	Steel/plastic	Grey/brass	
AO-1SCh	Cylinder/fins			156	49	Steel	Grey	
PTAB-2,5KO	Cylinder/wings			300	59	Steel	Grey	
MOTIV-3M	Cylinder/parachute			255	284	Steel		

Table 2-4 Parameters and relevant information for the submunitions described below.

2.2.4.1 BLU-61A/B

A U.S. submunition. This is an aerial dispensed, centrifugal armed, impact-fired, high explosive incendiary, anti-material, fragmentation bomb. It is detonated by an M219E1, all-way fuse. The bomb is painted olive drab without markings. Each hemisphere is made from a coined steel fragmentation liner, and a liner of pyrophoric material (for incendiary effect) of zirconium-tin. The hemispheres are encased in a urethane plastic shell. The clamp ring is stainless steel.

2.2.4.2 BLU-63

A U.S. submunition. These are all small, aerial dispensed, centrifugal armed, high-explosive fragmentation (HE-frag) bombs. The bombs all consist of two hemispheres held together by a

crimp ring. The BLU-63/B, and the BLU-63A/B bombs are impact-fired and the BLU-86/B and the BLU-86A/B bombs are time-delay-fired. The outer wall has a weakened area which ruptures when the fuse functions. These bombs are olive drab with a small yellow dot on one hemisphere. Designation and loading data may be stencilled in yellow on all the bombs except the BLU-86/B, which has no markings. The BLU-26(T-1)/B, BLU-36(T-1)/B, BLU-63(T-1)/B, and BLU-86(T-1)/B are painted blue with white markings.

2.2.4.3 BLU-97A/B/IM

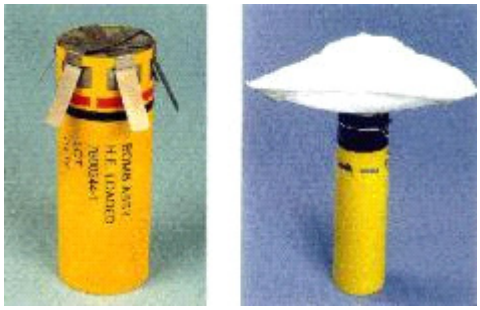

A U.S. submunition called Combined Effects Bomb (CEB), widely used in recent conflicts around the world. The BLU-97 munitions are soda-can-sized bomblet submunitions that are dispensed in large numbers (approximately 150-200 bomblets per weapon) to attack “soft” area targets. The body of the submunition is cylindrical in shape, approximately 20 centimeters long, and has a 6 centimeter diameter. It is bright yellow when new.

The BLU-97/B Combined Effects Bomb (CEB), effective against armor, personnel and material, contains a shaped charge, scored steel casing and zirconium ring for anti-armor, fragmentation and incendiary capability. The bomblet case is made of scored steel designed to break into approximately 300 preformed ingrain fragments for defeating light armor and personnel.

CEB is an effective weapon against such targets as air defense radars, armor, artillery, and personnel. However, because the bomblets are dispensed over a relatively large area and a small percentage of them typically fail to detonate, there is an unexploded-ordnance hazard associated with this weapon. These submunitions are not mines, are acceptable under the laws of armed conflict, and are not timed to go off as AP devices. However, if the submunitions are disturbed or disassembled, they may explode, thus, the need for early and aggressive unexploded-ordnance clearing efforts.

2.2.4.4 BL-755


The BL755 submunition dispensing cluster bomb has been in service with the RAF for over 27 years. The 272kg BL-755 comprises a finned casing containing 147 High Explosive Anti Tank (HEAT) bomblets packed in seven sections of 21 rounds each. Following separation from the aircraft the outer casing covers are jettisoned by a gas ejector at one of four pre-set times. The bomblets are then ejected sideways as much as 18m at pre-set intervals. Each of the ejected submunitions are then orientated by the deployment of a parachute while a spring mounted base plate is activated to give the correct stand-off for the shaped charge. The warhead is designed to explode on impact, being triggered by a piezoelectric fuse which is located under the base plate. Upon detonation the shaped charge produces a jet of high velocity, high temperature plasma which can punch through up to 250mm armour. In addition the release of 2000 pieces of shrapnel produces a secondary anti-personnel effect.

2.2.4.5 KB-1

Former Yugoslavian submunitions.

2.2.4.6 AO-1SCh

Russian submunition. These bombs are used against personnel and light material targets such as airplanes and motor transports. They are often carried in a cluster container. The body is gray.

2.2.4.7 PTAB-2,5KO

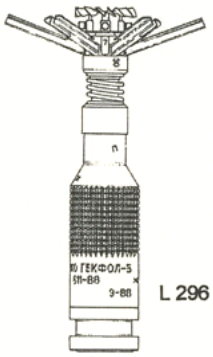

PTAB-2,5KO (AT/AP)

Russian submunition. This is a high-explosive antitank (HEAT) fin-stabilized dispenser-deployed bomb. It employs a point-initiating nose fuse which is mechanically armed and electrically fired. The bomb is painted gray with a black color band and markings stenciled in black. The fuse is unpainted with markings stamped into the metal of the impeller guard.

2.2.4.8 MOTIV-3M

This is a Russian SFM under development. It is designed to hit armoured targets from above with an Explosive Formed Penetrator (EFP). It is similar in design to other SFMs like BONUS, SMArt 155 and SADARM.

2.2.5 Improvised Explosive Devices (IEDs)

This category of weapons pose a serious threat to military forces in conflict areas where irregular forces and insurgents can use IEDs as a way of means to limit movement, terrorise and fight their enemies on a psychological level.

In this report the IEDs are discussed, but not evaluated at this time.

2.3 Examples of mines used in some countries

An example of used mine types encountered, or in service, in mine affected countries is given in Table 2-5, from [11].

Country	Types of mines
Somalia	DM-11 Germany, M/71 Egypt, M-15 United States, M7A2 United States, Mk-7 UK, MV-5 Russian Federation, PRB M3 A1 Belgium, PRB M3 Belgium, PT-Mi-Ba-III Czech Republic, SACI Italy, T-72 AT China, TM-46 Russian Federation, TMN-46 Russian Federation, TM-57 Russian Federation, TM-62 Russian Federation, TM-62M Russian Federation, TMN-46 Russian Federation, Type-72b China
Angola	C-3-A Spain, FFV 013 AVM Sweden, M-15 United States, M-19 United States, M-24 United States, M6A2 United States, M7A2 United States, MAT 76 Romania, Mk-5 HC UK, MV-5 Russian Federation, No. 8 South Africa, PRB M3 Belgium, PT-Mi-Ba-II Czech Republic, PT-Mi-Ba-III Czech Republic, PT-Mi-K Czech Republic, TM-46 Russian Federation, TM-57 Russian Federation, TM-62 Russian Federation, TM-62M Russian Federation, TMA-2 Yugoslavia, TMA-3 Yugoslavia, TMA-4 Yugoslavia, TMA-5 Yugoslavia, TMD-41 Russian Federation, TMD-44 Russian Federation, TMD-B Russian Federation, TMK-2 Russian Federation, TMN-46 Russian Federation, TMN-46 Russian Federation, Type 69 China, Type-72a China, UKA-63 Hungary
Bosnia and Herzegovina	MAT 76 Romania, PT Mi-Ba II Czech Republic, PT Mi-Ba III Czech Republic, PT-Mi-K Czech Republic, TM 57 Russian Federation, TM 62 M Russian Federation, TM-46 Russian Federation, TMA-1A Yugoslavia, TMA-2 Yugoslavia, TMA-3 Yugoslavia, TMA-4 Yugoslavia, TMA-5 Yugoslavia, TMM-1 Yugoslavia, TMN-46 Russian Federation, TMRP-6 Yugoslavia
Afghanistan	Mk7 UK, MV-5 Russian Federation, SH-55 Italy, TC-2.4 Italy, TC-3.6 Italy, TC-6 Italy, TCE / 6 Italy, TM-41 Russian Federation, TM-46 Russian Federation, TM-57 Russian Federation, TM-62 Russian Federation, TM-62 M Russian Federation, TMA-5 Yugoslavia, TMB-41 AT Russian Federation, TMB-44 AT Russian Federation, TMD-B Russian Federation, TMK-2 Russian Federation, TMN-46 Russian Federation, Type 69 China

Table 2-5. Examples of landmines used in some countries.

2.4 Future Mine Threats – A 10 Year Perspective!

2.4.1 Strategies – Future Mine Systems

Different long-term mine development strategies exist, depending on country and the historical and political situation in surrounding region of that specific country. The U.S. Intelligent Munition System (IMS) is one example (Figure 2-16), which is described in [12]

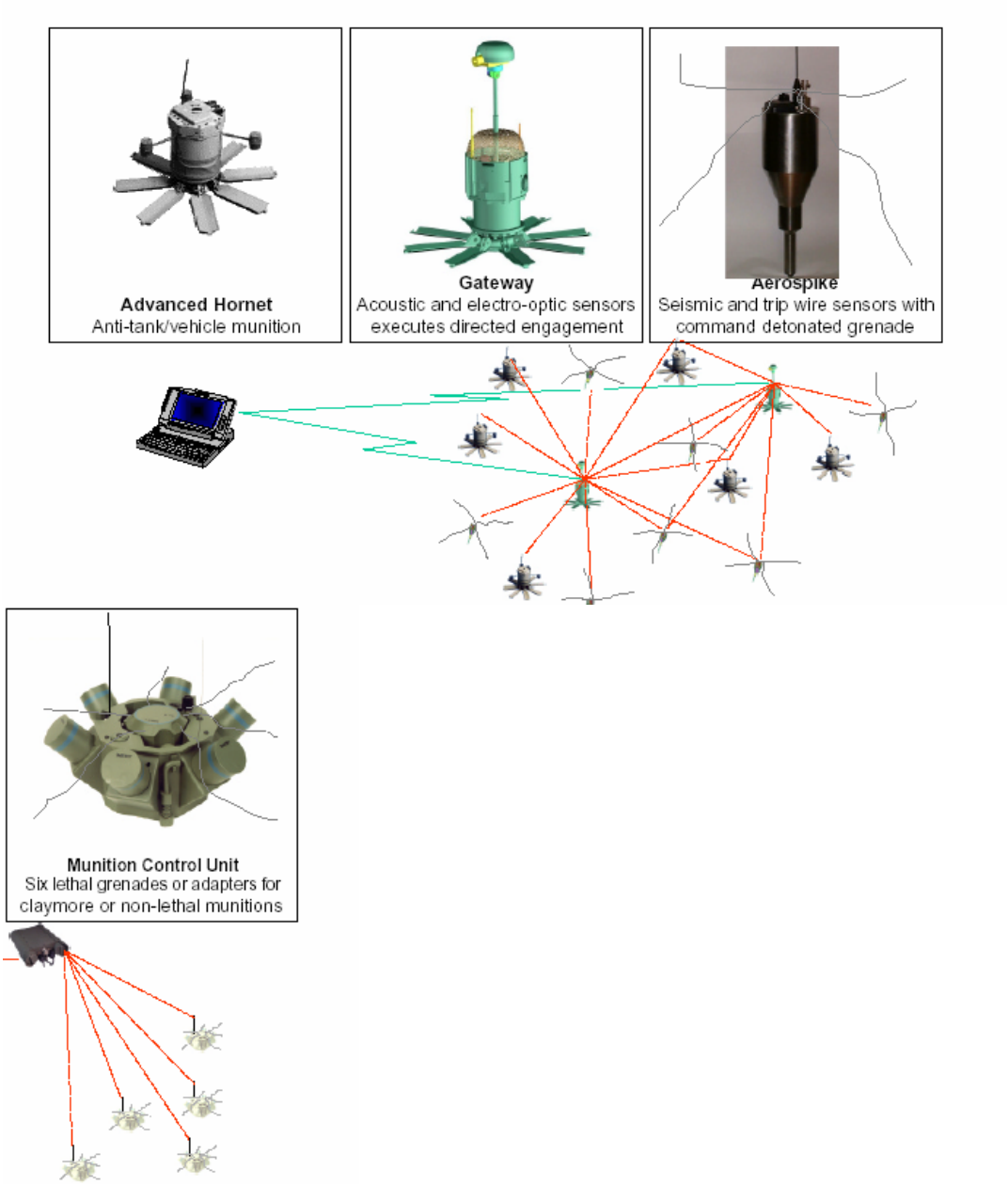

Figure 2-16. Example of modern mine development. Images represent parts of the U.S. Intelligent Munition System (IMS), which uses modern sensors and networking capabilities in order to defeat enemy targets. From [12]

IMS includes several different parts which are specific for U.S. related military activities, such as the Anti-personnel Landmine Alternative (APL-A), Non-Self Destruct Alternative (NSD-A) and "Self-Healing Mine Fields". In these sublevel strategies, different, new mines (WAM, AHM) will be implemented, but also some systems used today will be used as well (DPICM, CEM, SFM). Other western countries are following the U.S. development strategy in mine warfare. Russia and China seem to adopt parts of western mine development strategies at present.

Important aspects of the new types of mine threats, in a 10 year perspective, are: networking, mine field gradients (from non-kill to kill capability), "man-in-the-loop"-concepts, advanced

munition and submunition sensors, on-off-on-capabilities, friend or foe distinction, real-time surveillance and digitalised control systems.

2.4.2 Advanced Submunitions (DPICMs and CEMs)

DPICM and CEM submunitions will continue to be used in large quantities. The use of these submunitions will probably increase, as seen in a world-wide perspective, due to the extreme amounts of DPICMs and CEMs already produced and being produced the coming years.

2.4.3 Sensor Fuzed Munitions (SFMs)

SFMs are in use today in several military forces around the world. These types of submunitions pose a very serious threat to heavily armoured tanks today and there are at present no countermeasures to be used against this type of weapon. SFMs will probably be produced in much less numbers than DPICMs and CEMs, due to their high implementation level of advanced technology and therefore much higher unit price. SFMs will continue to pose a threat to armed forces for many years to come.

2.4.4 Wide Area Munitions (WAMs)

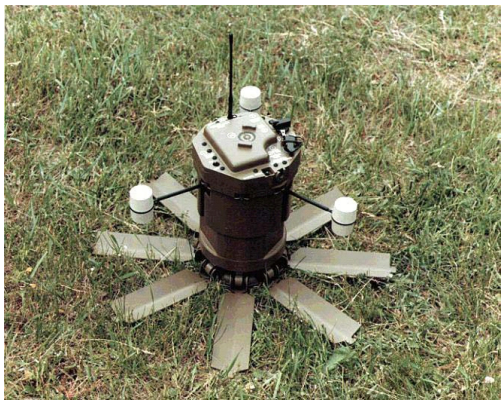

WAM is a concept designated to mines or munitions acting over a large surface, with the capability of locating and defeating its targets autonomously with the use of advanced sensors. M93 Hornet is one example already existing today.

2.4.5 Anti-helicopter mines (AHMs)

The AHM is a type of Wide Area Munition. Status of present anti-helicopter mine development is unclear. Two examples are shown below in Figure 2-17 [REF: Textron Product Info Sheet, REF: Jane's Mines 2000-2001], but the American AHM development has probably ceased to exist or is put on hold at present time.

Figure 2-17. Example of two anti-helicopter mine concepts. The U.S. AHM (left) and the Russian TEMP 20 (right).

The Russian TEMP 20 seems to be under development, still, and is, like the U.S. AHM concept, using seismic, acoustic and infrared sensors to detect, discriminate, locate and defeat its targets [9]

Obviously these type of mines will be very important to detect before they can do harm to an airborne search platform, if they will be deployed in future conflicts.

3 Environmental aspects

This chapter deals with a survey of environmental aspects of relevance for MOMS.

Environmental studies are normally carried out in close connection with experiments and modelling and simulation (MoS) tools.

3.1 General aspects

In order for a mine to be detectable, it must have observable properties that distinguish it from its surrounding environment. This makes the characterization and understanding of the mine environment just as important as understanding the properties of the mine itself. The set of relevant environment parameters will vary depending on the choice of sensor.

To reach a successful or sufficient level of detection of suspect objects, the interaction between the object and its neighbouring background needs to be understood. The physical properties of the mines and UXOs are normally constant in terms of its influence on the arising optical signature in the sensor. But for the background the situation is quite different.

The environmental background could consist of living materials, grass, trees etc., with different properties depending on the interaction with time of day or year and with earlier weather situations and probably most important the actual weather. In the case of urban environments, the physical properties in the scene are a mixture of human made objects, like building materials, and natural environment.

To understand the target and background dependence for different scenarios a lot of field experiments have to be carried out as well as supporting laboratory tests. A describing image of this is shown in figure 3-1. However, the understanding could also derive benefits from the use of physical and statistical based numerical modelling and simulation work described in chapter 5.

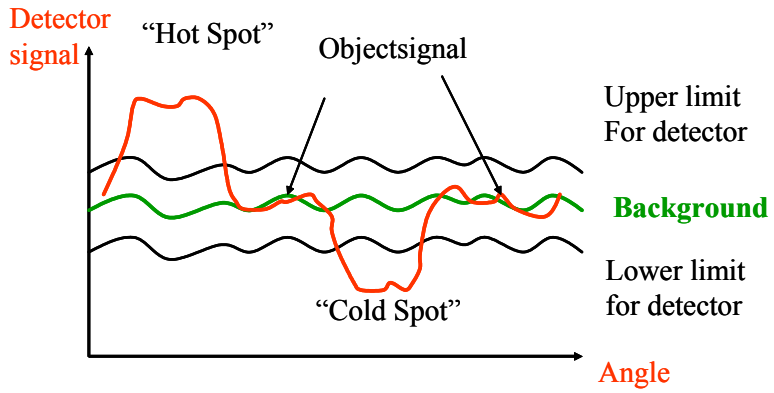

Figure 3-1. The target in background phenomena

The scientific area of environmental research is enormous. There are hundreds of journal magazines covering areas from global heating of earth down to microclimate studies of the photosynthesis in single leafs. The scientific approach to study a given problem normally

follows the same pattern. First, an observation of the studied phenomena, then analysis followed by a modelling work and at last the simulation in order to be able to reproduce the observed phenomena. Hopefully the simulation will increase the understanding of the observed phenomena and bring some answers to specific questions.

In MOMS, studies of relevant backgrounds will be carried out in close connection with FM and SWEDEC. The focus of environmental parameters will be on the optical phenomena. This is a complex task because of the wide spectrum of expected situations and environments that a MOMS concept will be studied for.

The parameters affecting the optical signatures that arise in the environment are shown in figure 3-2. Another important parameter is the vegetation layer influence on transmission of radiation from e.g. lasers.

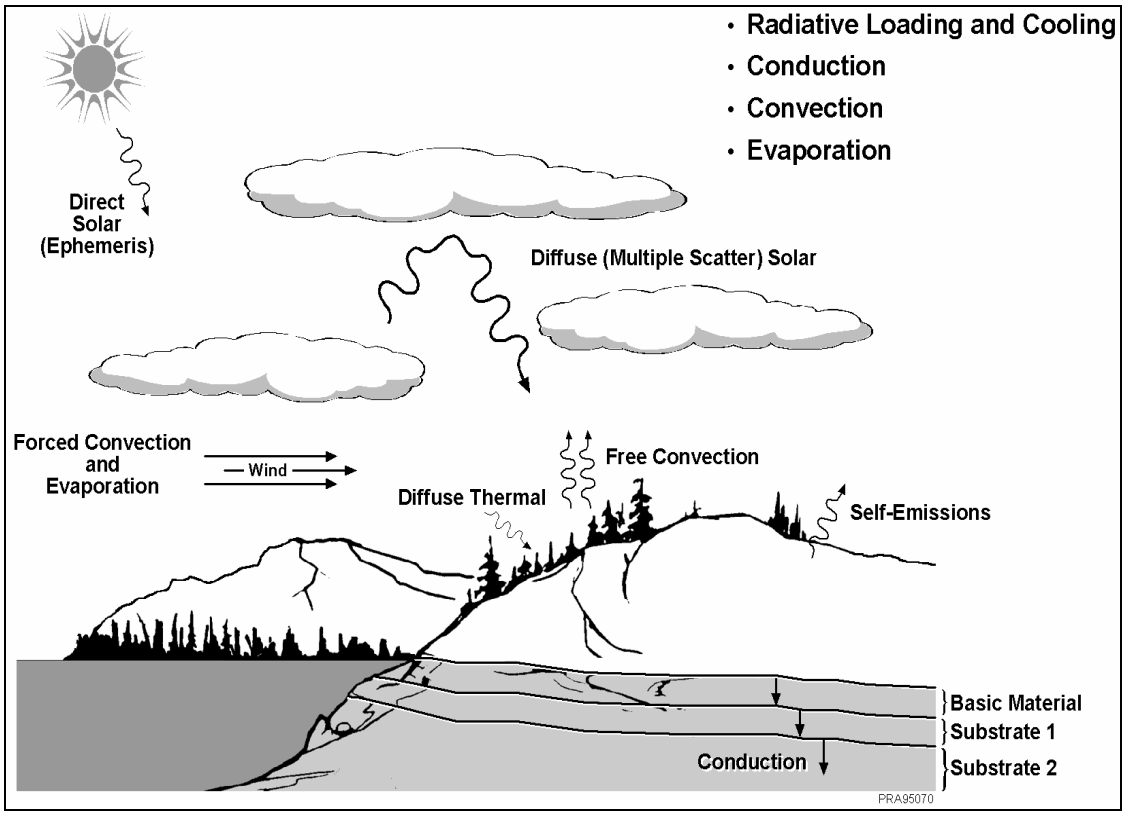

Figure 3-2. Some of the environmental parameters which needs to take into consideration when studying EO signatures of mines and UXOs. Figure from [13]

3.2 The environment

Many studies of optical methods to detect land mines also discuss the interaction with the environment. There are several papers [14-17] that discuss the influence of the background and environment. At present, there is no accessible universal theory for thermal modelling of environmental backgrounds, only rough approximations.

The complex energy exchange between the surface of the soil and vegetation, including mines and minelike objects, and the atmosphere is shown in figure 3-3.

Some careful prepared assumptions of the environmental parameters have to be made, see e.g. [16, 18, 19]. The basic equation for the principle of conservation of energy in the domain soil volume surface-atmosphere is given by:

$$\sum_{i=1}^{n} \dot{Q}(i) = 0$$

where $\dot{Q}(i)$ are n different energy transport processes per time unit between the studied objects and the local environment, and could in this case be derived from 7 different processes shown in figure 3-3.

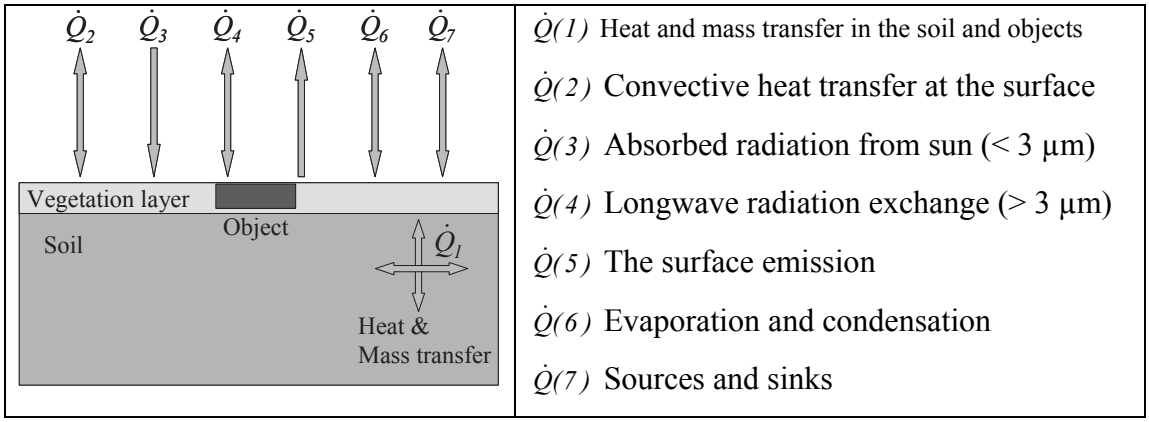

Figure 3-3. The energy transport processes between the studied object and the local environment. The arrows also shows the possible direction of the energy transports.

In the soil volume, the most important parameters from heat conductivity, see figure 3-4., are specific heat capacity and density. The mass transfer due to moisture is also of vital importance.

A rough method is to summarize the soil content in the following way, see e.g.. de Vries [20] and Miller [19]

$$\rho c_p = 1.9x_m + 2.5x_o + 4.2x_w \qquad (10^6 \text{ Jm}^{-3}\ \text{K}^{-1})$$

where x_m, x_o and x_w are the volume fraction of minerals, organic matter and water. Air is neglected in this approach.

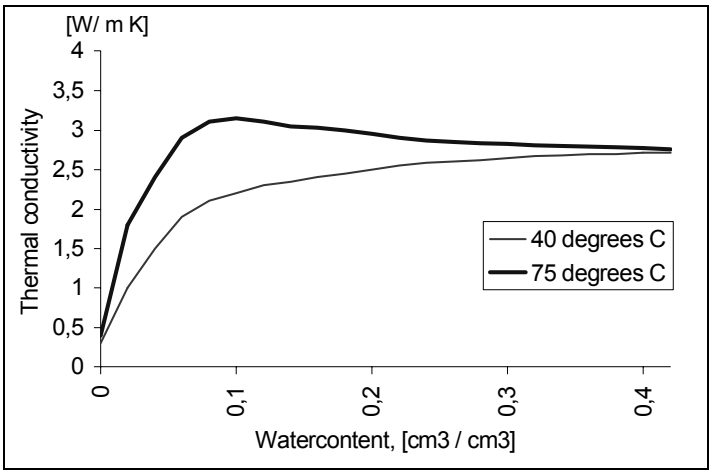

Figure 3-4. Upper, thermal conductivity of sand with a high degree of quartz as a function of soil moisture content, from Jacobs [17]

If the mass transfer is taken into consideration the moisture itself is a highly non-linear parameter. The addition of water to a dry soil volume causes an increased thermal conductivity. The thermal diffusivity normally rises to a maximum of 2 to 3 times the dry value when the moisture content is between 5 to 10 percent. In that case coupled differential equations are needed to solve the problem. For porous materials, like soils, there are two governing differential equations, which depend on each other. From e.g. [20, 21] we can obtain the general differential equations describing the heat conduction and the moisture movement in porous materials with combined temperature and moisture gradients.

Carter [22] demonstrated the importance and effect of different moisture levels when using infrared systems to detect shallow buried mine-like objects. Infrared cameras were used to record surface temperatures in buckets of wet sand. The results showed that the most favourable moisture level for enhancing the thermal contrast on the surface was approximately 5 weight.%.

The wavelength dependent reflectivity of an object or background is an important parameter for all EO sensing systems. This parameter is discussed in a number of chapters in this report and many examples will be shown. One example of dry and wet sand is shown in figure 3-5. Due to its importance, FOI is considering the purchase of a good instrument for research purposes.

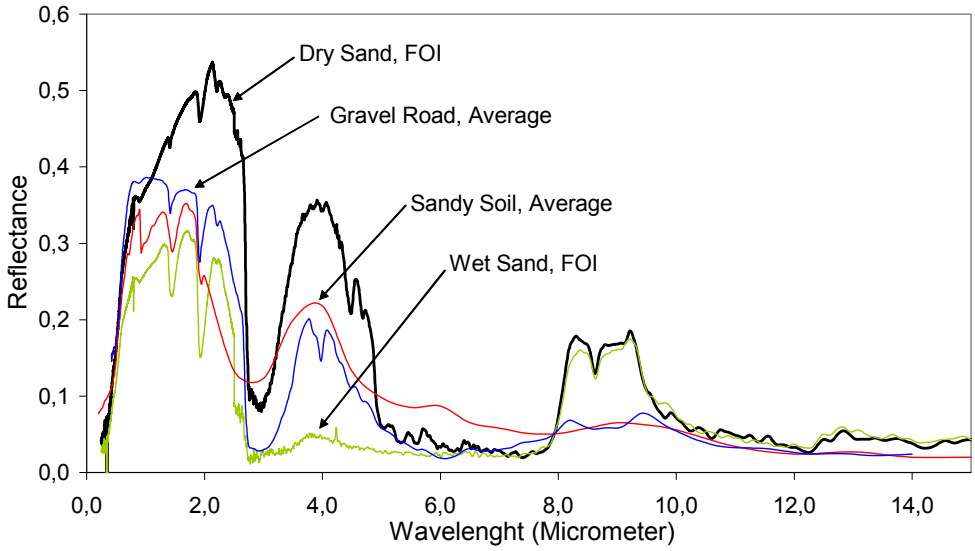

Figure 3-5. FOI measured reflectance of dry and wet sand and from literature, eg. [23], the average reflectance for sandy soil and gravel road are obtained.

The vegetation layer differs from inorganic materials due to its internal physiological processes. The vegetation canopy and the Leaf Area Index (LAI) is discussed in [24-26]. Besides the heat exchange through radiation, sensible heat and latent heat losses to the atmosphere are the dominant effects. Examples of that are the evapotranspiration that occur due to outer stress from e.g. the sun and the stomatal resistance due to humidity gradients and carbon-dioxide in surrounding air. In [27] a parameterization of the vegetation parameters is studied. All physical processes are transformed into parametrical terms that allow basic studies of thermal IR sensing.

The atmospherical effects and the different contributions of radiation are studied in [28] and its effect on the signatures due to the presence of land mines in [29]. A weather station is of vital importance when carrying out field trials.

Concerning studies of environmental aspects with modeling tools, the table 3-1 from [17] could be obtained. The table 3-1 shows the individual model responses from different parameters.

Very Sensitive	Moderate Sensitive	Very Insensitive
Air temperature	Relative humidity	Air Pressure
Solar irradiance	Target height	Cloud cover (high level clouds)
Solar absorption coefficient	Windspeed	Time Step
Thermal emission coefficient	LWIR sky irradiance	Thermal diffusivity
Top layer heat conductivity on ground	Thermal conductivity	Mesh Size
Cloud cover (middle layer clouds)	Bottom heat flux (if the model is deep enough)	
Cloud type		Diurnal repetitions
Initial conditions		
Vegetation		

Table 3-1. Relative model responses to the variation of several input parameters, from [17].

3.3 Active imaging

Active illumination is a way of controlling the external conditions by dominating the natural illumination. Active imaging will thus in many cases have similar properties during day and night measurements. A prerequisite for active imaging is that the emitted radiation can reach the object and that enough photons are reflected back to enable detection. There must also be a contrast between the background and the imaged object. The word contrast has a broad meaning in the sense that it can reflect a wide variety of properties such as shape or colour. Reflectance, surface structure and geometry are among the important environment parameters for active imaging.

3.3.1 Active range imaging environment

Various environment parameters including the reflectance and the penetration of vegetation are characterized in [30] using an active 3-D laser radar system as well as a passive camera under solar illumination at the wavelength of 1.5 μm. Reflectance values were found to exceed 50 % for grass and the tree trunks of various species, while lower values in the 13 %-18 % range were measured for foliage. Seasonal variations in the penetration depth of the laser imager were measured. While more than 80 % of laser reflections were found beyond a depth of 20 m into a softwood forest scene during early springtime, this number decreased to 55 % during winter time with the scene covered in snow, and in early summer it was only 30 %. This variation is shown in figure 3-6. Another interesting effect was discovered during the winter, when the low reflectivity of snow at this wavelength was found to provide good contrast to many man-made objects.

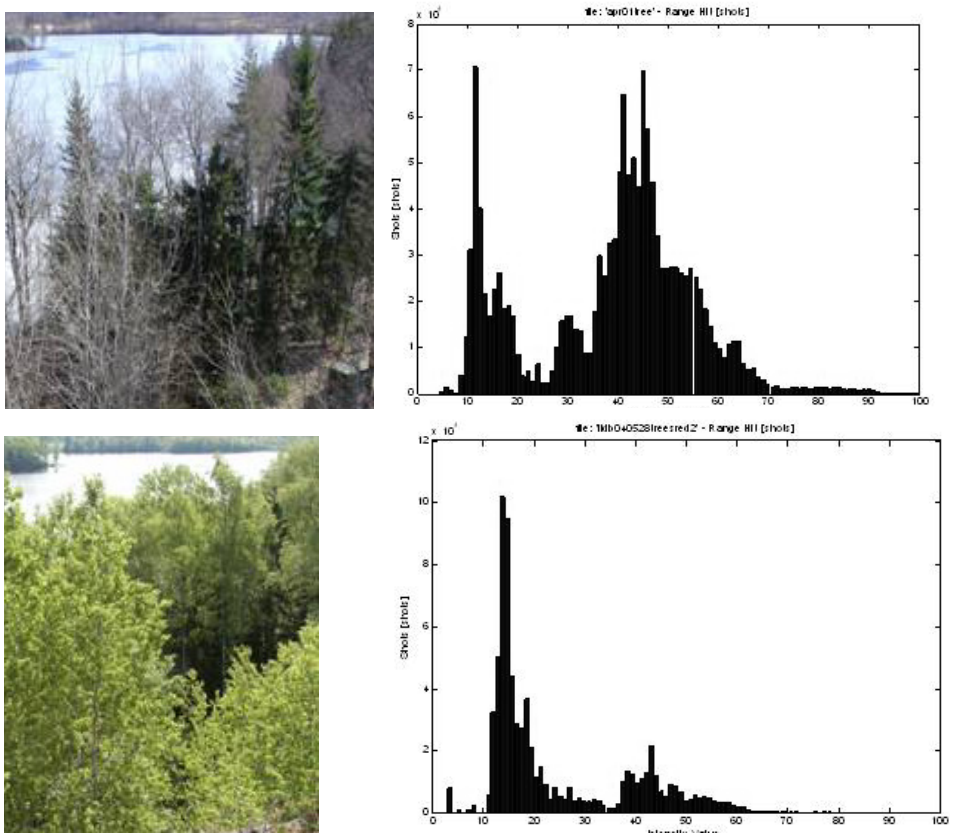

Figure 3-6. Measured distribution of laser reflections from a site during spring (top image) and summer (bottom image).

A high-resolution scanning laser radar is used in [31] for characterizing minefield sites and generating surface and terrain models. Surface "micro topographical" elevation contour and vegetation height maps are created from scanned data from dirt and grass minefield sites. The surface heat flux under a vegetation canopy is an important parameter in the transfer of heat to and from the ground, and thus for the detection of mines in this environment. A measure of the ground shading effect of the grass canopy is the leaf area index, LAI. Laser radar data from the same grass field as in [31] are used in combination with a photosynthetically active radiation ceptometer to derive an approximate correlation between the vegetation height and the LAI [25]. A model for estimating the distribution of solar radiation reaching the ground for different solar zenith angles is developed, thus resulting in a correlation between the laser scanner measurement and the heat flux existing at the soil surface.

3.3.2 Active polarimetry

Standoff detection of mines in some different environments has been subjected to initial investigation by [32], using a prototype laser illuminated active polarimetric system. These tests featured varying background materials, mines and levels of solar radiation at standoff distances of 660 and 1000 ft. It was found that the degree of polarization, DOP, of the detected radiation was lower for various background samples such as soil, sand, grass and rock than it was for the majority of mines. Performance was improved when solar subtraction was used. The presented system also includes a passive thermal FLIR sensor, and it is shown that the dual sensor approach using IR detection provides some capability in one case where

the mine did not show good DOP separation. It is thus clear that one sensor will not necessarily work for all mines in all environments, speaking in favour of multi-sensor approaches.

A property of green leaves is their ability to bind solar energy by photosynthesis. The typical absorption pattern of the chlorophyll may differ from man-made objects such as mines. The approach studied in [33] is to achieve detection at close range (2.7 m) using a two-colour laser scanner with one wavelength in the chlorophyll absorption dip around 675 nm and the other wavelength above it at 778 nm, in order to distinguish the grass from other types of materials using the ratio of reflectance values at the different wavelengths. This two-colour laser system is used in combination with another active scanner based on tungsten halogen lamp illuminators with four wavelength bands between 1400 and 2300 nm, and a third system based on a TV camera with spectral or polarization filters. It was noted in [33] that real surface laid mines that can be overgrown by vegetation or partly covered with dust or soil which will greatly reduce the contrast against the background. The solution that they suggest is to use a water spray system to clean the area of interest.

3.4 Examples of FOI research results

An example of a result [29] on how FOI continuously has measured an area, with different sensors, containing a buried mine and thereafter developed a model for investigation of different parameters is shown in figure 3-7. The used sensors are a LWIR-sensor and some Pt-100 temperature sensors. A simulated surface temperature from the model is also shown. Figure 3-8 shows some simulated effects due to different boundaries and the depth of burial and how boundaries affect the temperature difference on surface above the buried mine subtracted with the undisturbed area. The basic model is setup with parameters directly from the measurements. An increased cloud level to 50% is modelled and shown, but does not differ so much compared with the basic model. Two different convection models is shown in the figure but has minor effect compared with the basic model. Also if we double the windspeed the effect is marginal. Decreasing the irradiance on the ground from sun by 50% gives a slight decrease of the contrast. The original burial depth of the hole is 20 cm. Changing this into the new burial depth of 15 cm gives a large effect on the surface temperature contrast. Overall, this model shows how different parameters could be changed and interpreted to increase the knowledge of phenomenons.

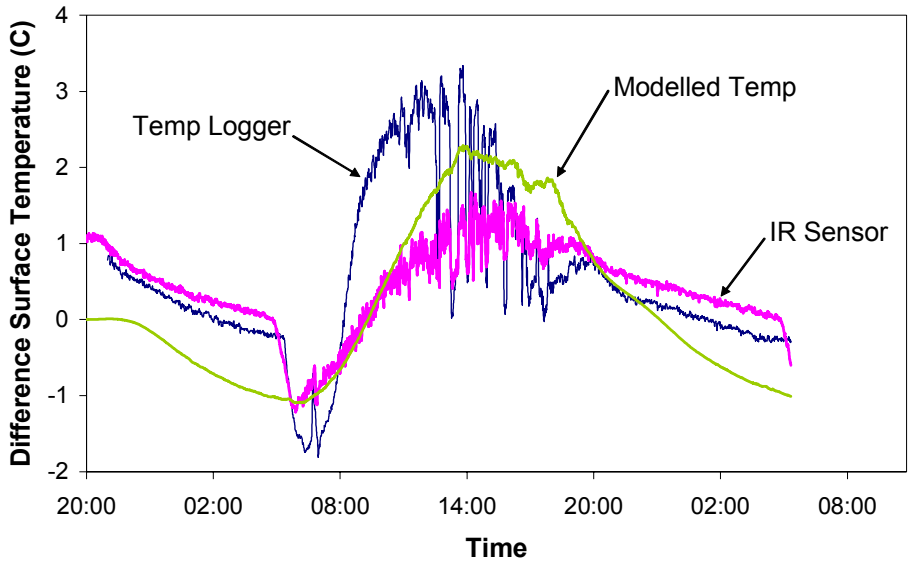

Figure 3-7. Comparison of the three different methods for surface temperature estimation, IR-sensor, Pt-100 temperature logger and simulated surface temperature from the model.

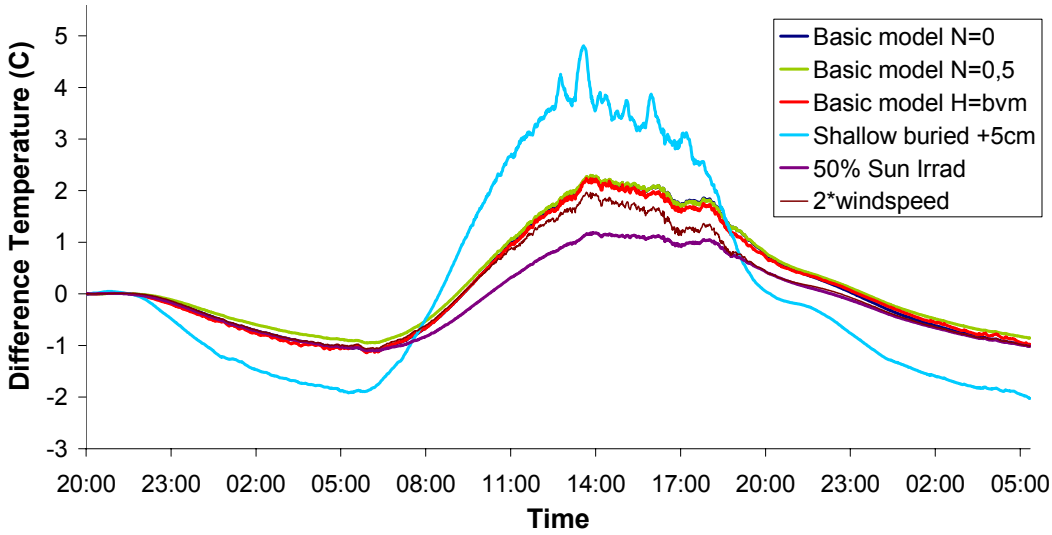

Figure 3-8. Modelled and simulated temperatures when changing environmental parameters. The temperature differences are between a point above the buried mine subtracted by the local background. Comparison of the effects of different modelling parameters: The basic model. Different Nebulosity, Convection coefficient, Depth of burial, 50% of sun irradiance and double windspeed.

3.5 Summary of the chapter

Understanding of the environment is a large area of research. An overview of some parameters of importance has been made in this chapter. Several factors influencing the heat transfer in the mine environment have been described, as well as the impact of reflectance and vegetation density on both passive and active electro-optical detection. Because the field is large and the expected environment is highly scenario-dependent, FOI will collaborate with SWEDEC concerning relevant environment issues.

4 Evaluation of Sensor Concepts

This chapter deals with a survey of sensor technologies of relevance for MOMS. Emphasis is put on laser sensing since this is relatively unexplored technology for land mine detection and classification. The chapter starts with listing the system requirements as a background before presentation of different phenomenologies and sensor technologies limiting performance and serves as a base for initial evaluation of sensor candidates.

4.1 Requirements

In this chapter some requirements for the optical sensor system are presented. Some of the requirements can be extracted from background documents, other are introduced as proposals. The MOMS project is intended to support design of the technical demonstrator succeeding the MOMS project. This means that requirements for the technical demonstrator also will govern research activities in MOMS. In case there are requirements not already specified that are essential for governing research in MOMS, input from the reference group is expected.

4.1.1 Adaptation ability

A modular approach for the MOMS system ensures that the system can be adapted to different conditions, demands and restrictions. Some examples of factors that influence the demand for adapting capacity are listed below:

- Weather conditions will influence the function of different sensors as well as the object signatures..
- Light conditions, day/night capacity
- Different ground conditions. Snow, ice, water, bare soil, asphalt, grass, bushes, trees have different optical properties (reflectance, emittance, polarisation, fluorescence) and will influence the need for sensor adaptation as well as the need for tuning lasers to different wavelengths.
- Platform, type and stability. It makes a difference if the sensor system is mounted on a ground or an airborne vehicle e.g. concerning vibrations, weight, power consumption, space requirements.
- Different user priorities in different situations. In some situations, time is a limiting factor but in other situations a user might give priority to high detection probability, possibly in combination with a demand for low false alarm rate.

4.1.2 Time and velocity requirements

The ability for the system to present results in real time is a very challenging requirement. In [15] "Real Time" is defined as: "Pertaining to the timeliness of data or information which has been delayed only by the time required for electronic communication". According to this

definition, data analysis is unfeasible for the purpose of this study. Instead, for MOMS it seems that the definition of "Near Real Time" is more appropriate: "Pertaining to the timeliness of data or information which has been delayed by the time required for electronic communication and automatic data processing. This implies that there are no significant delays". Referring to this, a definition for MOMS could be: "The user shall not experience any significant delay".

Some examples of time requirements under discussion are:

- 0.6 km^2 reconnaissance in a couple of hours.
- 2800 m^2/s at a speed of 50 km/h.
- Check roads with respect to re-mining in international operations at a speed of 40-50 km/h.
- Velocity for detection in terrain is set to 40-50 km/h for a swath width of ± 100 m.
- Operations shall be sustainable for more than one hour.
- Capacity all around year and day.
- Demand for extremely good distance accuracy will give a demand for short pulse length and/or fast modulation of the emitting laser.
- Fast algorithms to meet the real time requirements

4.1.3 Geometric requirements

There is a requirement to be able to "see into the forest". Spatial resolution in imaging sensors should be well in accordance to objects of interest, which means millimetres to centimetres depending on object size and if the intention is wide area screening or detailed investigation of suspicious objects.

- There is a range requirement of 100 m for detecting directional fragmentation mines.
- Sweep width ± 100m.
- INS/GPS navigation system with 5 cm accuracy for geo localisation of objects.
- Detection of partly occluded mines.
- Detection of mines in water down to a depth of 2 m.

4.1.4 Stealth and EW

There is no explicit statement regarding requirement for taking signature of own equipment into account.

4.1.5 Probability of detection and false alarm

There is no quantitative statement of requirements for probability of detection and false alarm. There are statements saying that the false alarm rate should be low and that the level should be clarified. It is stated that algorithms for detection and classification should be robust. The ambition is not to declare areas as mine free if situation related ambiguity is prevailing. See some comments about performance measures in the chapter 7 dealing with the total concept.

4.1.6 Environmental constrain

The sensor system proposed by MOMS should be robust against all kind of weather conditions. The platform is supposed to be stable enough not to introduce limiting factors on sensors from a vibrational point of view.

4.1.7 End user requirements

Some requirements are:

- The results should be presented in such a way that they are valuable as a decision support to a commanding officer.
- The system should be able to operate under moderate risk of hostile activities.
- Suspected objects with estimated area of action should be presented in GIS.
- Ability to point out areas containing mines as well as areas not containing mines are essential.
- A decision support for selecting alternative routs.
- A priori knowledge is utilized e.g. in the form of threat library.

4.2 Phenomenologies

4.2.1 3-D shape

High resolution 3 D imaging is interesting because it has capability to see through vegetation and water. It utilizes utilize shape and texture signatures which are hard to get from a passive EO sensor. 3 D imaging has good capability for trip wires and on all surface lying objects but limited capability on buried mines although some potential could be explored to find some pattern in changes of the terrain height due to a mine filed.

Recent development in high resolution imaging laser radars [34] offers range resolution in the sub-cm level. In order to use range and shape information either for detection or for classification the pixel size as well as the range resolution should be in the cm or sub-cm level.

Important shape and texture features may be revealed by using range gated 2-D techniques or even better full 3-D information in each pixel. The range capability should make it possible to extract the target from the vegetation above and beside the mine. The difficulty will be to extract the mine from background and to determine the shape as being man made. Methods similar to those being developed for the DARPA program JIGSAW [35] might be used.

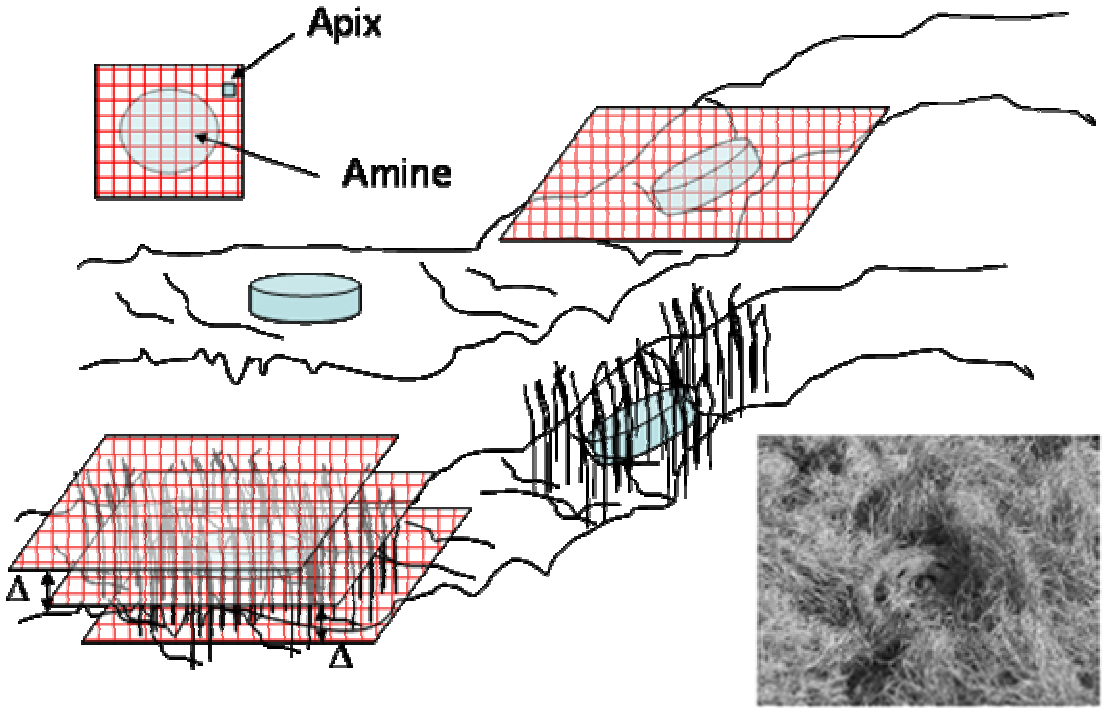

Figure 4-1. Illustration of the mine detection problem for bare mines and mines partly covered by grass. As the characteristic dimension of an AP mine is in the cm level we will demand a sensor resolution in the cm or sub cm region in all directions.

The mine might be covered or buried and then the high resolution range for classification will not work. Range resolution in combination with intensity imaging may be suitable for finding tracks or disturbances in the soil?

The range gated 3-D imaging with full resolution will be of high interest for tripwire detection.

The 3-D structures on the cm level of various terrain types and backgrounds are not easily found and have probably not been measured and systemized in detail. There exist more data with a range resolution of about 10 cm for terrain features relevant to vehicle detection and environmental mapping [36] and attempts to systemize those data [37] is under way.

The promising feature of 3-D range imaging looking for shape, instead of intensity only, is that, when presented in range coding, these images can have a very high “contrast” to background compared to passive EO imagery, where small reflection differences and shadows may make it difficult to detect targets. The absolute measurements of geometry by a high resolution laser radar will simplify classification.

Range accuracy and resolution for laser radars has been investigated by waveform simulation by Steinvall and Chevalier [38]. For angular non-resolved targets (1 D profiling) the analysis of the waveform offers the possibility of target recognition due to range profiling. For 2 D and 3 D imaging the angular and range resolution are the critical parameters for target recognition. In other applications, such as in lidar mapping, the range accuracy plays an important role for the performance. Figure 4-2 illustrate the complexity of the problem due to the different waveform shapes for different elevation angles for the case of one pixel covering the target scene. One pixel sampling for the whole mine is not the way to go, even if the range jumps in the waveform may give some indication of an object on ground.

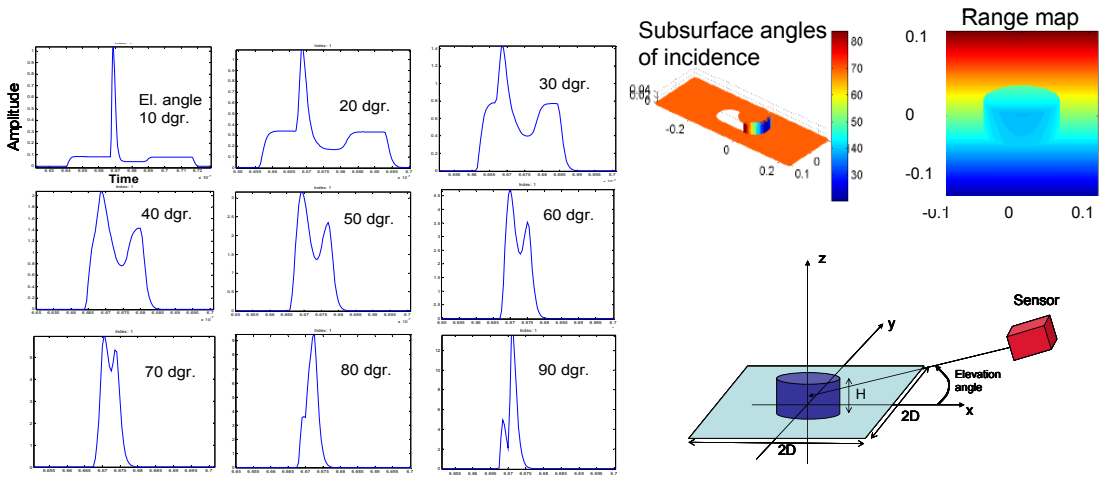

*Figure 4-2 Left: waveforms from different elevation angles for the one pixel covering the scene. Laser pulse length 3 units and cylinder height 4 units. The cylinder diameter is 10 and the bottom plate 20*20 units. Right above: range map and a map indicating the angle of incidence for different parts of the target scene. Right below: the target scene.*

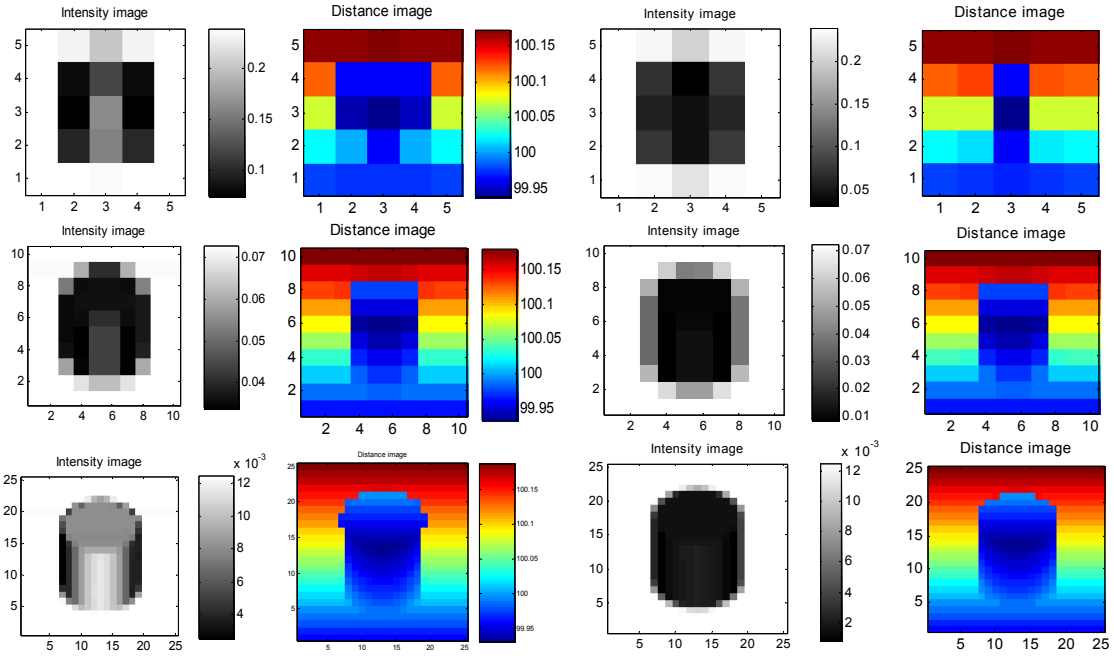

*Figure 4-3 Intensity and range images for different positional resolution (5*5, 10*10 and 25*25) pixels. Left: BRDF 1. Right: BRDF 3 (more glintlike) for the cylinder. For the definition of the BRDF's used in the simulation see [38].*

4.2.2 Retro reflection

In band retro reflections from optical sensors are very profound and easy to detect. Mines using optical sensors for target sensing can therefore be detected using this technology. Optics detection using retro reflection from optical sensor like sights and binoculars has been studied

in great detail at FOI and elsewhere. The capability to use scanning or flood illuminating laser beams to detect and pinpoint optical sights before weapon delivery is an attractive feature that could be combined with laser jamming.

The laser reflection signature from optical sensors is of high interest for laser radar because it enables warning, precision tracking target identification and a possibility to optimize the laser defeat procedure from a spectral and timing point of view. The reflection can be a surface reflection from the entrance optics or a retro reflection from a focal plane in the optics. The retro reflection laser radar cross section can be measured in units of m^2/sr and depends on the specular and diffuse reflection from the target optics focal plane, the focusing range, the target aperture, the target optics transmission, the detector collection angle, the target range and the laser wavelength.

4.2.3 Spectral

Visible and near infrared hyperspectral imaging. Detection of surface-laid landmines by classification of their visible/near infrared (VNIR - 400 to 1000 nm wavelength) spectral signatures. Near infrared imaging offers enhanced contrast against vegetation. Anomaly detection has proven its usefulness. Hyperspectral signatures for surface mines can have substantial variability due to the environmental conditions and subpixel mixing. Signatures are also affected by the condition of the mine. Shape detection might be useful for detection and classification of side-attack mines. Clutter suppression can be obtained by adaptive learning of features.

Short wave infrared (SWIR) hyperspectral imaging. There is a lack of availability of SWIR hyperspectral imagers. Preliminary indications are that a simple generic classification decision boundary should be able to distinguish surface-laid landmines from many human-made artifacts and natural materials in this spectral region.

Mid wave and long wave infrared spectral imaging. Contrasts observed due to fact that mines and/or the disturbed soil retain or release heat at a different rate than their surrounding. Detection is obtained by observing the area during natural temperature variations. Results are also heavily dependent on the environmental conditions. In particular, the effect of wetting and drying cycles has an influence on IR spectra possibly depending on a higher packing density of the particles following the wetting process. A better understanding of the spectral characteristics of soil in the mid-infrared spectral domain could provide improved interpretation of data retrieved from disturbed soils during hyperspectral imaging. IR images can also support sensors more suitable for classification. Hyperspectral imaging could possibly enhance the thermal sensitivity and also distinguish between temperature and spectrally distinct emissivity. Thermal imaging has day/night capability since it is the radiation emanating from the target that is detected.

Active reflectance imaging. Performs active imaging at key spectral wavelengths for improved detection and classification. It is possible to perform imaging in spectral regions that are not easily available in passive imaging. Active illumination gives also night capability at short wavelengths. Range gating is not necessary but gating is used for cutting down on influence of ambient radiation when needed. Uniform illumination is needed for good performance.

A large number of spectral signatures of mines and background are available in the literature. The difficulty is that the data often is collected during laboratory conditions and encompasses only a subset of the potential mines and background combinations which could be envisioned

in a real tactical situation. We will shortly exemplify with some results from recent papers mainly from the last 4 years of SPIE conferences on mine detection.

Coath and Richardson [39] give spectral data for the diffuse and specular reflections of four representative scatterable anti-personnel landmines ultra-violet, visible and infrared regions and compare this to potential backgrounds in which such anti-personnel mines are likely to be found. The mines were all made by polyethylene or polycarbonate and, with one exception, they were all used in recent conflicts. The comparative results were used to highlight the regions where a high contrast is exhibited between the mine and the background. According to the authors the spectral regions of particular interest, which exhibit tens of percent contrast, are shown to be in the near ultra-violet (UV A and UV B) and near infrared (IR A and IR B).

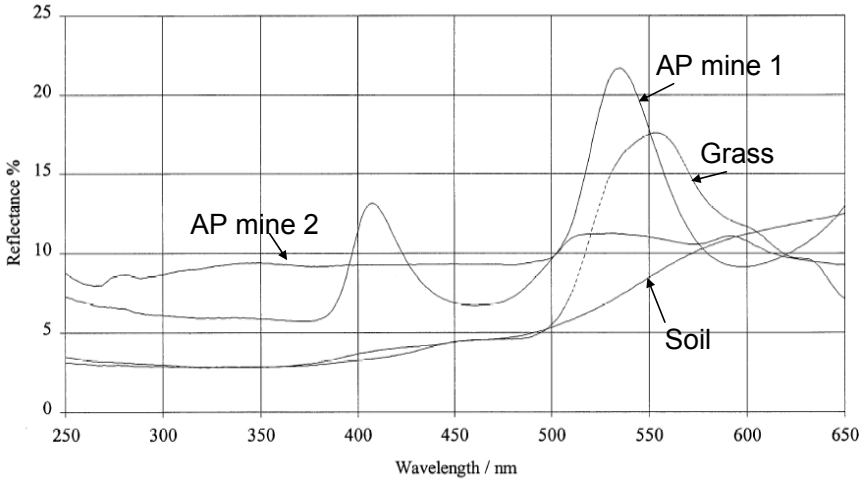

Figure 4-4. Example of reflectance from mines and backgrounds (total refection measured with an integrating sphere) in the UV and visible regions. From Coath and Richardson [39].

Figure 4-4 shows examples of total UV-reflection (integrated over all angles) some personal mines and backgrounds of grass and soil. The average reflectivity in the UV (250-400 nm) was 5-10 % for the six AP mines investigated and the average reflectivity for grass and soil was 2.8 % resulting in contrast (defined as the reflection difference divided by the reflection sum) between 30-50 %. The threshold detection contrast for the human eye is between 2-5 %.

Figure 4-5 shows the same for the IR region. Several wavelength bands will be of interest judging from these results. For example the 800-900 nm region suitable for laser diodes, the Nd:YAG laser wavelength 1.06 μm and also the eye safe wavelength region above 1.5 μm. In the NIR regions the mines can have both positive and negative contrast to the grass and soil backgrounds.

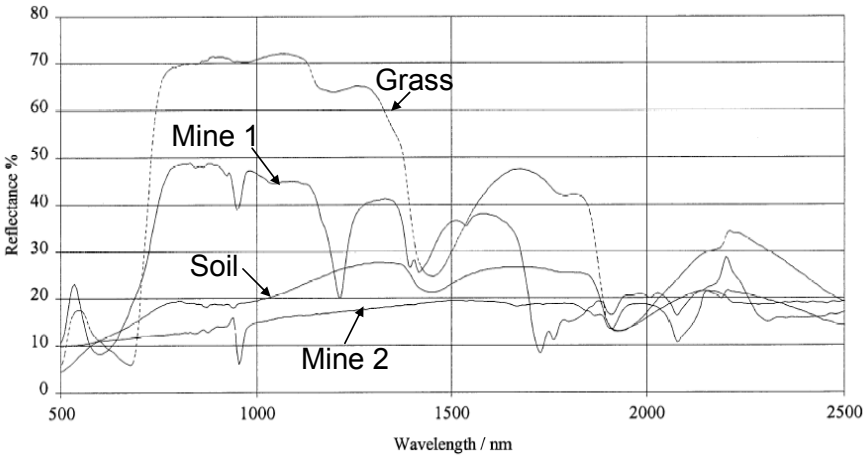

Figure 4-5. Example of reflectance from mines and backgrounds in the IR region. From Coath and Richardson [39].

Arie de Jong et al. from TNO [40] investigated active ground illumination to improve the detection performance of EO sensors compared to passive skylight illumination. Active illumination gives nigh time capability but also avoids the temporal variability of sky and sun radiation. Active sources can range from lasers to Xenon or halogen lamps. In the report results from a two-colour laser scanner (using 675 nm and 778 nm) with one wavelength in the chlorophyll absorption dip and from another active scanner operating at 4 wavebands between 1400 and 2300 nm, using tungsten halogen lamps were presented. A conventional TV camera with either a set of narrow band spectral filters or polarization filters in front of the lamps was also used. The targets consisted of an array of mixed objects, most of them real mines. The results showed great promise in enhancing the detection and identification probabilities of EO sensors against small surface targets.

The ratio between the reflection coefficients ρ_1 and ρ_2 in the chlorophyll dip at 675 nm and the near IR at 778 nm shows that all objects are greatly different from the grass background. So the primary use of rationing is for target detection: all non-vegetation objects are easily detected, of course also open soil, which is not taken in the table. The ratio $\rho 1/\rho 2$ shows however also that we can discriminate a few classes: values between 0.25 and 0.45, between 0.60 and 0.75 and around 1.00. Most objects fall into one of the three classes. It is noted however that not only the ratio between the two signals can be considered, but also the absolute signal level. The investigation also included active imaging at 1600 nm and 2200 nm. The source was a Xenon lamp which gave a rather limited SNR. However these wavelengths also show very good contrast between the objects and the grass.

According to de Jong, the experiments with the active multi-spectral sensors have shown the power of discrimination when using a variety of target and background features. It was clear that a combined sensor package is capable to provide near 100% detection probability for the 25 objects presented.

The data taken in those examples above are of course ideal in the sense that the mines and objects were uncovered. In reality the mines although laid on the surface will be partly or completely covered by dust and sand or by vegetation which makes spectral discrimination much harder. Maybe a water spray system or a flame-thrower in some cases would make sense to clear the mines from the background, if the tactical situation allows that.

Although the present MOMS study shall deal primarily with surface laid mines the spectral information of disturbed soil around buried mines are of course also of great interest for the

reason given above. Haskett et al. present the quantitative detection performance of buried mine reflectance signatures for various soils and burial durations [41, 42]. The spectral signatures (extending from 0.35 to 2.5 μm, for the entire region there were 1512 channels prior to interpolation) of mines buried with different durations were examined. The statistical analysis of the signatures including the distributions representing class separation between mines and background was performed. Statistical analysis and quantitative performance of mines buried in various soils and burial durations indicate that the more the disturbed soil (over the mines), the more difference the signatures between the disturbed soil and the background, hence the performance benefits; the longer the buried time, the less different the signatures between the disturbed soil and the background, hence the performance suffers. In short, the physics of soil disturbance using the hyper spectral sensing hold -- the physical disturbance of the soil results in a phenomenon that was detectable by hyper spectral sensing. Haskett et al. also investigated the spectral properties in the 3-5 and 8-12 μm region using 425 bands in 3-5 μm, 130 bands in 8-12 μm regions [42]. Those wavelength bands did not give as good performance as the shorter bands.

The short wave IR region (SWIR, 1-2.5 μm) gives high reflection for grass and thus often enables better detection potential for green mines and for obstacles compared with the visual wavelengths. Both these wavelength regions should however be uses in a real system using the benefit form of data fusion. This is discussed by Wolff et al. [43], see Figure 4-6.

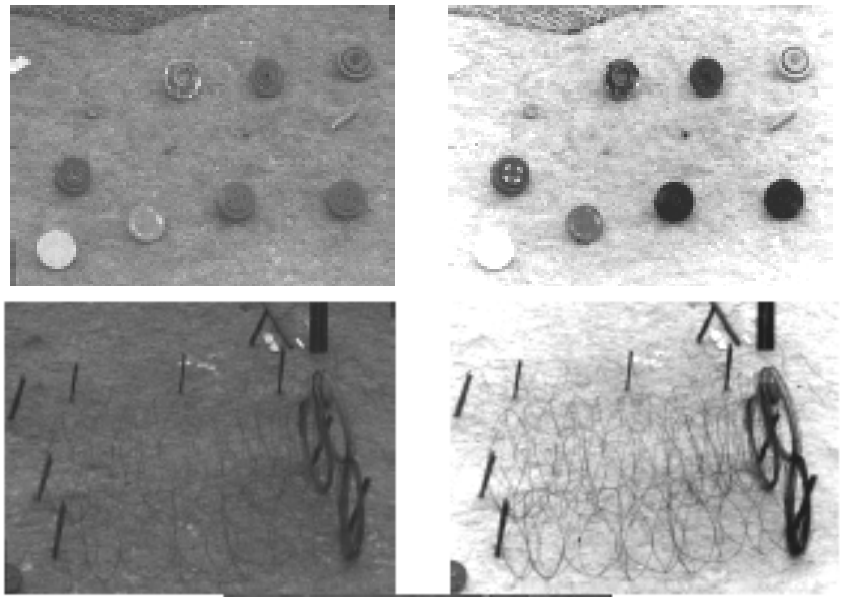

Figure 4-6. Example of visible and sort wave IR (SWIR) images of mines and obstacles against grass. From Wolff et al. [43].

An interesting work which combines the NIR and visual bands for mine detection is given by Crosby et al. [44, 45] in two papers. A multi-spectral wavelength tuneable camera was flight-tested using optimized wavelength combinations which were found using field test data over a variety of backgrounds and altitudes. The wavelength combinations (Enhanced Band Sets) in Table 4.1 were found to be of interest for the test area (beach with sand and vegetation). The findings points out the advantage of an adaptive wavelength tuneable system for both active and passive spectral discrimination. Example of ROC curves are given in Figure 4-7.

	Dry Sand	Sand/Grass	Vegetation	Wet Sand
Enhanced Band Set	406, 450, 867	435, 731, 671	447, 584, 879	385, 533, 855

Table 4.1. The (Enhanced Band Sets) found valid for finding mines in a beach environment. From Crosby et al. [44]

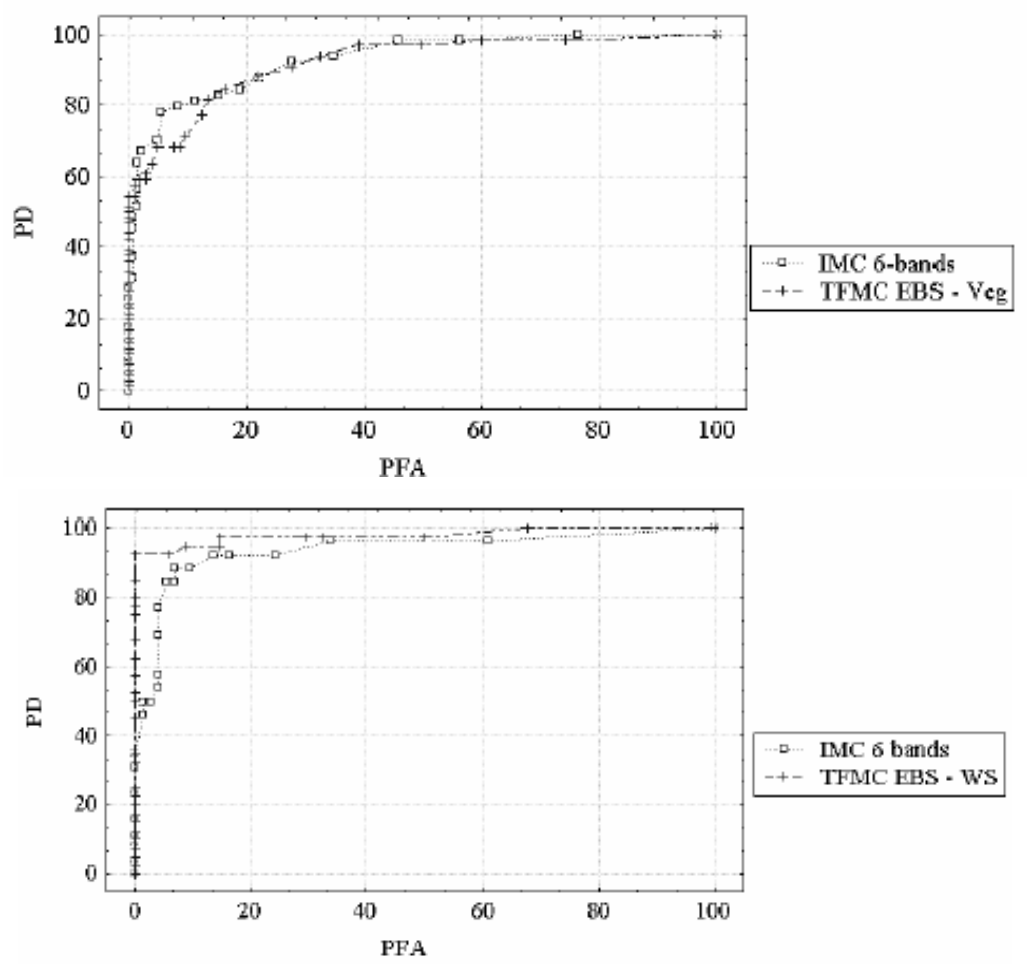

Figure 4-7. Example of ROC curves comparing a six wavelength spectrometer and a three band optimally selected band camera (TFMC) over a grass only (above) and a sand/grass site (below). From Crosby et al. [44]. Passive multi-spectral cameras were used.

Snow is a background which has to be taken into account although there seem to be rather few investigations relevant to mine detection, both from an active and passive point of view. The spectral properties of snow are presented in the IR and EO handbook [46] and references therein. One example of a spectral reflectance is shown in Figure 4-8. While the reflectance at shorter wavelengths (visible to 1.2 μm) is high, the reflectance at the important wavelength 1.5 μm is just a few %. The exact value strongly depends on the age, structure and water content of the snow. As we have not seen very much published on snow reflection related to laser radar we decided to look a little more in detail on snow reflection incorporating different kinds of snow and also the angular reflection properties.

Figure 4-9 shows an example of a 1.5 μm reflection image of the snow covered ground. Due to the low reflectance from the snow objects like buildings, containers and trees stand out

quite clearly. Note how clear the car tracks are seen due to the change in reflection of about a factor 3 in this example. Also shown in Figure 4-9 is another interesting example where the snow has melted so that grass and asphalt is breaking through the snow cover. The temperature was around 0 C° and we can see how the structure of the road is much more evident in the laser reflection mode than in the colour CCD image. Also note the snow patch on the garbage container for example as well as well as the small parts of grass that are popping up here and there giving a clear reflection that is considerably stronger than that of the snow.

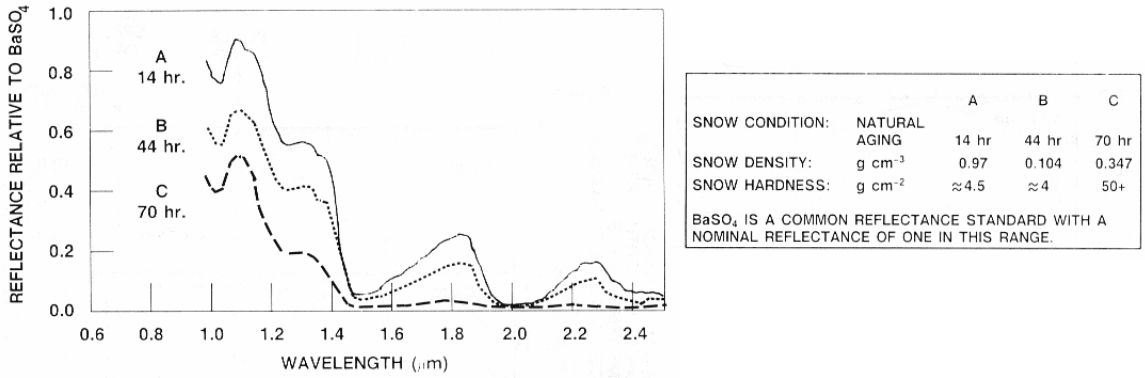

Figure 4-8. Changes in snow spectral reflectance with age. From [46].

The very low reflection at 1.5 µm for snow and water should give very good contrast to bare mines, (maybe even for white painted) in snow and in wet surroundings.

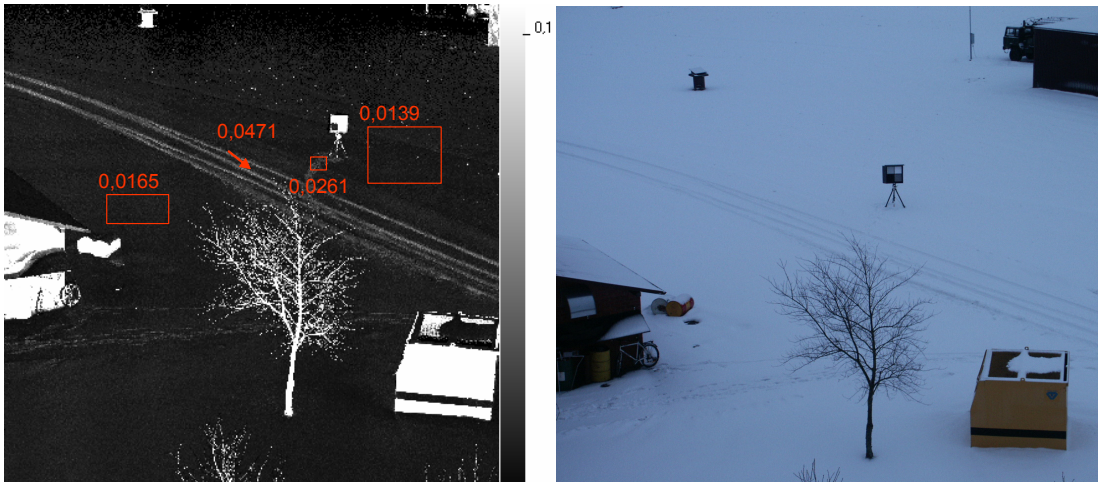

Figure 4-9. Example of snow reflection on the ground outside our laboratory measured with the laser scanner at 1.5 µm. Example of reflection values are shown. The dark section of the reference target has a calibrated value of 1,7 % at 1.5 µm. Date 040112 , time 10.08 a.m. – fresh snow, a couple of hours old. The temperature +2 ℃ and relative humidity > 95 %. From [47]

For mines in water the capability to detect them with lasers depends much on the beam attenuation and backscatter amount. For scanning laser radars (lidars) FOI has made a substantial work on charting and on large object detection [48] at depths down to 20-30

meters but also on the detection of mines and mine like objects [49]. We have also reviewed the work on imaging laser radar systems.

The mines in water conditions of interest for MOMS are mines on the beach and in the surf zone as well as mines on river lets, and ponds etc. of relevance for army operations. By experience a laser system can detect objects at depths which are many times larger than the visibility depth (Secchi disc depth). For real turbid water however very short laser pulses and fast camera/detector systems are needed to reject backscatter.

The objective of the Office of Naval Research (ONR) project's LAMBS (Littoral Assessment of Mine Burial Signatures) effort is to determine if electro-optical spectral discriminants exist that are useful for the detection of land mines in littoral regions. Statistically significant buried mine overburden and background signature data were collected over a wide spectral range (0.35 to 14 μm) to identify robust spectral features that might serve as discriminants for new airborne sensor concepts. LAMBS has expanded previously collected databases to littoral areas – primarily dry and wet sandy soils – where tidal, surf, and wind conditions can severely modify spectral signatures

The surf zone is a challenging environment for conducting mine countermeasures operations. The performance of acoustic sensors in this environment is extremely limited. Airborne lidar sensors have significantly better prospects for successfully working in this environment. However, the complex environment will be a driving factor limiting their performance. Breaking surf action causes bottom sediment resuspension and the formation of bubbles and foam. The resuspended sediments then begin the process of settling, while the bubbles and foam begin to dissipate. All of these phenomena influence the optical properties of the water, which, in turn, have an impact on the performance of the lidar system. Strand et al. [50] have found that that the optical properties in the surf zone can be remarkably patchy and spiky in space and time. Turbidity variations by a factor of >3 in 2-3 hour intervals were common. Isolated breaking events typically had an impact for time intervals approaching 1 minute before settling back to baseline behaviours. The performance limitations by foam form braking waves can be reduced by multiple looks at time intervals longer than those of a wave break.

For the other water conditions in river lets and ponds relevant for army operations, there is probably few data available on water turbidity and backscatter. That is an area which may need investigation.

4.2.4 Angular reflection properties

Surface scattering of optical radiation is described in many textbooks e.g. [51]. An excellent introduction to surface scattering is written by Bennett and Mattsson [52]. Target and atmospheric effects on laser radars are also summarized in a FOA report [53].

Most of the data presented so far has either been relevant for total reflection or for backscatter reflection from mines and backgrounds. For passive systems using the sun as an illuminator the bidirectional scattering is important and bi-static systems may also be of interest for laser systems. An airborne laser could act as an artificial sun and illuminate an area where detectors and cameras could be placed on vehicles or on other airborne platforms.

The angular reflectance from a surface is described by the bi-directional reflection distribution function (BRDF).The monostatic backscatter relevant for laser systems may be modelled as [54]:

$$BRDF = BRDF_{spec} + BRDF_{diff} = \frac{A}{\cos^6(\theta)} \exp(-\tan^2(\theta)/s^2) + B\cos^m(\theta) \quad (1)$$

$BRDF_{spec}$ and $BRDF_{diff}$ represent the specular and diffuse components, s is the surface slope and θ is the angle of incidence and reflection, see Figure 4-10. We have found that the BRDF's of many different types of surfaces can be fitted by this expression.

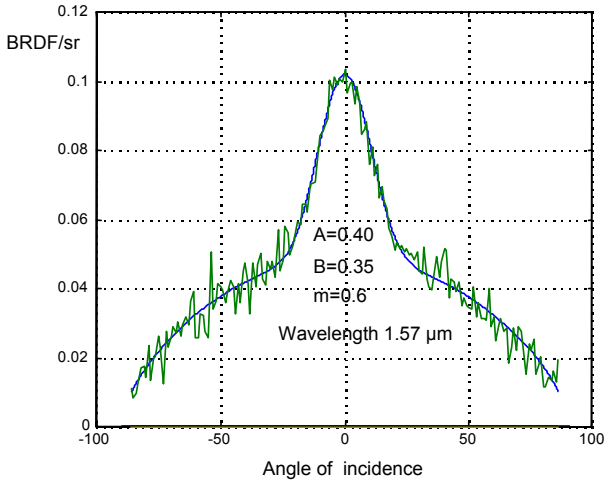

Figure 4-10. Measured and fitted monostatic BRDF using Eq. (1) for a rough surface. Laser wavelength 1.57 µm. The rms of the surface height is 2.13 µm and the rms value of the surface slope is 0.2958.

Typical for military target surface reflections is the specular behaviour for longer wavelengths (wavelength > 2-3 times the rms surface height). This in combination with a high total reflection will pinpoint targets with curved surfaces, wires, poles etc. A very modest assumption must be that mines and mine like objects have a different BRDF characteristics compared with that from the natural background, maybe with water as an exception. It will therefore be of interest to study multiple look or bi-static configurations for laser assisted detection systems.

Derzko et al. [55] measured the absolute reflectance of a large number of landmines using a single-mode laser diode operating at approximately 814 nm, Figure 4-11. Approximately thirty different anti-tank (AT) and anti-personnel (AP) mines were irradiated with a highly polarized laser beam configured in a monostatic geometric arrangement. The in-plane (p) and out-of-plane (s) linear polarization components were measured as a function of incidence angle of the transmitted laser energy.

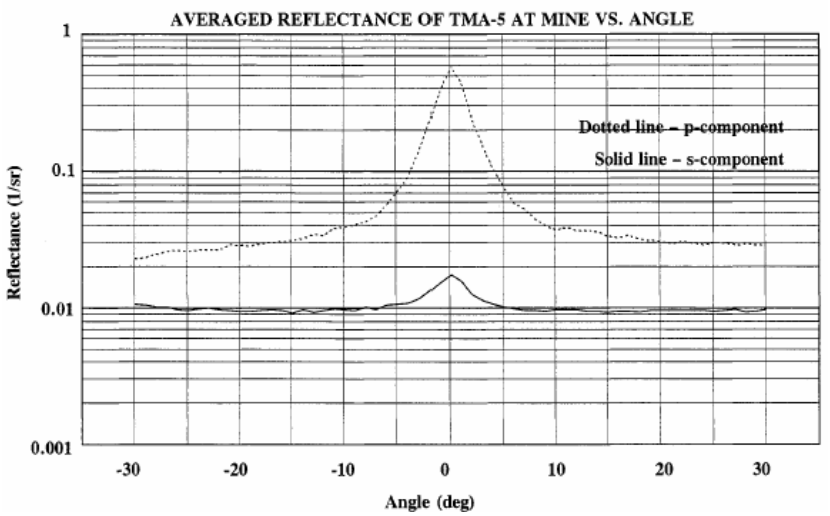

Figure 4-11. Plot of the Averaged Reflectance of a TMA-5 Anti-tank Mine vs. Angle. From Derzko et al. [55].

In some cases, the initial contact will not be with the mine but will be with the trip wire that activates the mine. This case is particularity true for off-road anti-vehicle and wide-area, shrapnel anti-personnel mines. Without an effective method of detecting these tripwire-activated mines, the costly, high technology sensor will be destroyed prior to its use. Because of their small size, tripwires are difficult to observe in their operational environment. One way to enhance their detectibility is to find a wavelength region where the contrast between the tripwire and the background is a maximum. The UV/VIS/SWIR reflectance spectra of various tripwires and natural backgrounds [56]are shown in Figure 4-12. The bold coloured lines represent natural backgrounds and the thin lines are data from representative tripwires. The spectra show the lack of contrast between tripwires and backgrounds in both the ultraviolet and visible regions. Therefore, these wavelength regions would not be good candidates for tripwire detection. For the studied samples, the greatest contrast occurs for wavelengths greater than 700 nm.

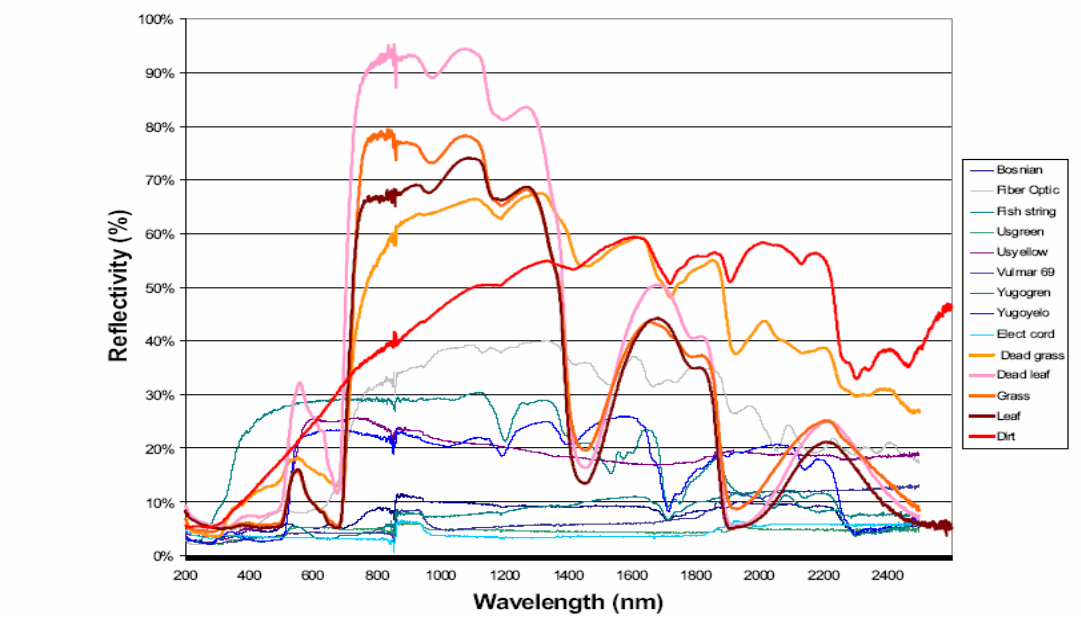

Figure 4-12. Reflectance spectra of trip wires and natural backgrounds from 0.2 to 2.5 µm, from[56]. The reference unfortunately is sparse on information about the angular reflection properties of the wires.

4.2.5 Temporal

To combine image information from sensors captured at different times and at different locations with a moving platform raises a high demand for implementing and developing algorithms for motion compensation and matching the signals from the different sensors to each other and to the ground. Good navigation data are required in order not to be depending on image content for the coregistration of sensor data.

IR Temporal processing uses apparent temperature variation for objects and background to detect meaningful features, see Figure 4-13 and Figure 4-14 for example of diurnal IR variation of an AT-mine buried in a gravel road.

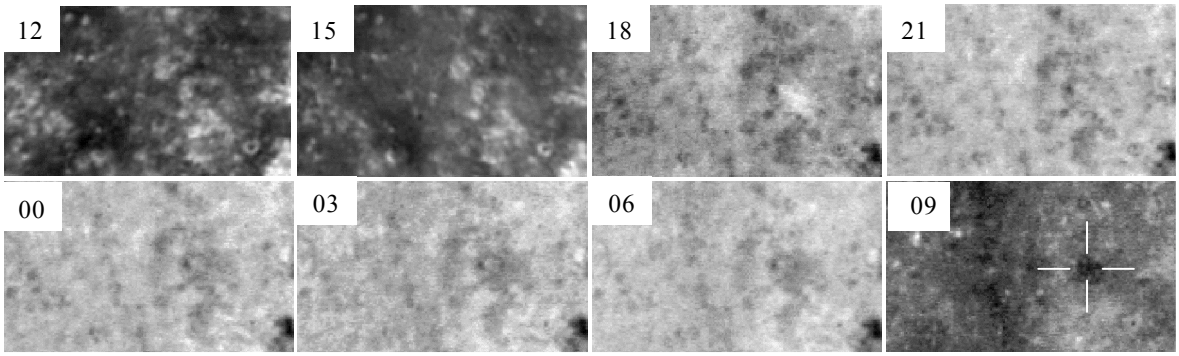

Figure 4-13. IR-images of a gravel road with a buried AT-mine captured at different times of the day, 12 is at noon and 00 is at midnight. In the 09-image the position of the mine is marked. The bottom of the mine is at 29 cm depth and the top of the mine is at about 20 cm depth. Registrations are made two and a half year after burial, from [57]. The images are automatically scaled.

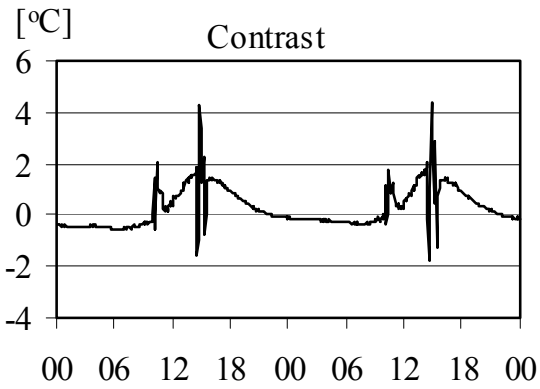

Figure 4-14 Diurnal contrast variation of the AT mine in Figure 4-13.

In order to use IR images for classification of objects it is a great advantage to have a reliable model of temporal behaviour of different objects of interest. In Figure 4-15 and [58-60] , the FOI method used in earlier projects is presented The method can be used in MOMS as a prediction tool for IR signatures. Repetitive registrations of IR images in order to get a more elaborate model will probably not be a standard mode in MOMS. For MOMS application a

model based prediction of IR signature has to be compared with an IR image captured at times given by other priorities than achieving optimal IR signatures for objects of interest.

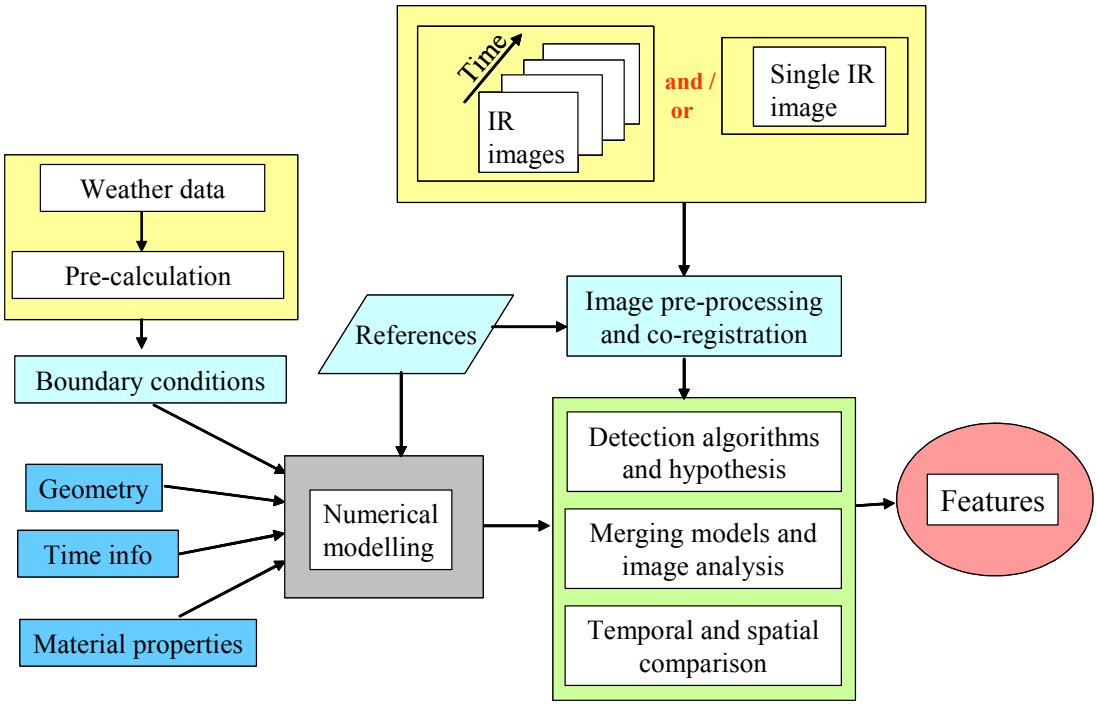

Figure 4-15. Data flow for the model based diurnal temperatures

All images are recalculated before the analysis with parameters for atmospheric compensation. The purpose is to achieve a better estimation of surface temperature from the IR-images. This is important for increasing correspondence between temperatures estimated from the images with results from the physics-based model. Also a procedure during the flights is proposed where IR images of temperature reference markers are recorded from operational heights. This procedure is necessary to increase the correspondence between the diurnal based modelling results and the collected IR images. Change detection is an important application of repetitive image registrations utilizing temporal information. The intention is to detect presence of new or absence of old objects rather than using diurnal variations as a tool for feature extraction. In order to be able to coregister image data from repetitive acquisition of data, a terrain model is needed.

4.2.6 Spatial

For objects at infinity, the F-number (F/#) is defined as the ratio between focal length and the diameter of the aperture stop (normally the diameter of the optics), [61]. From a sensor specification point of view, there is a trade off between aperture, field of view and aberrations. Small F/# (large aperture) and large field of view leads to a high amount of radiation reaching the detector. In addition, a smaller F/# will give a better ability to form a point image. But the disadvantage is that aberrations get worse. A standard criterion for detection is the Johnson criterion [62]. According to this criterion, one line pair is needed across the minimum dimension of the object. For a CCD camera this criterion is converted to a demand of two pixels across the minimum dimension of the object. For MOMS applications there is an important design trade off between spatial resolution and demand for real time performance of the system.

4.2.7 Polarization

Polarimetry is the analysis of the polarizartion state of scattered radiation from a surface either narural or artificial. Polarimetric imaging is an interesting approach for detection of non-buried objects in the presence of grass and other types of clutter. Polarimetric signatures of various landmines and other target classes are present both in the visible and infrared wavebands as well as in the infrared spectral region. In the thermal infrared, the surface radiates polarized radiation with properties depending on the detailed geometry. In the SWIR spectral region, a polarised illuminator and cameras fitted with SWIR filters and polarizers could be useful. Different polarization properties are being measured in the passive and in the active mode depending on both the scattering properties of the target surface and the polarization state of the illumination. Degree of surface scatter to bulk scatter is an important depolarization mechanism. The usefulness of circular polarized radiation as a feature is not well known.

Laser polarimetry, the analysis of the polarization state of a backscattered laser radiation, is a valuable tool in distinguishing different surfaces from each other and to gain information about a specific surface. In remote sensing the polarization has been used to provide information about for example plants, soil, sand, minerals, snow, ice and cloud properties.

The amount of depolarization is to a large extent depending on the diffusivity of a surface, meaning that multiple scattering results in diffuse refection which is depolarized while the specular component is not. Passive EO sensors can measure depolarization using the unpolarized sun as a source, the effect is usually hard to control as it depends on the angle between the position of the sun and the direction of observation. Laser polarimetry on the other hand has a larger potential for gaining target information because it is independent of natural illumination, and can provide the full Mueller matrix by changing both the emitted and the received polarization states. The Stokes vector S is defined by [63]:

$$S = \begin{pmatrix} I \\ Q \\ U \\ V \end{pmatrix}$$

with

$$I = \left\langle E_x E_x^{\,*} + E_y E_y^{\,*} \right\rangle$$

$$Q = \left\langle E_x E_x^{\,*} - E_y E_y^{\,*} \right\rangle$$

$$U = \left\langle E_x E_y^{\,*} + E_y E_x^{\,*} \right\rangle$$

$$V = j\left\langle E_x E_y^{\,*} - E_y E_x^{\,*} \right\rangle$$

where $E_{x(y)}$ are electrical field components along the x(y)-axis. The propagation is along the z-axis. The total intensity is I, Q is the amount of linear polarization (horizontal or vertical). U is the amount of linear polarization + 45 or –45 degrees in relation to x-axis. V is the amount of right or left-hand circular polarization.

Relatively few values of depolarization measured by laser radar are found in the literature. Concerning backgrounds Karlshoven et al. [64] measured the depolarization D_p of crops to monitor plant conditions. D_p is defined as:

$$D_p = P\perp / P\|$$

where $P_\perp$ ($P_\|$) is the amplitude of the perpendicular (parallel) backscatter polarization vector. Using an angle of incidence of approx. 65 degrees, they found D_p = 0.55-0.85 for crop using 532 or 1064 nm wavelength. This corresponds to P_{dpol} = 0.45-0.80, a rather high value. Breugnot [63] reported values for $P_{dpol} \approx$ 0.10-0.35 for wood, 0.10-0.30 for stone, steel and painted plastic ≈ 0.85.

Zallat and Stoll [65] investigate the polarization from natural soils using 10.6 μm wavelength. Their data seem to indicate large effects for scattering angles larger than the angle of incidence but not so pronounced effects in the backscatter direction.

For mines and mine like objects Derzko et al. [55] have made an interesting investigation as mentioned above. For this laboratory experiment, real landmines were positioned horizontally with provisions for tilting them at known angles from the vertical in order to measure their absolute reflectance at a specific laser wavelength. They use a metric referred to as "degree of polarization", which is defined as:

$$P = (r_p - r_s)/(r_p + r_s) \quad (2)$$

where r_p is the absolute reflectance of the in-plane (p) component and r_s is the absolute reflectance of the out-of-plane (s) component. This degree of polarization is presented for 0 degrees only. Their measurements of the polarization components of the reflectance of common materials like grass, asphalt, gravel and dirt are tabulated in [55] for comparison with the mine data.

Figure 4-16 is a plot of the degree of polarization versus the out-of-plane (s) component of reflectance for all the mines & clutter objects. The degree of polarization parameter tends towards one for reflectance returns that maintain a high value of r_p to r_s, and tends to zero for returns that show "depolarization", i.e. r_p approximately the same as r_s. It is apparent that almost all of the landmines have a substantially higher value of *P* than the clutter objects, reiterating the earlier assertion that "man-made" objects tend to "depolarize" less than natural ones.

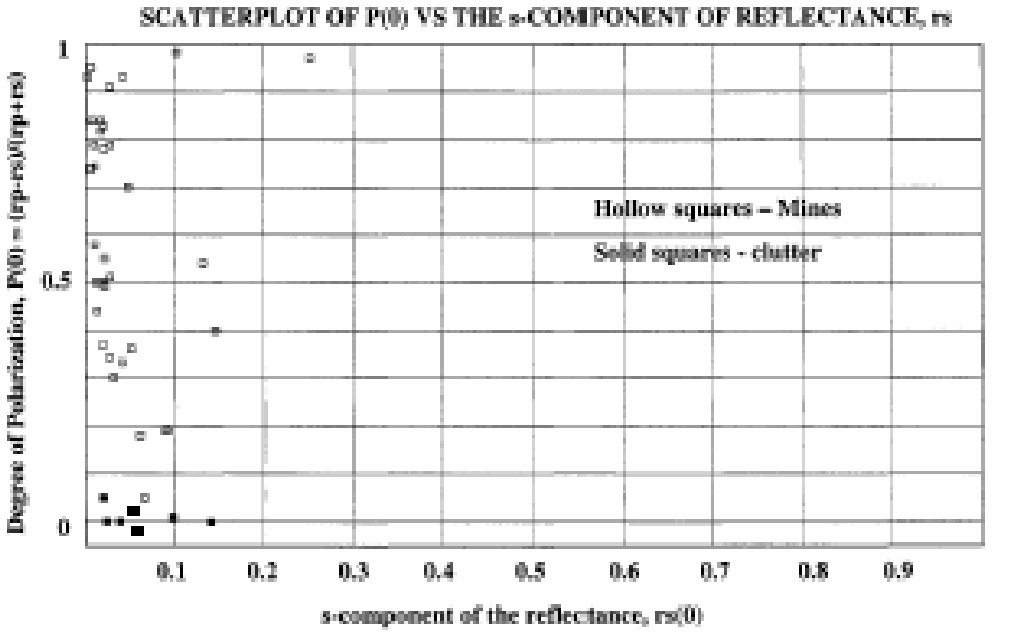

Figure 4-16. Scatterplot of the Degree of Polarization, P(0") vs. the cross-plane (s) Component of reflectance. From Derzko et al. [55].

Haskett et al. [66] quantifies the overall detection performance for laser based polarization detection of landmines in various background and solar conditions. Specifically, for comparison purposes, this paper quantifies the detection performance based on the RX detection algorithm [67] RX implementation as a correlation operator, and intensity thresholding approach using airborne laser imagery. This paper includes generated receiver operating characteristic (ROC) curves with and without man-made objects to access the effect of the man-made objects based on these algorithms. One example of ROC curves are shown in Figure 4-17. Some of the conclusions in this paper were:

- Man-made clutter seems to have minimum effect, statistically, on the performance based on the used algorithms.
- Additional analysis needs to be performed to determine the mine detection operation point for optimal mine-field detection performance. However, this might be considered sufficient enough for the mine performance bound in the airborne system to obtain acceptable minefield detection. Mine detection performance can also be improved with a higher quality sensor, for example, higher laser power, and nadir reference.
- In general, performance seems to be worse in the high sun than low sun scenarios across the implemented algorithms in the report.

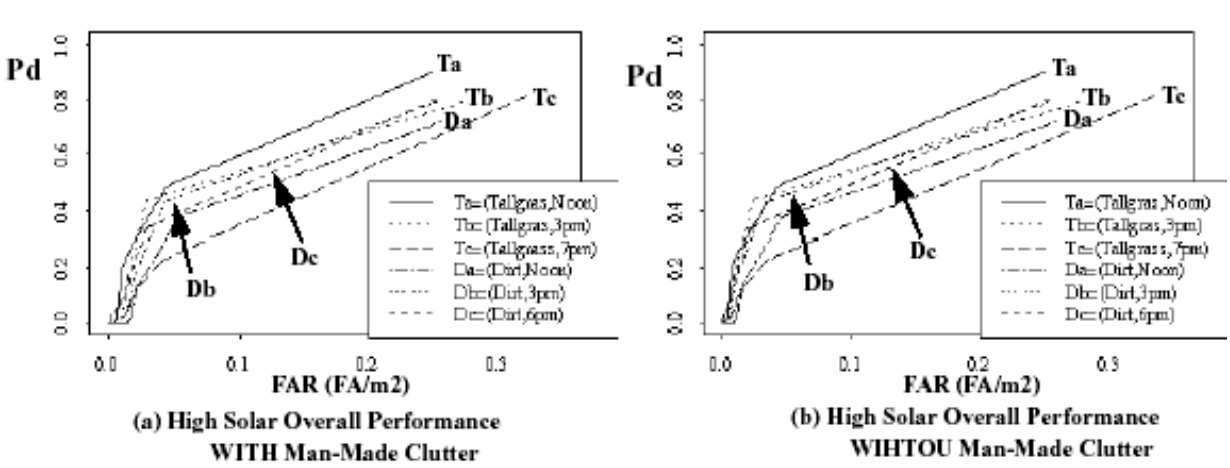

Figure 4-17. High Solar, 808 nm Laser Overall Performance of using P Polarization, see Haskett et al. [66] Note that the FAR (false alarm rate) is written in /m^2.

In another paper Haskett et al. [68] used the same data base as above and showed that the class separability between mines and backgrounds remains similar for the low and high solar angles. This seems to indicate that different solar angles do not effect the class separability between mines and backgrounds. P polarization alone seem to be sufficient as other polarization statistics such as S, P-S, or DoP contribute little or nothing to intensity count and class separability for this data set. This may be due to limited specular returns for mines as the nadir look preference was not precisely achieved due to aircraft roll, pitch and yaw.

There are also a great number of papers dealing with polarimetry for mine detection using passive EO sensing. W. de Jong, et al. [69] used IR and visual cameras with polarisation filters to study detection and mine classification. The detection performance was evaluated with ROC curves. It was shown that, for higher detection rates, classifiers based on polarisation features perform better than classifiers based on the intensity cue only. A

combination of both gave the best overall performance for the scenes considered. The infrared camera outperformed the visual light camera in the difficult scene. In another paper [70] the same authors presented a simple model of infrared polarisation .This model predicts the radiation due to reflection and emission from a perfectly smooth surface under a number of assumptions. This model shows that if the source illuminating the target has a different temperature than the target, the irradiation is partly polarised.

All polarization modelling efforts have mainly been devoted to passive EO detection. Sendur et al. [71] developed a model of scattering from randomly rough surfaces, e.g. mines and natural surfaces. A second order small perturbation method/small slope approximation (SPM/SSA) formulation for the rough-surface scattering problem was used. Emissivities seen by both polarized and unpolarized sensors were studied for smooth and rough surfaces.

Another polarisation model is presented by B. A. Baertlein and J. T. Johnson [72]. The model simulates high-resolution images formed from Stokes parameters that describe thermal emission and reflection of sunlight and skylight. The intensity image in Figure 4-18 (from [72]) shows a maximum on the sunlit vertical face, which is due to a combination of reflected sunlight and thermal emission, both of which are driven by solar illumination. In the shadow region, the image intensity is low, and multiple interaction terms (not included here) assume greater importance. The Q image (Figure 4-18 (b)) shows a peak depolarization on the sunlit face, which is primarily due to thermal effects. There is also a region of decreased Q along the edge of the top surface. This region is due to a combination of positive Q from the sky radiance offset by a negative Q from the thermal radiance. The U image (Figure 4-18 (c)) shows an anti-symmetric behaviour due to the solar and sky components. The authors found that these images were in good qualitative agreement with experimental images presented elsewhere.

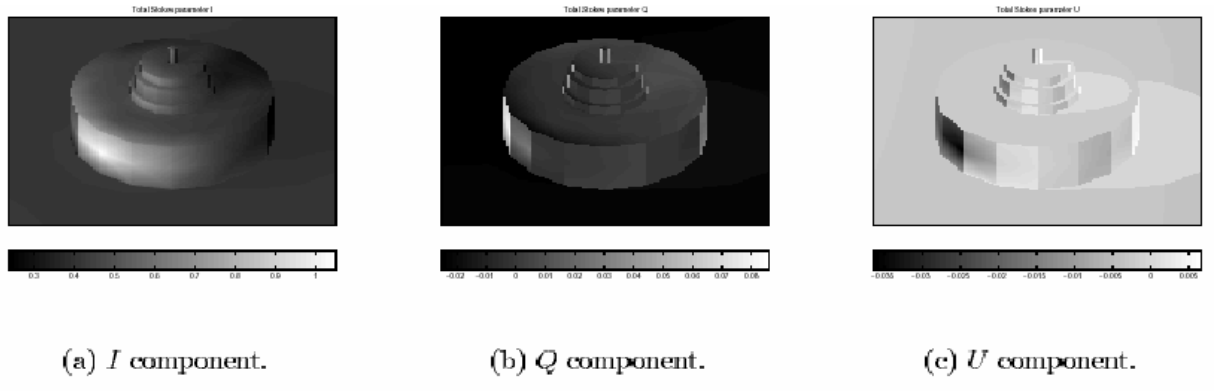

Figure 4-18. Stokes components due to all sources. The total intensity is I. Q is the amount of linear polarization (horizontal or vertical). U is the amount of linear polarization + 45 or –45 degrees in relation to x-axis. From [72].

Williams et al. use another metric than the conventional Degree of Linear Polarisation, DoLP [73]. It has not been found to be the best metric, for several reasons, one of them being that one of the polarisation components (let's say S2) often has a low SNR and if DoLP is thresholded, the majority of false detections will be due to spurious non-zero S2 rather than S1 values. The separability measure used by Williams et al. was instead chosen as the Bhattacharyya distance, a standard metric for the separability of probability distributions.

At FOI work on passive polarisation in the IR region [74, 75] has been studied for covered, non covered mines and trip wires with limited success maybe due to shortcoming in the used equipment.

Polarimetry both in the passive and active mode has been shown to give promising performance in detection of tripwires [56, 76-78]. Few range resolved 3-D laser radar data exist on the tripwire detection problem.

4.2.8 Fluorescence

Fluorescense is characterized by the phenomenon that an object that absorbs light of a certain wavelength emits light of a longer wavelength. This is due to excitation of a molecule from a ground state to a higher (excited) state followed by a deactivation process through intermediate energy levels [79]. Information can be retrieved from the excitation/emission steady state spectra, Figure 4-19, life time fluorescence spectra, Figure 4-20, and long time variation of fluorescence spectra of organic materials depending on natural changes or environmental stress [80].

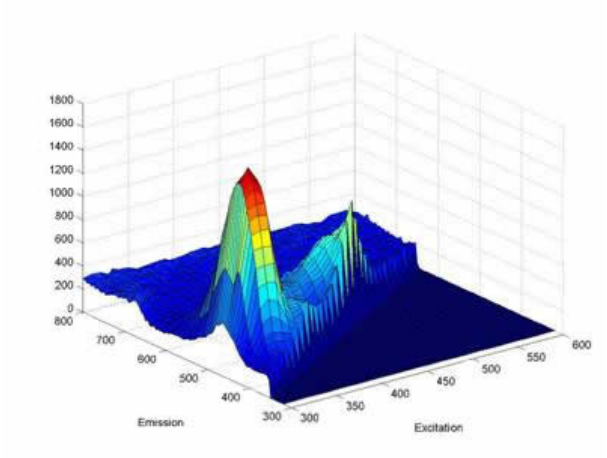

Figure 4-19 Example of Emission-Excitation spectra, from [81]

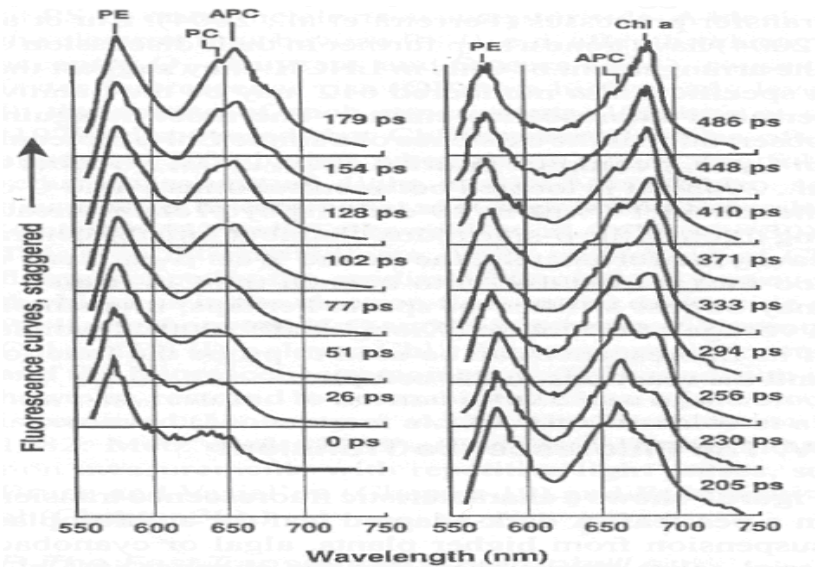

Figure 4-20. Examples of short time emission spectra 0 to 486 ps after excitation with a 6 ps pulse at 540 nm, from [82].

There are a wide variety of applications of fluorimetry, e.g. monitoring of metabolic processes in plants in order to describe and understand photosynthesis and how it is influenced by

different stress factors [82], detection of harmful agents or environmental threats [83], ecological monitoring of land and sea, detection of minerals, archaeology, medicine, forensics, combustion analysis [84], detection of landmines [85], fungal growth [86]. At FOI, department of laser systems, development of a laser system for biological sensing is performed [87].

Different light sources can be used for fluorescence measurements, e.g. arc lamps, (compact arc lamps, Xenon lamps, Mercury-Xenon Lamps, Tungsten Lamps) and lasers. Passive satellite and airborne fluorescence measurements can be made at wavelengths where the solar spectrum is attenuated in the solar or terrestrial atmosphere (Fraunhofer lines). Attenuation in the solar atmosphere at 656 nm due to hydrogen gas and attenuation in the terrestrial atmosphere at 687 nm and 760 nm due to oxygen gas are some examples. Passive fluorescence daytime measurements at those wavelengths will have a higher S/N ratio compared to other wavelengths because a large portion of the detected radiation will be fluorescence radiation and not reflected. If 24 hour capacity is a demand for MOMS application, an active light source combined with detector sensitive for radiation in Fraunhofer lines could be a concept to consider. Fluorescence from vegetation is strong and easy to detect. Excitation can be performed both in the ultraviolet spectral region as well as in the visible wavelength region. The main emission is in the near infrared. The operational potential to use fluorescence for detection is not yet clear. The system has to be optimized for the specific task.

Laser induced fluorescence (LIF) is an important tool in medicine, remote sensing [88] and other applications for detecting and quantifying constituents and contaminants in the atmosphere and in the hydrosphere. Fluorescence contrasts in mine detection may be manifested by either lack of signal or specific emitted fluorescence for the mine itself or from the disturbed soil or vapour released from the mine. The fluorescence signal from vegetation is well investigated and emanates primarily form chlorophyll.

Fluorescence of vegetation has been investigated for many years monitoring different pigments and environmental stress on plants. Chlorophyll *in vivo* has main fluorescence peaks between 670 and 750 nm. As a result of partial overlap of a chlorophyll absorption band and the 685 nm fluorescence peaks, the intensity ratio I(685)/I(740) is depending on fluorescence re-absorption which in turn is chlorophyll-concentration dependent. Thus long term stress on green plants can be monitored as a higher I(685)/I(740) ratio as a result of lowered chlorophyll concentration [89]. This is illustrated in Figure 4-21, where the images were recorded using an image intensified CCD-camera.

Hoge et al. [90] showed that airborne lidar (AOL, NASA) could be used to monitor fluorescence of vegetation using a 3 MW pulsed frequency doubled Nd:YAG laser at 532 nm, and a XeCl laser at 422 nm from an altitude of 150 m. Using the laser data from the AOL we can estimate the fluorescence efficiencies for 2-3 μm oil films to be 10^{-3} to 10^{-1} $\mu m^{-1}sr^{-1}$. We used the NASA:s AOL lidar data [90] for terrain fluorescence to estimate the efficiency F to be in the range 10^{-5} to 10^{-6} using blue excitation at 422 nm. If a UV excitation had been used we would expect a factor of 2 higher values. The yield from sun-excited florescence measured at Fraunhofer lines in the sun spectrum, the so called FLD (Fraunhofer line detection), seem to be in the range 10^{-3} for steady state and the broad spectral excitation caused by the sun light [91].

Recently other groups[92-94] have investigated vegetation fluorescence using imaging and spectral methods. They generally show that using information from both the blue-green fluorescence ($\lambda <$ 650 nm) and the red fluorescence ($\lambda >$ 650 nm) give much information about composition and status of plants.

Atmospheric laser fluorescence has been in use for remote sensing a long time [65]. Recently fluorescence has shown to be of interest for sensing of bio-aerosols [95, 96]. Furthermore, laser paints [96] and laser dyes [97] are discussed as markers for search and rescue systems.

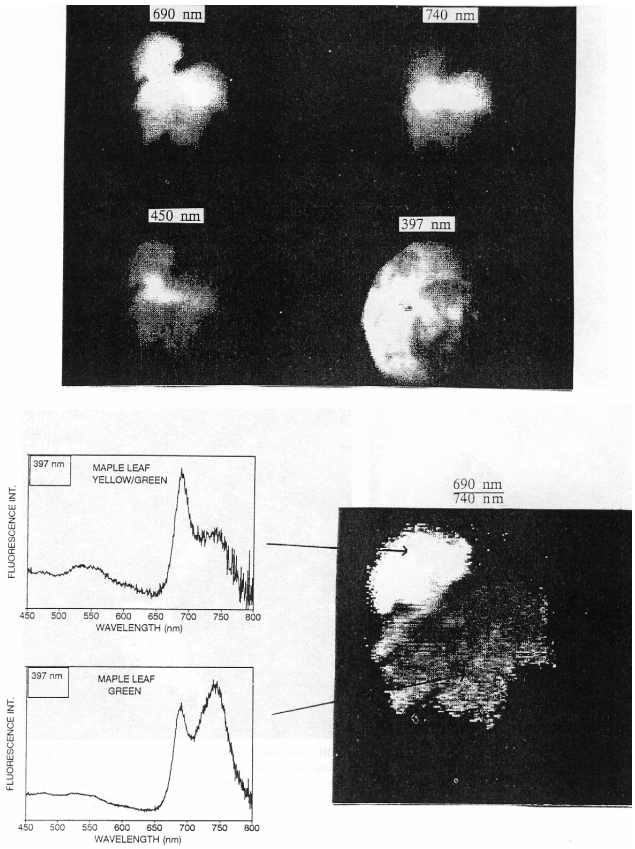

Figure 4-21. Simultaneous fluorescence images of two maple leaves recorded at 690, 740 and 450 nm using laser excitation at 397 nm (about 30 mJ) from 50 m distance and averaging over about 20 laser shots. A reflectance image at 397 nm is also shown. A computer based ratio image 690/740 nm shows the discrimination capability between the green and the slightly yellow leaf. The spectra taken from 50 m range are also shown. From Edner et al. [89].

An interesting approach to the mine detection problem using fluorescence is presented by Burlage [4, 98]. The idea is based on indirect detection of the explosive packaged inside the mine. The Microbial Mine Detection System (MMDS) described by Burlage is an example of a living system that responds to explosives and provides the operator with an identifiable signal. A common soil micro organism has been genetically engineered to recognize an explosive (DNT and TNT) and to respond to it by producing a fluorescent protein. These bacteria are sprayed over a field and allowed to make contact with the explosive that resides in the bulk phase of the soil. The concentrations of explosive are much higher here than in the vapour phase, and research has shown that ppm concentrations are available to the microbes— which is ideal. As fluorescent protein is produced, the bacteria become detectable using any of several fluorescence detection techniques. The fluorescent signals are mapped, and the area is examined for the source. The performance of this detection method seem unclear, the method is complex and probably not proper for tactical mine detection but may be of interest for humanitarian demining.

Fluorescence have also been tested for underwater mine detection and classification [99]. A Fluorescence Imaging Laser Line Scan (FILLS) sensor demonstrated that fluorescence

imagery provides strong signatures which may be used to separate the coral clutter from mines. Figure 4-22 and Figure 4-23 demonstrate the ease with which a human observer can differentiate the mine like objects (MLOs) from the natural clutter in an environment that is difficult for sonars. Images like these make it worth considering this technology also for the surface land mine detection problem.

a *b* *c* *d* *e*

Figure 4-22. The images produced by the a) elastic scatter channel, b) red fluorescence channel, c) green fluorescence channel, and d) yellow fluorescence channel. e) shows the pseudocolor image produced by mapping the red, green, and yellow channel images to RGB, respectively. From Strand et al. [99].

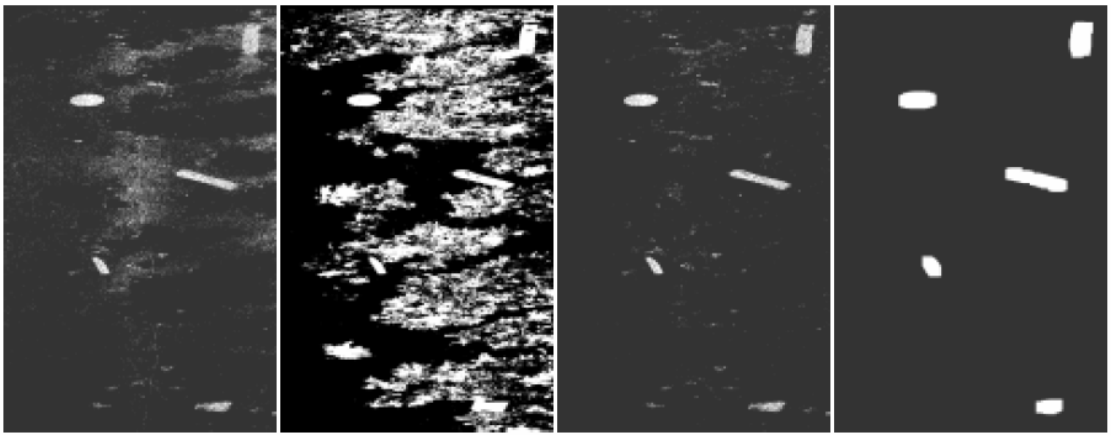

a *b* *c* *d*

Figure 4-23. a) and b) show the background masks formed by thresholding the red and yellow channel images, respectively. c) shows the AND-ing of masks a) and b). d) shows the final object mask formed by cleaning-up mask c) using standard mathematical morphology operations. This final mask selects the manmade objects, while rejecting the extensive coral clutter. From[99]

Potential use of fluorescence for MOMS tasks can be to distinguish between vegetation and mines painted with colour similar to vegetation, it is probably very difficult to develop an artificial paint that in addition to spectral signature also has fluorescence signature similar to vegetation. Another application could be to detect plants or small areas of vegetation that are exposed to stress factors originating from mine deployment or using vegetation as camouflage material for mines. It would be interesting to investigate time constants for fluorescence and spectral signature variations for vegetation exposed to such stress factors.

4.3 Sensor technology review

In this section we will shortly exemplify some sensors and sensor systems and techniques which might be of interest for the surface mine problem. An international review of projects on humanitarian mine detection can be found in [100]. FOI has during the years 2001 to 2003 been a partner in the European Union (European Commission) funded project ARC [101]. The FOI role in ARC was as supporter of EO sensors and signal processing & analysis. Some of FOI review articles on laser radars [102] may be relevant for different aspects of laser systems.

4.3.1 Laser illumination systems

Passive EO vision devices use thermally emitted radiation or ambient light. The performance of image intensifiers or low light level TV cameras can greatly be improved by adding a laser-illumination source. Typical applications include target identification, reading of car, aircraft or ship identification letters and numbers and search and rescue operations. Co-operative reflectors (traffic reflectors etc) have very long detection ranges when laser illuminated, typically 4-5 km. Recent advances in laser diode illuminators and fiber delivery make laser illuminators a very attractive “add-on” to existing FLIR/TV gimbals for example. It is also possible for shorter ranges to enhance thermal cameras in the 3-5 and 8-12 μm by adding laser radiation.

Other references related to the LAMD concept investigate the diode laser technology for illumination [45, 103, 104]. The Airborne Littoral Reconnaissance Technologies (ALRT) project has been developing night time operational minefield detection capabilities, under funding from the Office of Naval Research, using commercial off-the-shelf laser diode arrays. This has lead to the development of the most recent variant, the Airborne Laser Diode Array Illuminator wide field-of-view (ALDAI-W), in a line of laser diode array imaging test bed type systems [45].

Test results and phenomenology are found in several recent SPIE publications[44, 45, 66, 68]. Examples of images from diode laser illumination and a CCD intensifier camera is given in Figure 4-24.

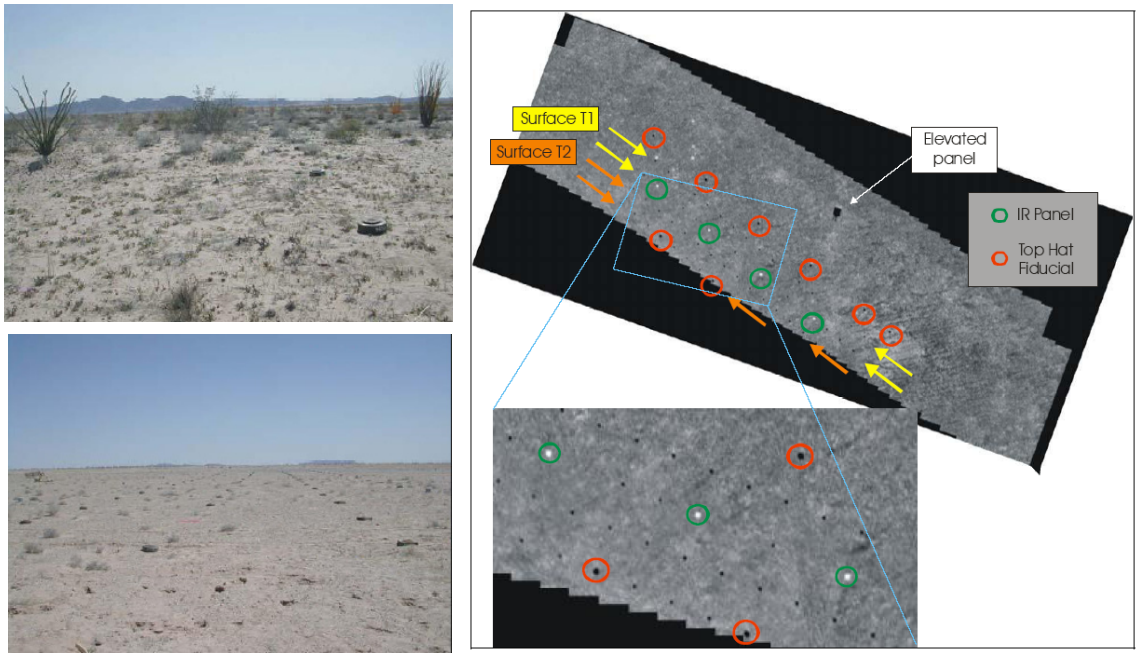

Figure 4-24. Examples of images from diode laser illumination and a CCD intensifier camera [45].

The LAMD-Laser system was developed for compatibility (in terms of size, weight and volume) with a tactical UAV. The system was required to meet performance requirements at an altitude of 330 m feet and a ground speed of 35-50 m/s knots. The performance specification requires that a 67 m cross-track swath be covered at a 2.5 cm ground sample dimension, at a minimum operational altitude of 330 m. The total weight of the system is 25 kg. Figure 4-25 shows an image of the sensor and the diode laser array.

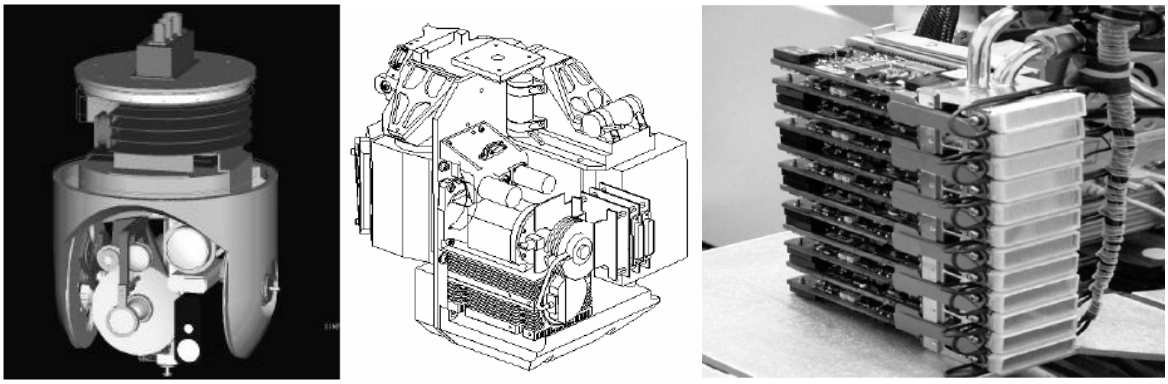

Figure 4-25. Left the LAMD gimbal with passive and active sensors. Middle, the LAMD sensor package and right the laser controller boards mounted on opposite faces of a cold plate shared by the laser head. The resulting fast axis, combined with the natural divergence of the laser diodes in the orthogonal axis, establish the required field of illumination (FOI) of 1.2° × 12.2°. Each laser bar consists of 60 laser diodes (or emitters). There are a total of 18,000 emitters in the laser subsystem [105].

The data for the LAMD laser and receiver are found in Table 4-2 and Table 4-3 below.

Specification Title	*Requirement*	*Measured Values*
Energy	≥14 mJ per 1-μs pulse (14 kW peak)	12.3 kW at I = 140 A
Pulse Width	Between 0.5 μs and 1.0 μs	~1.0 μs
Pulse Repetition Frequency	Between 285 kHz and 333 kHz	250 kHz
Pulse rise time	<100ns (20%-90% peak)	~120ns
Pulse fall time	<100ns (20%-90% peak)	~80ns
Burst Repetition Frequency	18 Hz to 50 Hz	50 Hz in most cases
Duty Cycle	0.5% average	0.46% in most cases
Average Power	≥ 70 W within the FOI	49 W at I = 140 A
Wavelength	$\lambda_C = 806 \pm 2$ nm	805 nm ≤ λ_C ≤ 806 nm
Spectral Bandwidth	≤ 7 nm FWHM	< 3 nm FWHM
Degree of polarization (DOP)	DOP ≥ 100:1	DOP > 300:1
Beam Divergence	FOI in cone of 1.2° × 12.2°	See Note 1 and Fig. 3-1
Beam Uniformity	< ±20% within the FOI	up to 40% at the corners
Boresight alignment	≤ 0.5°	0.07°
Beam Wander (Pointing Stability)	≤ 0.1° over the lifetime	< 0.085°

Table 4-2. Data for the LAMD diode laser [105].

Parameters	Specifications
Sensor	Sci-Tech Breadboard 808 nm Laser
Detector Array	CCD, backsided thinned 656 (horizontal) x 490 (vertical) Pixels (656 x 245 for P Polarization and 656 x 245 for S Polarization)
Frame Rate	24 fps (programmable), 24 fps max with flush
Readout Noise	< 5.4 counts rms
Dynamic Range	12 bits
Gate Integration Time	Imager 1.8 ms, FLC Camera Shutter 100us
Optics	84 mm / f1.5
Spectral Filter	800 nm ± 2nm
Field of View	2.3 (H) x 6.3 (W) (P&S)
Laser Array	7 Laser Modules @ 13 Rows Each w/microlens
Laser Power	1.5 Kw Peak for 100us
Platform	UH1- Helicopter
Height	500 ft.
Spatial Resolution	1 in

Table 4-3. Data for the LAMD-like receiver[68].

Multi-spectral laser systems are being considered for mine detection. One example is illustrated is in Figure 4-26. CTI in US [106] is developing a compact and efficient multi-spectral laser transmitter for surf zone and on-shore active imaging. The transmitter is designed to search for mines and surface targets in shallow water, beach, and low vegetation areas. The system will produce range-resolved, multi-spectral images suitable for automatic-target-recognition (ATR) algorithm processing.

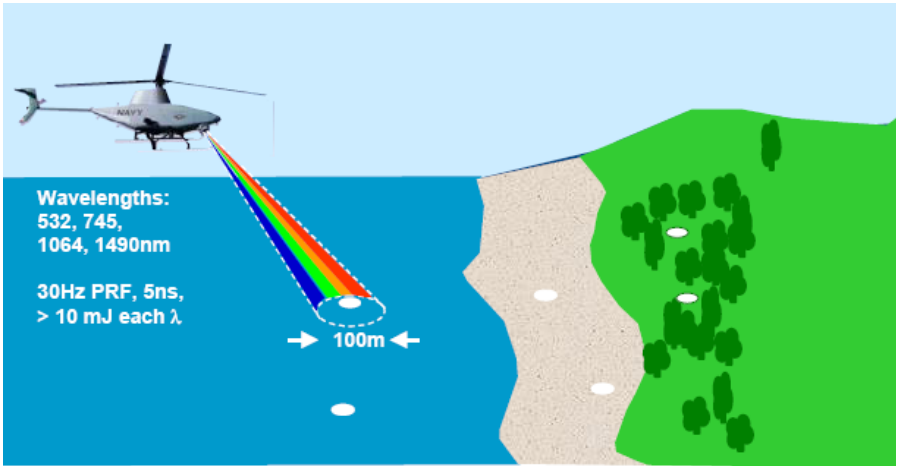

Figure 4-26. Assumed scenario for surf zone mine countermeasures demonstrations [106].

An example of a baseline laser illumination system is given in [107].

4.3.2 3-D imaging

There is a potential of combining high range and transverse resolution with high area coverage rate. A combination of intensity and range information seem to be the natural. One example of such a sensor is the Sandia laboratories scannerless range imager [108] utilizing a modulated intensified CCD Focal Plane Array and flood light illumination, Figure 4-27. The sensor has a 0.1 inch range accuracy over a 40 degree field-of-view with 30 Hz acquisition rates The nature of the measurement process is multi-frequency AM-CW. There are also a number of other laser sensors with this sort of capability.

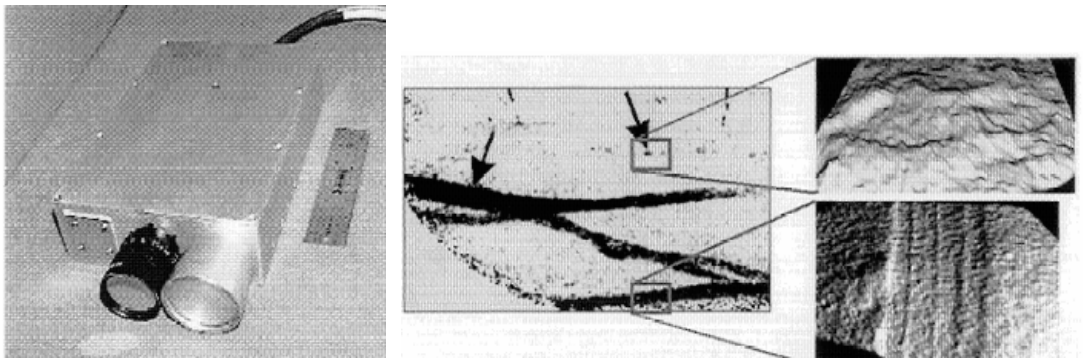

Figure 4-27. The Scannerless Range Imaging utilizing a modulated intensified CCD Focal Plane Array and flood light illumination. The sensor has a 0.1 inch range accuracy over a 40 degree field of view with 30 Hz acquisition rate [108]. Note the 3-D images of car track and a footstep in the soil.

There are some commercial systems relying on phase modulation for range measurements. FOI recently acquired a system from Canesta, see Figure 4-28. These 3-D cameras are first generation cameras for industrial applications with limited ranges (tens of meters) and accuracies in the mm-cm range.

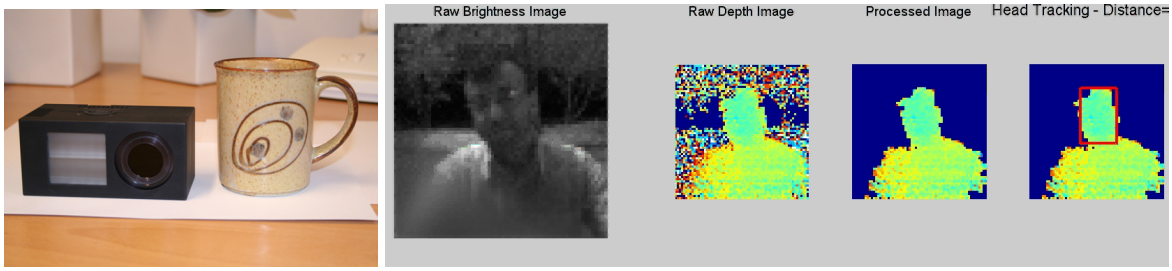

Figure 4-28. Left the Canesta camera and to the right some range images [109].

4.3.2.1 Scanning singel/few detector element laser radars

There is a growing interest and development in scanning laser radar technology for both airborne and ground use. Examples of scanning systems developed for this purpose are ILRIS-3D (Optech Canada) [44], RIEGL (Austria), Zoller and Fröhlich (Germany) [110] and Cyrax (US) (now Leica Geosystems) [111]. In the civilian field, scanning 3-D laser radars are used for engineering, construction, operations and maintenance activities in manufacturing plants and civil/survaillence markets.

Commercially available scanning laser radars are commonly single detector systems based on time-of-flight data technologies. Data rates have reached up to 100,000 points per second. Examples of systems are ALTM from Optech [44], Top Eye MkII from Top Eye AB [10] and Leica ALS50 from Leica Geosystems [76]. They can deliver sounding in x,y,z points with an accuracy about 10 cm or better and together with intensity values (proportional to reflectivity). The systems uses pulse lengths in the range 3-10 ns and the most recent systems also have waveform capture at every laser shot for post processing.

For military application compact scanning high resolution laser radars have been developed for seekers and UAV:applications. The laser radar adds a third dimension of high-resolution data for automatic target recognition (ATR) and target track in clutter. This capability requires a high probability of correct ID with simultaneous low false alarms. In wide-area search roles, LADAR can achieve more than ten times lower false alarm rates while maintaining a high probability of ID. Laser radars for seekers typically provide 50 µrad angular resolution and simultaneous 7.5 cm range accuracy, a capability unavailable in IR or RF radar systems. It can achieve these resolutions in a smaller and lower-cost package than a dual mode IR/RF sensor. These systems typically use linear detector arrays with 6-256 elements with avalanche photodiodes. Compact Nd:YVO_4 lasers with average powers in the 10 W range enables maximum ranges up to a few km. The depth resolution within a pixel is limited to 0.5 m range due to the due to the pulse width (a few ns). Example of compact missile laser radars are found in the US programs LOCAAS [112] and Figure 4-29 , LAM [18] and Cruise missiles real time retargeting [113]. An example of laser radar images from a state of the art scanning system is given in Figure 4-30

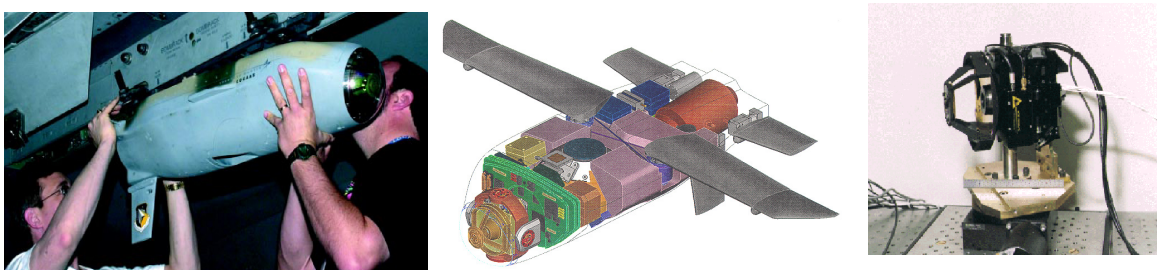

Figure 4-29. The LOCAAS - a weapon demonstrator program using a scanning laser radar [112]. LOCAAS is envisioned as a miniature, autonomous powered munition capable of broad area search, identification, and destruction of a range of mobile ground targets. Right picture shows an image of the compact seeker head.

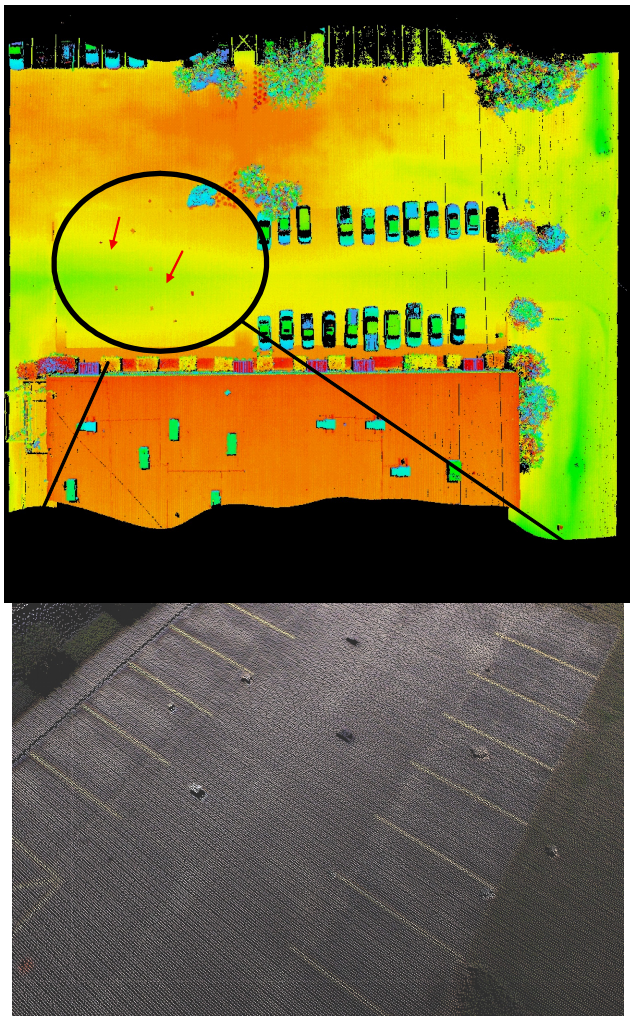

Figure 4-30. Example of laser radar images from a state of the art scanning system. Above "boxes"are detected in the color coded range imagery and enlarged in the image below. From [114].

4.3.2.2 3-D Focal plane detectors and systems

Exciting development is taking place concerning 3-D sensing focal plane arrays (FPA's). With these devices a full range and intensity image can be captured in one laser shot. For laser

radars (lidars) this will lead to more accurate positioning of the different pixels relative to each other and also to higher resolution and area coverage. The demands on scanning will also be much reduced compared to present single detector element systems. 3D – FPA's will enable integrated true active/passive imaging and multifunctional systems by changing the detector voltage, a CMR APD array can switch from passive thermal sensing to active sensing. A recent FOI report gives an overview of the area [34].

A laser flood illuminates a target area with a relatively short (1-10 ns) pulse. The time of flight of the pulse is measured in a per pixel fashion. The position of the detecting pixel yields the angular position of the target element, and the time of flight yields the range. With a single "shot", the complete 3-D image of a target is captured. An important feature to make this type of FPA a reality is to have a Readout Integrated Circuit (ROIC) to capture information that determines the range of a return at each pixel field-of-view (FOV). In this fashion, though all the 3-D information is captured in an instant, it can be read serially at a rate compatible with passive IR readout circuits.

Photodiode arrays for laser radars have been demonstrated in silicon, InGaAs and CMT. Due to eye safety issues present military (high power) laser radar developments is mostly concentrated towards InGaAs and CMT for operation at 1.5 µm. The avalanche photodiodes made in silicon have been relatively unsuccessful in arrays much greater than about 10×10. Figure 4-31 gives an example of see through vegetation concept based on microchip lasers and a 3 D APD (avalanche photo diode) Geiger mode single photon sensitive detector array.

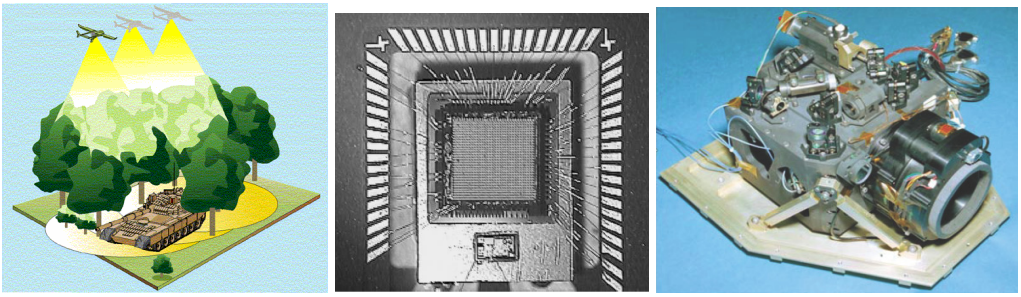

Figure 4-31. Above the JIGSAW [35] concept intended to detect targets under trees using 3-D FPA laser radar in a UAV and an image example with vegetation removed. In the middle is the 3-D FPA (32×32 element) array and the total sensor [115].

Figure 4-32. Example of a compact 3-D camera including laser and laptop for visualization and data storage [116].

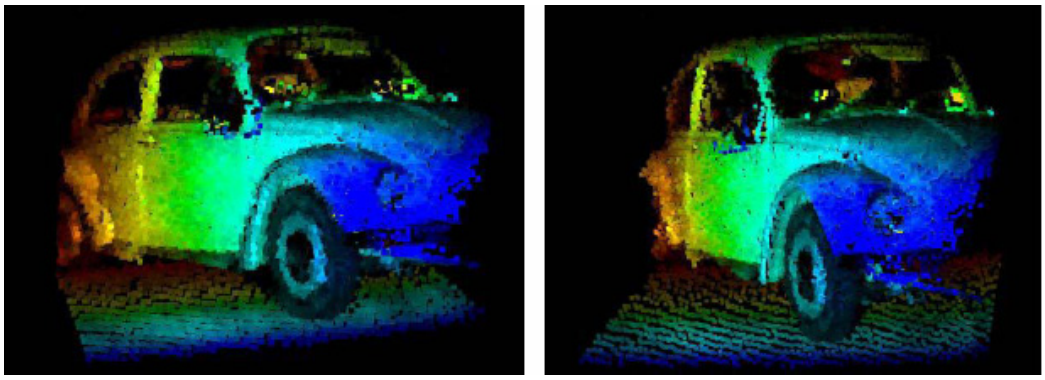

Figure 4-33. Two orientations of the same single-laser-pulse raw 128×128 3-D image. Color-coded for depth. Although a raw image, the vehicle type is clear [117].

The Geiger mode detector does not capture the whole waveform which is a disadvantage as much information about the target and target surroundings is hidden there. An interesting Readout Integrated Circuit (ROIC) that captures the waveforms and processes this waveform has been developed by Advanced Scientific Concepts (ASC) by Stettner and others [116].The ROIC is bump bonded to a solid state detector array to form a hybrid. Each unit cell, operated independently of the other unit cells in the array, is bump bonded to an independent detector in the detector array. Fundamentally each pixel contains circuitry, which independently counts time from the emission of a laser pulse, from the camera, to the capture of the reflected pulse in a pixel. In addition pixel circuitry captures temporal information about the returned pulse. Figure 4-32 and Figure 4-33 refer to a system and images witch such a detector.

A very interesting FPA under development is the CMT APD array from BAE systems [118] (now Selex) in Southampton. The detector (named SWIFT) is a 320×256 array of HgCdTe photodiodes operating with high avalanche gain to achieve sensitivities as low as 10 photon rms per gate interval (50-100 ns). A custom silicon multiplexer performs the signal injection and temporal gating function, and adds additional electronic gain. The detector is encapsulated in an integrated-detector-cooler-assembly and utilizes standard thermal imaging electronics to perform non-uniformity correction and grey scale images. Imaging trials using the camera have shown little excess noise, crosstalk or non-uniformity due to the use of avalanching in the HgCdTe photodiodes up to gains of over 100. An example is given in Figure 4-34. The detector can also be run in a passive mode and can be expanded into full 3-D capability. The pixel size is only 24 μm.

An example of a baseline 3-D FPA system is given in [107].

Figure 4-34. Left passive WFOV thermal image and right a range gated image at 1.5 μm for identification [118].

4.3.2.3 High resolution range gated cameras

Range gated cameras have been around for some time. Usually they have been tested for long range target reconnaissance applications with range gates on the order of 50-100 ns efficient to segment target from the background and for target recognition. At FOI there have been several studies on range gating [47, 119, 120].

By using a specially developed processing technique a series of 2-D images from a gated viewing image sequence can be used to construct a 3-D object with higher resolution than that given by the convolution of the pulse length an gate length [47]. In this way 3-D imaging can be done with as much as 10 times higher accuracy than that predicted by the pulse length or gate step length, example image in Figure 4-35. Range gating is thus a technique applicable for full 3-D imaging. The drawback for the range gated 3-D imaging is the high collection time to create a 3-D image which is proportional to the number of steps within the total range interval but also on the image capture rate.

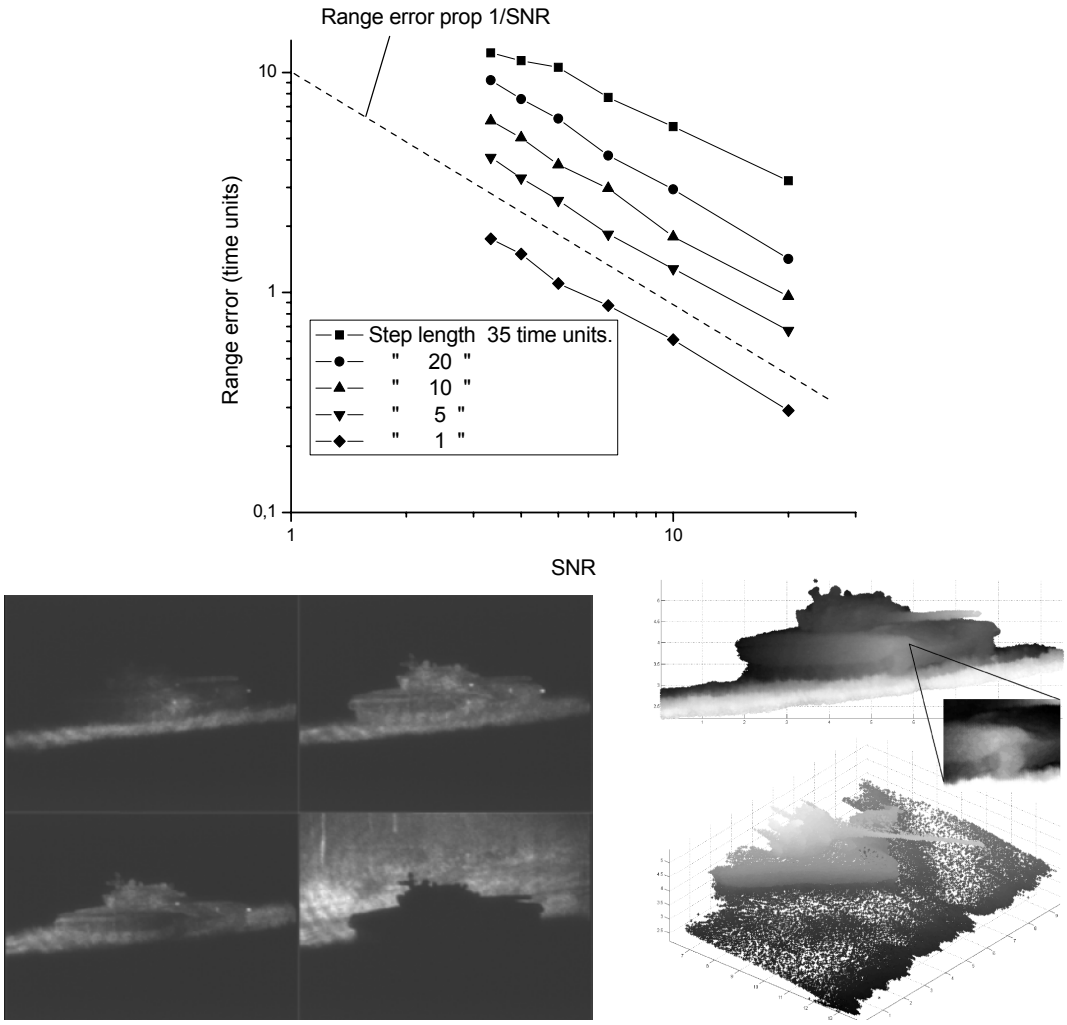

Figure 4-35. Left a series of gated images of a tank with a gate length of 40 ns (6m) and a 10 ns (1.5 m) step length which gives the high 3-D accuracy on the order of 10 cm (0.6 ns). From [47].

A novel CCD sensor camera being developed by Kaman Aerospace Corporation[121] and Dalsa Corporation, capable of operating in a burst mode at 100 million frames per second This ultra-high frame rate provides a temporal sampling element 10 ns in duration. The application for this camera is to generate the volumetric 3D imagery required for the ocean surveillance application. The initial design point of 64 x 64 x 16 layers at up to 380 Hz. Each 16-frame burst establishes an image data-cube. At maximum frame rate, the data-cube covers a temporal sample 160 ns in duration The sensor is equipped with a custom micro-lens-array to overcome sensor fill factor limitations. A means of processing the camera's output to achieve range resolution on the order of 1 inch has been demonstrated. A 2nd generation version of this camera with enhanced sensitivity to achieve true application utility is now being planned.

Jens Busck et.al. at FOFT in Denmark has recently demonstrated [122] high resolution imaging with sub mm accuracy for the identification of sea mine and other applications like personal identification. The main components of the laser radar system are a green pulsed laser and a fast gating intensified CCD camera. The laser radar system innovation is a combination of the short laser pulses (0.5 ns), the high laser pulse repetition rate (32.4 kHz), the fast gating camera (0.2 ns gate width) and short camera delay steps (0.01-0.1 ns). The

signal processing for generating the 3-D images is similar to the one developed by FOI, but simpler. The camera works at 50 Hz frame rate and integrates about 650 laser pulses for each frame. To scan a range with 50 time steps then takes about 1 second. If the range gate is 30 cm for example then a range resolution of about 0.8 cm is possible.

For our mine detection problem there are some disadvantages with this kind of system in the search mode due to the finite time for creating high resolution with a varying gate due to a varying terrain profile. Figure 4-36 gives some image examples from the gated images.

An example of a baseline system is given in [107].

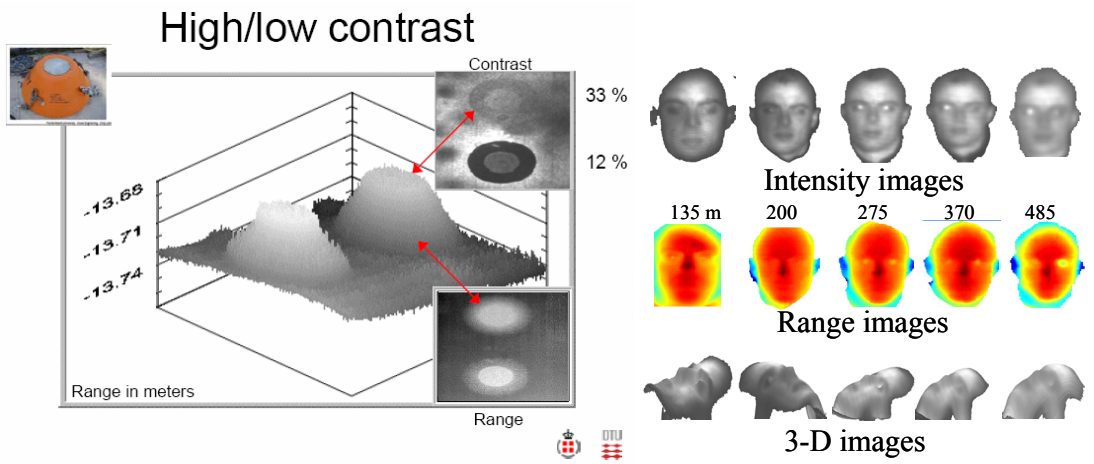

Figure 4-36. Left example of a 3-D image of a 5 cm small mine model. Right 3-D images of persons up to almost 500 meters. From [122].

4.3.2.4 Streak tube imaging lidar (STIL)

Streak-tube imaging lidar (STIL) [123] is a new technique for obtaining high 3-D images from land and ocean. The principle is shown in Figure 4-37. A pulsed laser transmitter in conjunction with a time-resolved streak tube forms the basis of the system. The laser diverges to form a fan beam on the scene and the reflection is imaged onto the slit photo cathode of the streak tube. The fan beam moves in the flight direction. Photoelectrons liberated from the photo cathode are accelerated, focused, and deflected in time using parallel-plate electrodes. A sweep voltage applied to steer the beam in time along an axis orthogonal to the fan beam allows a range-azimuth image to be formed on each laser pulse. This range-azimuth image is digitally recorded by conventional CCD technology. Synchronizing the PRF of the system with the forward speed of the platform means the in-track dimension is swept out in a push broom fashion.

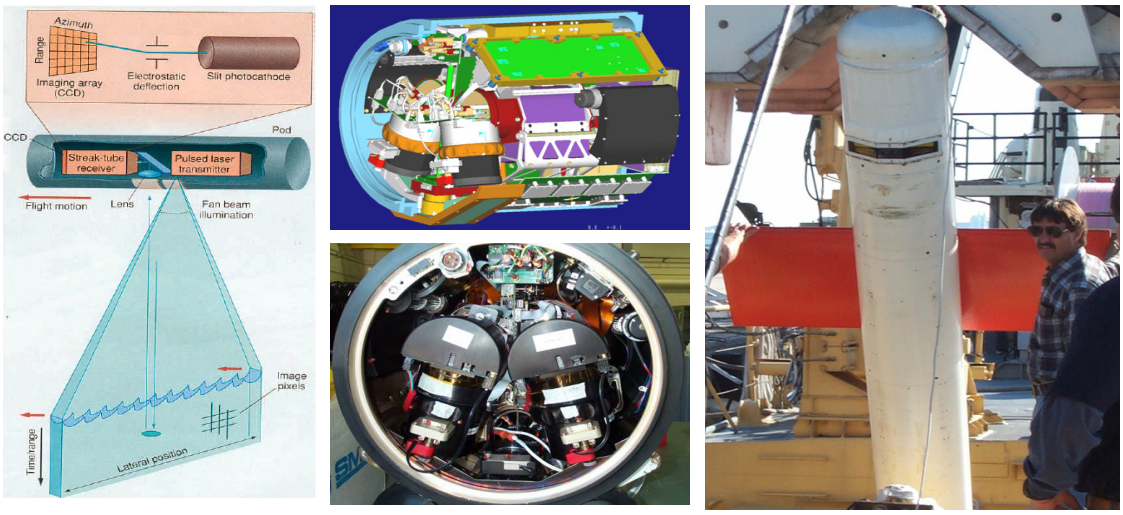

Figure 4-37. Left the principle of the streak camera and middle and right show two streak camera tubes installed in an underwater vehicle for mine classification.

Figure 4-38 demonstrates the range and contrast imaging capability, and also demonstrates the high resolution range information that the system can generate [124]. Because the STIL system can collect multiple samples within the laser pulse length, the range resolution of the system is not governed by the sample period, but is given by:

$$\sigma_{range} = 0.6 \cdot \frac{c\tau}{SNR}$$

where τ is the FWHM value of the laser pulse width.

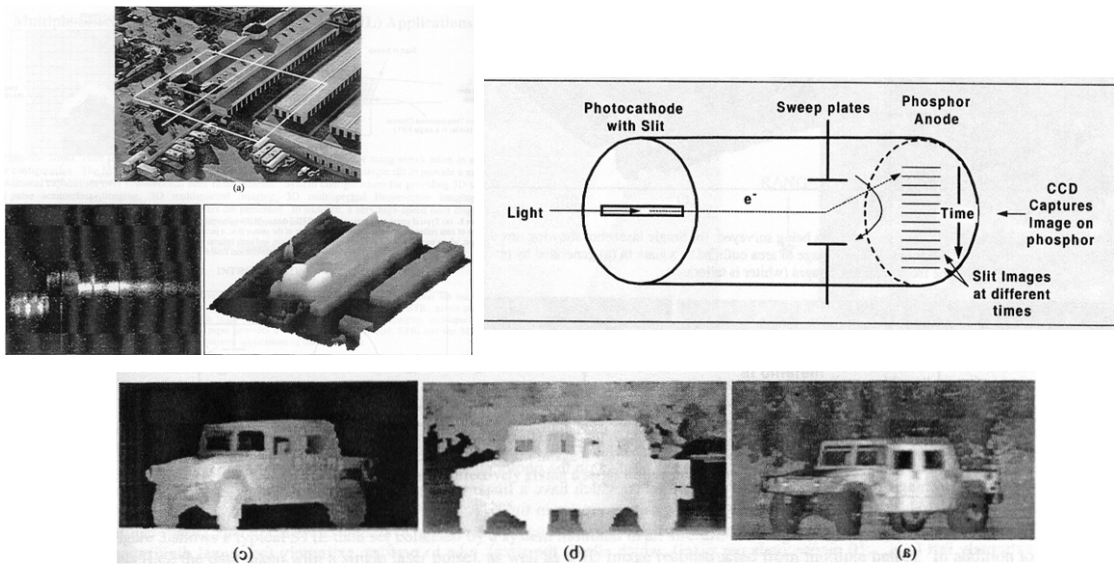

Figure 4-38. Above example of airborne 3-D imaging using a streak camera and below a scan across a vehicle from range within vehicle only, range image of the whole scene and reflectivity image of the whole scene. The range resolution on the vehicle images was 1 inch [124]. The target is at close range (60 m) and the laser wavelength 532 nm.

In Figure 4-39 we illustrate the combined reflection and high resolution imaging of bottom mines using a streak camera [125] and a laser.

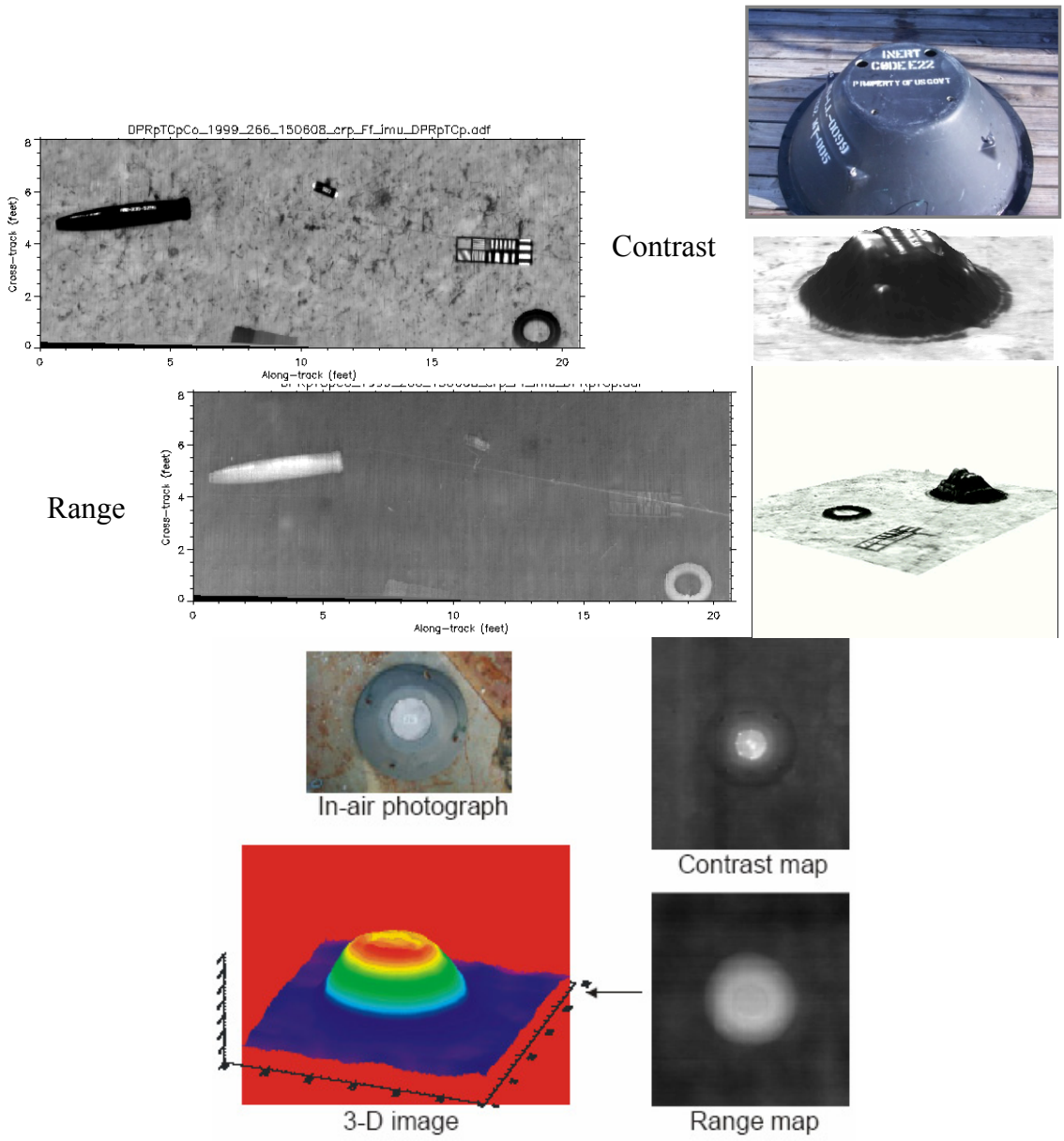

Figure 4-39. Example of laser based high resolution reflectance and range imaging for detection and classification of bottom mines. From Arete, USA [125]. The combination of reflectance and range should be very interesting both for detection and classification.

Streak Imaging Lidars [125] (STIL) technologies are also of interest for imaging in turbid waters, as shown in Figure 4-40. They have a high spatial resolution in all 3 coordinates.

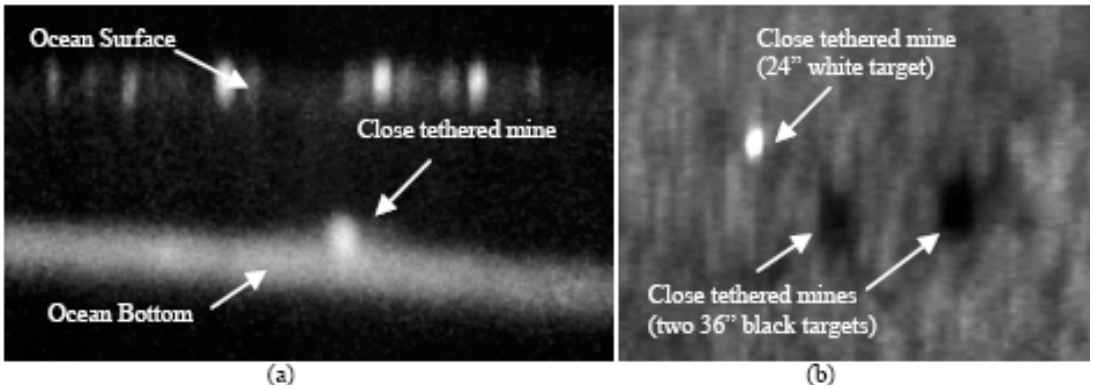

Figure 4-40. Airborne detection of bottom mines in the VSW region (10-40 feet water depth). In this case a close tethered 24 inch sphere moored 18 inch above the bottom in 27 feet of water. (a) Single frame slice through the ocean showing the bottom. (b) Reconstructed top view of three targets (one white and two black) sitting on bottom. From [125].

An interesting extension of the streak camera can be made by using multiple slits, see Figure 4-41. In addition, the technique can also allow a significant number of applications to be explored, in which different spatial data is imaged onto the additional slits (e.g., different wavelengths or different polarization states).

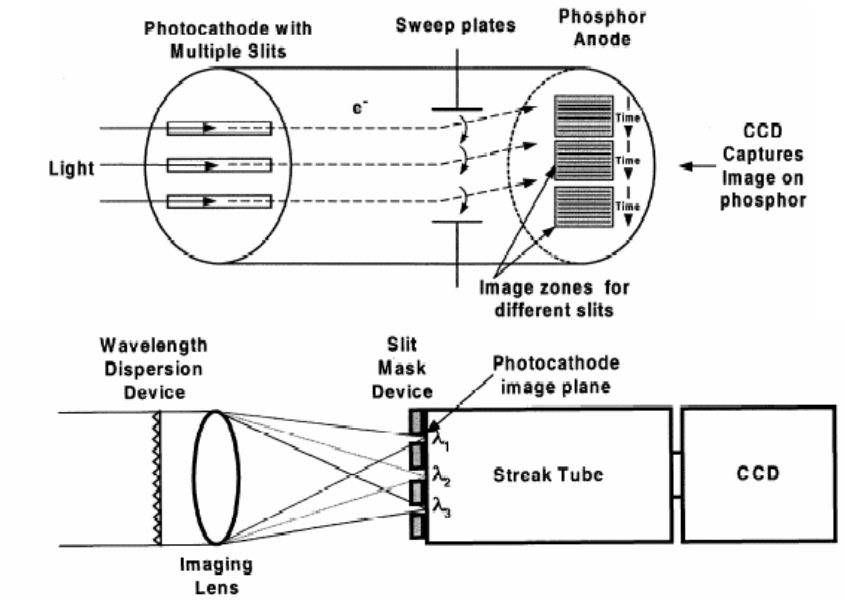

Figure 4-41. Above, arrangement for the multiple slit streak camera system. Below, example of how to implement multi-spectral imaging for the multiple slit streak camera

For multi-spectral imaging and fluorescence imaging, the additional slits are used to capture different wavelengths. The wavelength dispersion device (e.g., a diffraction grating) splits the wavelengths, while the slit mask device (a spatial light modulator, for example) provides a programmable set of slits for selecting desired wavelengths. The transmitter can be a multi-wavelength source, with each of the transmitted wavelengths going to a different slit. Alternatively, it can be a single-wavelength transmitter, with one slit dedicated to the laser wavelength, and the other slits positioned at longer wavelengths in order to capture fluorescence phenomena. Each wavelength region will have a time and space resolved image.

It is important to note that there are a number of trade-offs between the various dimensions of resolution, since the total number of pixels of the CCD is limited.

Figure 4-42 shows an example of an image showing reflection, fluorescence and range from a single laser exposure. The figure shows the results from a laboratory demonstration of a STIL fluorescence imager [126] operating at an excitation wavelength of 532nm and collecting three spectral bands: 532 nm, 550-650 nm, and 650-850 nm. The scene consists of a green plastic trashcan with a house plant on top, located about 1 meter in front of a white wall containing three paper resolution panels with black bars. The bar targets have a 50% duty cycle and a period of 37mm. The resulting three spectral band images are coloured blue, red, and green, respectively. The 3-band composite displayed in RGB colour enables the three spectral bands to be displayed simultaneously. The colour image is overlaid on top of a surface map to simultaneously display the spectral and range data. Three views of the 3D multi-spectral data are shown.

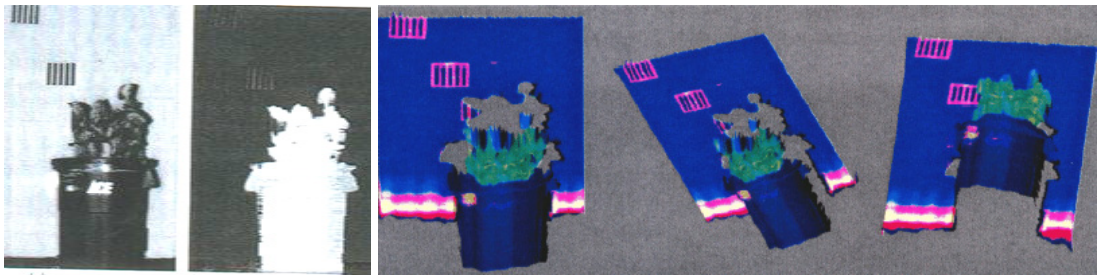

Figure 4-42. Picture of a trash can plus a houseplant seen with a SLIT camera in reflection, range and combined fluorescence and range [126]. See text above for more details.

A 64×64-pixel lidar system that uses a streak tube to achieve range-resolved images was recently demonstrated. An array of glass fibers maps light from an area in the focal plane of an imaging lens to multiple rows of fibers on the streak tube's photocathode. Data processing yields 64×64-pixel contrast (intensity) and range images for each laser pulse. Range precision better than 2.5% of the range extent is exhibited for a wide variety of targets and terrains at image rates up to 100 Hz. Field test imagery demonstrated the capability of the Flash lidar system for imaging vehicles hidden by a tree canopy as well as for imaging sub-surface mine-like targets in the ocean [125].

Examples of advantages for the streak camera approach are:

- Versatility- a variety of laser radar configurations can be combined into several different measurements, such as 3-D, multispectral, hyperspectral, multi-excitation hyperspectral, fluorescence-lifetime and polarization onto a single sensor taking data simultaneously.
- High range resolution (cm level)
- High time resolution (in principle ps) allows fluorescence lifetime to be added to observed parameters.

Examples of disadvantages are:

- Scanning or sensor movement in one direction is needed.
- Complex equipment using high voltage (kV)
- Not very compact
- Relatively high cost?
- Complicated processing

An example of a baseline system for fluorescence detection is given in [107].

4.3.3 Retro reflection

The large laser radar cross section due to retro reflection enables optics detection and classification at long ranges. In these kinds of systems (often called Electro-Optical Counter Measures, EOCM) the strong signal enables long detection ranges over wide areas. It also enables the active system to pinpoint the target position and precision direct the jamming or damaging laser.

If the side hitting mine contains an optical sight or an optical sensor it's thus possible to detect the sensor within its FOV. Outside the sensor FOV the retro reflection signature practically disappears. The detection can be made with a simple camera with added bore sighted illumination. There is however an advantage if the sensor can have a 3-D imaging capability because this also strongly extends the capabilities to detect non optical side hitting mines hidden in the terrain.

4.3.4 Passive multispectral sensing

Spectral signature are often used for detection, classification and identification of different materials or objects. For a given material, there is a wavelength dependent reflectance, see Figure 4-43. Spectral analysis are often applied on wavelengths UV-VIS-NIR (ultra violet, visual, near infrared), but IR wavelengths, 3-5 μm and 8-12 μm, have become more common for spectral analysis.

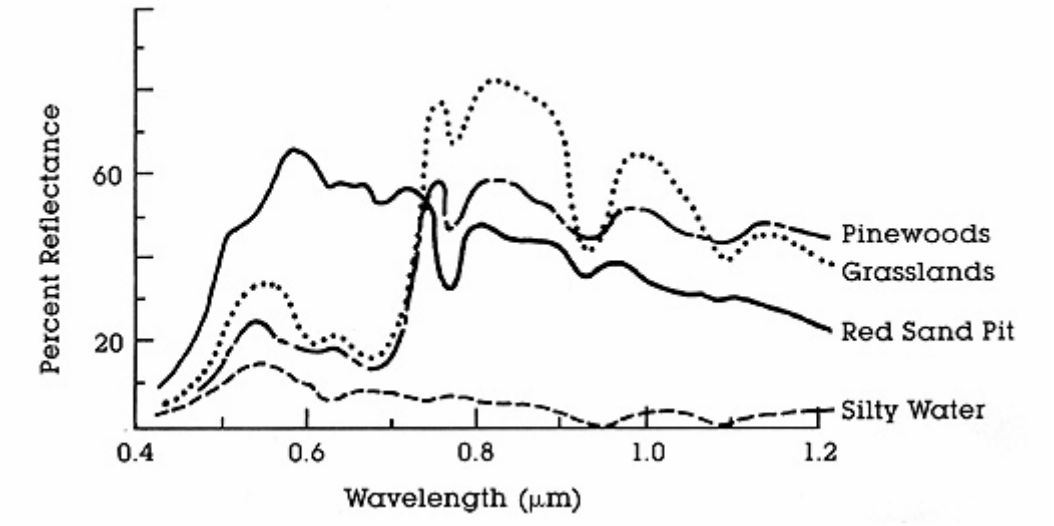

Figure 4-43 Spectral reflectance variation for different objects, from [2]

Depending on the number of wavelength bands, cameras can be monochromatic, multi- or hyper- spectral. Monochromatic means that only one wavelength interval is registered, usually a rather broad interval in order to collect many photons in low light conditions, e.g. a black- and white camera. A colour camera has three bands: red, green and blue. Multispectral cameras divide the spectrum in a larger number of bands, up to the order of 10. If the

spectrum is divided into a larger number of subbands, the camera is said to be hyperspectral. In remote sensing applications, a division of subbands of 0,2 µm is considered as low and 0,01 µm as high resolution. There are different techniques available to performing the wavelength separation. One example is optical filters, possibly mounted in rotating filter wheel synchronized with the detector read out. The method causes images representing different wavelengths not to be registered simultaneously. This leads to a need for special procedures to align the different images in case the platform is moving or the scene is dynamic. In Figure 4-44, an example of multispectral IR camera with rotating filter wheel is presented. In Figure 4-45 and Figure 4-46 some examples of images are presented.

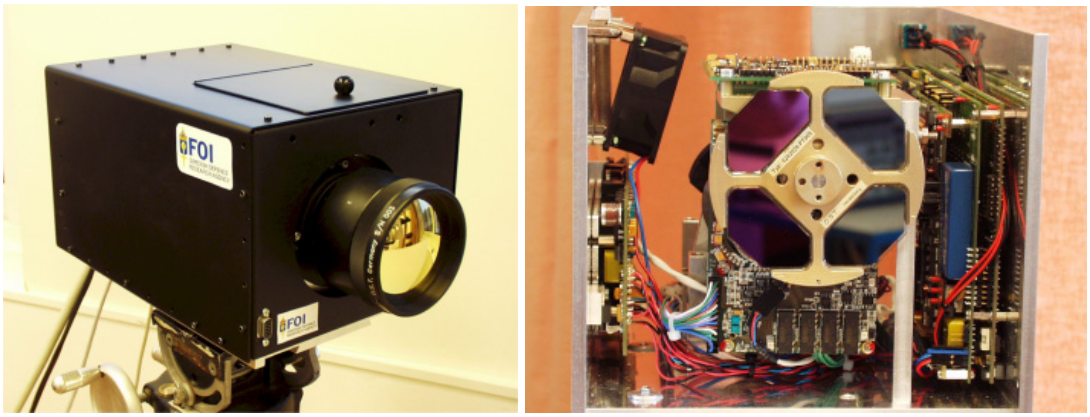

Figure 4-44 Example of multispectral IR camera (Multimir) with rotating filter wheel, see chapter 8 for camera data.

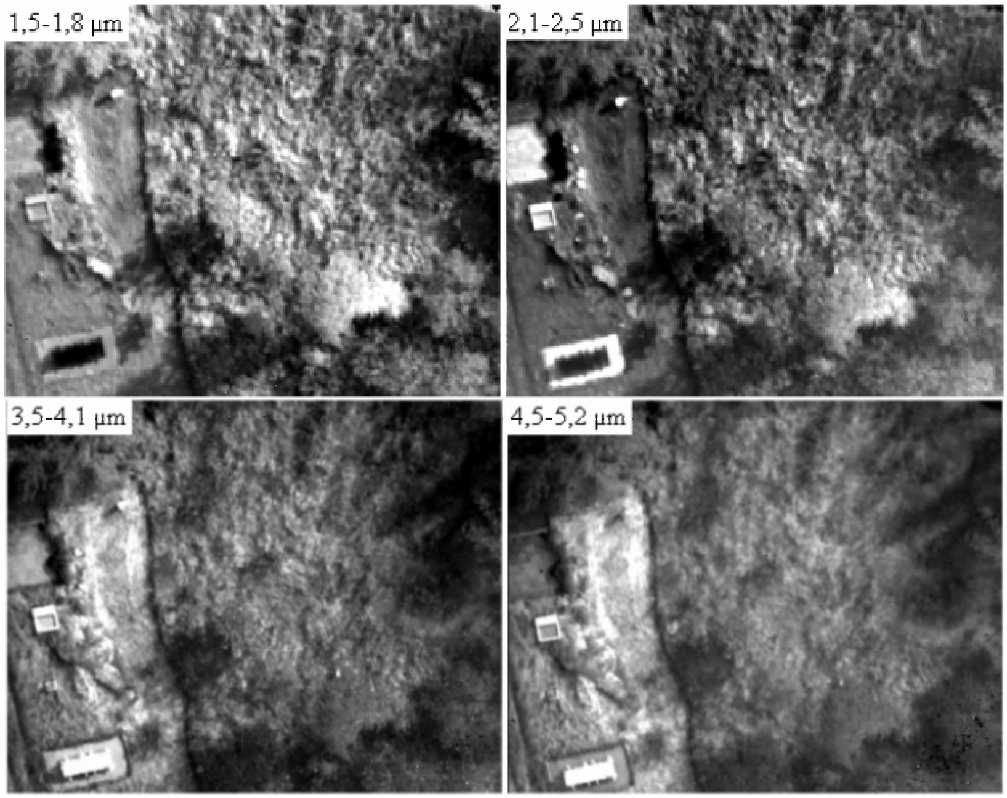

Figure 4-45. Example of airborne registration from an altitude of 1000 m with the Multimir camera.

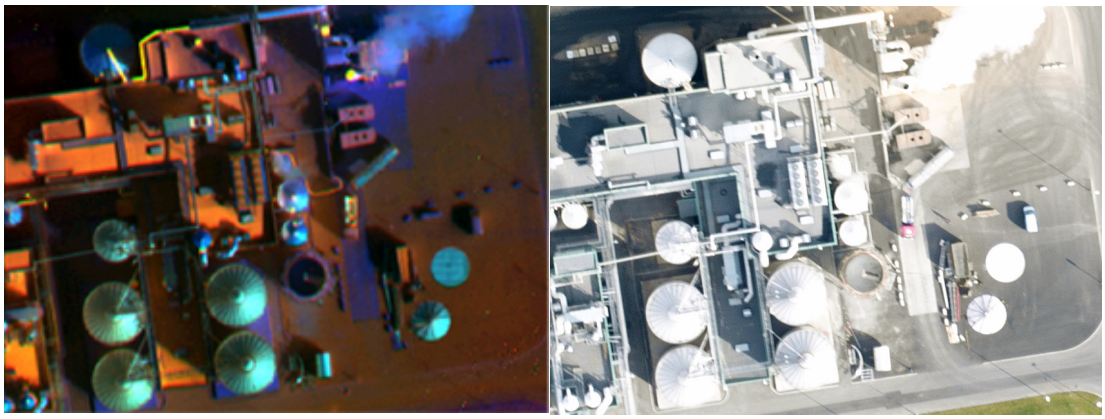

Figure 4-46. Images registered from an altitude of 1000 m. To the left is a merged image from the four spectral IR bands of the Multimir camera. To the right is a corresponding colour image.

Another way of obtaining multispectral registration is to use prisms and filters to divide the beam into different sub bands. This method overcomes the problem with time synchronisation, but for practical reasons a limited number of wavelength bands can be extracted with this method. A camera example is given in Figure 4-47.

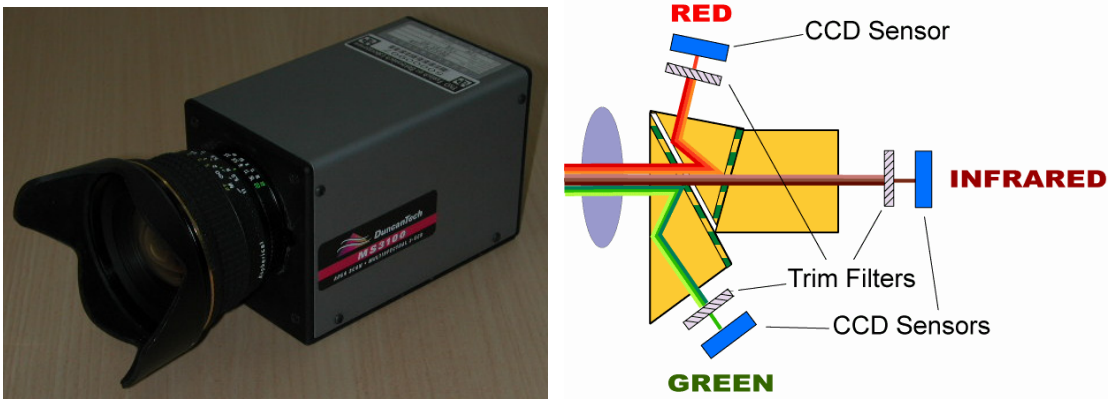

Figure 4-47. An example of multispectral camera, Redlake (former: Duncan Tech).

In Figure 4-48 an example of hyperspectral camera and principle of operation is given. Every read out from the 2-Dimensional detector represents spatial information (line) in one direction and spectral information in the other. Camera movement can be used to build up a 3-Dimensional hyperspectral cube representing two spatial and one spectral dimension, see Figure 4-49 for an example.

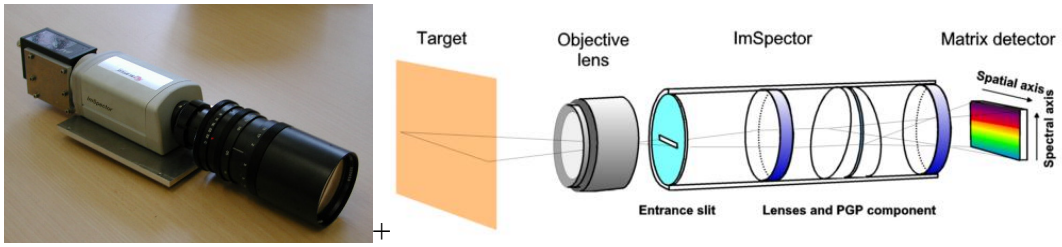

Figure 4-48. An example of a hyperspectral camera (Imspector).

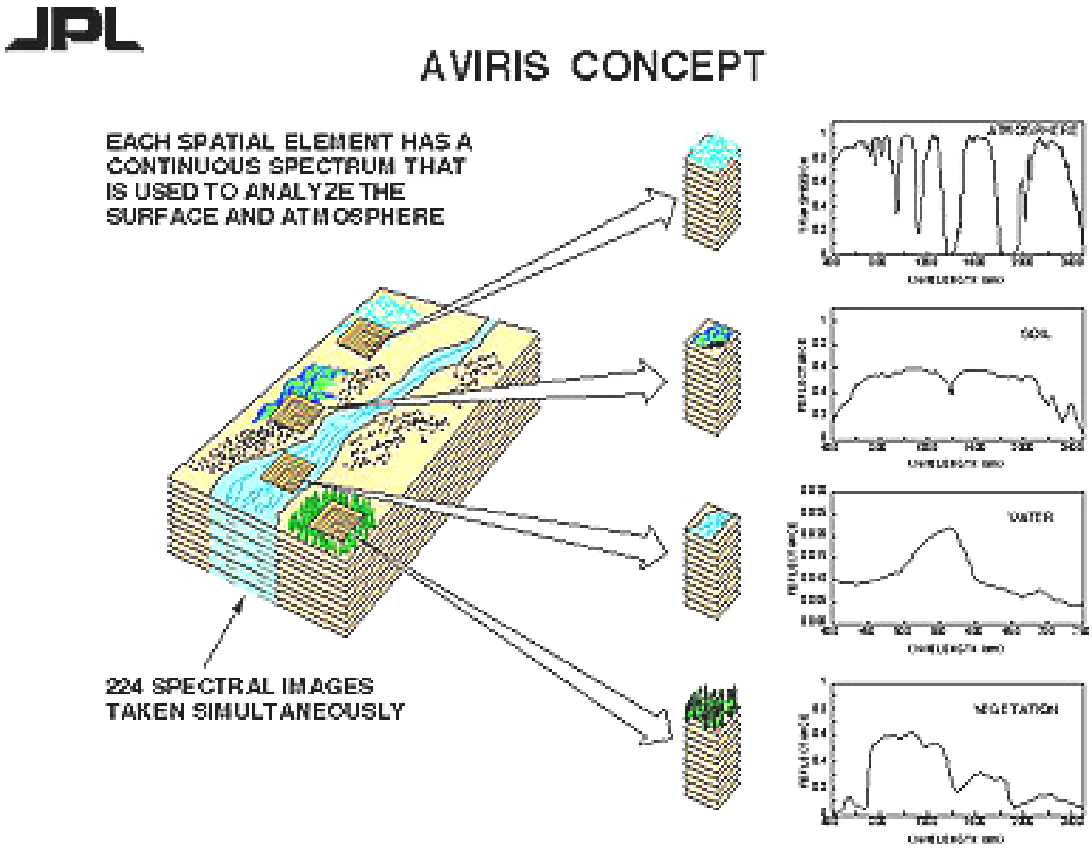

Figure 4-49. Example of a hyperspectral cube, from [2]

Different scenarios have different characteristics regarding spectral contrast between objects of interest and background. In order to meet the demands for adapting a multispectral sensor for those varying situations, tunable filters can be used, in [127] an overview of different methods is given.

4.3.5 Active multispectral 3-D sensing

Laser systems enable active reflection, polarisation and 3-D imaging at the same time using from example STIL technology. Figure 4-50 exemplifies this using colour coded intensity and polarisation together with 3-D volumetric projections [128].

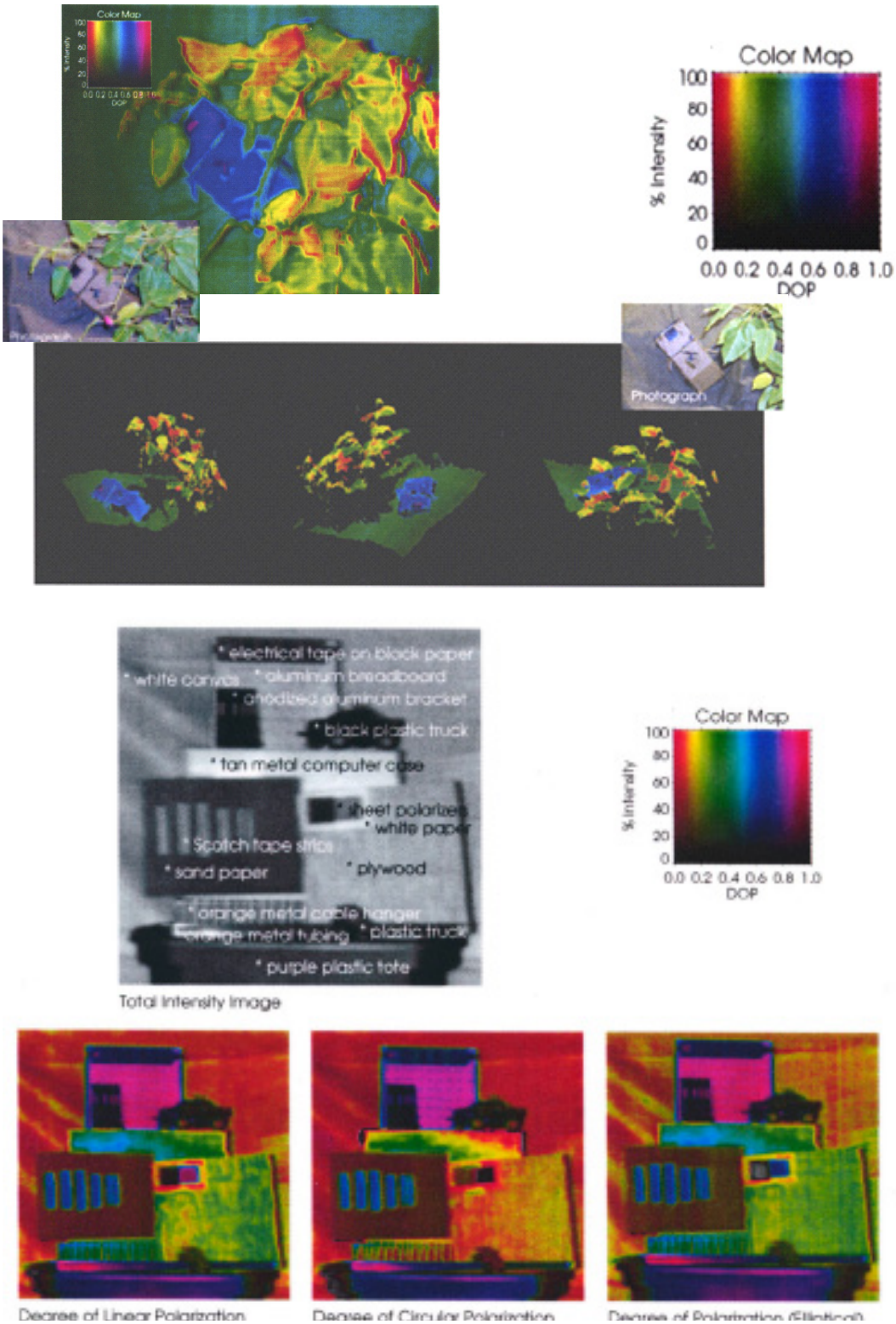

Figure 4-50. Simultaneous rendering of the degree of polarisation (DOP) and reflectance images. The DOP is indicated by the hue and the intensity by the lightness in the HLS colour system (see colourmap). Below imaging polarimetry using linear, circular and elliptical polarisation for different man made targets. From [128].

A recent interesting experiment using a multi-spectral mid-infrared laser stand off imaging was reported by Wang et al [129]. The system was applied to diverse targets that consist of

man-made and natural materials and objects, and shown capable to resolve and distinguish small spectral differences among the various targets. Colourless objects in the visible were shown with "colourful" signatures in the mid-IR, see Figure 4-51. Image processing algorithms based on spectral contrast was shown most effective to exploit the laser sensitivity and accuracy, as opposed to algorithms that operate mainly on the image spatial intensity. The results also showed the complexity of laser imaging phenomenology, involving both spectroscopic and geometrical scattering effects. A demonstration of 3-D multi-spectral imaging was also given. The system design is suitable for compact packages with semiconductor lasers, and the results suggest that laser-based multi-spectral imaging can be a unique and powerful technology for target discrimination.

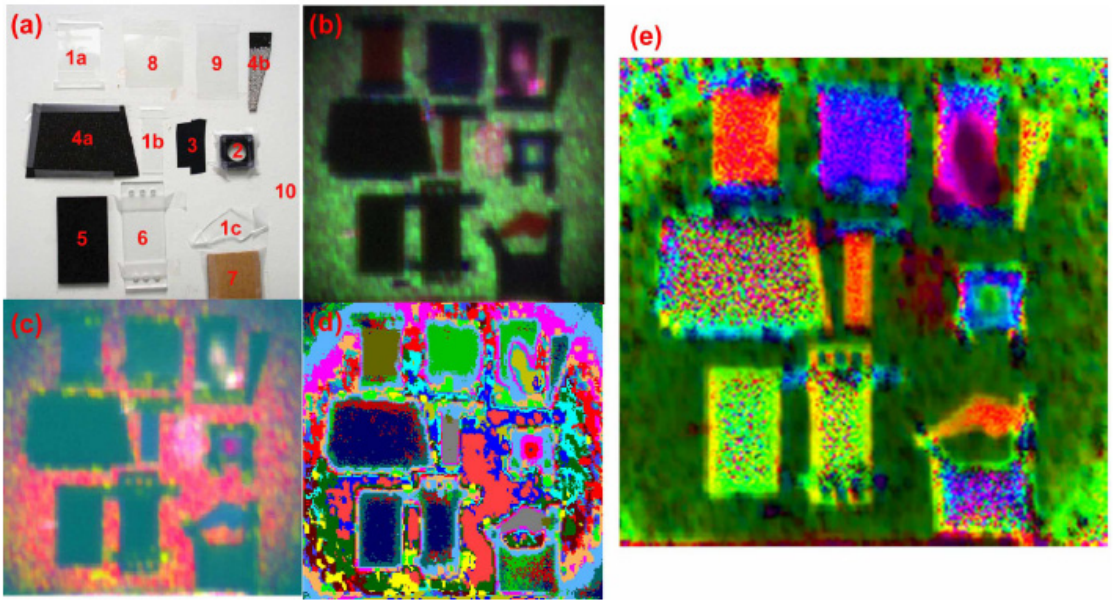

Figure 4-51. (a): visible image of the target. (b-d): False colour images from the same IR spectral images with different phenomenological algorithms (see text). The algorithms for (b) and (c) lose or distort some spectral information, and some objects become dark. The algorithm for (d) over-classifies and makes more colour distinction than physically meaningful. The algorithm for (e) is designed to preserve laser spectral data in lieu of intensity. The resulting false colour image has reasonable correlation with the object IR spectra. Notice that colourless objects (black or transparent) in (a) have "colourful" mid-IR signatures in (e). From [129].

4.3.6 Fluorescence

Fluorescence contrasts in mine detection may be manifested either by lack of signal or specific emitted florescence for the mine itself or from the disturbed soil or vapour released from the mine. The fluorescence signal from vegetation is well investigated and emanates primarily form chlorophyll. One example of a system study on a multifunctional system using fluorescence is found at MIT [62]

> *"An active hyper spectral imaging system for the detection of concealed targets has been developed. A novel microlaser-pumped fiber Raman source that provides high-brightness, subnanosecond-pulse-length output spanning the visible through near-infrared spectral range, is used. The hyperspectral-imaging system is comprised of a compact, grating-based spectrometer that*

uses a gateable, intensified CCD array as the detector element. The illuminator and the hyperspectral imaging system are mounted on a small platform that is itself mounted on a tripod and scanned in azimuth to build an image scene of up to several hundred spectral bands. The system has been deployed under a variety of environmental conditions, including night-time illumination, and on a variety of target scenes, including exposed and concealed plastic and metallic mine-like targets. Targets have been detected and identified on the basis of spectral reflectance, fluorescence signatures, degree of polarization, and range-to-target information (via range gating). The combination of laser-like broadband illumination and hyperspectral imaging offers great promise in concealed or obscured target detection. Ongoing developments include the incorporation of broadband illuminators in the 1 to 2 µm and 3 to 5 µm spectral bands, with corresponding increases in spectral coverage of the imaging and detection systems".

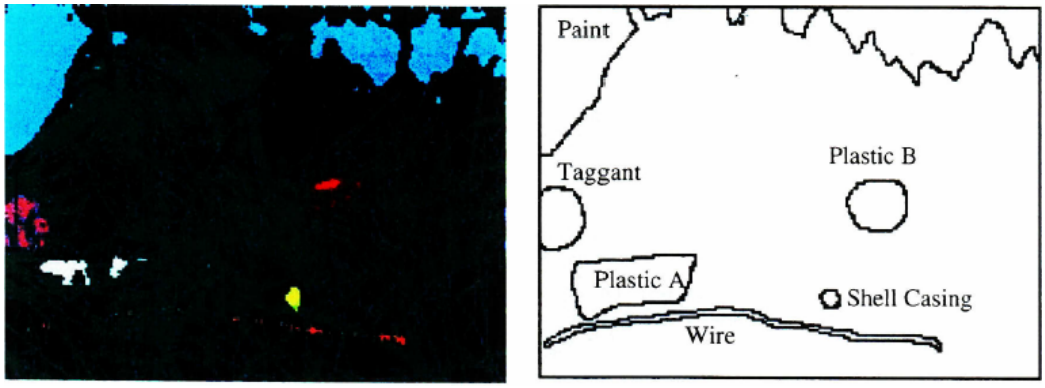

Figure 4-52. Laboratory target scene containing soil, grass, weeds, partially-obscured plastic and metal objects:A: Dark-green plastic, B: Bright-green plastic, Wire, Shell casing, Green paint, Taggant. Fused fluorescence, polarization, and reflectance data displayed in one scene and compared to target placement. From [45].

One problem with laser induced fluorescence is the relatively low yield against vegetation chlorophyll. The values found in the literature are sparse and have to be derived from experiments. We used the NASA:s AOL lidar data [90] for terrain fluorescence to estimate the efficiency F to be in the range 10^{-5}-10^{-6} using blue excitation at 422 nm. If a UV excitation had been used we would expect a factor of 2 higher values. The yield from sun-excited florescence measured at Fraunhofer lines in the sun spectrum (the so called FLD (Fraunhofer line detection) seem to be in the range 10^{-3} for steady state and the broad spectral excitation caused by the sun light) [91].

The low yield for laser excitation limits the practicality of a lidar fluorescence for large search areas rates. A baseline laser fluorescence sensor is found in [26].

4.3.7 Examples of sensor images

In the figures Figure 4-53 to Figure 4-56 below, some examples of the phenomenology discussed in the sensor context above, is given. Not all the phenomenology is exemplified. Test systems should be developed that can be used for evaluating the phenomenology based information content as it relates to specific situations.

Figure 4-53. Left: Green plastics in vegetation as viewed in reflection with a RGB sensor. Right: Green plastics in vegetation as viewed in reflection with a NIR sensor.

Figure 4-54. Left: Green plastics in vegetation as viewed in fluorescence with a NIR sensor. Right: Green plastics in vegetation as viewed in reflection with a RGB sensor and fluorescence suppression mask.

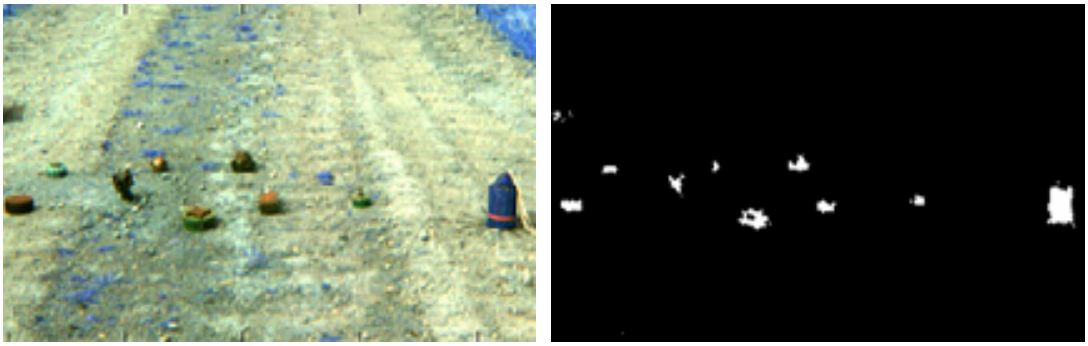

Figure 4-55. Left: RGB-rendering of hyperspectral image. Right: Information based target detection based on hyperspectral data.

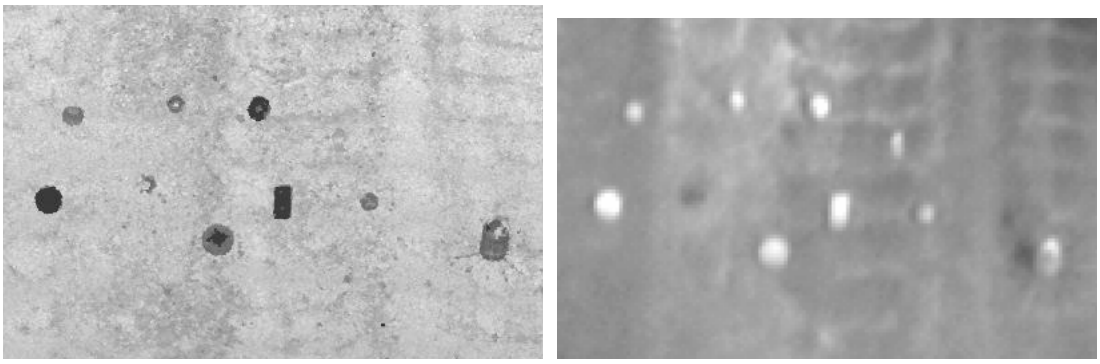

Figure 4-56. Left: 3-D LADAR image. Right: Thermal infrared image.

4.4 Combinations of sensors

In chapter 6, description of some data fusion techniques are given. Prior to fusion of sensor signals, selection of sensors are a major concern in order to exploit the benefits of cooperation between sensors. At FOI, some earlier work has been done regarding mine detection in order to select sensors for data fusion, Brusmark [130]. Methods and technologies as potential part of a multisensor system for mine detection were discussed. As system requirements were different compared to MOMS, preliminary evaluation of the capability for single sensors in different environments (background, target, clutter) favoured the combination of radar, metal-detector and biosensor. In Haugstad [131], claims and requirements regarding combinations of sensors for mine detection and mine clearance are given. One important statement is that the different methods should be statistical independent. The work deals with demands for combinations of different clearance methods in humanitarian demining, but has relevance for combination of sensors for all demining pruposes. In Dullum [132] a sceme is given regarding correlation between different clearance methods, Figure 4-57

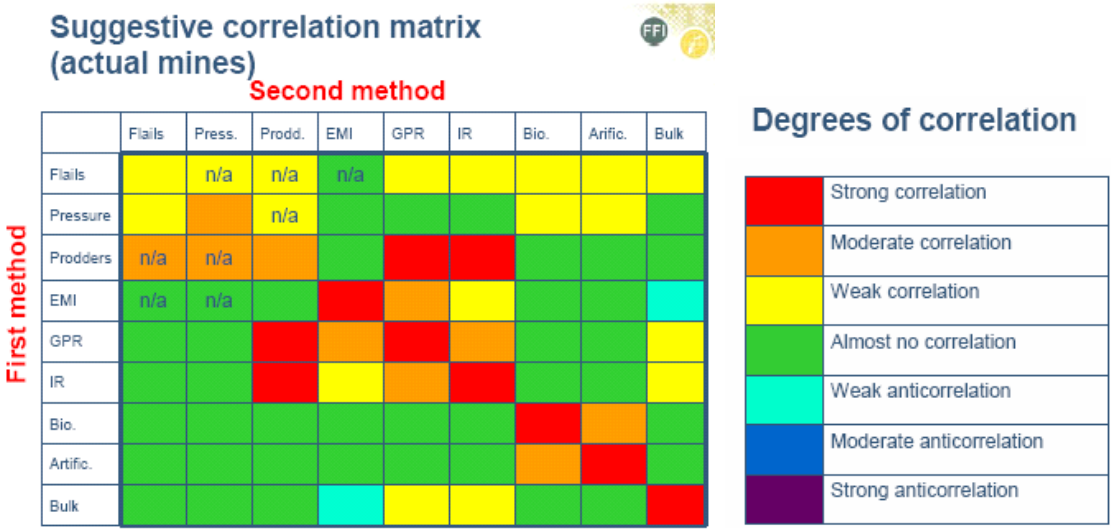

Figure 4-57 Correlation matrix for two demining methods taken in sequence, from [132]. IR is the only optical method in the matrix.

Some concluding remarks from Dullum [132] are:

1. Two combining methods should:
    a. have low or negative correlation coefficient
    b. have low false alarm rate for at least one method
2. Making a general correlation measurement between two methods is very difficult
3. Assessment of correlation requires an intimate knowledge of detection physics
4. Values for correlation will be of great valus, if they can be provided as a function of the environmental variables.

During 2001-2003 FOI was a partner in the EU-project ARC [101]. A pyramidal approach was applied for combining sensors with different resolutions, see Figure 4-58. Data fusion was a part of the project. In Figure 4-59 some results are shown as an illustration of data fusion.

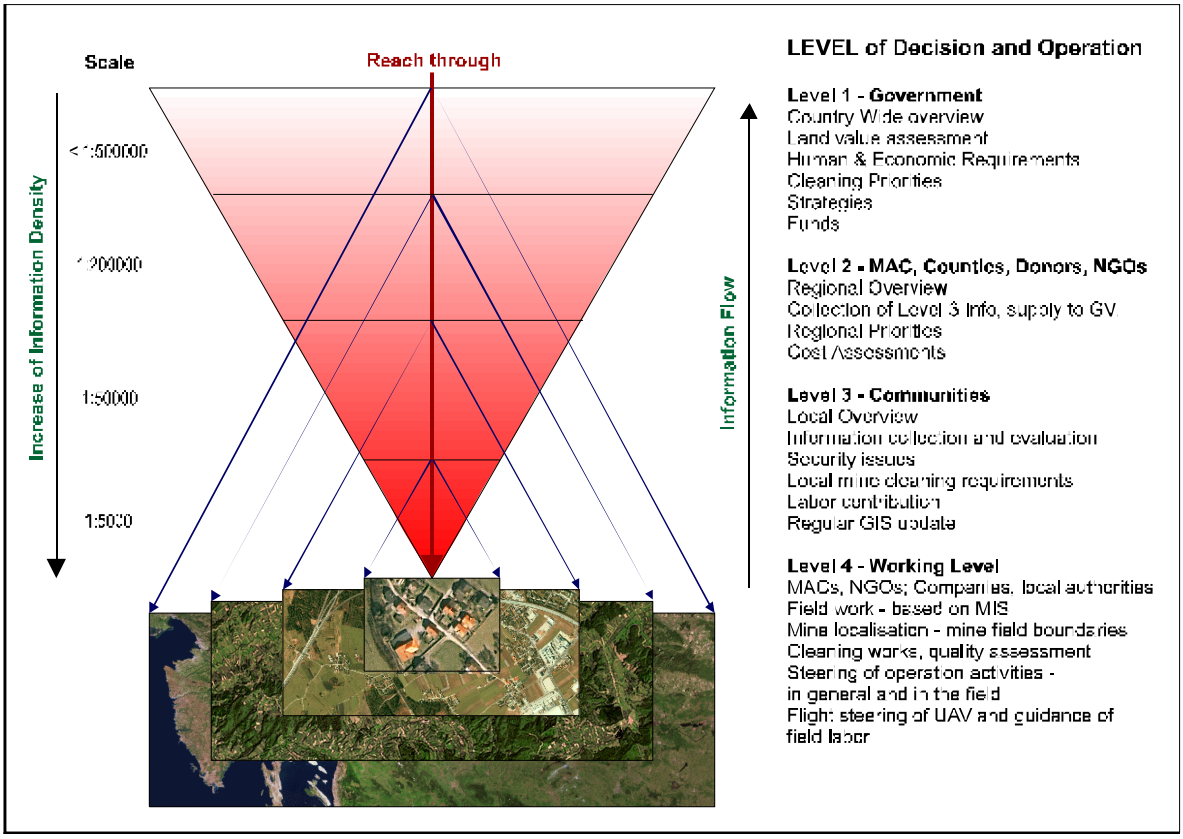

Figure 4-58 Schematic view of data content and information flow in a pyramidal approach applied in EU-project ARC.

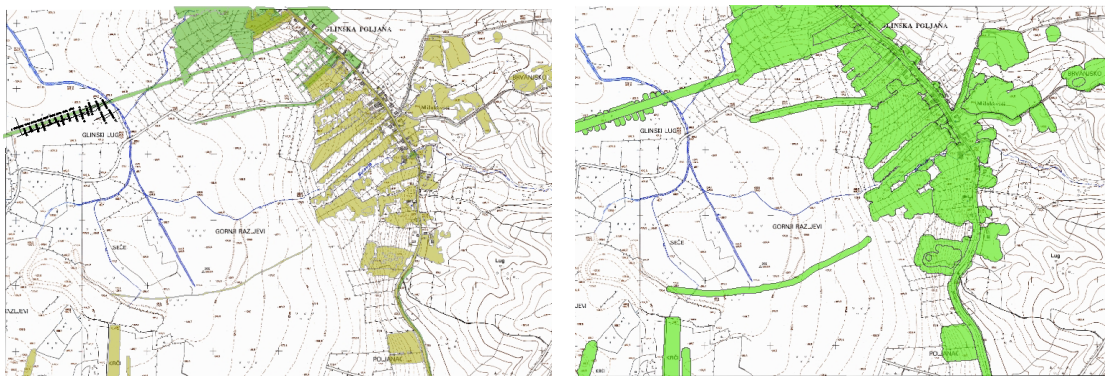

Figure 4-59 Data fusion from EU-project ARC. Left: Input features; Right: Safe Area output (using the union operator and halo).

4.5 Preliminary evaluation

We restrict ourselves to the land scenario. Mines in the surf zone can be detected by short pulsed laser system using the green wavelength but this application was not high priority for the study although mines on in water filled ditches and holes will definitely be a problem. After this literature review and feasibility estimation on performance we make an initial evaluation of the potential for different sensing techniques according to the Table 4-4.

	Surface land mines	Side-hitting mines	Buried mines	IDE (surface)	OXA (surface)
High res. 3-D laser radar (cm res./accuracy)	3	3	1	2	2
Reflection incl. retro reflection and potentially multiple wavelengths	2	2	1	2	2
Polarization	2	2	0	2	2
Fluorescence	2	1	1	2	2
Multispectral UV VIS NIR	2	1	1	2	2
IR	3	2	2	2	2

Table 4-4. Initial evaluation of different sensor techniques for land mine detection/classification. Code: 3 = high capability, 2 =some capability, 1= low capability, 0 = no capability

Some comments: We put the highest capability on the high resolution 3-D imaging sensing because it has some capability to see through vegetation and uses a signature that is very hard to get from a passive EO sensor. 3-D imaging has good capability for trip wires and on all surface lying objects but limited capability on buried mines although some potential could be explored to find some pattern in changes of the terrain height due to a mine field. IR imaging has high capacity for surface land mines and for buried mines compared to other sensors. The active reflection imaging including multiple wavelengths if necessary gives night and low daylight capability. The passive multi-spectral reflection imaging is feasible under daylight conditions. The reflection contrast can be high for man made objects against the terrain. An example is the glints obtained from glossy surfaces and retro reflection from side hitting

mined containing optics. Polarization imaging is also a strong indicator of man made objects. Fluorescence imaging might be of interest for detecting plastics or objects in dense grass by sensing the chlorophyll fluorescence. Some paints may also fluoresce but the technique is not well explored yet and the demand on high illumination intensity at UV or blue-green wavelengths, e.g. from a laser, may be too high to be practical and cope with the search rate need.

We suggest a scanning high range resolution laser radar to be the main emphasis for further studies regarding laser systems. Such a sensor could combine range, multi-wavelength reflection and polarization sensing in the same package. The sensor should use a detector array to be compatible with the high ground resolution (cm) and coverage speed demand. It should be integrated with passive sensing exploring advantages of such systems e.g. regarding area coverage, speed, low system complexity, flexibility and sensor maturity. In Figure 4-60 a possible configuration is outlined.

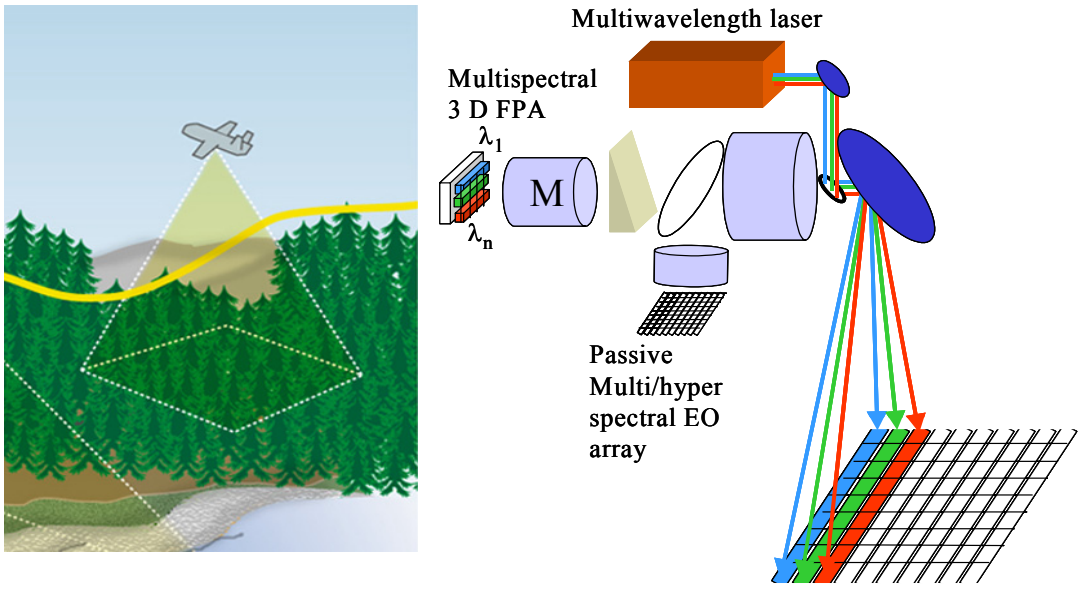

Figure 4-60. Potential for a passive/active EO system for mine detections.

4.6 Summary of the chapter

In this chapter we have tried to evaluate some potential sensor candidates for MOMS. For a deeper evaluation there is a need to collect more data and to perform more modelling and signal processing tests before the sensor candidates are chosen. Due to the large variability on target background characteristics anomaly detection and change detection may be a more proper way for detection than direct feature evaluation.

In Steinvall [107], the base line for different laser sensor performance is given. From this and the above descriptions we conclude that a scanning high resolution laser radar combining cm class resolution with (multi- or single wavelength) reflectivity and polarization would be a potential laser sensor to be combined with a passive multi- or hyperspectral sensor. The laser fluorescence techniques seem unpractical at least for the search case due to the high demand on laser power. Passive FLD (Fraunhofer line detection) using sunlight seems to be of interest.

At this stage of the project only subjective concluding remarks can be done.

- There is no support for excluding any candidate technique
- Other candidate techniques might be added to the list, especially regarding different sensor solutions for exploiting phenomenologies.
- It remains to be done to introduce an approach for systematic evaluation of sensors and combinations of sensors
- Statistical or mathematical evaluation of sensors and sensor combinations can only be made on a limited number of trials, scenarios and situations.
- Modelling and simulations can be used to extend the foundation for evaluation.
- The final recommendations regarding sensor systems will probably be made based on subjective expert reasoning, but with input from results and experiences achieved during project life time.

5 Modeling and Simulations

This chapter deals with a survey of modelling and simulation (MoS) technologies of relevance for MOMS.

A presentation of the EO modelling and simulation work in general terms follows by the FOI work in general and the more specific work concerning land mines. FOI have well acknowledged and established capacity in these areas.

5.1 MoS in order to increase the knowledge

At development of large and complex information systems a reliable simulation environment is needed where different parts and phenomena's can be studied and pretended. Modelling and simulations, MoS, is often used as a bridge between analysis and experiments. This is also discussed in [133]. In this chapter the modelling and simulation concepts are used in at wide sense. It is important to take into consideration that the used models are as long it is possible verified. This means that the model is designed right according to the specifications. The models should also be validated. This means that the model replies against the reality with certain approximation. Balci discuss this important process in [134].

Models are needed in different levels. Likewise they could be formulated in a simple or more advanced manner. Development of detection and data fusion methods require access to synthetic data in a big scope. In a study by RAND institute [4] it was established that no single technology available today seems to be sufficiently effective for detection of all types of mines in different conditions, so combinations of sensors, algorithms, fundamental knowledge, data fusion etc. could raise the probability of detection. RAND suggest dedicated physical based models where more effective methods, as well as models itself, could be developed to enhance the possibilities to predict signatures for detecting mines using EO systems.

Models that are developed can have various aims, for instance:

- Interpretation and analysis of the scene
- Complements to, and interpretation of experimental data
- Analysis and evaluation of experiments, inclusive signal processing
- Sensor-, atmospherical-, target and background effects due to influences and interactions
- Target and object interpretation
- Detection methods
- Prediction studies
- Model based statistical data bases

At development of models, access to experimental data, preferably calibrated, is required. The area of MoS is not an isolated area without collaboration with as well experiment as analysis and signal treatment should take place continuously.

A number of coupled physical phenomena have to be considered in modelling of EO signatures. Modelling of surface properties, geometry, heat and mass dependent properties, atmospheric effects, vegetation and radiometry are all needed in order to calculate the in-band radiance detected by EO sensors. There are a large number of models and methods, with varying degrees of complexity and accuracy, for calculating the individual physical processes involved in modelling of EO signatures from targets and backgrounds.

The areas that needs to be studied on the basis of relevance for MOMS describes below.

5.1.1 Modelling areas:

- Specific objects. Precise signature models and studies of individual mines/UXO in three sub areas:
    - Temporal analysis. Probably the area that needs to be most complex described. This includes geometry and material composition in three dimensions. Further is required a good description of the surface's properties as emissivity, reflectivity and possible a BRDF-description. Time dependent.
    - Spectral and multispectral analysis. The studied objects geometry and the surface wavelength dependent properties are mainly studied. The surface's polarisation influence is probably important.
    - Spatial analysis. The objects geometry along with the surfaces signature properties and different aspect angles is needed in order to predict the objects signature. Three dimensions.
- Background models in two areas:
    - Buried objects.
        - Sensors without thermal ability can only consider indirect evidences for occurrence of buried objects. Thermal sensors can detect buried objects due to the presence of an objects itself or due to burial effects. Complex task. Needs information of several physical processes.
    - Surface laid objects.
        - A statistical description of the local environment, in several scales, is needed in order to distinguish mines/UXO from natural background objects.
        - A physical based approach gives the opportunity to predict the characteristics of the local background due to influence from weather.
- Interacting between object and environment:

- Depends on the studied sensor. To predict surface temperatures require extensive models. Atmosphere properties are perhaps the dominating factor. The position of the sun influences largely on the signature of the object due to heat transfer while shadow effects has an big impact on multispectral and spatial analysis. For laser systems it is possible to separate geometric properties from surface properties.

5.1.2 Simulation areas:

- Thermodynamic simulation for analysis and prediction of IR signatures of individual objects. Simulations are based on experimental data for studies of different parameters.
- Simulations of scenarios for analysis and studies of system performance. Simulations as a base for planning field measurements.
- Simulations of mines/UXA based on both experimental and synthetic data for development and analysis of different detection algorithms.

5.2 General modelling tools for objects and environments

A general overview of EO signature modelling tools is presented in [135]. Another paper describing the target in background problem is presented in [136] also a simple thermal model for natural background elements is described in [137] At FOI several commercial programs have been used for optical signature predictions. These are for example CameoSim, RadThermIR and Sensorvision. Some of them have been used for quite some time and others are more recently acquired. Validation of the programs is an important task that has to be fulfilled. The validation work is also an excellent way of improving the knowledge of the program and helps the development of efficient methods for the actual use of the programs. Many of the programs require huge amounts of input parameters and the work needed to properly assign values to these parameters should not be underestimated. Validation of commercial programs is of course being performed at other institutions [13, 138-141], and the work at FOI is to be seen as a complement to these previously reported validations. Validation work carried out by FOI with these modelling tools have been reported in [142] and more specific in [143, 144].

SensorVision is a VEGA-based application that produces IR scenes in real time with a certain amount of simplifications in order to obtain the real time capacity.

The Camouflage Electro-Optic Simulation System (CameoSim) is an advanced IR program aiming at producing high fidelity physics based images originally applied to camouflage assessments. With information on 3D-geometry, material properties, weather data and simple sensor characteristics (such as position, field of view, resolution and spectral response) CAMEO-SIM generates images. The radiation transport equations are solved on an image pixel-by-pixel basis to form a spectral-spatial representation of the radiation arriving at the front of the optics.

RadThermIR is a 3-dimensional (with some restrictions) heat transfer program which predicts the temperature distribution for objects and backgrounds and also a prediction of the actual IR radiance, or signature, is possible. RadThermIR models 3-D conduction, convection, and multi-bounce radiation and solves the equations using algorithms based on Finite Difference Methods (FDM). Material properties, e.g. density, heat capacity, heat conductivity and paint or surface properties, and boundary conditions are read from built-in or imported data files, wavelength dependent properties and/or parameter constants. The weather that is influencing the model is imported as text files or modelled by the built-in algorithms.

All three programs have their specific applications and they therefore complement each other. FOI has previously showed how RadThermIR can be used for improving the target signature modelling of SensorVision [111]. The software's handles wavelengths between 0,3 up to 20 micrometers. In a close future the two programs CameoSim and RadThermIR will run close together, with respect to sharing and iterative interaction of data through the solving process, on the same computer.

Examples of FOI modelled and calculated scenes and objects are shown in figure 5-1. Normally these simulations are calculated for time periods between some minutes up to several days.

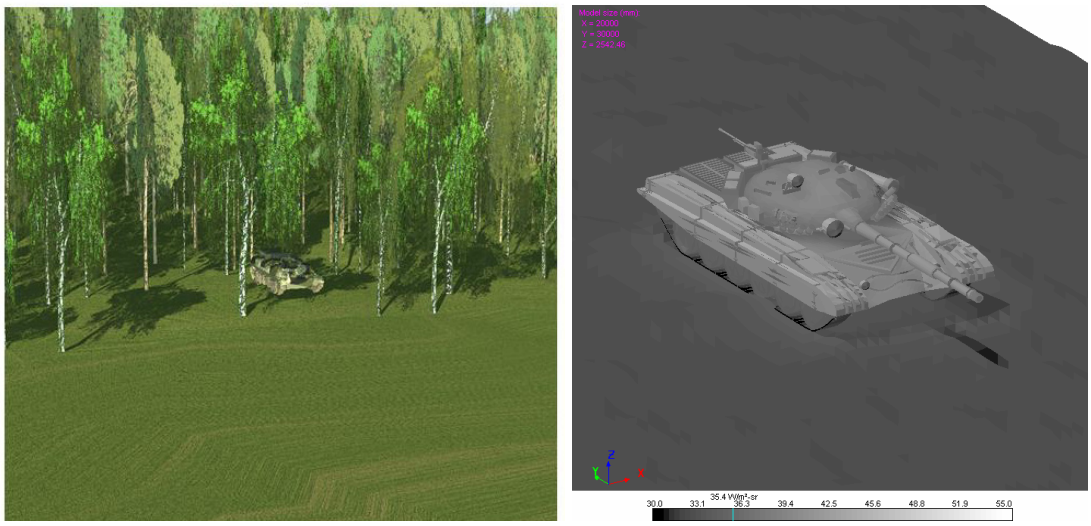

Figure 5-1. Snapshot from a, Left, CameoSim VIS rendering of a vehicle in a forest background, Right, RadThermIR calculated LWIR image of a main battle tank.

Input data to the simulation software consist of for instance material thermal and optical (spectral reflectance) data, triangulated (CAD) models for terrain and/or objects, weather data and model and rendering options. When using SensorVision or CAMEO-SIM a sensor response function should also be provided. The main output from the simulation software is radiance maps of the synthetic 3D scene or objects. Calculated surface temperatures or apparent surface temperatures can also be obtained as output data.

In order to exemplify differences between the three simulation software, we have listed some features of the software in table 5-1. In SensorVision a number of simplifications and approximations have been used in the implementation of the radiation transport equation in order to reach real time performance. A more accurate solution of the radiation transport can be obtained by using CAMEO-SIM. A major difference between RadThermIR and the scene simulation programs SensorVision and CAMEO-SIM is that RadThermIR models three-

dimensional thermal conduction while SensorVision and CAMEO-SIM use one-dimensional conduction models. This makes it possible to model internal structures more accurately with RadThermIR.

	SensorVision	CAMEO-SIM	RadTherm IR
Dimensions in heat conduction	1D	1D	”3D” + internal sources (finite difference)
Real time	Yes	No (but depends on method)	No
Rendering and radiometric solution	Simplified ray tracing, simplified radiometry	Ray tracing with MonteCarlo etc. Accurate radiometry	Ray tracing
BRDF	No, but specular lobe	Yes	No, but specular lobe
Weather history in thermal solution	No	Yes	Yes
Atmospheric modelling	MOSART (isotropic atmosphere)	MODTRAN4 (3D parameterisation)	No (but sky irradiance according to Subarctic summer model)
Interaction between objects	No	Radiometrically, thermal shadowing	Thermally and radiometrically
Scene simulation	Yes	Yes	”No, not in general”

Table 5-1. Examples of differences between the FOI used simulation software

MoS will facilitate the understanding of phenomena’s and thereby support the analysis and the development of algorithms. MoS will also support predictions of e.g. when during the day and night cycle that the best conditions for detection exists. RadThermIR and CameoSim is examples on MoS tools for objects and backgrounds.

From the beginning the chosen solver for the calculations was THAFEM, Thermal and Heat Analysis by Finite Element Method, see Loyd et al.[145]. Later the modelling environment was transferred to the more general tools Matlab and FEMLAB [146] which gives the possibility to study details and physical phenomena more in detail and also in direct cooperation with analysis- and development of methods. The open Matlab/FEMLAB environment permits also directly linking of experimental data to the signal treatment area. Also these sets of models are based upon physical laws implemented with FEM. One reason for using FEMLAB-based models is the higher flexibility and the possibilities to couple different physical problems e.g. heat transfer, mass transfer and fluid mechanics in the same model. Also the possibilities to calculate in three dimensions and the collaboration with image processing algorithms are quite important factors.

An example of simulation result gives the temperatures in all nodes in the FEM model, for every time step during the calculated period. We can choose to show the results in spatial or temporal dimension. A simulation can give the interesting answer on the question “Do we have favourable contrast for successful detection of landmines, and when?”. The modelled objects could be buried as well as surface laid. In figure 5-2 is shown some simulation results, carried out at FOI, for a specific time and weather condition.

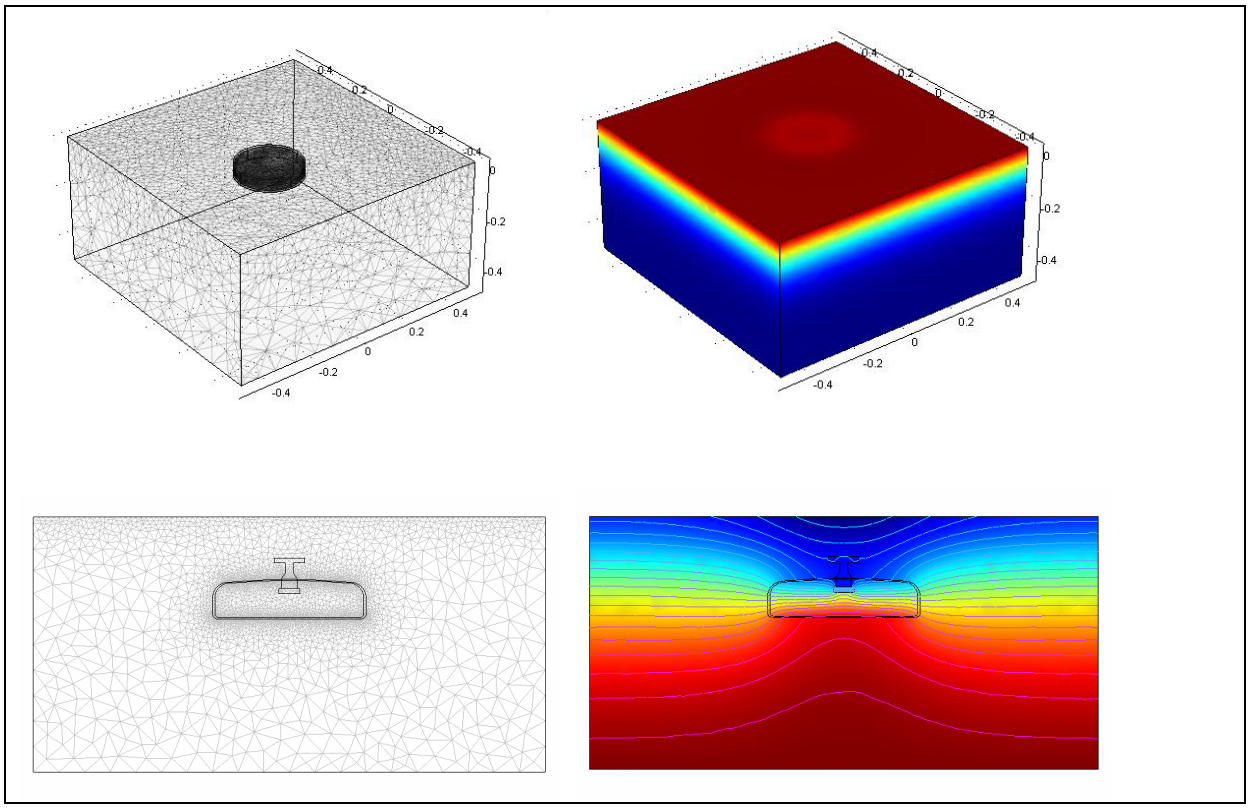

Figure 5-2. Examples of buried mines. To left, meshed models. To right, simulation results.

5.2.1 The vegetation layer

The MoS aspects on the vegetation layer is a very complex task. The purpose is to explain and predict different phenomena in the layer between the soil and the atmosphere, thereby enhancing the detection of hidden and buried objects. Some of the developed models build on statistical or empirical results, others on strictly physics-based equations. The easiest way to take the influence from the vegetation layer into consideration, for the energy transports, is to calculate its presence as a dampening layer/factor. This approach is not good enough due to active sensors aspects. Here needs nearly a modelling resolution close to individual leafs and single blade on grass.

A survey of different background models, specific for thermal effects, and how to handle the influence from the vegetation layer can be found in F G Wollenweber [14], W R Reynolds [15], Clement [16] and in Jacobs [17]. The vegetation canopy and the Leaf Area Index (LAI) is discussed by Ballard [24, 25] and Lhomme [26]. At present, there is no accessible universal thermal model for terrestrial surface background behaviour, only rough approximations.

5.3 The more specific case of physical modelling of mine signatures

Extensive measurements have been performed and a number of models with different levels of complexity have been developed in recent decades. The purpose has been to explain and predict different phenomena in the layer between the soil and the atmosphere, thereby enhancing the detection of hidden and buried objects. Some of the models developed build on statistical or empirical results, others on strictly physics-based equations. Some relevant papers dealing with MoS of the land mine problem are presented in Vavilov [147], Khanafer [148], Martinez [149], Muscio[150], Miller [19], Mahmoodi [151], Pregowski [152], McFee [153], Sendur [154], Cathcart [155] and Baertlein [156]. The most authors have written several papers in this area but are only mentioned by one paper here. At FOI several papers have been written by Sjökvist [133, 157-164].

One of the objectives of the ongoing modelling part of the research work carried out at FOI has been to improve the understanding of the heat and mass transfer mechanisms around buried objects with the purpose to utilize the most favourable conditions for detection. This area is basically presented in Hartley [165]. The detectable contrast depends to a great extent on the history and the actual environmental properties interacting on the surface and the buried objects. Other issues are to support image analysis and feature extraction algorithms and as a decision support tool to predict when to carry out flights to achieve maximum contrasts.

During the last five years a sensor modelling tool for three-dimensional laser radar has been developed [102, 166]. The purpose has been to get a tool for active sensor modelling that is an appropriate compromise between speed, complexity and user friendliness. The model takes into account the laser source properties as well as the receiver characteristics, together with the atmosphere and target reflection and geometry properties. Along with the increasing performance of computers more and more complexity has been built in, but always with a near-real-time simulation in mind. New requirements when modelling sensor systems used in searching for mines are the geometry and other features for low vegetation, i.e. bushes or grass. This has due to the small scale been disregarded in the previous work. It is a complex task as mentioned in section 5.2.1, but is very important to understand the mine searching capabilities.

5.3.1 Examples of simulation results

Figure 5-3 shows some simulated effects from Sjökvist [161] due to different boundaries and the depth of burial and how they affect the temperature difference on surface above the buried mine subtracted with the undisturbed area. Increased cloud level to 50% (N=0.5) is modelled and shown, but do not differ so much compared with the basic model. The basic convection coefficient model is “McAdams plate model” another model based on $h = a \cdot v^m$ is shown in the figure but have minor effect compared with the basic model. Also if we double the windspeed the effect is marginally. Decreasing the irradiance on ground from sun by 50% gives a slight decreasing of the contrast. The original burial depth of the hole is 20 cm by changing this so the new burial depth is 15 cm gives a large effect on the surface temperature contrast.

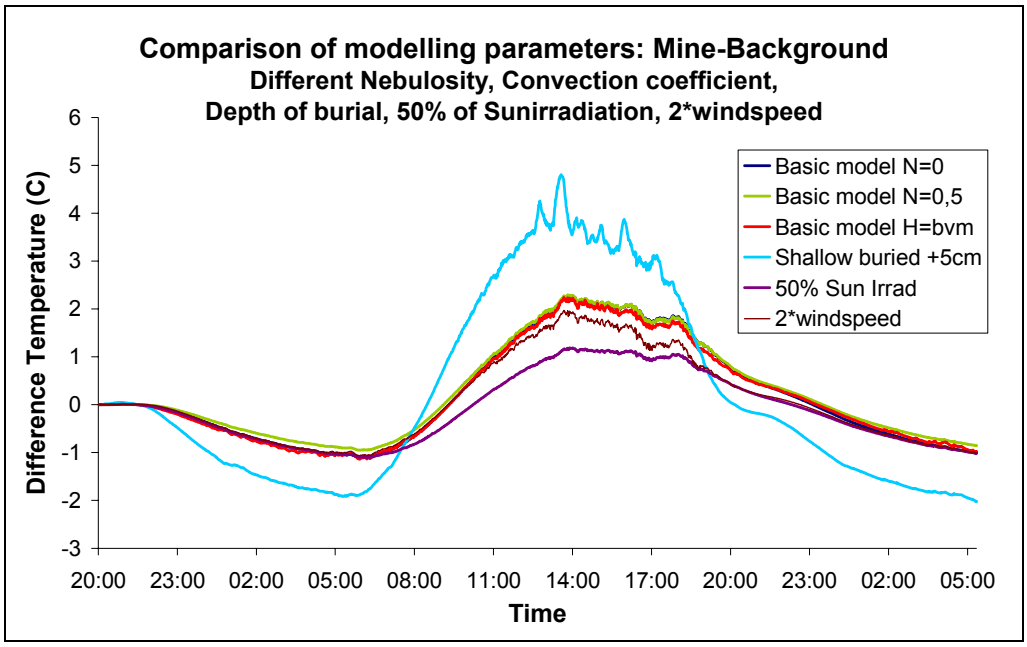

Figure 5-3. Temperature differences between a point above the buried mine subtracted by the local background. Comparison of the effects of different modelling parameters: The basic model. Different Nebulosity, Convection coefficient, Depth of burial, 50% of sun irradiance and double windspeed

Another example of how the MoS work could increase the understanding of phenomena is shown in figure 5-4. By using the Femlab code with different casing parameters some interesting result could be obtained. In this simulation real data from a field campaign is used as boundary conditions. The modelled object is a shallow buried and visible AT mine see figure 5-4.

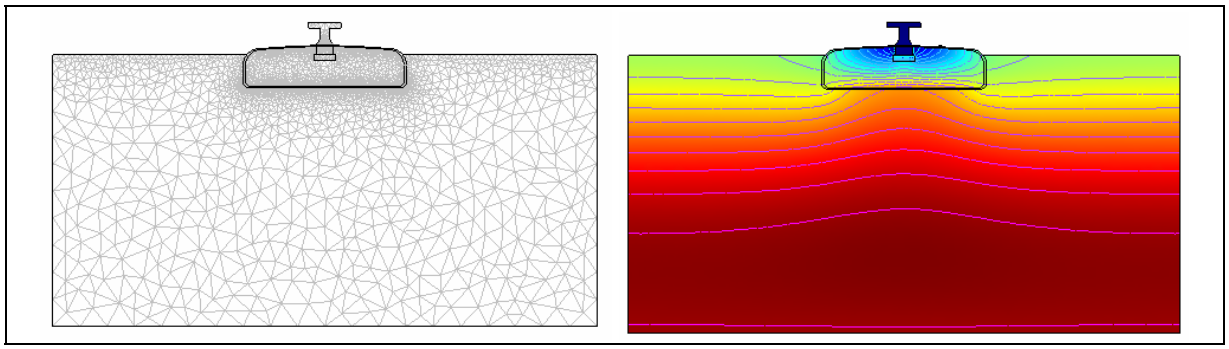

Figure 5-4. The model. Left, the mesh consis of approx 10000 elements. Right, The isotherms for one time step at the end of the diurnal simulation.

Those parameters that are changed are, casing material and colour. The diurnal result during a 33 hour simulation is shown in figure 5-5. The curves represents a point on the upper side on the half buried mine.

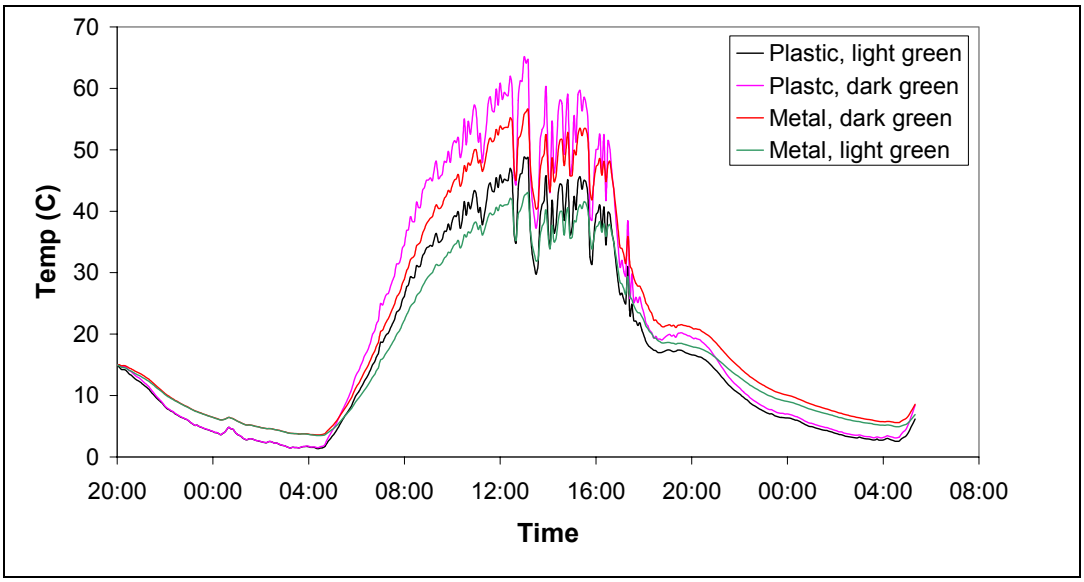

Figure 5-5. Effects due to different casing materials and colours.

A simple example of active sensor modelling is shown in Figure 5-6. A 3-D laser radar is simulated measuring a cylinder on flat ground. Future simulations will also have to include vegetation, more complex reflection functions, atmosphere effects and receiver and optics characteristics.

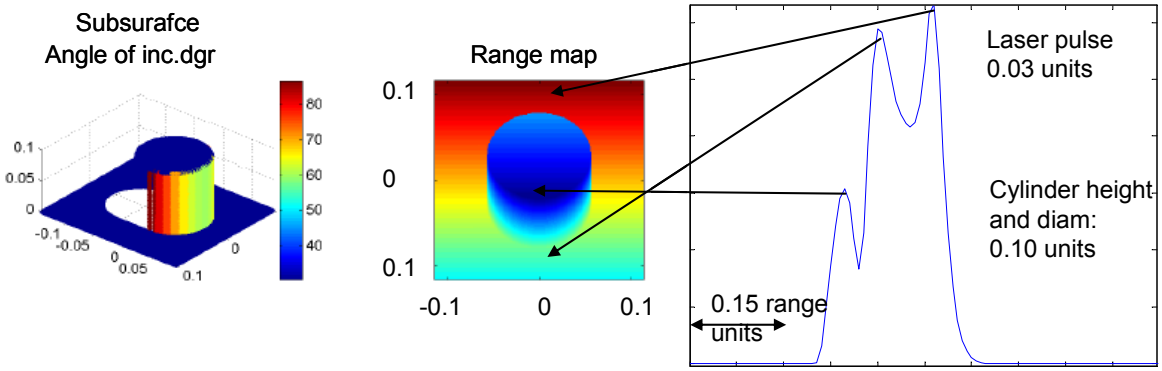

Figure 5-6. Partial results from a simple active sensor modelling. The middle image shows the distance map, while the left image shows the angle of incidence on each part of the target. The right graph shows the temporal response for a one pixel sensor.

5.3.2 The use of thermal inertia in MoS

The temporal variation of ground surface temperature reveals several properties of the ground. In the area of remote sensing a very useful method is the use of thermal inertia. The definition of thermal inertia [167] is: The resistance of a material to temperature change, indicated by the time dependent variations in temperature during a full heating/cooling cycle (a 24-hour day for Earth); defined as $P = (Kc\rho)^{1/2} = c\rho\,(k)^{1/2}$. Interpreting thermal data and images of temperature distribution over an area is complex. In many instances, one must look for

patterns of relative temperature differences rather than the absolute values, because of the many complex factors that make quantitative determinations difficult, such as:

- Number and distribution of different material classes in an instantaneous field of view
- Variations in the angle of thermal insolation relative to sensor position
- Dependency of thermal response on composition, density and texture of the materials
- Emissivities of the surface materials
- Contributions from geothermal (internal) heat flux; usually small and local
- Topographic irregularities including elevation, slope angle, and aspect (surface direction relative to the Sun's position)
- Rainfall history, soil-moisture content, and evaporative cooling effects near the surface
- Vegetation canopy characteristics, including height, leaf geometry, and plant shape
- Leaf temperatures as a function of evapotranspiration and plant stress
- Near surface (1 to 3 meters) air temperature; relative humidity; and wind effects
- Temperature history of the atmosphere above the surface zone
- Cloud-cover history (during heating/cooling cycle)
- Absorption and re-emission of thermal radiation by aerosols, water vapor, and air gases

An example from FOI shows the variation in apparent temperature due to the heat capacity and heat exchange properties for different parts on the ground. The simple model used is that the current temperature depends on the sun radiation during some time interval before. A series of LWIR images where recorded on a field where conceivable garbage, which can be found in post-war fields, had been put out is shown in figure 5-7. The figure shows to the left the first thermal image from a three-hour sequence. In the right part the time constant due to the heat capacity is shown. The time constant is estimated from around 40 frames, with a frame-to-frame time of five minutes. However, due to several simplifications the right image is only related to the time constant. As expected the heat time constant image has a great similarity with the original image.

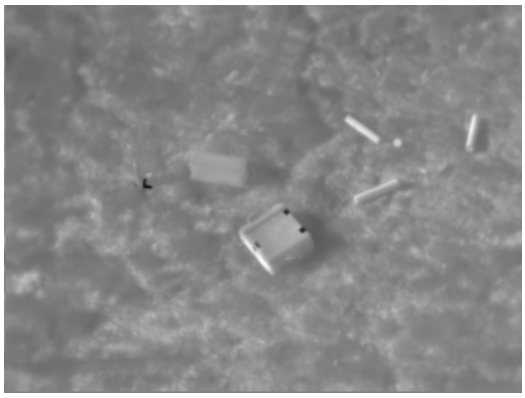

a

b

Figure 5-7 Time constant from a sequence of IR frames. In (a), the first frame of a sequence is shown, and in (b), the time constant image is shown. In (a) bright parts correspond to a high apparent temperature and dark parts to low apparent temperature. In (b) bright parts correspond to high time constant and dark parts to low time constant.

5.4 3-dimensional model of mines and UXOs

3 dimensional geometrical models developed in MOMS for further studies are shown in figure 5-8. These models are correct according to scale. The aims with these models are to study their arising signature due to different vegetation backgrounds and different weather conditions, also the influence of different surface properties are a topic for further research.

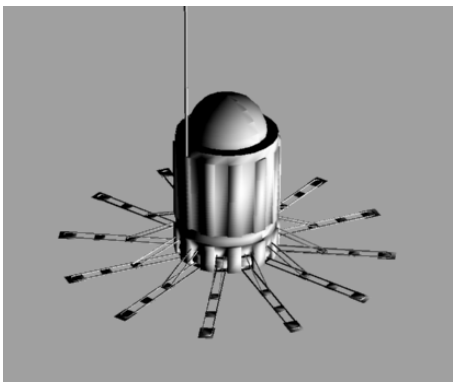

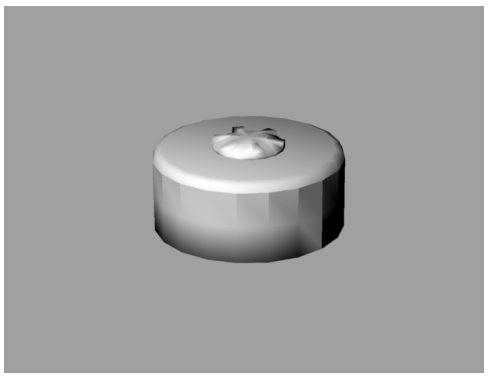

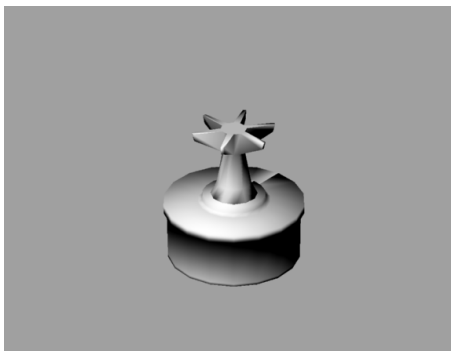

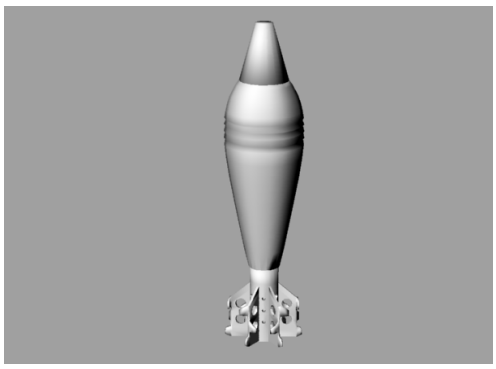

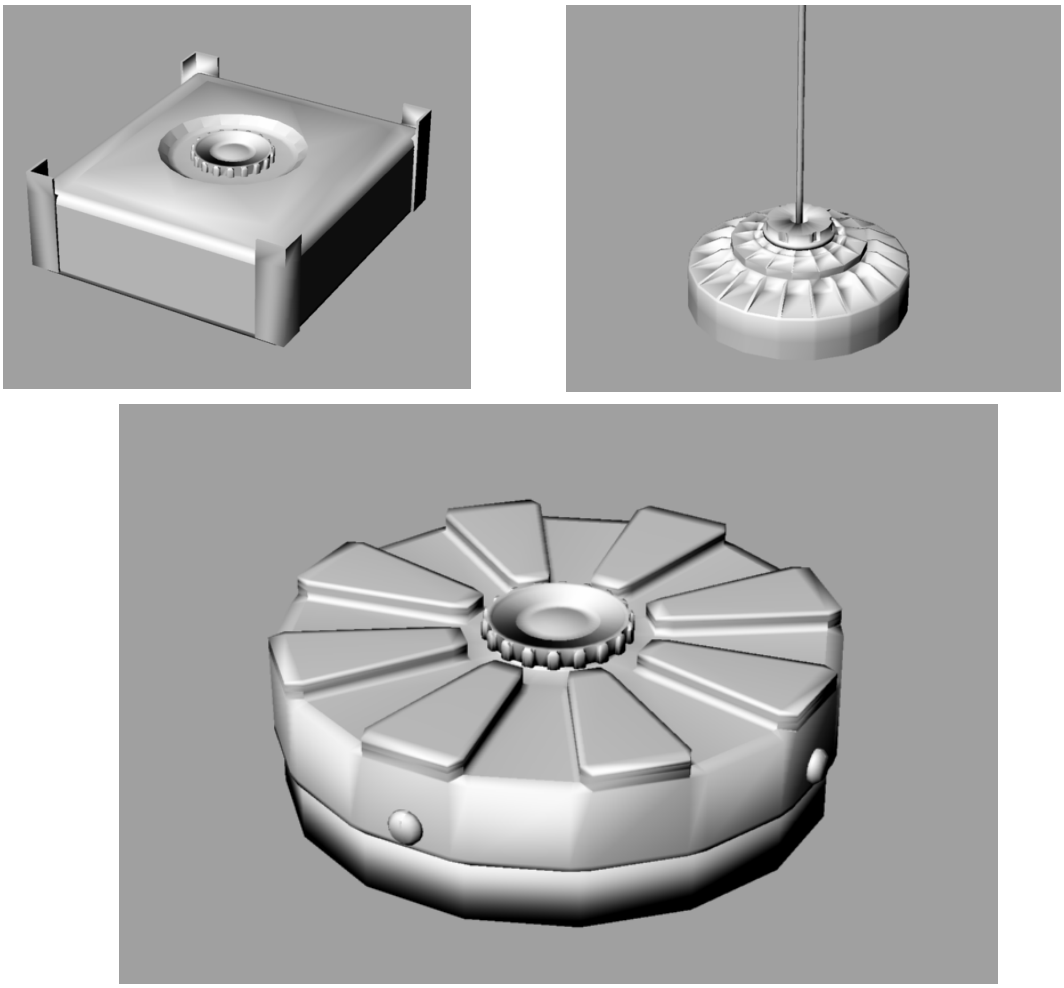

Figure 5-8. 3-dimensional models of mines. From upper left: AT-2, DM-11, PMA-2, Sving-8, TMA-5, TMRP-6, and TMA-1

5.5 Summary of the chapter

This chapter discuss the modelling and simulation aspects concerning buried and surface laid objects. Both active and passive methods and models are presented.

The conclusion of own work and all refereed work is that the MoS needs an emphasized focus to replies against expectations due to reliable outputs. FOI holds today experimental equipment, software (both commercial and in-house developed) and knowledge to support the development of validated and verified models. The validation and verification work of used codes are also important for reliable results.

Wise used the MoS could be used as a bridge between analysis and experiments, and also for increase the possibilities with signal processing.

6 Signal and image processing

In this chapter, we present an overview of existing signal processing techniques related to mine detection. In Section 6.1, we review literature for signal and image processing based on IR, visual and laser radar data. In Section 6.2 we illustrate some of the ongoing mine detection-related work at FOI. Results are presented in chapter 8.

The data processing can be divided into five different steps, each with a specific processing goal. In the first step a piece of land, large or small, is searched for small areas where the properties are considered unnatural. This can be done, for example, by *anomaly detection* or *change detection*. In *mine field detection* a larger piece of land is analyzed than when single mines are the subject. In the next step, the small areas are analyzed for *mine detection*, where a set of pixels/voxels are determined to be either mine or non-mine (background). The mine detection process may contain several processing step to reduce the number of false alarms. The objects in the scene that are detected as being mines can be further analyzed in the *mine classification* step, where the mine class (AT or AP) is determined. In *mine recognition* the mine's model/make is determined (AT type 1 or 2) and finally in *mine identification* detailed physical characteristics of the mine is detected (AT type 1 with explosive type A or B). In some approaches several steps in this hierarchy can be treated simultaneously. Previous studies have shown that anomaly detectors and even sophisticated ATR techniques fall short of the performance achieved by human analysts for mine detection [168]. However, considering the hazards related to manual, on-site inspection automatic methods are highly desirable.

6.1 Literature survey

In this section, we describe approaches to anomaly detection (Section 6.1.1), change detection (Section 6.1.2), mine detection (Section 6.1.3), sensor fusion (Section 6.1.4) and 3-D shape detection (Section 6.1.5).

6.1.1 Anomaly detection

The goal in *anomaly detection* is to find small regions whose characteristics deviate from those of the surrounding background clutter, without worrying about what has caused the anomaly. However, the ability to pinpoint certain suspicious-looking regions for further analysis is of vital importance, since an explicit search for mines may be inhibited by atmospheric disturbances, natural variations, poor resolution, lack of proper sensors, or simply ignorance of the characteristics of the mines.

From the signal processing point-of-view, existing methods for anomaly detection differ mainly in the way the background characteristics are modelled. In the RX algorithm [169] the background spectrum (mean vector and covariance matrix) is estimated locally using a sliding window. Anomalies are then detected as being significantly different from the background, in terms of a large Mahalanobis distance. A key assumption in the RX anomaly detector is that

data corresponding to the background and the sought-after target are normally distributed with different means but the same covariance matrix.

In the kernel-RX algorithm [170] the assumption is that the data consists of two Gaussian distributions in some high-dimensional feature space. By mapping the original data to this feature space, higher-order correlations between spectral components in the data that are not detected with the original RX algorithm, can be captured. The algorithm showed improved performance over the conventional RX algorithm when applied to a couple of hyper-spectral image sets.

An anomaly detection approach based on Gaussian clustering was presented in [171]. A probabilistic model of the background is created using an adaptive Bayesian classification algorithm, with *k*-means clusters providing the initial state for the algorithm. Anomalous pixels are then detected as being sufficiently dissimilar to the clusters. The experiments were carried out on two multi-spectral IR (6 bands) datasets. A comparison with the standard RX-algorithm was performed, indicating a favourable performance of the proposed technique. In the paper, a method to add local adaptivity (re-estimating cluster parameters locally) is also described. In [172] a similar cluster-based approach is presented, the main difference being that the image is segmented using Vector Quantization instead of the *k*-means algorithm. The algorithm was tested on some multi-spectral satellite images (visible, reflective IR and thermal bands). Instead of using Gaussian clustering, Hazel [173] suggested using a Multivariate Gaussian Markov random field approach for segmenting the scene, which seems to result in better ROC characteristics. Like all methods based on unsupervised clustering, these techniques suffer from the delicate problem of finding the best number of clusters, as this choice strongly affects the performance.

Chang and Brumbley [174] proposed a Kalman filtering approach, based on a linear mixing model. The state and measurement equations correspond to the abundance equation and linear mixture model, respectively. The idea is to update the abundance equation for pixel *k*, predict the abundance at pixel *k+1* and then detect anomalies at pixels where the prediction differs substantially from the observations. Using this approach, improvements over Orthogonal Subspace Projection (OSP) methods [175] were demonstrated on multi-spectral images. In this context, it should be mentioned that the OSP techniques were originally proposed for hyper-spectral data.

Furthermore, the delicate problems associated with accurate model and parameter selection were recognized and briefly discussed.

In the CLEARFAST project [176] mathematical morphology is used to select small objects brighter than their surrounding background. They also perform image registration and mosaic processing.

6.1.2 Change detection

Like anomaly detection, c*hange detection* is also closely related to the de-mining problem. It refers to detecting a (small) region in the scene that has undergone significant change from one moment in time to another. A major problem is to distinguish between changes that result from human activity (e.g. digging marks) and perceived changes due to other effects (e.g. natural variations, different sensor characteristics, noise).

A very simple approach for detecting *spectral* changes is to quantify the dissimilarity between every pair of corresponding data vectors in two consecutive images, e.g. by computing the Euclidean distance and detecting changes by thresholding. Analogously, *spatial* changes can

be detected by comparing 3-D data, e.g. acquired with a LIDAR and detect changes as 3-D points/structures with no correspondence in the previous data set. However, such simple approaches are typically subject to significant problems in practice, since false response occurs even at slight misregistration of the data. In fact, the general "mosaicking" problem is a field of research of its own.

The approach presented in [172] was also applied to change detection. This is performed without explicitly comparing the pixel values between the images. A background cluster model of image I_t is first formed. Then, these clusters are mapped onto the consecutive image I_{t+1}. If no significant change has occurred, the data in I_{t+1} is still approximately Gaussian. The appearance of pixels at a significant Mahalanobis distance from the clusters indicates that objects have appeared. Disappearing objects are detected by running the detector in the reverse direction, i.e. first clustering I_{t+1}. The approach was claimed to be relatively insensitive to image misregistration (≤ 4 pixels).

In [177] two techniques for change detection based on difference images are presented. It is demonstrated that change detection results obtained by treating pixels as independent of one another can be improved by taking inter-pixel class dependency information into account. The rationale is that a pixel belonging to a certain class is likely to be surrounded by pixels belonging to the same class. Obviously, such an assumption requires higher spatial resolution (alternatively larger objects). As both techniques require a priori knowledge about the statistical distribution of changed and unchanged pixels in the image, an Expectation-Maximization optimization scheme is adopted for estimating the respective statistical distributions.

In [178] Yamamoto *et al.* proposed a 3-D segmentation (split and merge) technique for change detection in a *sequence* of multi-spectral images. The image data is represented as a 3-D block that is first split using a division rule based on Mahalanobis distance and Student's *t*-test. The resulting sub-blocks are then merged into clusters, after which cluster boundaries perpendicular to the time axis are identified as temporal changes. The technique was applied to multi-spectral and multi-temporal images. It was claimed that applying this block-based technique on multi-temporal images may lead to reduced response to spurious, noise-induced changes. The proposed framework allows for observing areas at different times with different sensors. However, in order to be able to perform meaningful clustering along the temporal axis, it requires registration of several (>2) images.

Detection of mines on a road is the subject of the paper by Donzelli *et al*. [179]. The system is airborne, with an operator detecting the differences between a previous sequence and the currently sensed one. The signal processing, mainly an anomaly detector, acts as a cue to the operator helping him or her in difficult situations. The cueing algorithms work in real time with stabilization and mosaic-building without delay.

6.1.3 Mine detection

In order to determine whether a certain anomaly or change is really due to the presence of a mine, a classification has to be performed, based on *a priori* knowledge about the expected mines e.g. related to spatial, spectral or thermal characteristics.

Hardly any references deal with the problem of detecting mines using spatial operators. The main problem is the large number of mines that exist that have different sizes and shapes. This often leads to an unacceptable amount of false alarms when trying to detect and classify mines. Some spatial operators that utilize invariant characteristics are tested on images from the infrared sensor. The properties used are curvature [180], convexity [181], symmetry [182]

and Laplacian operator [183]. Normally, three scales (degrees of resolution) are used in the detection process. There exist a lot of other features that can be used in this connection (e.g. Gabor and Harris) and are described in the literature concerning image stabilization, where one problem is to find invariant features to be used as landmarks.

In [110] it is shown that taking spatial characteristics of the sensor response into account may lead to improved detection performance, compared to treating each pixel individually. A similar idea is pursued in [184]. The main difference lies in the way the spatial information is incorporated. The detection in [110] is performed via two cascaded 2-D generalized likelihood ratio tests of vector corresponding to the measurement for the neighbouring pixels. In [184] the sensor response is thresholded, giving an initial set of possible target points. The number of possible target pixels is reduced by only keeping the pixels around which a certain number of neighbours are above the threshold. Both groups verify their approaches with EMI sensor data provided by DARPA. However, only a limited dataset mainly containing metal calibration objects was investigated. Still, both techniques were considered useful for reducing the number of false alarms.

Martínez *et al.* [185] address the problems of detection and depth estimation of surface-laid and shallowly buried landmines from IR images. First, anomalies are found as deviances from the expected thermal evolution when no buried objects are present. For this purpose, a cellular neural network (CNN) is used, with expected (modelled) and actual (measured) data corresponding to four time instances as inputs. The design and training of the discrete-time CNN is described in [186]. Each anomaly is classified as *mine* or *unknown* by comparing the measured data to a thermal model corresponding to a mine at a particular depth. The depth that gives the smallest error indicates the presence of a mine, provided that this error is smaller than a threshold. The approach was demonstrated on a sequence of IR (8-9 μm) images acquired in an outdoor test field (10m x 3m x 1.5m) containing 43 objects, among which 34 were mines, with a spatial resolution of about 1.5 cm/pixel in each direction. The final detection and false alarm probabilities for the experiments were 0.92 and 0.25, respectively. It should be noticed that this approach requires data to be collected during a relatively long period of time (45 min in the experiments) which obviously severely limits the speed with which an area can be investigated. The authors note that the training of the image processing system must be repeated for any new physical environment or atmospheric condition, which typically takes 1-2 hours [187].

Bowman, *et al.* [188] presented phenomena that can be registered with a hyper-spectral IR camera, when measuring surface and buried landmines. Temperature and spectral phenomena were reported. Mines are spectrally distinct from the major background in the scene, they tend to be more homogeneous than mixed backgrounds and they are spatially-localized phenomena in contrast to the background which usually is either, not both. Based on the phenomena study, a mine detection algorithm is outlined. First the hyper-spectral data set is reduced by spectral projections. Then an adaptive spectral clustering is processed and each pixel is classified. A local area around each pixel is then analysed by a spectral likelihood filter and clusters are formed. Finally, the clusters are analysed using size and shape constraints. Performance of the algorithm is not presented.

In [189] a mine detection system and results of field tests are described. The goal is to locate and detect buried and surface land mines. A six band visual camera with 720x480 pixels is mounted on a helicopter. The helicopter flies on 250-450 ft (75-135 m) elevation over a field containing various metal and plastic AP and AT mines and mine surrogates. The pixel size on ground varies between 1.1-2.5 cm/pixel. The image processing, described in detail, consist of pre-processing, pixel classification, region formation and post-processing. The pre-processing is a high-pass filter to remove artefacts in sensor data. Each pixel is then classified by

calculations of nine amplitude histograms for a local area. The histograms features are loaded to a probabilistic neural network for classification. Each pixel is classified as either “mine” or “background” and the results are stored in a binary image. The binary images are subject to event region formation using the Bhattacharya distance. Finally, size and shape constraints are applied to lower the level of false alarms. The metal mines were detected with high probability, although the level of false alarm was quite high. The detection of plastic mines was less successful, as those have spectral characteristics similar to the background in the visual wavelengths. Further, the current post-processing lowered the detection rate.

Shimoi *et al.* [190] describe a remote mine detection system with an IR camera (8-12 μm). The system is mounted in a crane to receive forward-looking perspective. The system hardware and software concept is described. The mined area is sprayed with cold water (4 ºC) and the temperature gradient is studied. A sequence of IR images is collected after the area has been sprayed. The image processing is based on subtraction images. The subtraction images are searched for cylindrical objects, i.e., objects of elliptical shape. Also, shading effects are removed by local normalization and then a binary image is created. The binary image is subject to region division and labelling, not further described.

Thermal modelling used for identification of mines is reported in [29, 191]. Nguyen *et al.* study the inverse problem to solve for mine parameters such as position under the ground and different size parameters. Good agreement between calculated and actual parameter values was obtained.

A hyper-spectral sensor was used for landmine detection in [192]. The visible sensor covers the band 400-1000 nm and the short wave infrared 850-2450 nm. Preliminary indications are that a simple generic classification decision boundary should be able to distinguish surface-laid landmines from many human-made artefacts and natural materials. No details were reported. An example of fusing aerial multispectral images has been shown by Bajic [193]

In Wolff *et al.* [194] argues that two wavelength bands are just as effective as a multi-band suite of bands in differentiating objects from background. They use two broadband spectrums: visible and shortwave infrared. In remote sensing two ratios are commonly used to estimate cultural land area usage, the ratio vegetation index and the normalized difference vegetation index. For cultured features these indices are close to one but significantly higher for vegetation. Simply thresholding these indices usually give quite poor results. A better segmentation is obtained by a simple Gaussian model. The two-dimensional distribution is iteratively estimated providing a good segmentation. Lundberg presented also a dual band detection study in [195].

A method to detect side attack mines and roadsides devices is described in [196] where a Morphological Shared-Weight Neural Network (MSNN) is used. The authors argue that near infrared (NIR) wavelengths give a good contrast between vegetation and mines, since vegetation reflects NIR well. Good performance is obtained if the neural net has been properly trained.

6.1.4 Fusion techniques

There is no single sensor that is inherently best suited for the mine detection problem. Since each type of sensor has its particular merits it is commonly understood that the most promising system would be based on a combination of different sensing technologies. Fusion techniques are usually grouped into different classes depending on the amount of pre-processing of data that is performed prior to the fusion. In *pixel-level* fusion signal/images of similar type, for example two imaging systems, are fused. A simple pixel-level fusion is the

combination of colour channels (e.g. RGB) into intensity (R/3+G/3+B/3). Understandably, accurate positioning of the sensors is crucial.

Another type of fusion is *feature-level* fusion, where features are extracted by one or several algorithms on each sensor data set, and then the feature vectors are fused. The uncertainty associated with sensor readings and feature extraction is typically included in the fusion process, e.g. using the fuzzy set theory, Bayes or Dempster-Shafer frameworks.

In *decision-level* fusion the sensor's data are refined even further before fusion. The detection/classification/recognition decisions are calculated independently for each sensor-algorithm pair after which the individual decisions are fused. Simple decision-level fusion techniques include majority voting, conjunction (i.e. the decision must be unanimous) or disjunction (i.e. it suffices that one sensor/algorithm is positive). However, it is often desirable to have some type of belief value (or confidence/probability value) for each decision.

Gunatilaka, *et al.* [197] presented approaches to feature-level and soft decisions-level data fusion. The approach is applied to fusion of GPR, MWIR and EMI sensor data, for land mine detection. The sensors produce data of non-comparable form, as they differ in the dimensionality of the returned data and the samples are non-coincidental in location. A theory of feature-level fusion of randomly sampled multi-sensor data is outlined. The multiple hypothesis feature-level fusion algorithm can be referred to as an estimator-classifier technique in that the detection is based on the parameters rather than the residual errors in the model. The framework can also be applied to soft decision-level data fusion. A small experiment was conducted, in which 28 non-mine and 12 surrogate mines were placed in outdoor terrain. The feature level and soft-decision level fusion methods were superior to the single sensor detection and hard-decision level fusion. Further, the feature level fusion methods reduced the amount of false alarms.

Cremer, *et al.* [70] compare a number of decision-level sensor fusion methods (Bayes, Dempster-Shafer, a simple fuzzy technique, rule-based and voting) in the scope of AP landmine detection. The outputs of three sensors – Metal detector, IR-camera and GPR – are processed to produce the respective confidence (belief) levels. Sensor grids, representing the confidence level for the presence of a mine, are created and then fused to yield the final result. It was found that the rule-based technique performed poorly on an independent evaluation dataset, while the others gave quite comparable results with only seemingly more or less random variations.

Instead of fusing features acquired with different sensors, one could also fuse features extracted from applying an array of different algorithms to the same data. The underlying idea is that a true target can be detected with quite different techniques, and that the false accepts that normally follow vary with the choice of (statistical) model and respective parameters. Each of the algorithms is then tuned/optimized so as to obtain a low FRR and the fusion mechanism suppresses the false response, thereby increasing the robustness of the detection process.

A fuzzy fusion algorithm for GPR-based mine detection based on an extension of the Choquet fuzzy integral was proposed in [198]. The outputs of three different detection algorithms are combined, yielding significant ROC improvements over the individual algorithms. An approach for Dempster-Shafer fusion of GPR data was presented in [199]. Although applied only to GPR data, both articles illustrate the advantage of fusing different sources of uncertain information to improve the performance.

In [200] a framework for fusing detection statistics obtained with different background models into a maximum entropy joint distribution was proposed. Three models were used - a

local normal model (RX algorithm), Gaussian mixture model and a linear mixture model. Advantages in terms of improved ROC characteristics are demonstrated using hyper-spectral data.

In a paper by Meitzler *et al.* [201] several techniques are demonstrated for detection of mines. They use near, mid and long wavelength infrared imagery. The output of the process is a new image which is computed from the different images obtained from the sensors. The very detection is then done by a human.

6.1.5 Shape recognition

So far only a limited amount of work, if any, has been done on explicit shape-based recognition of mines. However, significant efforts have been devoted to develop image processing and analysis techniques for various other objects. In principle, many techniques can be readily transferred to the mine detection problem.

Model-based recognition implies matching a library of models with known geometry with the scene in order to find correspondences. The object surfaces can be represented in viewer-centred or object-centred coordinate systems [202]. Model matching in viewer-centred coordinates requires one representation of the model for every viewpoint being considered, which must be constructed and stored in a library. This approach is used in [203] for vehicle recognition from laser radar data. This requires the storage of a large number of model templates, and each template must be properly aligned to the scene before matching can take place. The *spin image* representation presented by Johnson [202, 204] enables matching in an object-centred coordinate system, without the need for initial alignment of the scene data to the model. The basis for the generation of a spin image is an oriented point, i.e. the spatial coordinates of a data point and the orientation of the surface normal vector in that point. For every oriented point, the surface can be represented using this object-centred coordinate system. The result is a spin image, a rotationally invariant 2D projection of the surface data, for every surface point. Correspondences between model and scene surfaces are established when many points have similar spin images. The starting point for recognition used in [202] is a set of densely sampled surface points, their connectivity and normal vectors – a mesh – from each model as well as the scene. 2-D template matching techniques are then used for establishing object correspondences in scene data. Principal component analysis is used to discard redundant information in the spin images and to increase the computational efficiency. Experiments show that the recognition rate remains very high and false alarm rate remains low in scenes with occlusion of objects of up to 70 % and clutter levels up to about 60 %.

The spin image technique can be generalized from using mesh representation of surfaces to using data point clouds. A prerequisite to do this is that the sampling of the surface be dense enough to enable a robust estimation of the surface normal vector for most points.

Based on a literature survey performed by Vasile and Marino [205], spin image-based detection and recognition is the most promising current technique for processing the 3-D laser radar data collected in the JIGSAW program [205], which aims at ATR given multiple views of occluded targets (vehicles). In their work, matching is initially carried out for 20 % to 50 % of all scene points using an a priori computed spin image library of vehicles, with a matching procedure following that of [204]. The distribution of similarity measures resulting from the correlation of the scene images to all the model images is subjected twice to similarity thresholds, and the remaining correspondences are grouped and checked for geometric consistency. Initial matches are then used as input to an iterative closest point (ICP) algorithm

for establishing final correspondences. Very good results are obtained for recognition of military vehicles with estimated model surface resolutions of 0.125 to 0.25 m. The recognition algorithm is also extended to include model-based automatic target detection in larger terrain scenes. The terrain scenes were of varying sizes between 25×25 m^2 and 100×100 m^2, and the average time for scene-to-model comparison was around 2 min/model for the combined detection and recognition algorithm on a desktop computer.

Another spin-image based framework, presented in [206], uses support vector machines (SVM) trained to recognize surface components and their spatial relationships for different object shape classes subject to intra-class variation. The authors also noted that when the scene data allow the surface normal vectors to be accurately estimated, spin-images are the preferred choice for surface shape encoding.

6.2 FOI-related work

In this section, we point specifically towards signal processing work related to the demining problem carried out at FOI. So far, as far as optical sensors are concerned, the main focus has been on anomaly and object detection with passive sensors. Active (laser) sensor data have primarily been used for recognition of relatively large objects, e.g. vehicles. Some preliminary results from the recently conducted FOI trials at Eksjö are presented in Chapter 8.

6.2.1 Anomaly detection

Multi- and hyperspectral image exploitation is a growing field not only in remote sensing within the civilian community but also in defense applications such as reconnaissance and surveillance. Multi- and hyperspectral sensors are electro-optical sensors (cameras) that sample the incoming light at several (multispectral sensors) or many (hyperspectral sensors) different wavelengths. Compared to a consumer camera that, typically, uses three wavelengths, corresponding to the red, green and blue colours, hyperspectral sensors sample the scene in a large number of spectral bands, typically several hundred. Moreover, these spectral bands can be beyond the visible range, *i.e.* in the infrared domain. Each sample, or pixel, thus forms a (spectral) vector of measurements in the different bands. This observed *spectral signature* contains information about the material(s) present in the scene, and can be exploited for detection, classification and recognition. If an observed target spectrum deviates from the observed background spectra, this deviation can serve as a measure of anomaly. In [207] algorithms and methods for target detection and classification in multi- and hyperspectral images are described. A simple and popular way to reduce dimensionality and also to extract interesting features is Principal Component Analysis (PCA). The drawback is that it is based on Gaussian assumptions and anomalies are therefore easily lost in the compression.

In order to be able to perform a unique classification or signature-based detection, the spectral properties of the scene elements or targets must be known from laboratory measurements or from *in situ* measurements. Observed spectra are analyzed both from a statistical point of view and compared with laboratory data, *i.e. a priori* knowledge is used in order to enhance detection probabilities and classification capabilities. The impact of illumination, weather and atmospheric transmission must also be estimated in order to relate observed spectra to laboratory measurements correctly. Reference panels and other reference sources in the scene

can help in calibrating the sensor systems and also in estimating the correlation in spectral scene properties from one trial to another.

Digitalization of data from a hyperspectral imager is done in three dimensions; the radiometric dimension, the spectral dimension, and the spatial dimension(s). The output can be regarded as a random variable taking values from a discrete alphabet, thus allowing simple estimation of the variable's entropy, i.e., its information content.
By modelling the target/background state as a binary random variable and the corresponding measured spectra as a function thereof, we can compute the information capacity of a certain sensor or sensor configuration. This can be used as a measure of the separability of the two classes. The procedure also gives a bound on the sensor's performance [208]. Changing the parameters of the digitizing process, basically how many bits and bands to spend, will affect the information capacity, and we can thus try to find parameters where as few bits/bands as possible gives us as good class separability as possible. The parameters to be optimized in this way (and with respect to the chosen target and background) are spatial, radiometric and spectral resolution, i.e., which spectral bands to use and how to quantize them. The paper [208] focus on the band selection problem, describe an initial approach, and show early results of target/background separation. Refer to Chapter 8 for some initial anomaly detection tests on data acquired in field trials conducted within the MOMS project.

6.2.2 Mine detection

This section focuses on temporal analysis of buried land mines. The presented methods are used by the Swedish defence research agency (FOI) when analysing IR images collected at real minefields as well as on experimental test fields. Different approaches and comparisons between methods are described in [209, 210]

Optical mine detection aims at finding objects or areas in an image having certain properties that in some respect differ from the normal background. Man-made objects have temperatures that differ from other parts in the scene depending on different material properties like emissivity, thermal conductivity and thermal capacity, amongst other things [210, 211].

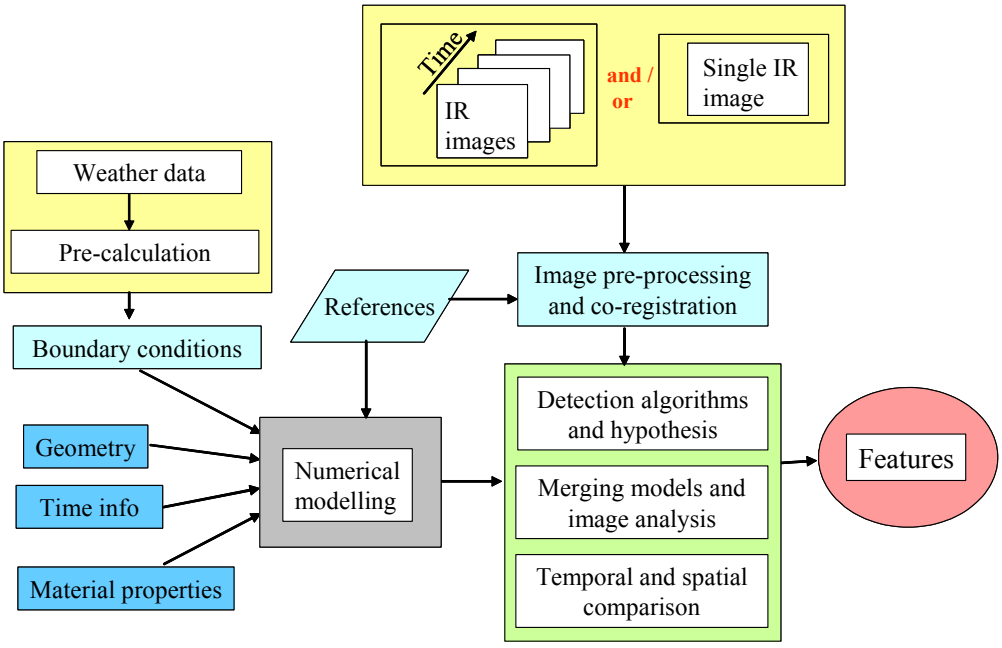

Figure 6-1. The FOI temporal analysis method.

The overall concept for optical mine and minefield detection at FOI can be described according to signal/image processing, experiments, and modelling/simulations, each are separate research areas but applied to the same problem: how to enhance the detection performance [211]. Here we show some results and performance tests when combining all these areas applied on the same data set. The data flow from a general point of view of the method is shown in Figure 6-1. Data collection, both sensor images and weather, as well as modelling is closely integrated with the signal processing in the temporal analysis method.

Temporal analysis is performed on image sequences collected from the same scene over time. The time increment between consecutive images can vary from seconds to days. Detection of different objects in the scene is based on the assumption that the apparent temperature of the pixel varies in the same manner as a corresponding reference object, formulated as a hypothesis test. Given the time for registration of the image, the model or reference object provides the expected temperature feature for the analysis. The measured features are compared to the reference feature estimated from numerical modelling or known objects. With this approach it is possible to detect and classify objects, buried as well as surface laid using different detection methods. In [59] three methods are presented:

1. Comparison of apparent temperature in the scene with reference temperature
2. Comparison of scene contrast with reference contrast
3. Analysis the difference between successive images

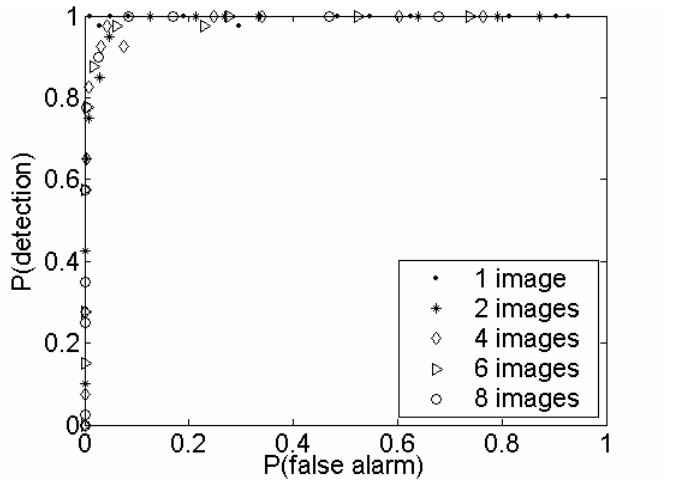

Figure 6-2. Matching candidate and known object values in the scene.

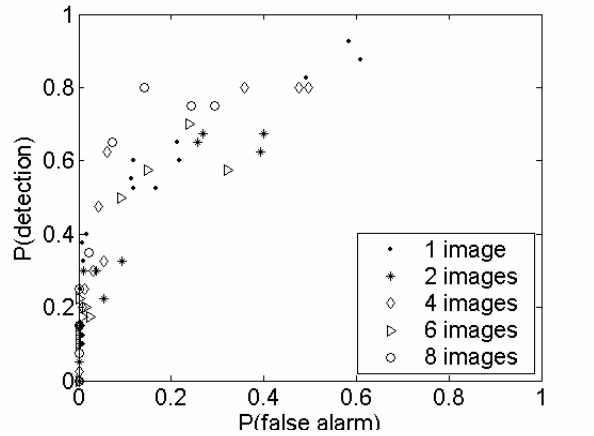

Figure 6-3. Matching candidate and model values in the scene.

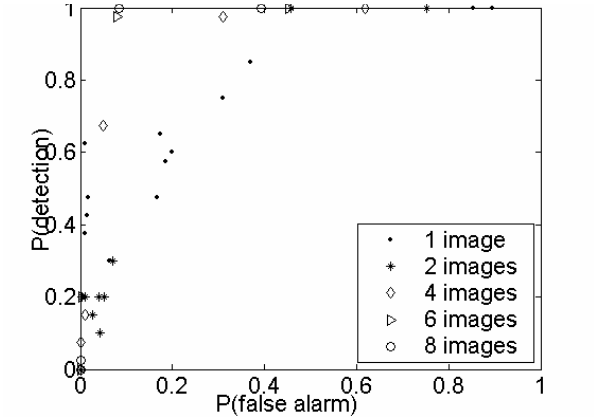

Figure 6-4. Matching candidate and model contrast in the scene.

The result from using different number of images is presented in Figure 6-2 to Figure 6-5. The images are chosen randomly from the image sequence. The number of images used was 1, 2, 4, 6, and 8. Different detection rates and false alarm rates are presented in the curves. Every point in the diagrams is the mean of ten detections with the same parameters but different set of randomly selected images.

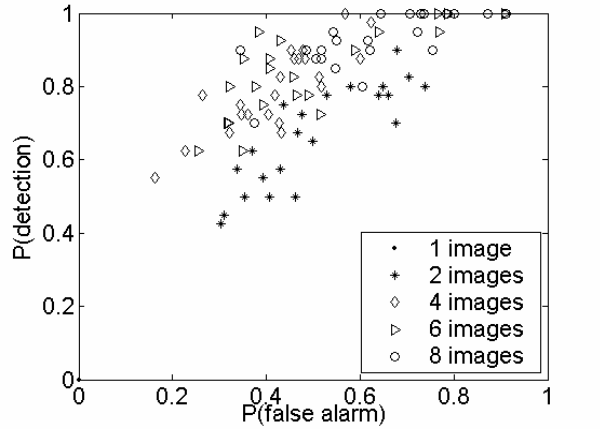

Figure 6-5. Matching candidate and model values in difference space.

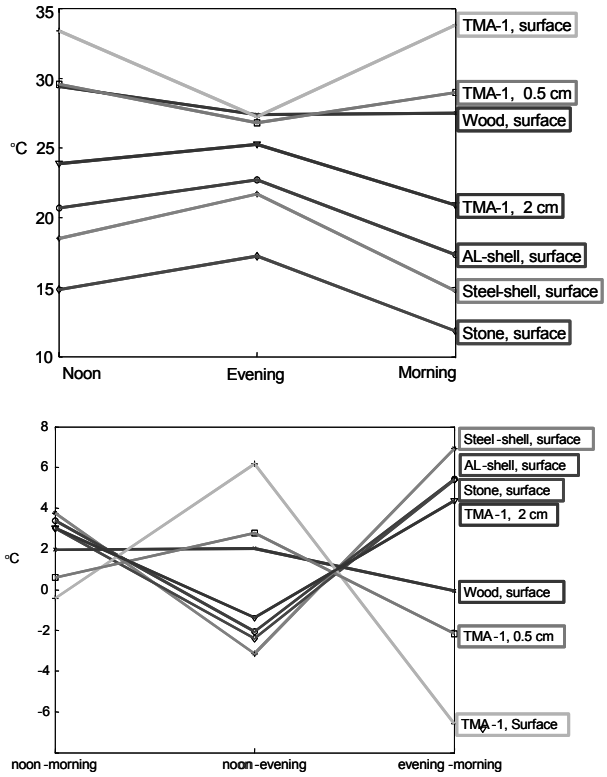

Figure 6-6. Top: The simulated object temperature values corresponding to the time of image capture represented in the image basis. Bottom: The corresponding temperature difference basis.

Figure 6-2 shows the performance when matching the temperature of the test area to the temperature of the known position of a mine. Figure 6-3 to Figure 6-5 show the result of using the detection approaches mentioned above with a model of a mine presented in Figure 6-6 as reference object.

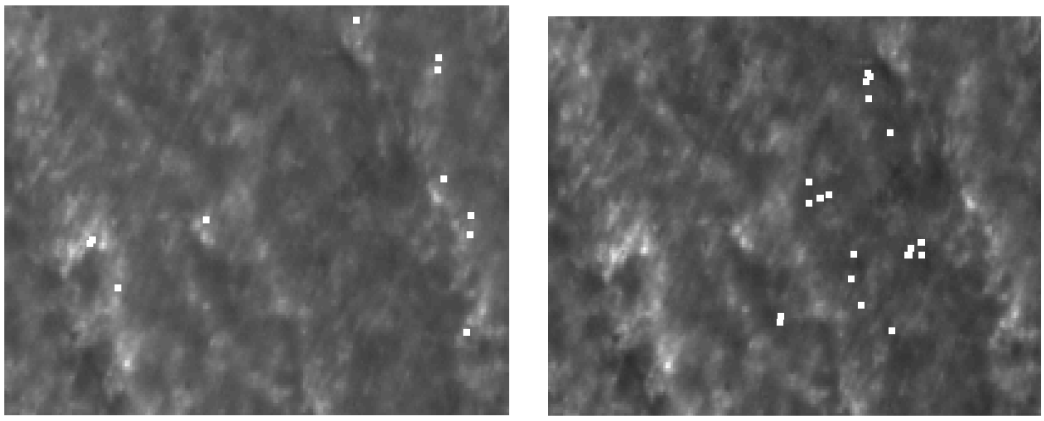

a b

Figure 6-7. Positions of detected objects. Marked pixels have a true correspondence due to the hypothesis test. a) The positions of the simulated surface laid TMA-1 mine. b) The positions of the simulated buried 0.5 cm TMA-1 mine.

Simulated temperature values of different relevant mine-like objects, corresponding to the time of image capture in the image and difference bases, respectively, are presented in Figure 6-6.

The next step is to use prior knowledge to select the time for data collection. Detection of the different objects in a real minefield, using the difference method and model as reference object are presented in Figure 6-7. We test for the difference between the temperature at different times of the day of the signal vector and the model vector. The positions correspond to pixels that have the same level of temperature change as the modelled objects, when $\Delta = 0{,}1\,°\mathrm{C}$.

The FOI temporal analysis method has been presented and tested on images randomly chosen from a diurnal sequence. Although the test sequence shows very little contrast, the detection methods presented show that mines can be detected using optical methods. Focus was on the question if increased number of data collection times affects the detection rate and false alarm rate. The results from the test with randomly chosen images show better performance than random for all of the tested cases, and excellent for some. Detection rate increases and false alarm rate decreases with increased number of images used for some of the tested cases. Using prior knowledge in the choice of data collection times, the result from testing the method on real mine field data shows good result.

6.3 Summary of the chapter

It is evident that a successful approach to the mine detection problem will require efficient techniques for anomaly, change and mine detection. Appointing a single winner among the existing techniques is not possible at this point, due to a number of issues: the difficulty of comparing experiments, the robustness to changing environment and sensory conditions, the computational complexity, the amount of *a priori* information required, etc. The RX-algorithm and its extensions are interesting for further analysis, mainly due to the relative simplicity of the algorithm and the inherent capability to detect anomalies locally, using the immediate surrounding background rather than the entire scene. It seems that clustering-based techniques may produce good anomaly and change detection results, but the main question is how to choose the optimal number of clusters.

Since different sensors and algorithms have their own advantages and drawbacks, a signal processing framework that allows for fusion of different sources of information is highly desirable. Recent work has shown that significant improvements are possible pursuing this idea.

Spin-images have emerged as some of the most promising tools for 3-D shape detection. The crucial step is the estimation of the normal direction in each data point, which requires a high sample density compared to the object size. For a mine, a sufficient density would probably be in the order of 1 sample/cm. Due to the great computational burden associated with spin-images, they are likely to be more useful for recognition/identification in limited, previously determined regions of interest.

For several years at FOI the main focus in mine detection has been on anomaly and object detection with passive sensors. Active (laser) sensor data have primarily been used for recognition of relatively large objects. The chapter shows relevant data processing methods and earlier work in this area carried out at FOI.

7 System concepts

This chapter presents different possible approaches to reach the goal of a Multi optical mine detection system. Such a system roughly consists of a Platform, a combination of Sensors, and dedicated Signal processing and detection algorithms. We here discuss the sensor systems, give some system examples and finally give some ideas for platforms.

7.1 Introduction

New and improved technologies will be studied in order to find roadmaps to increased effectiveness in mine detection. The sensors will, as described above, be based on electro-optics, multi/hyperspectral imaging, active/passive UV to LWIR imaging and polarimetric imaging. In order to be able to optimize these systems in an efficient way, improved understanding of environmental effects and material parameters must be obtained. The focus of the initial concepts will be based on seven basic approaches. After the evaluation of the potential of these approaches, the most promising concepts will be fused into sensor suits for evaluation. The basic approaches are: Hyperspectral imaging, Polarimetric hyperspectral LWIR, fluorescence, Polarization contrast imaging, 3-D imaging, Multispectral LADAR, and Retro-detection.

Each approach follows a similar development cycle:

1. Analysis of the basic concept based on the material data base and environmental conditions
2. Collection of data for basic concept study
3. Development of laboratory test system for evaluation and feasibility study
4. Initial field test for performance validation
5. Evaluate the concept vs. demands and practicality

The most promising approaches will be proposed to be a part of the mine detection concept and evaluated for the intended purpose. The details of these approaches will depend on the mixture of anticipated threats. It is quite likely that the sensors have to be adapted to both the environment and the types of threat that should be detected. This means that one set of sensors might monitor a road while another set is monitoring the road side and a third set is monitoring the off-road region. Sensors have to be selected in such a way that the detection probability is optimized. Sensors with high detection probability but possibly high false alarm rate have to be combined with sensors that have good false alarm discrimination capability but possibly not very good detection performance.

Suggested concepts should be based on field measurements and laboratory studies showing the impact of various environmental factors and processes (e.g., subsurface processes) on the resultant multidimensional signatures. Modelling of the scenarios will give further insight into the physics based phenomenology. Prioritized concepts should be realized as demonstrators for field measurements and signal analyses. These results can also guide the algorithm development to permit the development of robust processing techniques.

The combination of new sensor technologies and improved computational power will give rise to new sensing modalities and architectures. It is becoming increasingly clear that multi-sensor data can provide significant information for both manmade objects (targets) and natural background (clutter). Processing multisensor data is still in its infancy complicated by the fact that characteristics change from place to place in the scene. A short overview is given below with respect to a number of electro-optical sensor systems with potential for mine detection.

Tripwires are difficult to detect; 3 D laser imaging and polarisation imaging systems show some promise which have to be further exploited. Each sensor technology will find its specific area of applicability and work together in different combinations of sensor fusion. This joint decision space is modelled and decision boundaries should be computed from measured statistics. Since the approach adapts the decision criteria based on the measured statistics and possibly prior target training information, it provides a robust multisensor detection statistic. Anomaly detection has proved to be of great interest. This technique does not rely on exhaustive global statistics but rather on the local statistics and possibly some a priori information regarding the size and shape of targets. Iterative procedures of feature extraction and anomaly detection can be carried out in order to gradually reduce the false alarm rate while maintaining a high probability of detection. Morphological operations can subsequently be employed for extracting the size and shapes of anomalous objects.

The ability to distinguish between targets and non-targets automatically is an essential component of the system properties. One cannot expect a single solution to work in all scenarios and all applications. A variety of algorithmic approaches will likely continue to be developed over the years to come. The understanding and exploitation of the physical information, i.e. target features, is an important approach for deriving physical laws that defines probability density functions. Information theory is an important aspect of signal and imaging understanding, not only for derivation of performance bounds. The optimal processing of combinations of target features for detection and classification, as obtained using the sensor suit, constitutes what is meant by sensor fusion.

Change detection might be a viable technique for general threat indications. In change detection, obviously the same area is scanned repeatedly. Features being observed do not have to be classified but must be accurately geo-positioned. Efficient feature extraction in relevant scales is needed in the same way as in detection but false alarm rate requirements can be drastically relaxed. Huge databases will be created and must be processed with respect to relative sensor positions. Change detection has been demonstrated using both passive and active techniques.

7.2 Test systems

A proof-of-concept brass board system should be used to establish performance bounds for mine detection using different combinations of sensors under different conditions. The detection performance and type of false alarms and the conditions should be registered for further evaluation. The test system should also be used to evaluate how it can enhance the performance, which uses human operators. The management of sensors could be based on an information-theoretic approach that chooses sensors and sensor parameters that optimizes the detection in relation to a given false alarm rate. Of special importance is the detection vs. the verification (classification) process. These two functions may be done in series or in parallel

with different sensors. The issues that should be addressed in the analyses of the field trials are:

- Which observables differentiate targets of interest from non-targets
- What type of sensor combination is appropriate for obtaining the optimal information
- How can algorithms be developed in order to obtain robust discrimination
- What are the design and performance limitations

The resultd from field trials with realistic test systems should lead to proposals of concepts for mine detection and classification, signal- and image processing methods which are robust against clutter and varying environmental conditions and adaptive sensor fusion for meeting new threat conditions.

It is quite likely that the platforms must be found among those that are presently being developed for a number of different tasks. Those can be modified to accommodate the new sensor systems and software needed for the operations dicussed here. In some cases, other needs can be addressed that can be combined into the same mission.

The preliminary performance criteria are quite demanding and include the following capabilities:

- Decision support to the commander on presence of mines and advice for route planning
- Systems capable of detecting anti-personal mines, anti-tank mines, side hitting mines, concealed or signature adapted mines and explosives/UXO/IED.
- The system must have day/night and all weather capability
- The system should have a area coverage rate up to 50 km/h on roads and 15 km/h in terrain with a swath width of 200 m
- The system shall have a geo-positioning capability with high precision and work in conjunction with mine clearance units

For maneuver warfare, the speed and detection probability of the mine search is very important. The rate at which mines and minefields can be detected and marked has a significant impact on the timelines of the maneuver force. Relatively few technologies are compatible with the requirements for high-speed search of large land areas from airborne or fast moving land vehicles. In recent years, mines have turned from being a military weapon into a weapon that at times is indiscriminately used against civilians. “Improvised Explosive Devices" (IED’s) are characterized by varying employment techniques. In most of the techniques shown below, an unexploded ordnance (UXO) can easily be engineered to replace a mine or explosive device.

Booby traps and IED’s are similar to mines in that they are designed to kill or incapacitate personnel. They are also emplaced to avoid detection and improve effectiveness. Most are victim-activated, but some may involve remote or command detonation architectures.

The different shapes, material and colours of the threat devices from conventional mines to IDE’s stresses the importance of anomaly or change detection and compared to threat libraries with more or less well known signatures. The demands on search rate set for this program (1000 m^2/s) greatly exceed what was discussed in the US DoD report in the year 2000 .

The trade off between detection/classification performances must be evaluated vs. search rate for the different sensors in the suite and the best complementary sensor suite chosen. Figure 7-1 illustrates this process.

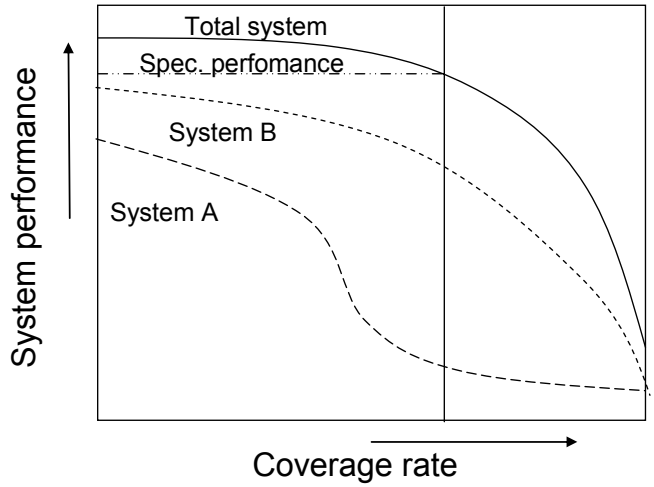

Figure 7-1 Trade off curves of performance vs. search rate for individual sensor and for the total sensor suite are shown.

To meet operational requirements, the different sensors and the suite must be evaluated to harmonize against a row of performance figure such as:

- Discrimination/selectivity
- Search rate
- False-alarm rate
- Probability of detection
- Sensitivity
- Missed targets

The chosen sensor suite should as much as possible measure orthogonal parameters in the signature space.

7.3 System examples

Many of the technologies considered here have been demonstrated, both ground based and airborne platforms. Many of the technologies have also been demonstrated with relevant stand-off capability. Examples are LAMD, COBRA, ARC and LOTUS. A useful discussion of overall system aspects are found in the RAND report [4]. The US DoD also discusses system aspects of land mine detection; see for example Developing Science and Technologies list [212]. What has not been demonstrated is a sensor fused system with adequate overall performance although encouraging results has been obtained. In 7.3.5 we illustrate a potential concept just to stimulate future discussion and modification. At present we believe that some

platform combination like the one in the example is needed to fulfil the system demands given above.

7.3.1 LAMD (Lightweight Airborne Multispectral Minefield Detection)

The LAMD, formerly known as the Airborne Standoff Minefield Detection System (ASTAMIDS), is intended to be a highly reliable airborne minefield detection system which will provide a commander with the accurate location of minefields [213]. The system will be required to detect and identify the boundaries of buried and surface patterned minefields plus scatterable mines and detect individual buried nuisance mines on unpaved roads. The minefield location, combined with other intelligence, surveillance and target acquisition operations, will provide alternatives for command decisions. LAMD will be an airborne mine detection system consisting of an imaging sensor mounted on an Unmanned Aerial Vehicle (UAV) and a processor/algorithm integrated into the UAV Ground Control Station (GCS). The system will allow the user to obtain information for formulating an operational plan and gather further information to modify that plan still more. The sensor, weighing less than 45 kg, will be mounted on the UAV and controlled by the UAV GCS, transmitting minefield imagery via a datalink to the GCS for processing in near-realtime by a very high-speed parallel processor. The resultant information will be displayed and disseminated to users in a manner similar to other reconnaissance, intelligence, surveillance and target acquisition data. The initial design included a Raytheon-developed sensor system involving laser diode technology, including a laser receiver and a UAV-mounted passive farband infra-red and active laser sensor detection system, Figure 7-2. The ground-based portion of the system included the Minefield Detection Algorithm and Processor (MIDAP). Technical Performance Objectives are given in Figure 7-3.

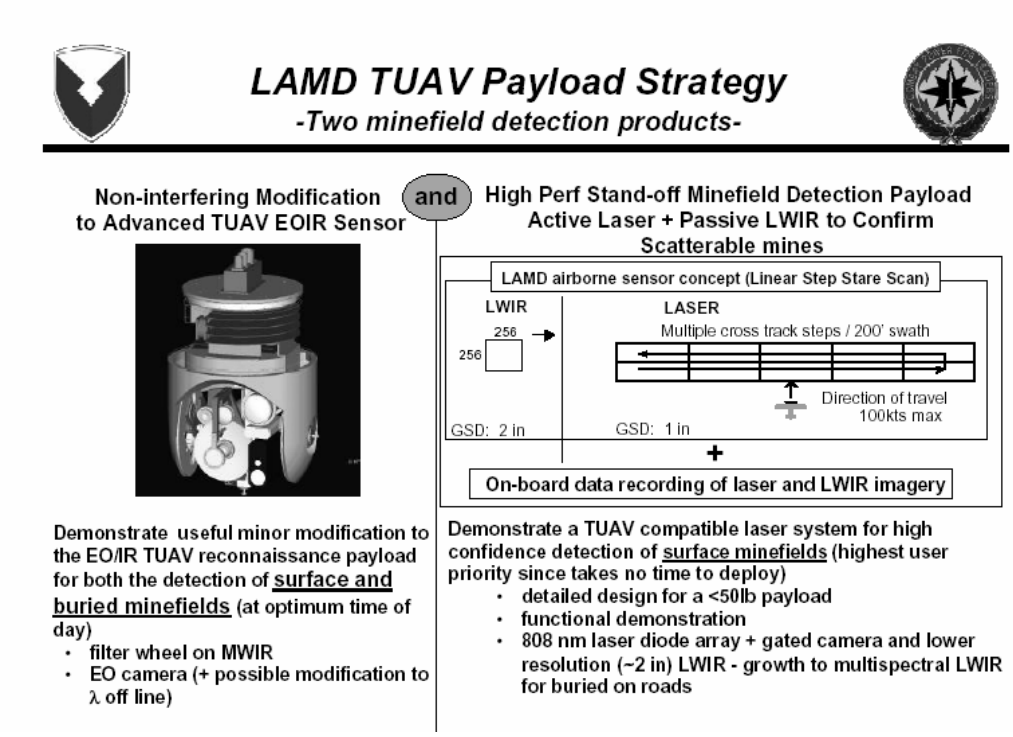

Figure 7-2 LAMD Payload Strategy, from [214].

Technical Performance Objectives

Operational Capability/Parameter	Exit Criteria	
	Minimum	Goal
Probability of Detection		
– surface patterned minefields	80%	*95%
– buried patterned minefields	65%	*80%
– surface scatterable minefields	70%	*85%
– buried nuisance mines on unpaved roads	60%	*75%
False Alarm Rate		
– false detections / square kilometer of area covered	FAR < 0.5	*FAR < 0.5
Detection Accuracy		
– minefield edge	< 150 m	< 100m
– minefield boundary	n/a	< 150m
Sensor Weight	< 65 lbs.	< 35 lbs.

* PD and FAR goals during defined operational conditions (i.e. time of day, environment, etc.). Conditions to be defined at the conclusion of the phenomenology investigations.

Figure 7-3 Technical Performance Objectives for LAMBD, from [214]

7.3.2 COBRA (COastal Battlefield Reconnaissance and Analysis)

Coastal Battlefield Reconnaissance and Analysis (COBRA) Advanced Technology Demonstration (ATD) incorporates advanced multispectral sensors into a UAV to provide daylight coastal reconnaissance of beach areas and craft landing zones. COBRA addresses the limitation in high-search-rate reconnaissance capabilities of minefields and obstacles on the beach and improves the capabilities of forces to determine precise minefield boundaries [215]. Figure 7-4 shows examples of scenario and sensor platform and Figure 7-5 shows an overview of capabilities for COBRA.

Figure 7-4 COBRA, examples of scenario and a sensor platform. (published by Nothrop Grumman).

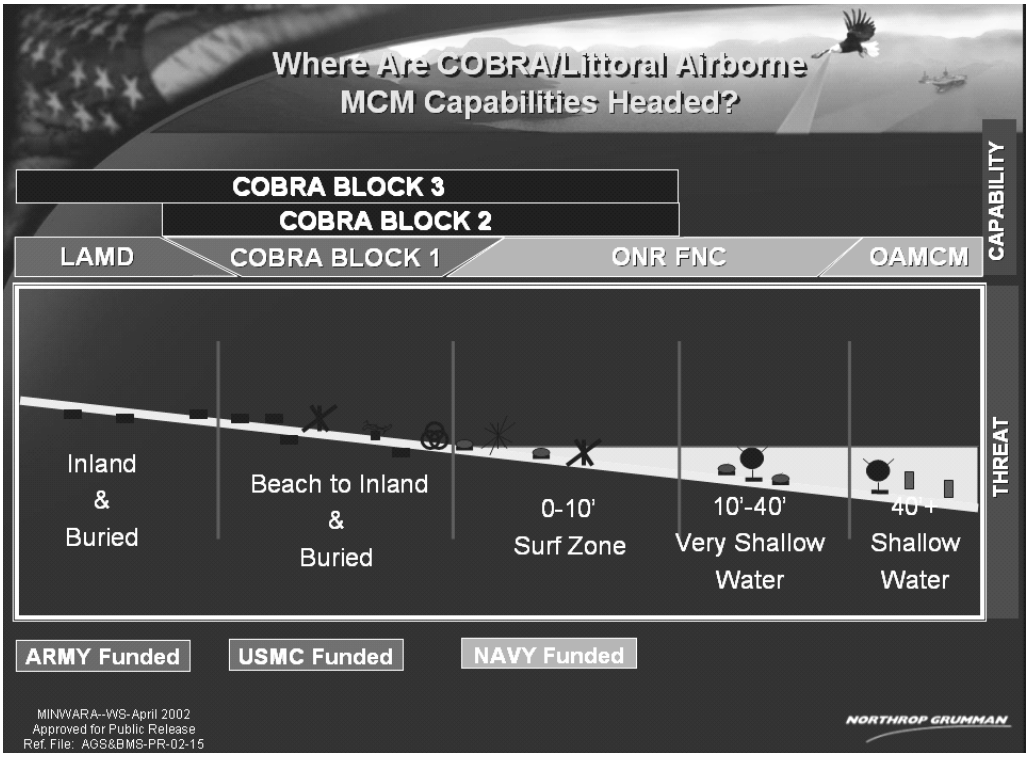

Figure 7-5 Capabilities for COBRA (published by Nothrop Grumman)

In Table 7-1 a comparision between the Advanced Technology Demonstration (ATD) and System Development and Demonstration (SD&D) Program Capabilities for the COBRA project is made.

	ATD	**SD&D**
Camera Rotation	Locked down	4 axis, gimbal
# of Cameras	2 for FOV	1 camera (non-ICCD)
Coverage Pattern	fixed stare	Step-stare, multi-area
Swath Width	50 meters	> 500 meters
Area Coverage Rate	4.5 km2/hr	80 km2/hr
Analog/Digital	analog, 8 Bits	digital, 12 Bits
Platform Adaptability	Single platform	multiple platforms
Operational Altitude	800ft AGL	variable

Table 7-1 Comparison of COBRA ATD and SD&D Program Capabilities (published by Nothrop Grumman)

7.3.3 ARC (Airborne Minefield Area Reduction)

ARC was an applied EC funded project for the design and implementation of a demonstrator system for airborne assessment of minefields in humanitarian mine action [101]. The project was running from beginning of 2001 and was finalised by the end of 2003. It was funded by 50% from EU and 50% from other sources. Partners were: FOI (Sweden), Geospace (Austria), GTD (Spain), Croatian Mine Action Center (Croatia), IMEC (Belgium), SCHIEBEL (Austria) and TNO (Netherlands). The ARC system consists of an UAV with IR and multispectral sensors (Figure 7-6), a ground control station for the UAV and a ground station with database, GIS, mission planner, image processing and data fusion (Figure 7-7). Data are stored on the UAV for later analysis on the ground station. The UAV can be preprogrammed to a pattern of waypoints where image recording automatically can be started or stopped. ARC can be used for general survey (mapping), area reduction, minefield delineation and quality control.

Figure 7-6 ARC UAV with IR and multispectral sensors.

Sensor data are fused with satellite data and other GIS data. A pyramidal hierarchical approach is used to logically integrate the different information levels using available state-of-the-art remote sensing tools ranging from (coarser) satellite data to very high resolution (cm range) data acquired from the UAV.

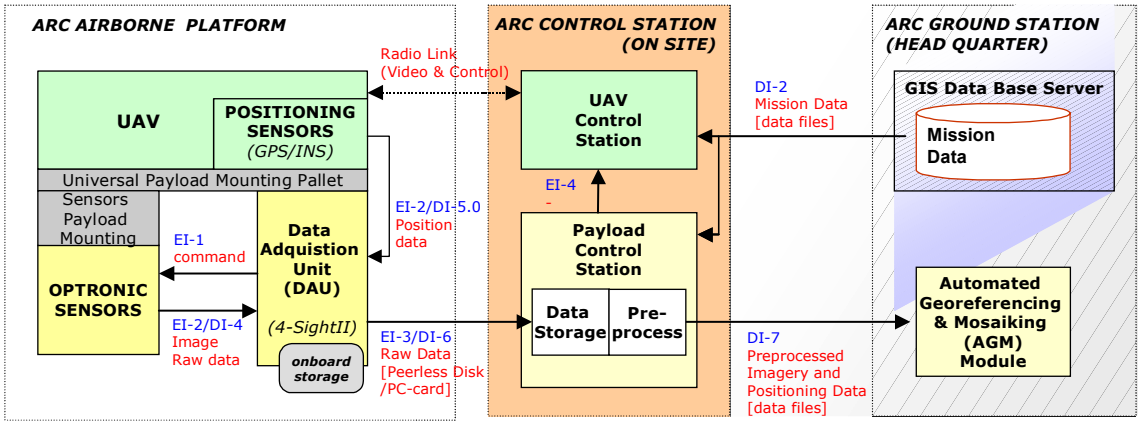

Figure 7-7 ARC overall system architecture logic view.

7.3.4 LOTUS

The Lotus project was an European Commission funded project running between 1999 and 2002 [100]. The objective of the LOTUS project was to provide a demonstration of the detection and marking of anti-personnel mines from a vehicle in real-time using a suite of sensors with data fusion. Involved organisations were: DEMIRA e.V. (Germany), EMRAD (UK), Institut Dr. Foerster (Germany) and TNO FEL (Netherlands). LOTUS was a demonstration of technology but it was supported by a detailed review of the scenarios to be addressed and of the system required. LOTUS used a suite of complementary detectors. These were a metal detector, a ground probing radar (GPR) and an infra-red camera. The LOTUS project involved the bringing together of all three sensors on to one sensor platform and operating them simultaneously in real-time, Figure 7-8. This included the real-time analysis of all the data by the individual sensors and the fusion of that data in real-time to give one overall system output. The sensors were mounted on the front of the vehicle, and a mine marking system on the rear. The output from the data fusion was also used in real-time by the marking system to allow the position of suspect objects to be marked in real-time as the system passed.

Figure 7-8. The LOTUS Vehicle. The metal detector is at the front, as far away from the vehicle and other metal as possible. The infra-red camera then follows within the framework and the GPR array is then immediately in front of the vehicle.

7.3.5 New ideas

Due to the high search rate (1000 m^2/s) an airborne system will be needed to cover the 200 m swath. This system could be a combined passive EO sensor and high resolution 3 D laser radar to localize mines at least on the minefield level. The sensors could also be used for route planning and for generating high resolution maps for mission planning, threat evaluation etc.

An (unmanned) ground vehicle is most likely needed to verify detections from the airborne system and to take care of the “leakers”, Figure 7-9. Of special importance is the detection of potential side hitting mines which may be difficult to detect by air under layers of vegetation.

Two separate side looking sensors might be needed apart from the down looking sensor from the boom of the vehicle to ensure detection of side hitting threats (mines or weapons in general). The down looking vehicle sensor could be a downscaled version of the airborne sensor combining active and passive operation. One option that might be considered is the bi-static configurations to utilize shadows and the glint like surface expected from many man made targets Figure 7-10. The vehicle sensor has smaller swath widths and may thus have higher resolution compared with the airborne sensor.

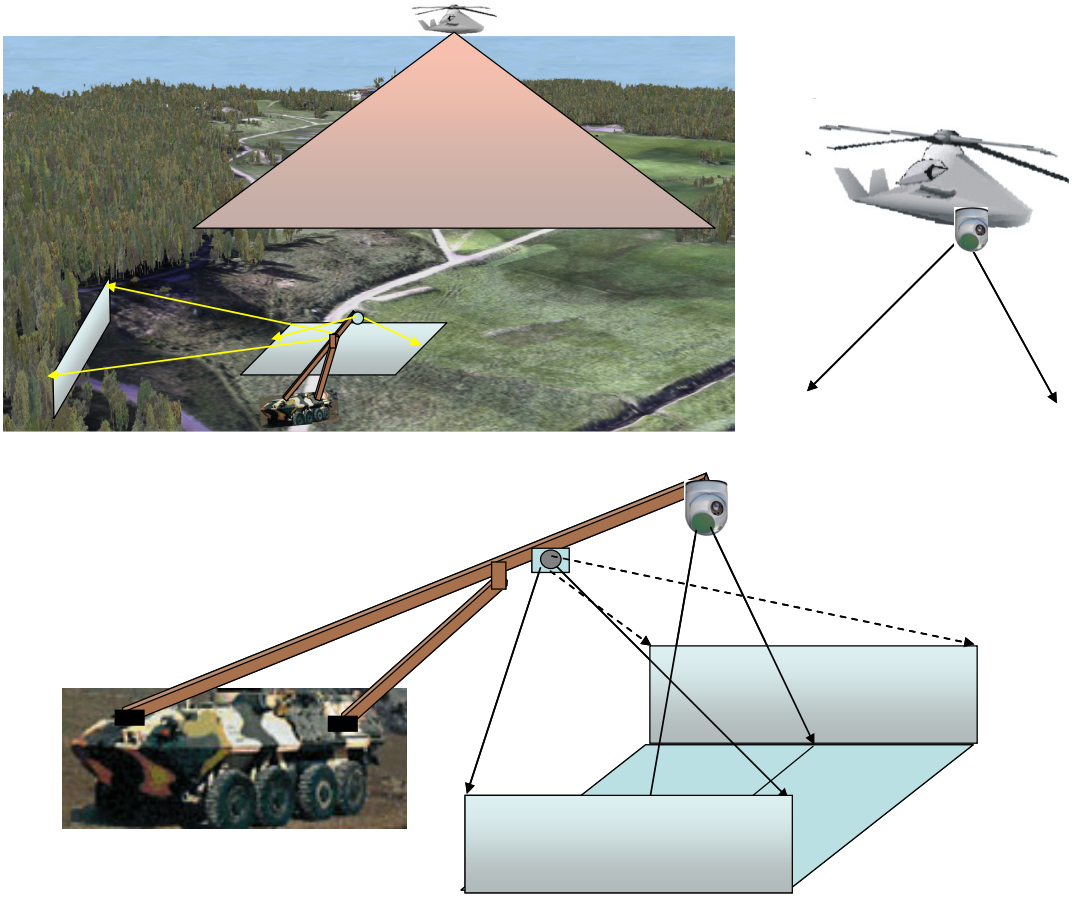

Figure 7-9 A potential system concept combines airborne and ground vehicle sensing.

Detection is obtained under a rather high false alarm rate while classification can be done at a lower rate in regions of interest. The final output from the system has to show a low false alarm rate. Anomaly detection has proven to be a very efficient way of finding regions with potential targets. The first step has therefore to be performed by sensors with both high coverage rate and with extraction of features that are typical for the targets but not necessarily unique for targets only. The second step should emphasize features that separate targets from clutter in the subgroup that has been selected by the previous set of sensors. There might be possible to employ an iterative approach with several views of the same target.

Several of the technologies discussed above have been demonstrated at a capacity compatible with a coverage rate of 1 km^2/h. This applies to visible and near infrared hyperspectral imaging, mid wave and long wave infrared spectral imaging, 3 D imaging, reflectance imaging, polarimetric imaging and retro-detection of optical targets.

The coverage rate requirements of the classification sensors depend on the false alarm rate of the detection sensors. More advanced versions of the previously mentioned sensors with improved classification capability are also compatible with this coverage rate.

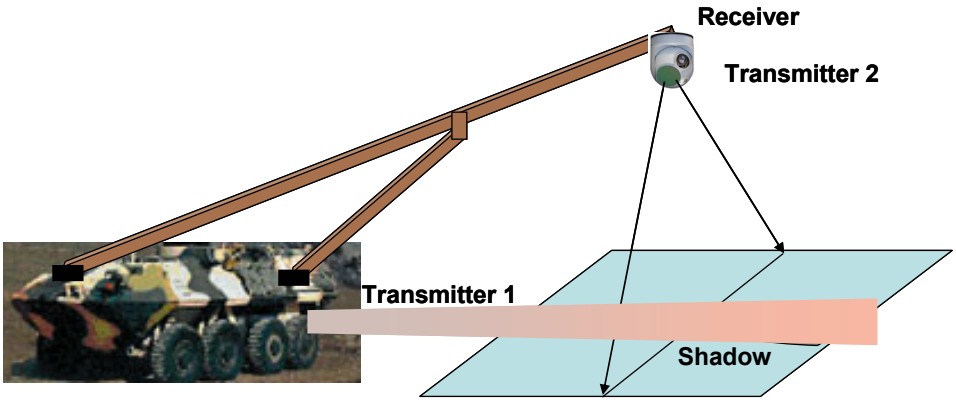

Figure 7-10 Potential bi-static configurations to utilize shadows, polarization and reflective properties for man made targets.

Demonstrator concepts should be considered both for airborne applications and ground applications. Together they will contribute to the overall threat mapping and the detailed mapping during escort service. Brass board systems could be placed on platforms simulating autonomous capability. These systems do not have to fulfill all tactical requirements as long as it can be shown that they can be scale properly. Important design features must however be considered such as protection against mine explosions, flexible mounts for adjustable sensor positions, easiness to change sensor suit and efficient signal processing capabilities. The vulnerability of the platform has to be considered. Unmanned helicopters and low flying UAVs could prove to be very useful but they also constitute easy targets. In situations involving other resources, this might still be acceptable. The airborne system could play a very important role in performing reconnaissance and threat evaluation. The high resolution sensors are suitable for that to be made at a safe distance.

7.4 Summary of the chapter

In this chapter different approaches to reach the goal of a Multi Optical Mine detection System are discussed. Some examples of existing systems have been described and an idea of a possible system with potential to reach the dimensioning goals was introduced. An (unmanned) ground vehicle is most likely needed to verify detections from the airborne system and to take care of the “leakers”. The basic sensor approaches are: Hyperspectral imaging, Polarimetric hyperspectral LWIR, fluorescence, Polarization contrast imaging, 3-D imaging, Multispectral LADAR, and Retro-detection. After the evaluation of the potential of these approaches, the most promising concepts will be fused into sensor suits for evaluation.

8 Conducted experiments and field trials

Experiments on polarization imaging of mines and tripwires have been conducted and are presented in 8.1.1. Spectral measurements have been performed on some sample mines with an integrating sphere. The measurements are described in 8.1.2.

A field trial was conducted at the Swedish EOD and Demining Centre (SWEDEC) in May 2005. The purpose was to take data on surface laid mines, UXO, submunitions, IED's, and background with a variety of optical sensors. The field trial, including all the sensors that were employed, is described in 8.2.1 and some initial results are presented in 8.2.2.

8.1 Laboratory measurements

8.1.1 Polarization

Three conference papers[216] have been published in mine detection and passive polarization. As reported in a conference paper in 2001 [216], a "worst case" scenario was arranged, with low temperature on the ground, and some of the mines was covered with grass. Figure 8-1 and Figure 8-2 show the mine field in visible light, in 8-12 μm without polarizer and 8-12 μm with polarizer. The images show that the mine covered with grass is possible to see when using polarizer calculating the Degree of Linear Polarization (DoLP) and not visible without a polarizer.

A systematic investigation was performed by constructing frames with cotton yarn mounted on the frames, as can be seen in Figure 8-3. The distance between the cottons was 1 mm and the thickness of the cottons varied from 0.2 to 0.9 mm, thereby constituting coverage ranging from 20% to 90% coverage. The following coverage was obtained: 20%, 45%, 60% and 90%.

The distance between adjacent cottons ranges between 0.1 and 0.8 mm, whereas the wavelength of the radiation is about 0.01 mm, which makes it unlikely to find any diffraction effects. Neither have such effects been observed. The conclusion is that the frames can be used as a clean damping material of the radiation.

The measurements of the worst case, in LW, clearly shows that polarization measurements can discover covered mines that the measurements without polarizer can not discover.

A trip wire can be clearly seen in DoLP (Figure 8-4) and is completely invisible in an image registered without a polarizer.

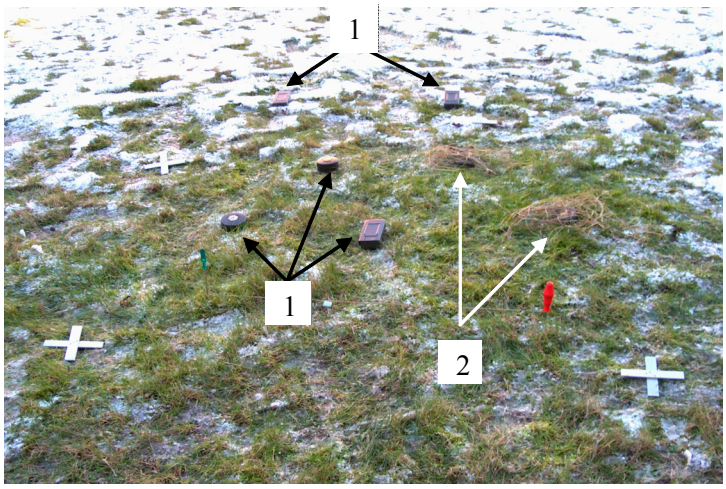

Figure 8-1. The constructed mine field observed with a camera in visible light. Mines are seen at the position marked with 1. There are also mines at position marked 2, but these mines are partly covered with dry grass. The crosses are orientation marks.

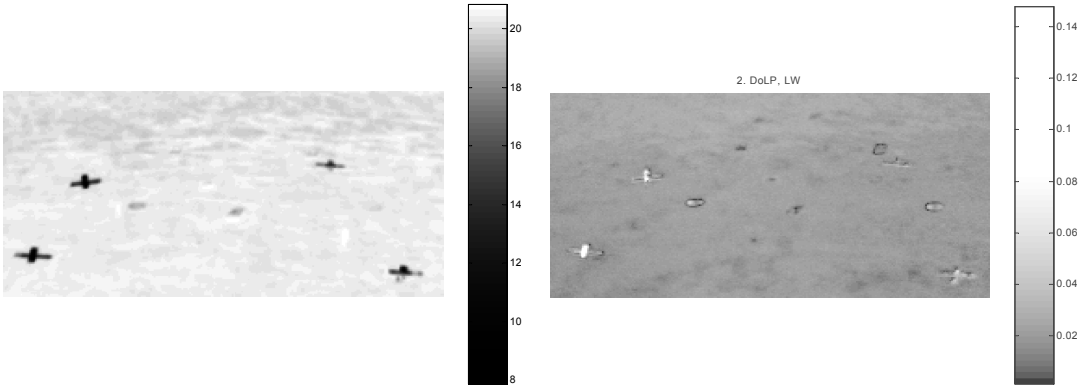

Figure 8-2. Image of the minefield, measured without polarizer to the left, and DoLP to the right, in the LW region. Two mines are clearly seen. The crosses are orientation marks.

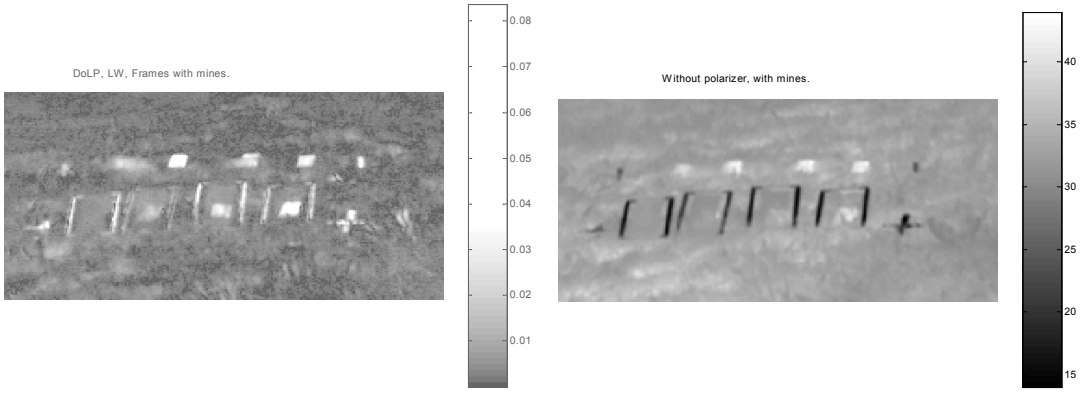

Figure 8-3. DoLP of the minefield, to the left and mines without a polarizer, in LW range.

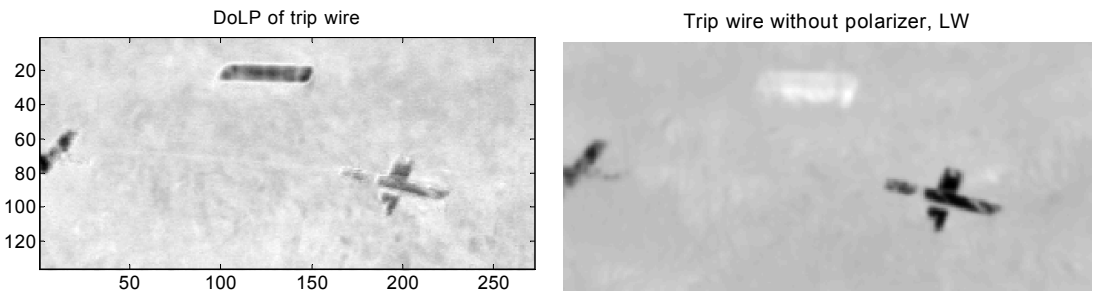

Figure 8-4. DoLP of a trip wire to the left and an image of a trip wire taken without a polarizer to the right. Both are taken in LW region. In the left image the trip wire is clearly seen as a white line between the two crosses.

In 2003, laboratory measurements of the coverage of mine surfaces were reported [74]. The equipment measured the emissivity as a function of emissive angle, for different coverage of the mine. The setup simulated a real case where a mine is partly hidden behind some obstacle, for example hidden in grass. Examples of the emissivity as a function of emissive angles are shown in Figure 8-5, left diagram, with no coverage and in Figure 8-6, left diagram, with 60 % coverage. Also shown is the DoLP, to the right in Figure 8-5 and Figure 8-6, calculated from the measured s-, p and 45˚ measurements.

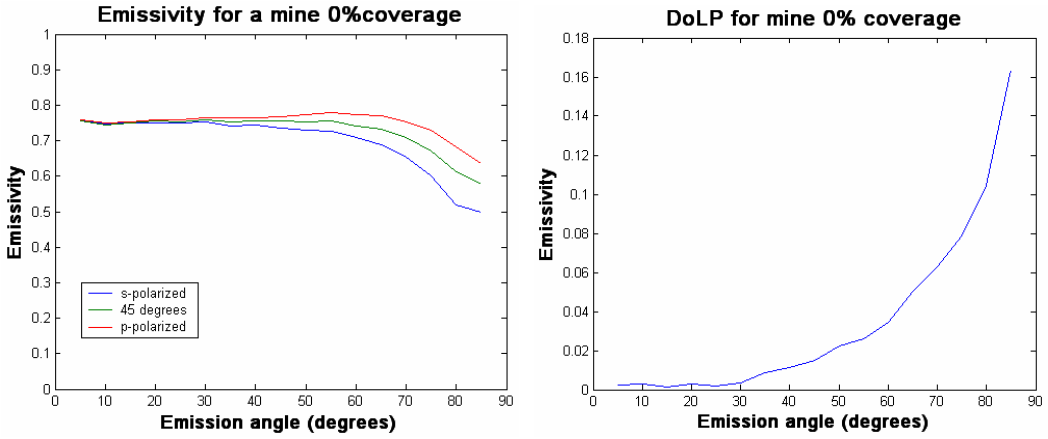

Figure 8-5. Emissivity as a function of emission angle to the left and DoLP to the right, for uncovered mine sample.

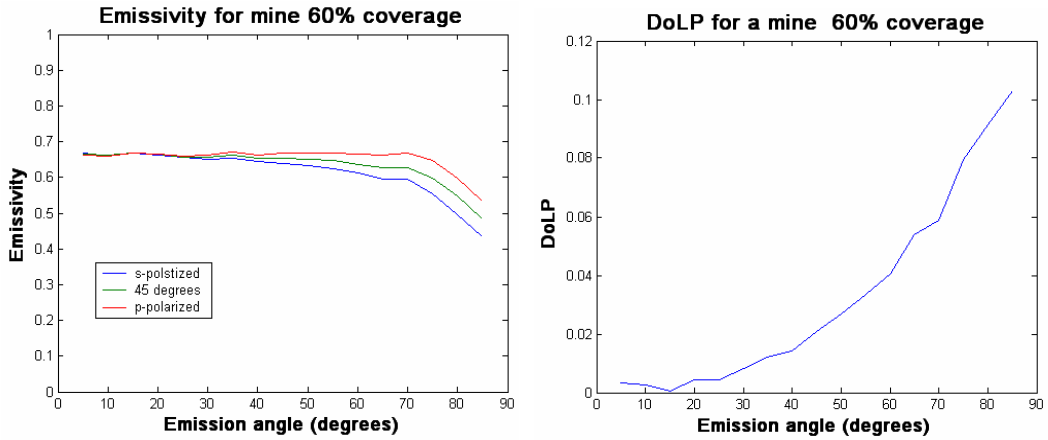

Figure 8-6. Emissivity as a function of emission angle to the left and DoLP to the right, for 60% covered mine sample.

The DoLP is not changing very much when the coverage is increased. A slight decrease is observed. This is consistent with the observation that the mines are well observed for all degrees of coverage studied.

The emissivity measurements give information about the surfaces and behaviour of the mines under different conditions. These measurements can be used for comparing with model polarization scattering calculations of the mine surface including the covering material.

The future work on mines will in be concentrated on model calculations of the properties of the surface of the mines and the effect of covering the mines. Also model calculations and measurements of trip wires will be done in both passive and active mode.

In the SPIE conference paper from Orlando 2004 [75], polarization measurements on realistic minefields, that have been setup by SWEDEC in Sweden, is reported. The goal has been to investigate how many mines and trip wires can be detected with polarization measurements in the LW region. The method is working well, but the present equipment is not very effective in finding mines and trip wires. The camera is old and with low resolution. The number of pixels is 272×136 and due to the size of the polarizer, the cameras are equipped with 20˚ optics. At a distance of 5 m the coverage of one pixel is about one cm and at 10 m the coverage is about 2 cm. Furthermore the dynamics of the grey level is low especially for the calculated polarization parameters. To calculate the polarization parameters, about 60 images are used. Twenty images are used for every polarization angle recorded with 15 Hz. The movement of the polarizer between the recordings takes about one second so the time it takes to register the 60 images is about 6 seconds. The consequence is that any movements within the sight of the camera will blur the polarization image. Any grass moving in the wind will appear as big as the whole amplitude of the movement. The restrictions can be summarized as:

- Low resolution 272×136
- Low dynamic range
- About six seconds to register all images for one polarization image. Movements in the image blur the images.

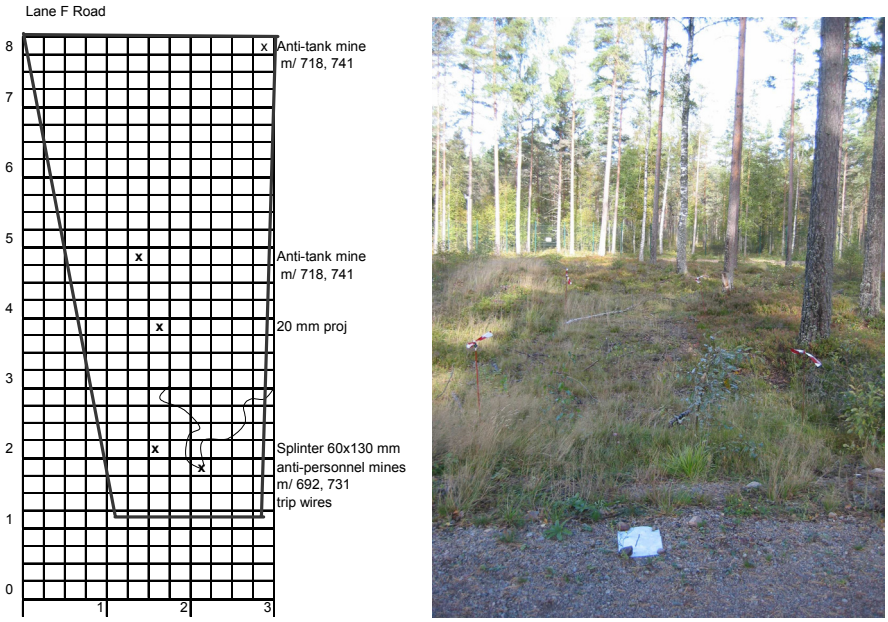

Figure 8-7. To the left is shown a graph of mine field F with objects. An image in the visible light is shown to the right.

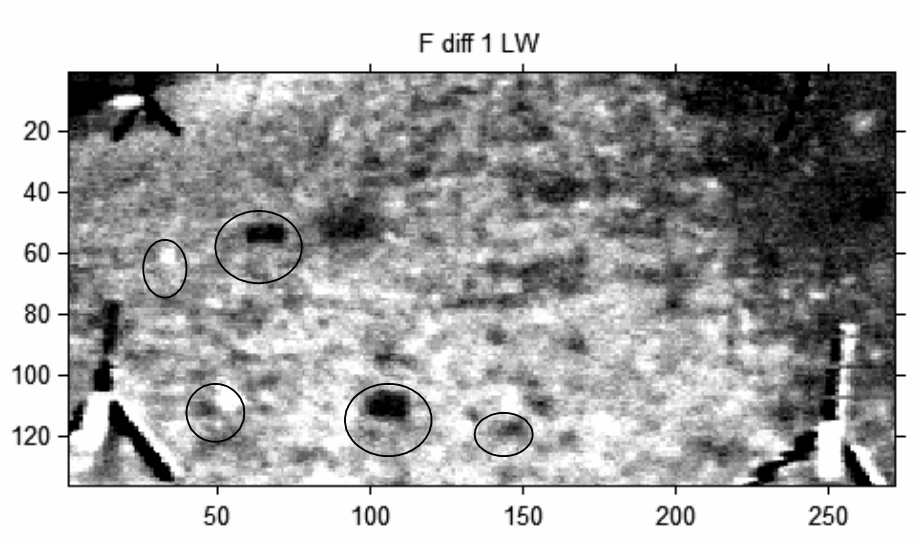

Figure 8-8. DoLP for the minefield F.

The conclusion is that the camera is not optimized for mine detection and therefore the use of these cameras for the demonstration is not expected to give good results. However, the procedure under investigation can be tested. So far, the equipment has been used for laboratory measurements were the circumstances and measuring parameters are well controlled.

Figure 8-7 shows the minefield built by SWEDEC. To the left is a drawing of the minefield, with the mines and trip wires indicated. To the left is a photo of the minefield. Figure 8-8 shows the DoLP where the analysis of the objects is indicated with circles.

As a summary, the model for testing the equipment used for mine detection, including measurements, interpretations and the analyses have been usable and good. The results for this equipment are, as expected, not very good. However the expectation was that it should be better than it turned out to be. In the future there will be polarization sensors available which are designed to measure the polarization of the radiation at the same time in several polarization directions. Hopefully these sensors will work better. A further improvement will occur if the measurements can be performed in both the atmospheric windows at the same time. Recent measurements of spectral reflectance reported in 8.1.2 show that for certain mines the emissivity in the 3-5 µm window is high, whereas it is low in the 8-12 µm window. For other mines the emissivity shows opposite behaviour. A careful investigation of the polarization signatures of mines and backgrounds would increase the certainty of the analysis.

8.1.2 Reflectance

Spectral measurements have been done, using a Brucker FTIR spectrometer; model IFS55 with a LabSphere integrating sphere. A calibrated gold sample is used for calibration of the integrating sphere. The instrument measures the total reflectance.

Fragments of real exploded mines and shells have been used as samples. These are described in Table 8-1.

Mine	Color in visible light	Material	Spectral curve in:	Emittance in 3-5 µm	Emittance in 8-12 µm
PMA-2	light green	plastic	Figure 8-9	0.055	0.06
TMA-4	light green	plastic	Figure 8-9	0.055	0.06
TMRP-6	light green	plastic	Figure 8-9	0.055	0.06
MRUD	light green	plastic	Figure 8-9	0.055	0.06
PMA-1	dark green	plastic	Figure 8-10	0.05	0.06
TMA-1	dark green	plastic	Figure 8-10	0.05	0.06
PMA-3	black	rubber	Figure 8-11	0.05	0.12
M29/32		metal, colour	Figure 8-12	0.18	0.09

Table 8-1. Mines and submunition used to measure the spectral reflectance in 1.6-25 µm.

The mines PMA-2, TMA-4, TMRP-6 and MRUD, seem to have the same kind of surface and the colour is similar in visible light (plastic and light green surface). Therefore the four spectral reflectance curves are grouped together in one figure (Figure 8-9). In the same way the two mines, PMA-1 and TMA-1 have similar surface (plastic with a dark green surface) and are grouped together in one figure (Figure 8-10). PMA-3 is covered with a black rubber and has unique surface and colour. The spectral curve is shown in Figure 8-11. The grenade, M29/32 is made of iron, painted with green paint. The paint has partly disappeared when the grenade exploded and therefore the spectral curve is a mixture of pure metal and paint. The spectral curve is shown in Figure 8-12.

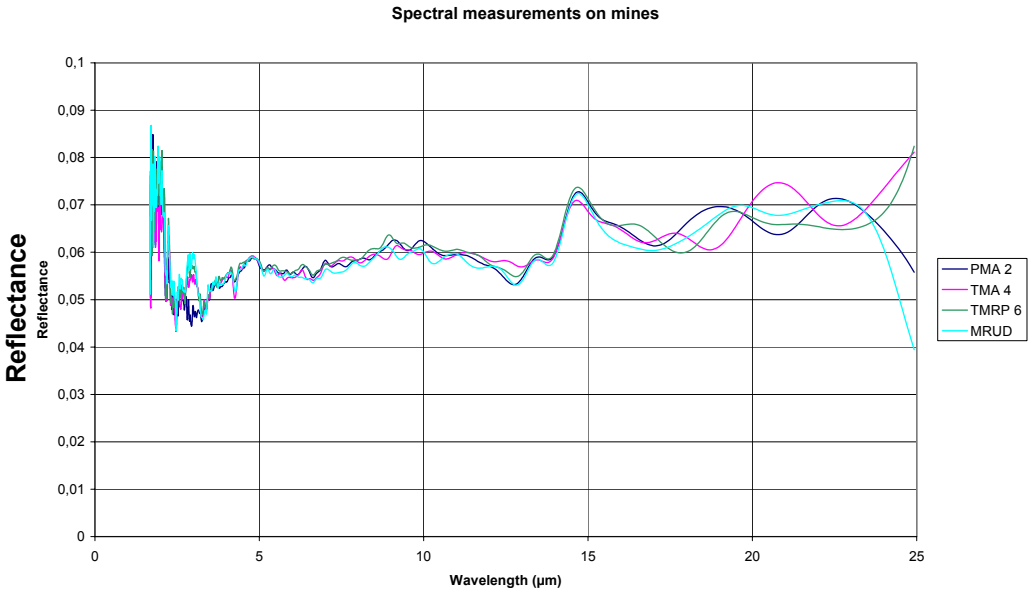

Figure 8-9. Spectral reflectance for PMA-2, TMA-4, TMRP-6 and MRUD.

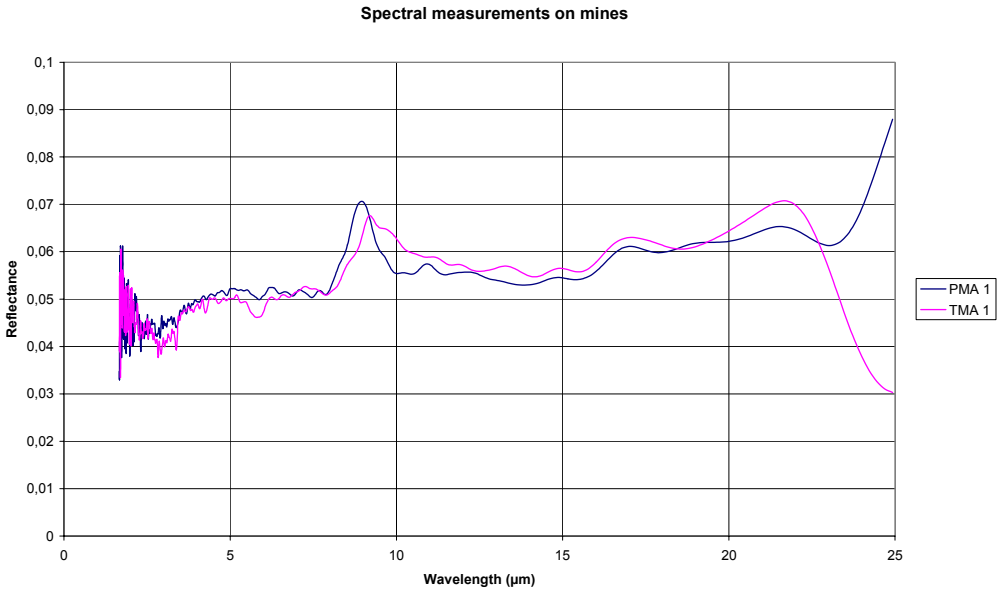

Figure 8-10. Spectral reflectance for PMA-1 and TMA-1.

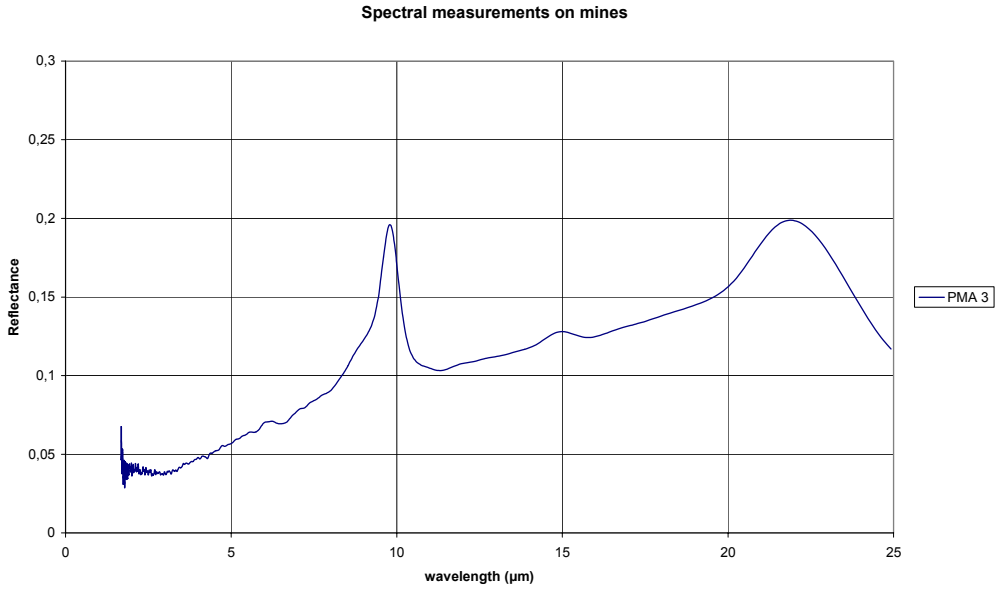

Figure 8-11. Spectral reflectance for PMA-3.

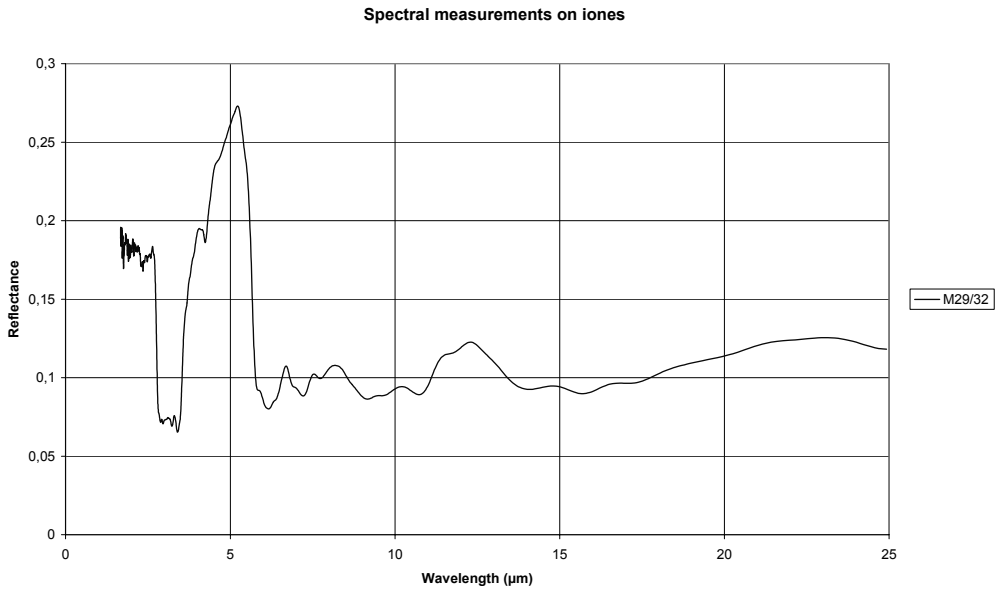

Figure 8-12. Spectral reflectance for the grenade, M29/32.

The four mines in Figure 8-9 have similar colour in the visible light. According to figure 1 the properties in the region 1.6 to 15 µm are also very similar. The reflectance is about 6% throughout the region except for a peak close to 15 µm. The mines in Figure 8-10 also have reflectance spectra that almost coincide, with a peak at about 9 µm. The reflectance is about 5 % which is a little lower than the reflectance curves in Figure 8-9.

As a conclusion, all the green coloured mine fragments, have low reflectance curves. That means that all the mines are highly emitting.

The mine PMA-3 in Figure 8-11 has completely different spectral properties. The spectral curve is that of a rubber band. The curve has a peak close to 10 µm, and a smaller peak at about 15 µm. As a consequence, the mine is highly emitting in the 3-5 µm atmospheric window (about 95 %), and has lower emittance in the 8-12 µm atmospheric window (10-15 %).

The grenade, M29/32 has a rough metallic surface partly painted with a green colour in the visible light. The colour has probably been evaporated at the explosion. The spectral reflectance curve is therefore probably a mixture of the rough metal surface and some colour. That can explain the low value (about 10 %) of the curve above the 6 µm. At about 3 µm there is a broad dip, the origin of which at the present is unknown, which gives a big peak at 3-6 µm. As a consequence the sample has low emittance in the 3-5 µm atmospheric window and high emittance in the 8-12 µm atmospheric window.

8.2 Field trial in Eksjö

A field trial was conducted at the Swedish EOD and Demining Centre (SWEDEC) in May 2005 [217]. The purpose was to take data on surface laid mines, UXO, submunitions, IED's, and background with a variety of optical sensors. The sensors that were used are listed in table 8-2. Some of the sensors were mounted in a skylift at about 10 m above ground, and

other sensors were place on tripods on the ground (about 1.5 m above ground). Three ground types were covered, see: forest (Site 1), gravel road (Site 2) and an area where all the vegetation had been removed some years previously, and where the vegetation had recovered (Site 3).

Sensor /System	Wavelength [µm]	Purpose/Phenomenon	Location	Remarks
ILRIS, 3D Laser	1.54	Active 3-D imaging	Sky lift	
Riegl	0.89	Active 3-D imaging	Tripod	
Emerald	3-4; 3.5-5; 4.5-5.2		Sky lift	
MultiMir	1.5-1.8; 2.1-2.5; 3.5-4.0; 4.5-5.2		Sky lift	
QWIP	8-9	Continuous registration, Temporal	Sky lift	Mounted on separate gimbal
THV900, LW		Polarization sensor	Tripod	Active illumination
Hyper-spectral VIS	0.4-1.0	Hyper-spectral VIS-NIR, ca 600 band	Tripod	
Multi-spectral LW, 900	4 band	Multi-spectral LW	Sky lift	
UV	?		Sky lift	
VIS	0.35-0.75		Sky lift	
NIR	0.83-1.1		Sky lift	
Digital camera	5 Mpixel	High resolution, optical zoom	Sky lift	

Table 8-2. List of sensors that were used in the field trial.

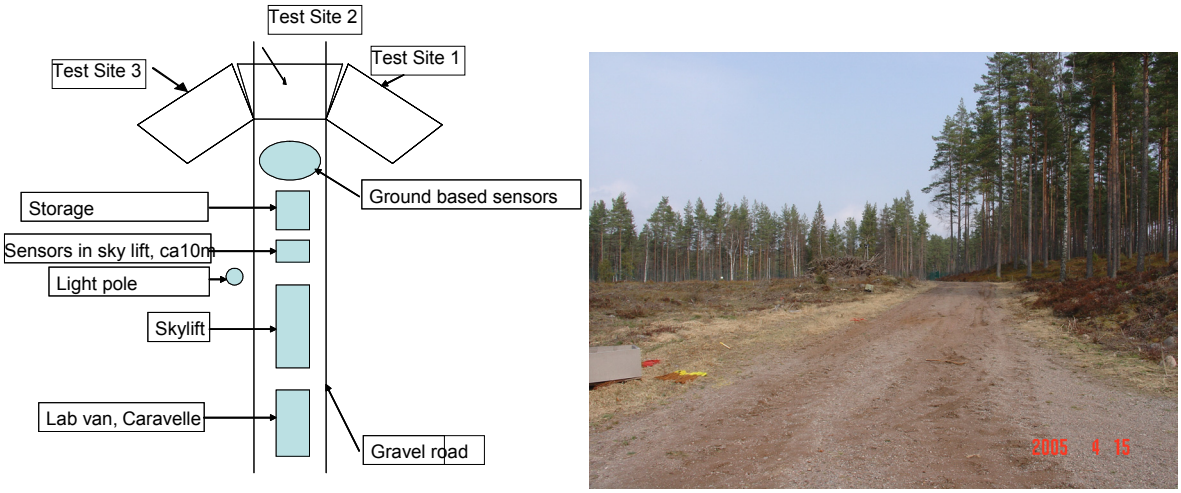

Figure 8-13. To the left a sketch of the measurement scenario, to the right a photo of the area.

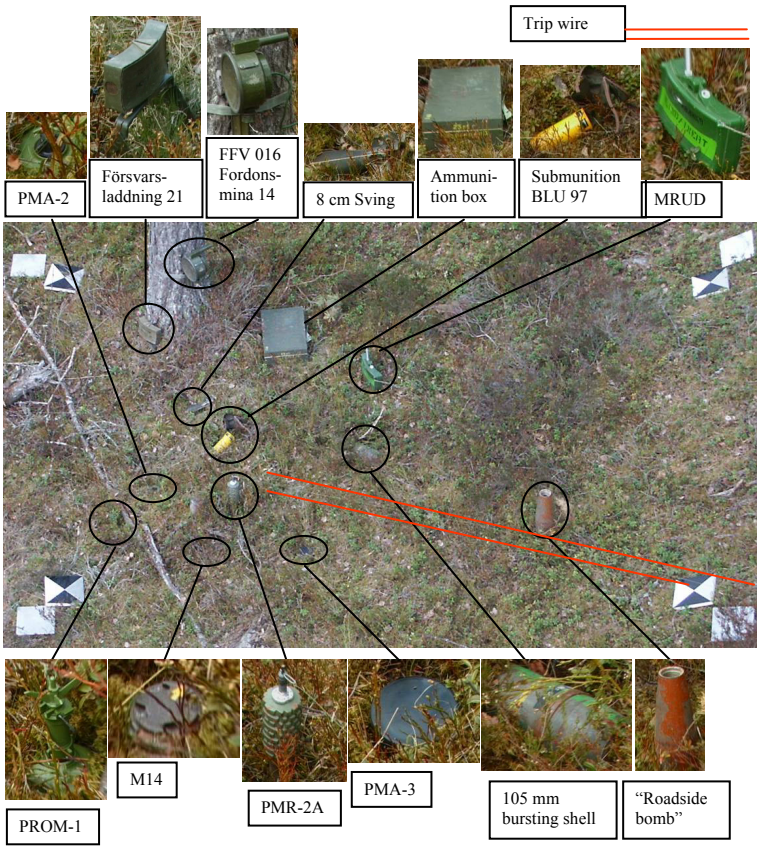

Figure 8-14. Test site 1, with target objects.

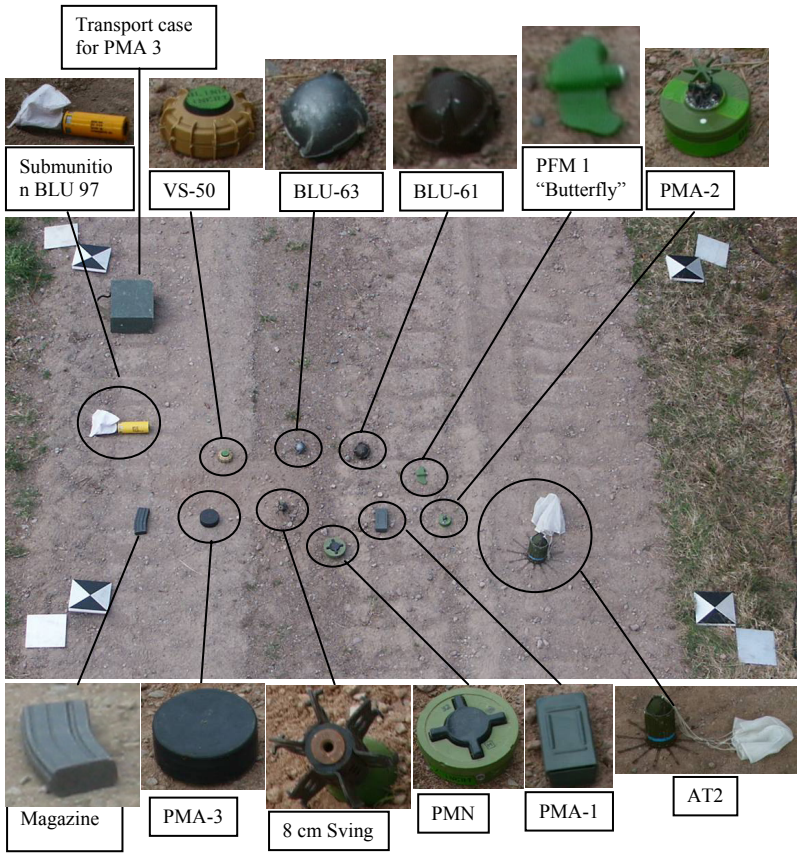

Figure 8-15. Test site 2, with target objects.

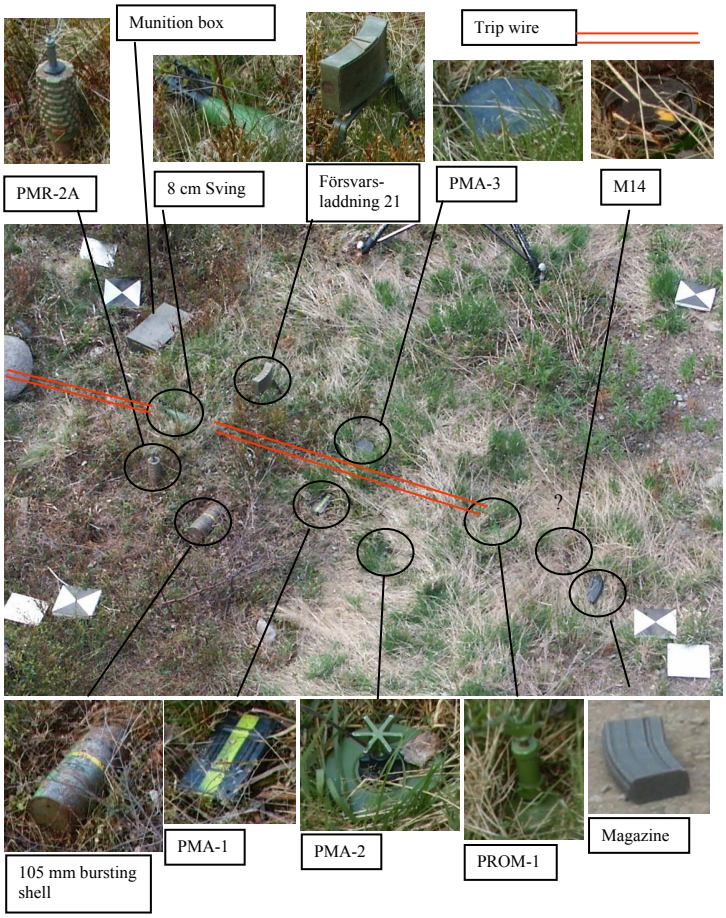

Figure 8-16. Test site 3, with target objects.

Figure 8-17. The sensors mounted on the gimbals in the sky-lift.

8.2.1 Description of the sensors

8.2.1.1 3-D scanning laser radars

8.2.1.1.1 ILRIS-3D

The scanning laser radar, ILRIS-3D, is manufactured by Optech Inc. [44] in Canada. The operating wavelength is 1.5 μm and the laser is eye safe class 1 for the scanning beam. The measurement principle is time-of-flight (TOF). Further specifications are given in Table 8-3. The measurement head, which is mounted on a tripod, contains a laser range finder, scanner and a digital camera, see Figure 8-18. An image from the digital camera is shown on a display on the measurement head. The operator runs the system with a Palm Pilot, on which parameters as scan area and spot spacing can be set. The Palm Pilot is connected to the measurement head with a cable. The data are stored as point clouds containing x, y, z coordinates and intensity value. The sensor is a commercial system, with mainly civilian applications, such as 3-D imaging and modelling. We use it also to measure laser radar signatures, i.e. reflectance (as function of aspect angle). With the laser radar, first or last echo can be selected. This means that a laser pulse that is partly transmitted through some sparse material (such as vegetation, camouflage net, etc.) and reflected from a target surface behind the concealment can be detected by the sensor in the "last pulse" mode, see Figure 8-19.

Parameter	Data
Wavelength	1.5 μm
Maximum range	350 m (4% reflectance); 800m (20% reflectance)
Accuracy	X-Y @ 100 m ±10 mm Z @ 50 m ±10 mm, Z @ 100 m ±10 mm
Field of view	40º (±20 º, programmable, horizontal and vertical)
Divergence	0.2 mrad
Range Resolution	1 cm
Angle Resolution	0.2 mrad
Sampling Frequency	2000 points/s
Working Temperature	0°C -- +40 °C
Size	30 x 30 x 20 cm
Weight	12 kg

Table 8-3. Specifications for ILRIS-3D

Figure 8-18. The laser scanner ILRIS-3D, front view to the left. The measurement head is mounted on a tripod. On top is the PalmPilot, which is connected to the measurement head with a cable. The photo to the right shows the display window on the back of the measurement head.

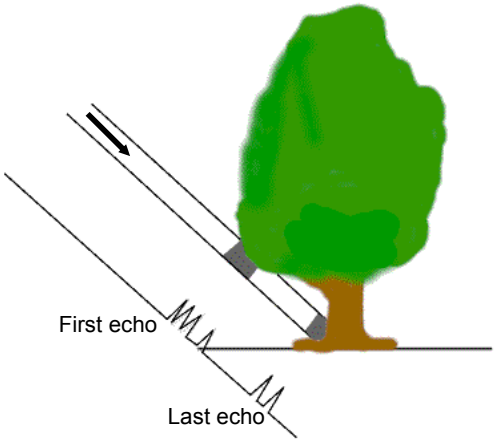

Figure 8-19. First or last echo can be selected on the ILRIS-3D.

8.2.1.1.2 Riegl

The scanning laser radar, Riegl LMS-Z210, is a commercial system manufactured by Riegl Laser Measurement Systems GmbH in Austria [27]. The operating wavelength is 0.904 µm and the laser is eye safe class 1 for the scanning beam. The measurement technique it uses is TOF. Further specifications are given in Table8-4. The measurement head, which is mounted on a tripod, contains a laser range finder and a scanner, see Figure 8-20. The scanner is controlled by a PC and the image is presented in real time. The data are stored as point clouds containing x, y, z coordinates and intensity value. For the LMS-Z210 is also a passive RGB-value collected for each point. The RGB-value can be used for a texturing.

Parameter	Data
Wavelength	0,904 μm
Laser Power	1 mW
Measurement range Accuracy	2-350 m (ρ≥50% reflectance); 2-150m (ρ≥10% reflectance) 2,5 cm (Sigma 1) for FOI's LMS-Z210
Field of view	340º (±170º hor.), 80º (±40º ver.), programmable, horizontal and vertical
Beam Divergence	3.0 mrad
Range Resolution	2,5 cm
Angle Resolution	0,018° (hor.), 0,036° (ver.)
Sampling Frequency	Nom 6500 points/s
Working Temperature	-10°C -- +50 °C
Size	44 x 21cm
Weight	13 kg
Classification	Class 1 under all operating conditions

Table8-4. Specifications for Riegl LMS-Z210

Figure 8-20. The laser scanner Riegl LMS-Z210, mounted on a tripod.

8.2.1.2 Polarization

For the first time, we have made active polarization measurements. A laser was placed close to the sensor and the laser ray was illuminating part of the mine field. The sensor, a

Thermovision®900 camera, was measuring the radiance for different polarization and the DoLP can then be calculated.

The illuminating laser was a CO_2 laser, model 48-G-2-28 from Synrad Inc. The laser delivered nominally 25 W of vertically polarized radiation at around 10 μm wavelength. The beam was transmitted through a beam expander, resulting in a footprint of about 0.6 m diameter at a range of 4 m. However, the beam quality was quite poor, and hence it was not possible to achieve a uniform (or even Gaussian) illumination of the target area.

The sensor used for the measurements reported in this work is an Agema Thermovision®900 camera working in the 8-12 μm region (LW), Figure 8-21. In front of the camera is a polarization filter (Graseby IGP-228-70) mounted. The filter is mounted so that it is possible to rotate it by a stepper motor. The properties and calibrations of the equipment are described in detail in other papers [218, 219]. Here it is summarized.

Both cameras are calibrated against a series of traceably calibrated black body radiators [220]. The equation that describes the relation can be written as

$$r = c_1 \cdot g + c_0$$

r is the radiance, in $Wm^{-2}sr^{-1}$, detected by the camera and g is the grey level of the image. The inclusion of the polarizer makes it necessary to include the emission of heat radiation from the polarizer, towards the detector. This radiation should be almost as big as the incoming radiation due to the fact that the temperature of the polarizer is about the same as the temperature of the scene. Thus the difference between the measured curve with a polarizer and the corrected curve without a polarizer is the correction term $h_{correction}$. It has been shown [218] that the correction term is almost constant. The calibration is done by first subtracting the calibration constant from the measured grey level for measurements with polarizer and then for all measurements, both with and without polarizer corrects the grey level with the equation above which gives the radiance in $Wm^{-2}sr^{-1}$.

Figure 8-21. Agema Thermovision®900 cameras with the polarizers mounted in front of the optics.

The camera takes 18 pictures for each of the polarization angles 0°, 45° and 90° respectively. A stepper motor rotates the polarizer between the angles. For every polarization angle, the mean value of the 18 pictures is calculated thereby reducing the noise. According to Stoke

theories, it is sufficient to measure the radiance for three polarization angles if the circular polarization can be neglected. Thus the three measurements above are enough to calculate the first three Stoke parameters and also the quantities DoLP and theta.

8.2.1.3 UV sensor

The UV sensor is a Hitachi, KP 160 E/K black-and-white video camera with a Si-detector with 752×582 pixel elements equipped with a filter that block the radiation above 350 nm. The camera was equipped with a Cosmicar/Pentax TV zoom lens 8-120 mm focal length. In that configuration the focus and zoom factor could be remotely controlled. Data acquisition was performed on digital video band (DV).

8.2.1.4 VIS sensor

The Sony FCB-IX470P is a one chip CCD colour camera with 18× zoom lens and a 1/4" detector. The camera has low weight (220 g) and low power consumption (4.2 W). Data acquisition was performed on digital video band (DV). The zoom factor was manually set in advance and auto focus was in use. Data acquisition was performed on digital video band (DV).

8.2.1.5 NIR

The camera for near IR is a SONY FCB-IX470P Black-and-white video camera with a Si-detector with 752×582 pixel elements. The camera was originally equipped with an optical filter removing radiation in the near infrared. This filter has been removed and exchanged with a filter removing radiation with a wavelength shorter than 830 nm. The upper limit 1100 nm is due to limitations in the Si-detector. The camera was equipped with a Cosmicar/Pentax TV zoom lens 8-120 mm focal length. In that configuration the focus and zoom factor could be remotely controlled. Data acquisition was performed on digital video band (DV).

8.2.1.6 Multispectral sensors

Two multispectral sensors were used, Emerald and MultiMIR, see Figure 8-22.

Figure 8-22 Multispectral sensors used in trial. Left: Emerald, Right: MultiMIR

Data for the multispectral sensors are given in Table 8-5.

Parameter	**MultiMIR**	**Emerald**
Detector	Cooled MCT (HgCdTe)	Cooled InSb
No. of pixelsl	384×288	640×512
Pixel size	20×20 µm (spacing. 4µm)	20×20 µm
Spectral range	1,5-5,2 µm	3,6-5,1 µm
NETD	<25 mK, 300 K	20mK, 298 K
Filter	4 filters: 1) 1,5-1,8 µm 2) 2,1-2,45 µm 3) 3,5-4,1 µm 4) 4,55- µm	4 filters: 1) <3,9 µm 2) 3,3-5,0 µm 3) >4,6 µm 4) empty
Speed	100 Hz, filter wheel still 25 Hz, filter wheel running 1000 Hz, max 16×16 pixlar	1-50 Hz full frame max 500 Hz subframe
Integration time	50µs-2,6ms	3µs-10ms, 1µs steg
A/D conversion	14 bits	14 bits
Power	12V / 10A	24V VDC, <3A
Size	b=225, h=180, l=310	b=130, h=162, l=275
Weight		5,5 kg
Lens 1	f=100 mm F/2,0	f=50 mm F/2
FOV	5,3×4,0°	18×14°
IFOV	0,24 mrad	500 µrad
Synfält 1000m	90×70m	320×250m
Pixel täck 1000		
Size		

Weight		
Lens 2	f=15mm f/2	f=250 mm F/2
FOV	35×26°	4×3°
IFOV	1,6 mrad	100 µrad
Synfält 1000m		64×51m
Pixeltäck 1000		
Size		
Weight		

Table 8-5. Data for the multispectral sensors.

8.2.1.7 Hyper-spectral sensor

The hyper-spectral sensor was rented from Barracuda AB, Figure 8-23. It is sensitive in wavelengths 400-1000 nm and can give hyper spectral images of spatial resolution of 1200×875 pixels. The band width can vary from 0.7 to 5.6 nm. If 5.6 nm is used then the hyper spectral cube will consist of 110 bands. The dynamic range is 14 bits.

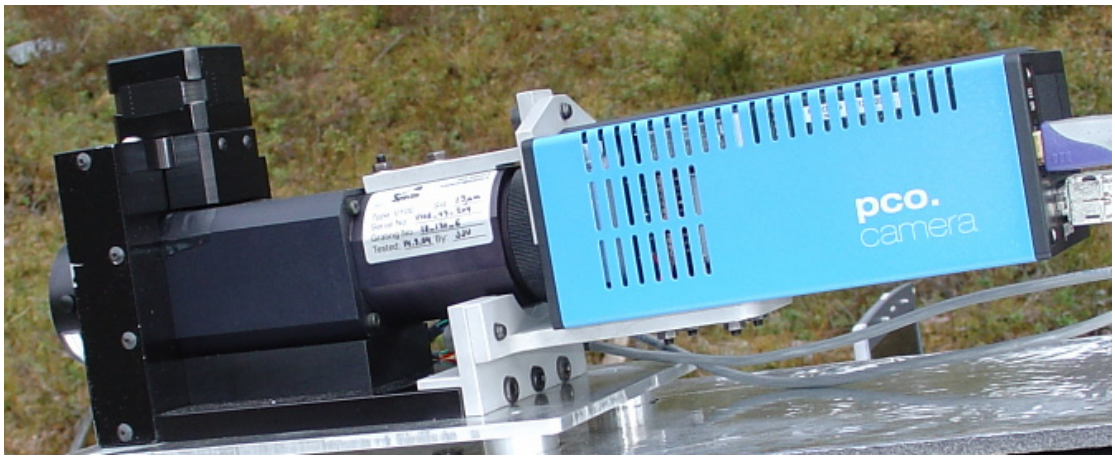

Figure 8-23 Hyper-spectral sensor supplied by Barracuda.

8.2.2 Initial results from the field trial

8.2.2.1 3-D scanning laser radar

For the laser radar data both the 3-D and the reflectance was studied. For all test sites several of the targets were detected by filtering of reflectance data, together with false alarms. The height profiles (projections of 3-D data) are harder to interpret by the eye for Test site 1 and 3, as the background's height profile varied in a similar way. Detection from height profiles is probably possible to perform automatically, for example by statistical methods. In Figure 8-24 - Figure 8-27 the method of analysis is shown for Test site 1. In Figure 8-24 the height profile of Test site 1 is shown. High objects, like the tree and the road side bomb, create occluded areas where no samples are retreived. In Figure 8-25 the reflectance data from Test site 1 is

shown. Some of the targets are visible by eye in this image. The complete data set contains over 300.000 samples, where most are non-targets, which makes it hard to interpret by eye. In Figure 8-26 the distribution of height and reflectance data are shown. We can see that the reflectance data contains a lower "tail" and in Figure 8-27 only these samples are shown. Using this simple filtering most targets are now detected. There are also several false alarm detections. For Test site 1, Försvarsladdning 21, M14, PROM-1, PMA-2 and the trip wire are not detected. There are also false alarms present. In the figures below the height data is not fully corrected for the forward-looking perspective, this introduces some sceweness in some of the larger targets.

At Test site 2 the background is flatter and more homogeneous and all targets are detected in 3D data, reflectance data or both. There are also several false alarm detections. The flatter background results in a profile where the larger targets can be seen easy, see Figure 8-29. The height data are almost equally distributed but the reflectance values have a distribution similar to Test site 1, see Figure 8-30. In Figure 8-28 the height profile of Test site 2 is shown. In Figure 8-31 the samples with low reflectance values are shown.

At Test site 3 the background is more varying. Still, most targets are detected in 3-D data, reflectance data or both. There are also several false alarm detections. The distribution of height data is similar to Test site 1 and the reflectance values have a distribution similar to Test site 1 and 2, see Figure 8-33. In Figure 8-32 the height profile of Test site 3 is shown. In Figure 8-34 the samples with low reflectance values are shown.

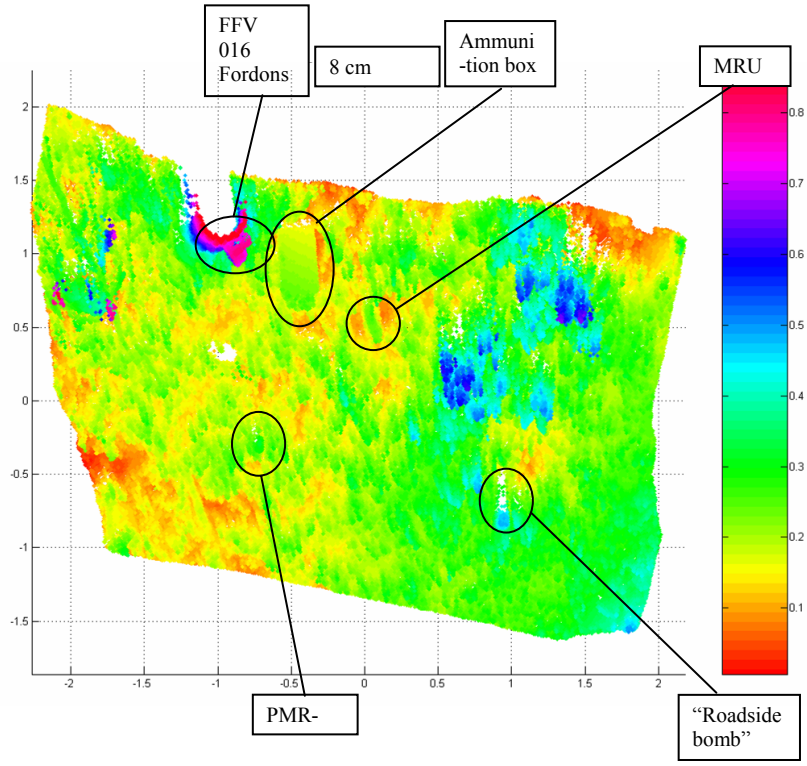

Figure 8-24. Test site 1, with target objects, in top view. 3-D data is shown, axes in meters. Only a few targets are detected by the eye.

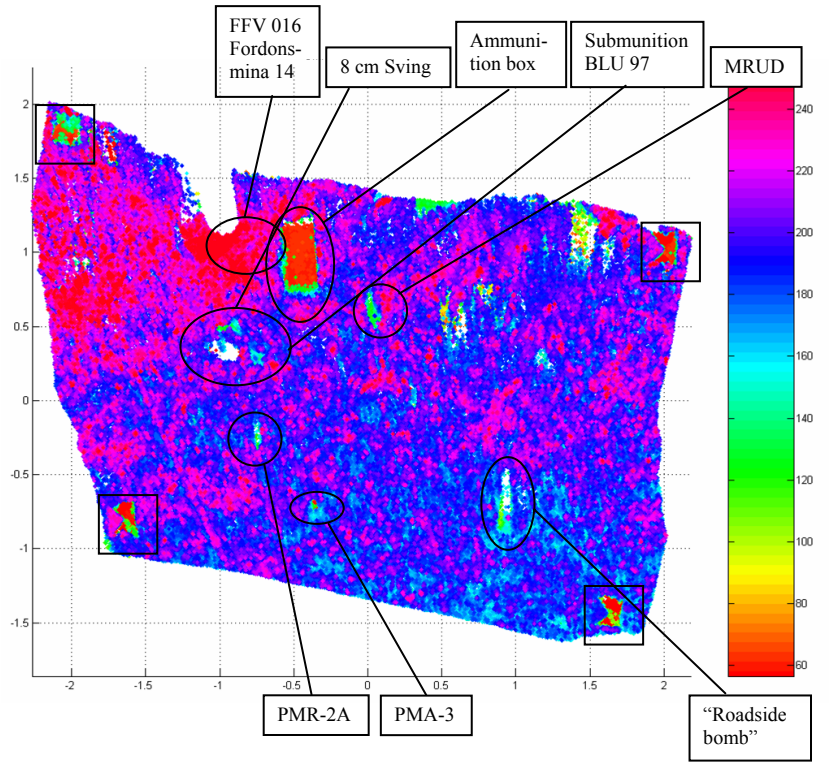

Figure 8-25. Test site 1, with target objects, in top view. Reflectance data is shown, the squares marks the test site markers, axes in meters. A few targets are detected by the eye.

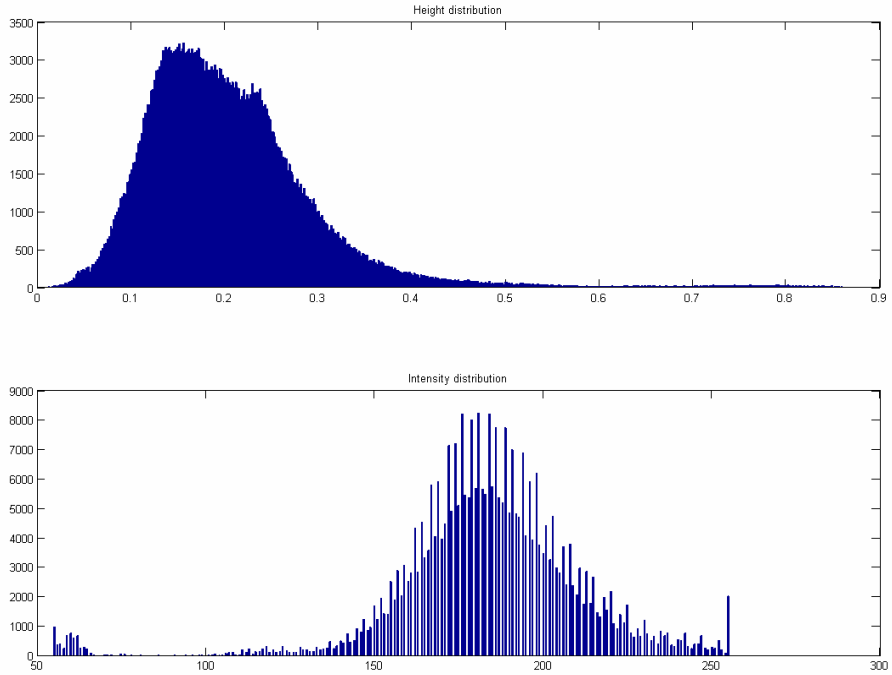

Figure 8-26. Test site 1, with target objects. Distributions of height data (top) and reflectance data (bottom) are shown.

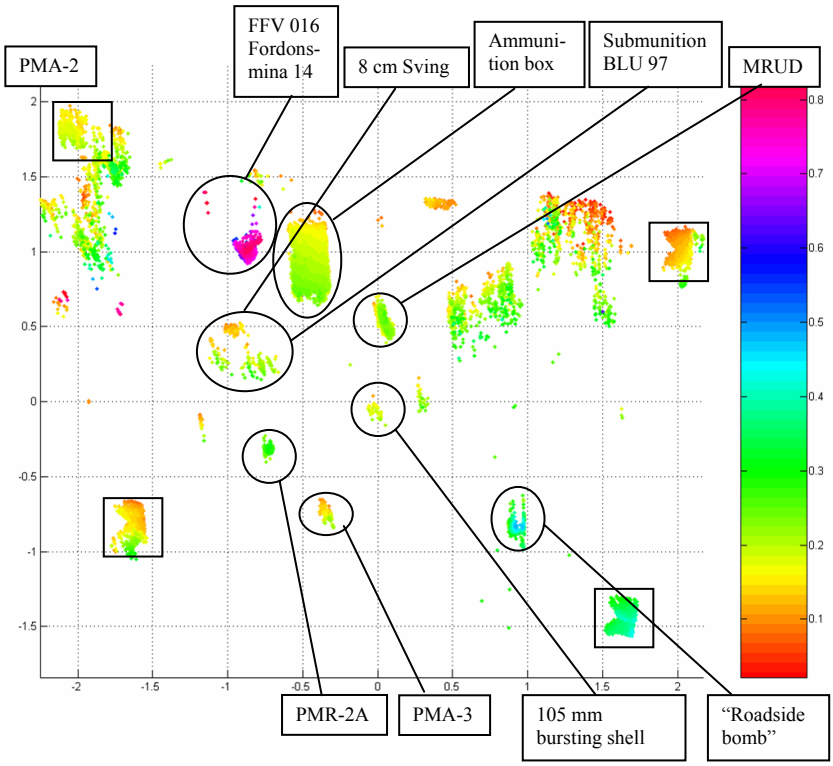

Figure 8-27. Test site 1, with target objects, in top view. Height profiles of positions with low reflectance values are shown, the squares marks the test site markers, axes in meters. PMA-2, Försvarsladdning 21, PROM-1, M14 and the trip wire are not detected.

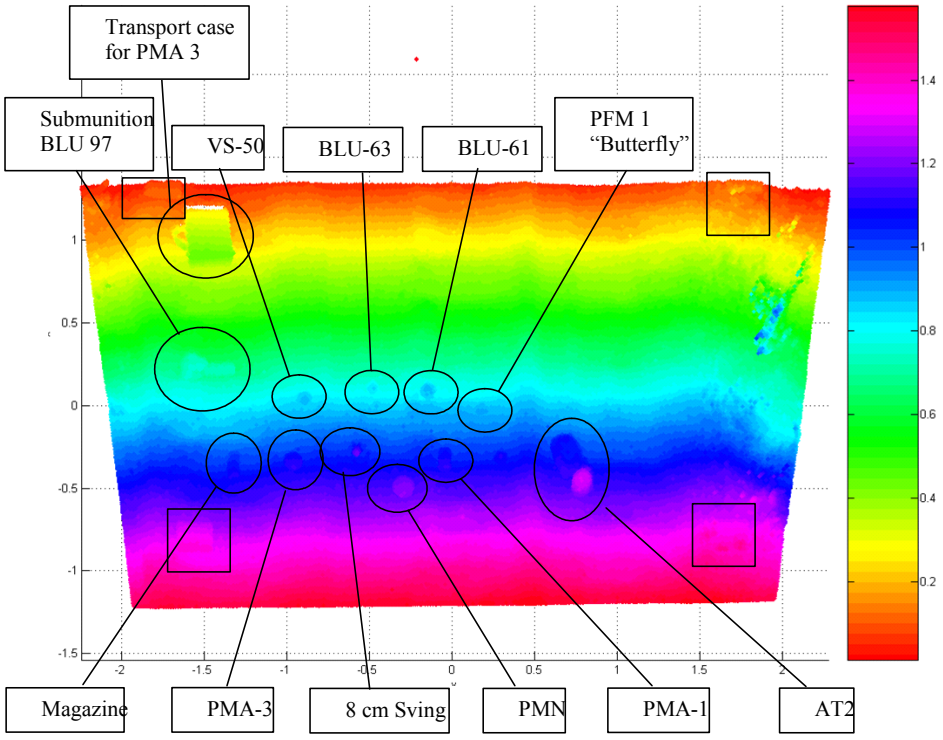

Figure 8-28. Test site 2, with target objects, in top view. 3-D data is shown, the squares marks the test site markers, axes in meters. The PMA-2 is not detected.

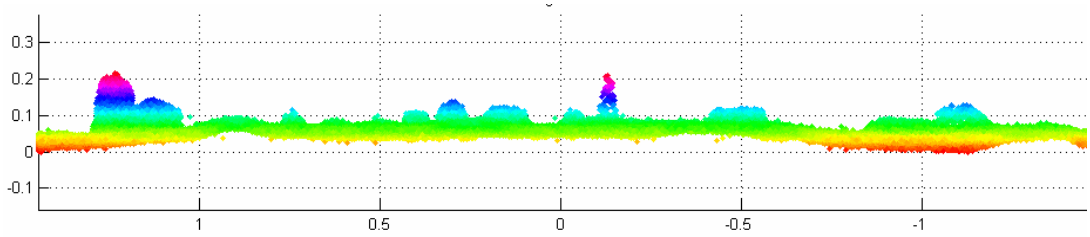

Figure 8-29. Test site 2, with target objects, in side view. Height profile (side projection of 3-D data) is shown , axes in m.

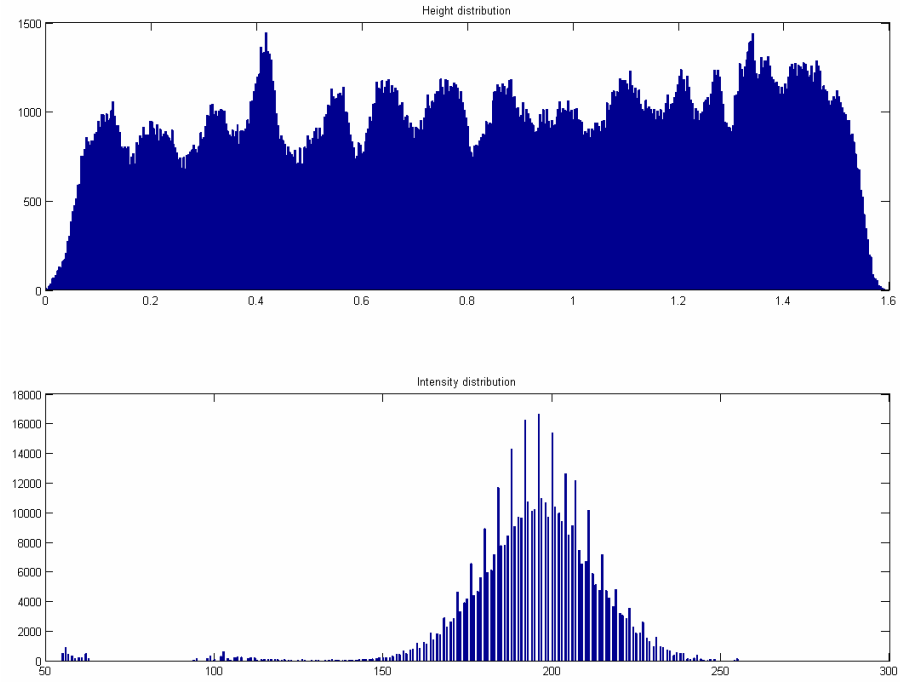

Figure 8-30. Test site 2, with target objects. Distributions of height data (top) and reflectance data (bottom) are shown.

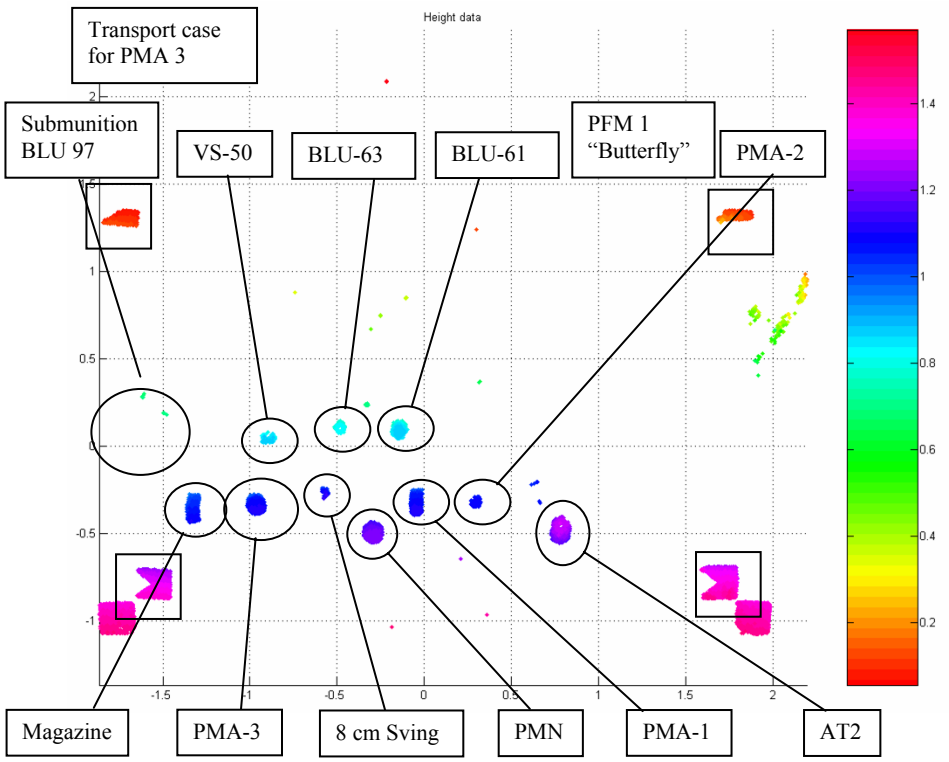

Figure 8-31. Test site 2, with target objects, in top view. Height profiles of positions with low reflectance values are shown, the squares marks the test site markers, axes in meters. BLU97, transport case and PFM1 are not detected by reflectance.

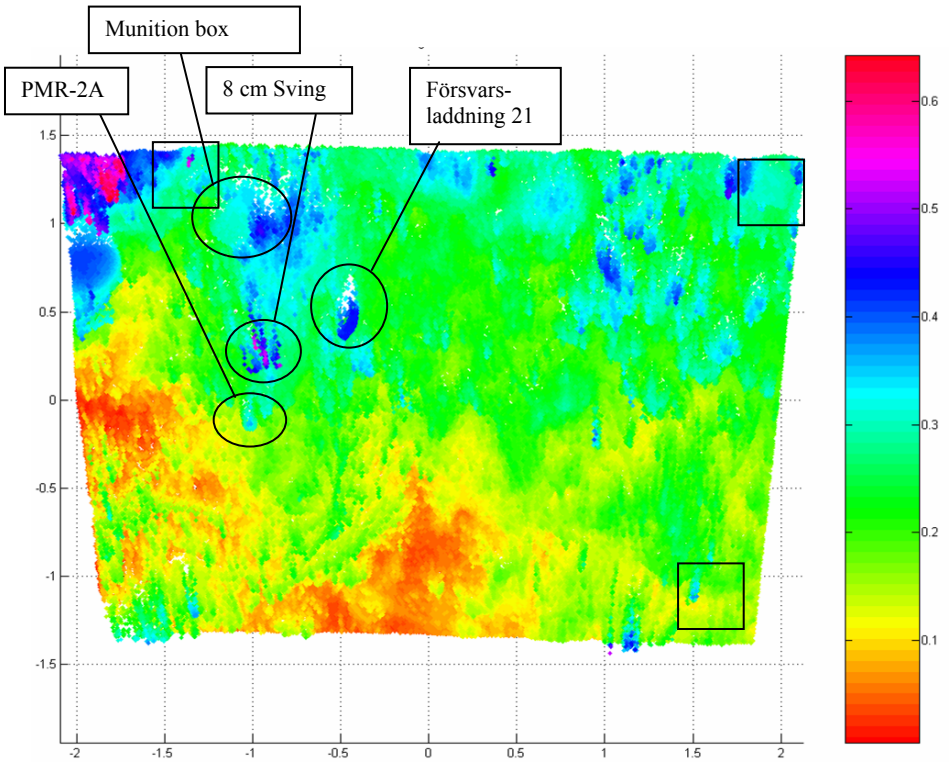

Figure 8-32. Test site 3, with target objects, in top view. 3-D data is shown, the squares marks the test site markers, axes in meters. A few targets are detected by the eye.

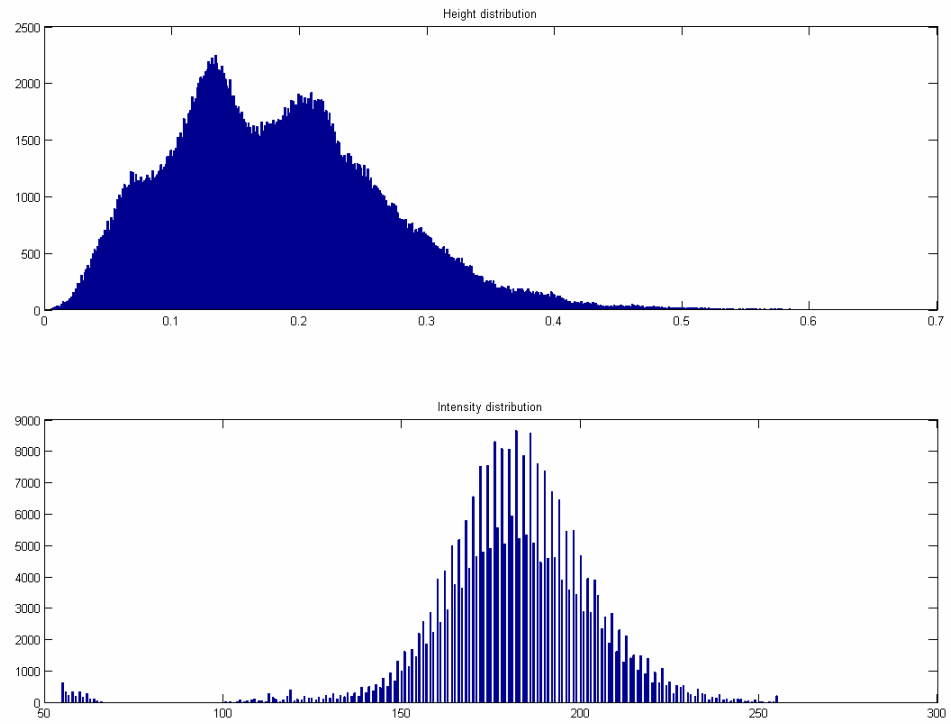

Figure 8-33. Test site 3, with target objects. Distributions of height data (top) and reflectance data (bottom) are shown.

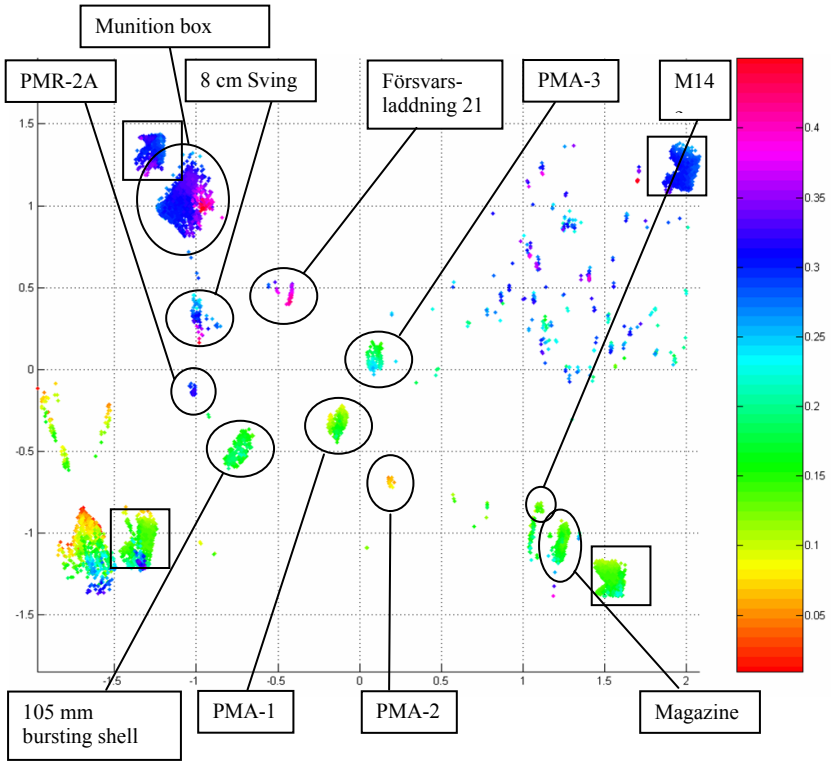

Figure 8-34. Test site 3, with target objects, in top view. Height profiles of positions with low reflectance values are shown, the squares marks the test site markers, axes in meters. PROM-1 and trip wire, and maybe M14, are not detected in reflectance mode.

8.2.2.2 Object recognition

Rectangle fitting

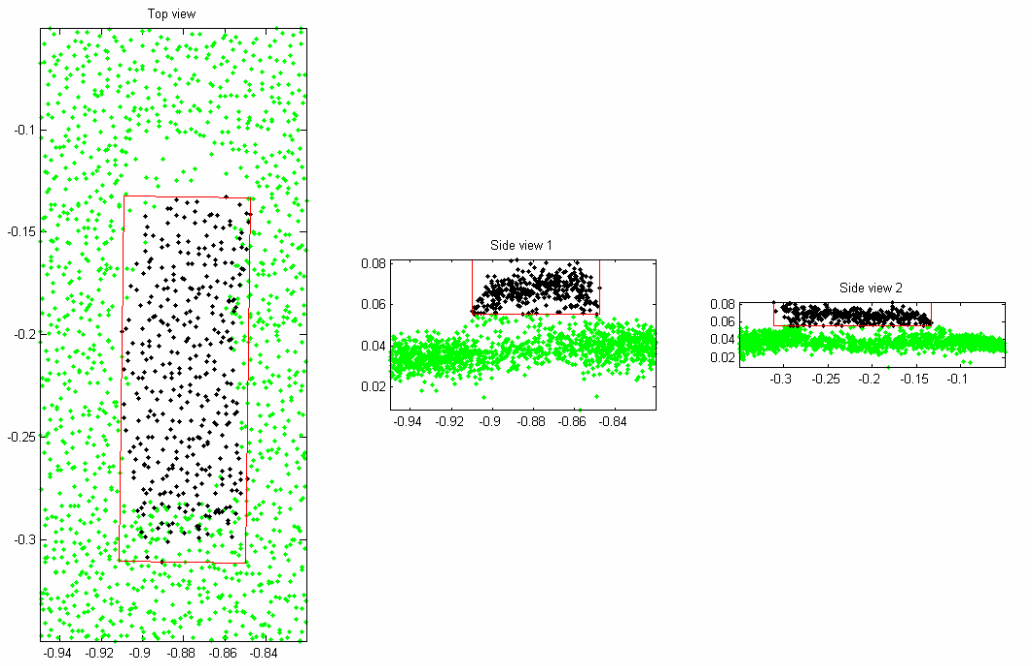

Figure 8-35. The AK-5 clip at Test site 2. Dimensions in m.

At FOI there is also research on recognition of ground vehicles based on laser radar data. If the target is registered with a 3-D imaging laser radar, its shape can be analyzed. One step in this analysis is to estimate the vehicle's dimensions, which is done using rectangle fitting [221]. This approach has been tested on some of the targets at Test site 2. It should be noted, though, that the detection and segmentation of the targets have been performed by hand. In Figure 8-35 – Figure 8-37 results of the dimension estimates are shown for an AK-5 ammunition clip, an AT mine and an AP mine. Due to the good resolution of the laser, the shape of the clip can be seen and the height profiles of all targets.

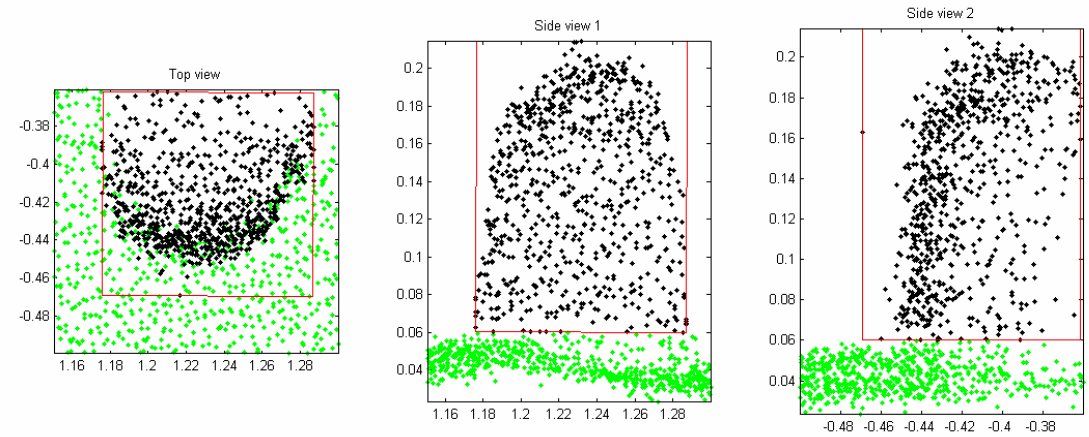

Figure 8-36. The AT mine AT2 at Test site 2. Dimensions in m.

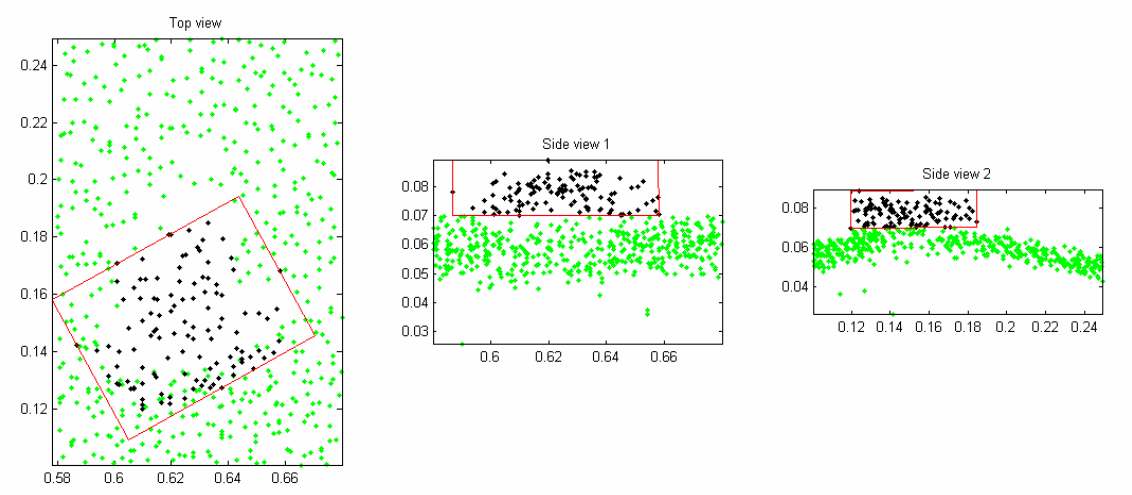

Figure 8-37. The AP mine PFM1 "Butterfly" at Test site 2. Dimensions in m.

Spin images

Due to the promising results obtained by other researchers, an implementation of the spin-image concept was initiated by FOI. The algorithm implementation follows the one described by Johnson [204] and was applied to 3-D laser radar data from scenes containing mines, collected during the FOI field trial. The stack of spin-images constructed from the scene can then be used for model-based detection and recognition. Because mines come in such a wide variety of shapes and sizes, a somewhat different model-based strategy has been selected. Instead of matching the scene with a spin-image library synthesized from actual mine models, we search the data for points matching certain generic surface properties. Figure 8-38 shows the result from running a match of the scene data against a template constructed so as to assign the highest scores to points on structured flat surfaces. We can see that the large ammunition case and the reference plates in the corners of the scene stand out from the surroundings. In a future implementation, this concept will be generalised to locate and cluster surfaces of different curvatures or other suitable properties. The idea is that this concept will show a potential for segmenting man-made objects present in a less geometrically structured environment.

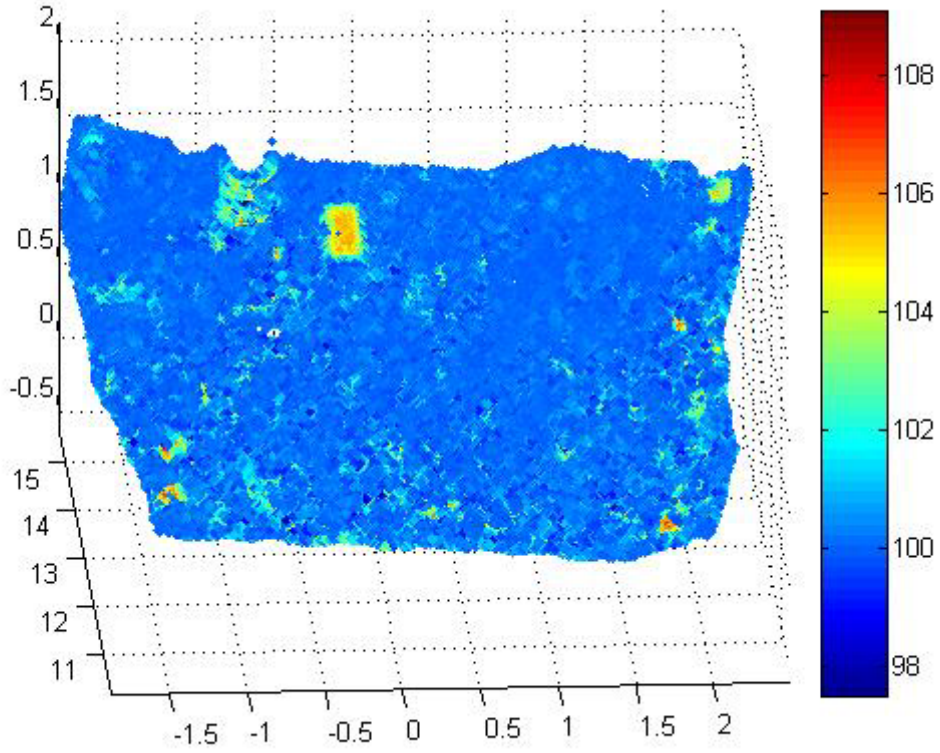

Figure 8-38 Scores obtained looking for structured plane surfaces in the scene data, using a spin-image template. A separate score is calculated for each point based on its spin-image, and the figure displays the result in colour-code. High scores are assigned to points on the large rectangular ammunition case, the reference markers in the corners of the scene and on part of the tree trunk.

8.2.2.3 Reflection from mines at wavelength 1540 nm

The three areas have been measured by Optech ILRIS-3D at 1540 nm. Measured reflections from the mines can be read in Table 8-6. As can be seen in the table, some mine types has been measured in several areas with different values. It depends on how the laserbeam has hit the surface of the mine (at what angle) and differences/age in the painting. Intensity images from the areas can be seen in Figure 8-39 to Figure 8-41.

Mine	Reflectance (Test site)
FFV016 “Försvarsmina 14”	0.08 (1)
MRUD (green surface) (Text field)	0.08 (1) 0.03 (1)
BLU97 (submunition)	0.32 (1), 0.36 (2)
BLU97 (parachute)	0.17 (1), 0.51 (2)
Ammunition box PMA3	0.03 (1), 0.42 (2), 0.03-0.08 (3)
VS-50	0.13 (2)
BLU-63	0.18 (2)
BLU-61	0.06 (2)
PFM1 “Butterfly”	0.28 (2)
Magasin	0.12 (2)
PMA-3	0.06 (1), 0.16 (2), 0.06 (3),
8 cm Swing	0.13 (1), 0.26 (2), 0.16-0,22 (3)
PMN	0.07 (2)
PMA-1	0.03 (2), 0.02-0.11 (3)
PMA-2	0.16 (1), 0.17 (2), 0.12-0.21 (3)
AT2 (submunition)	0.15 (2)
AT2 (parachute)	0.38 (2)
”Försvarsladdning 21” (upper side) (side)	0.25 (1), 0.28 (3) 0.21 (1), 0.15 (3)
PMR-2A (upper side) (side) (whole mine)	0.06 (3) 0.28 (3) 0.18 (1)
10.5 cm hand grenade (yellow stripe) (green surface)	0.08 (3) 0.19 (1), 0.17-0.23 (3)
PROM-1	0.27 (1) Not seen in gravel (Gravel 0.28-0.35) (3)
M14	Not seen in grass (Grass 0.24-0.5) (1) Not seen in gravel (Gravel 0.35) (3)
“Roadside bomb”	0.1-0.2 (1)

Table 8-6. Reflection values from mines measured from skylift.

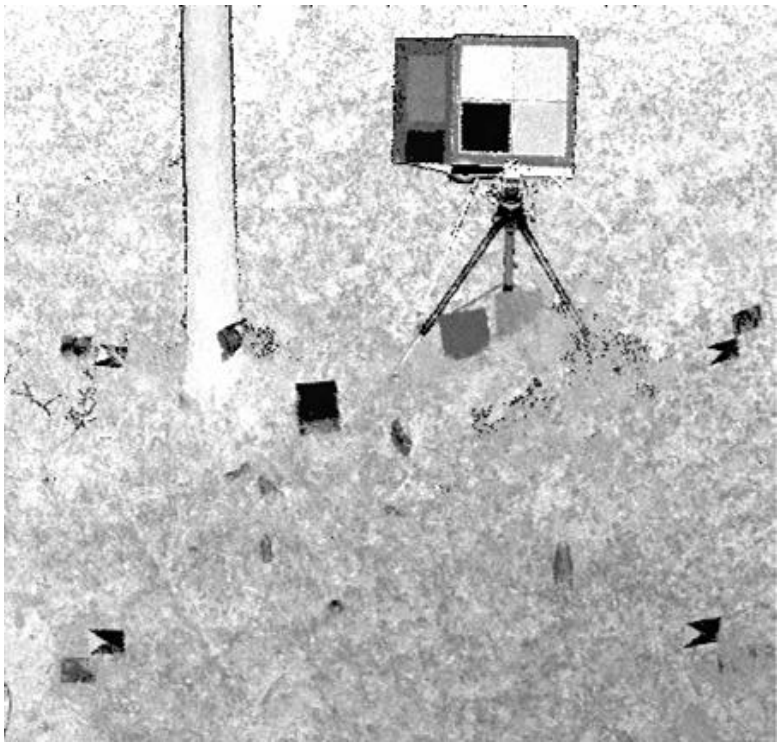

Figure 8-39 Intensity image in Test site 1 at 1540 nm recorded with Optech ILRIS-3D.

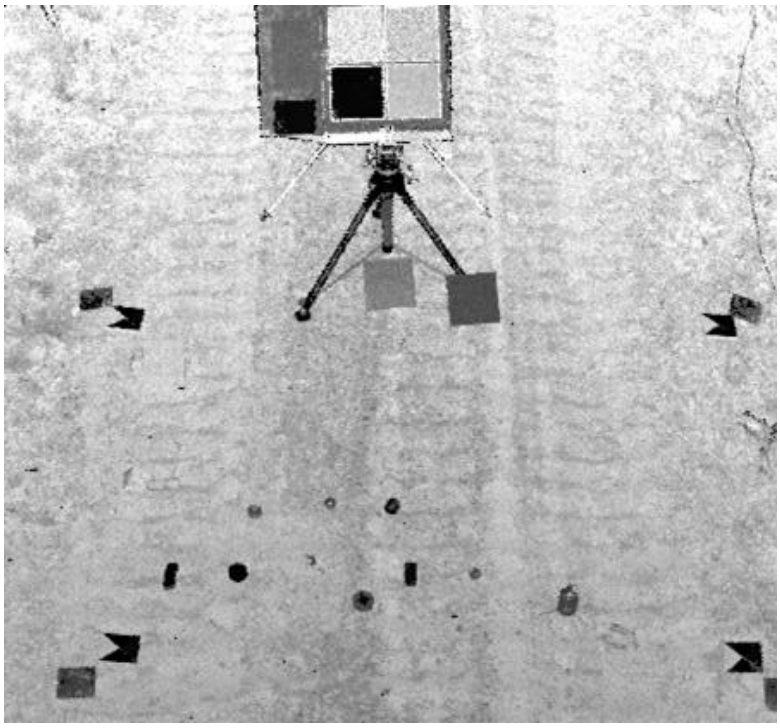

Figure 8-40 Intensity image in Test site 2 at 1540 nm recorded with Optech ILRIS-3D.

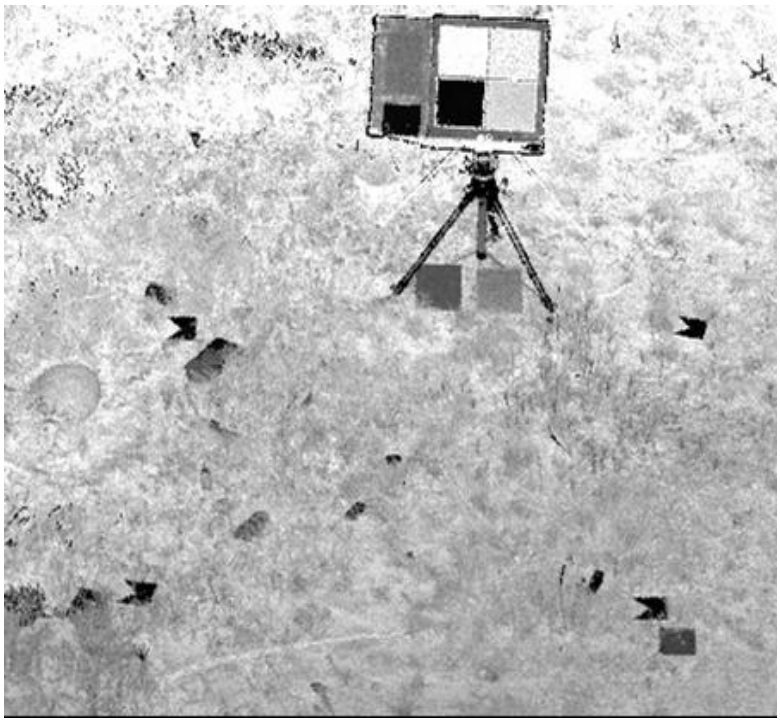

Figure 8-41 Intensity image in Test site 3 at 1540 nm recorded with Optech ILRIS-3D.

8.2.2.4 Reflectance at 1540 nm in comparison with 904 nm

Area 2 (road scenario) has also been measured with Riegl LMS-Z210i with wavelength 904 nm. In Table 8-7 reflection values are presented in comparison with values from 1540 nm. We have to keep in mind that measuring have not been made from the same place. The Riegl equipment was placed at a tripod on ground and therefore the laser has hit mines and ground with a very oblique angle of incidence. The values are not able to directly compare, but can give a small hint about differences between the wavelengths, see for instance how clear the submunition AT2 can be seen towards the gravel road at 1540 nm but is very hard to see in 904 nm.

Mine	**Reflectance at wavelength**	
	904 nm	**1540 nm**
BLU-63	0,13	0,06
BLU-61	0,16	0,18
8 cm Swing	0,09-0,16	0,26
Munition box PMA3	0,16-0,26	0,42
AT2 (parachute)	0,17	0,38
AT2 (submunition)	0,17	0,15
BLU97 (parachute)	0,25-0,47	0,51
BLU97 (submunition)	Not seen!	0,36
Magazine	0,07	0,12
PFM1 “Butterfly”	Not seen!	0,28
PMA-1	0,07	0,03

PMA-2	0,06	0,17
PMA-3	0,06	0,16
PMN	0,03	0,07
T/79	0,17	0,13

Table 8-7 Reflectance from mines in Test site 2 (road scenario) at wavelength 904 nm compared with 1540 nm.

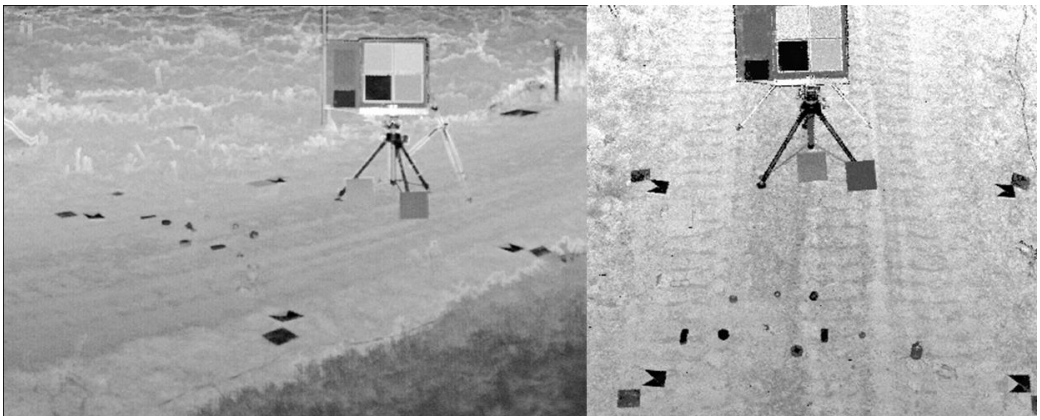

Figure 8-42. Comparison between wavelengths, 904 nm to the left and 1540 nm to the right.

8.2.2.5 Reflection from background

From intensity measurements and known reflectance values from calibrated reflectance targets, some background reflections have been calculated in each area at 1540 nm. Some results can be found in Table 8-8 and the results are illustrated in Figure 8-43-Figure 8-45. There is a large variation in the reflectivity of vegetation.

Kind of vegetation/background	**Reflectance (test site)**
Blueberry twigs	0,23 (1)
Pine	0,56 (1)
Ground in Pine forest	0,30 (1)
Ling	0,24 (1)
Road (Marks from tracks)	0,35 (1)
Gravel road	0,28 (2)
Packed dry loam	0,39 (2)
Vegetation in gravel	0,36 (3)
Gravel	0,28 (3)
Parched grass	0,50 (3)
Fresh grass	0,24 (3)
Tree stump (upper side)	0,22 (3)
Tree stump (side)	0,40 (3)

Table 8-8. Reflectance from vegetation/backgrounds at 1540 nm.

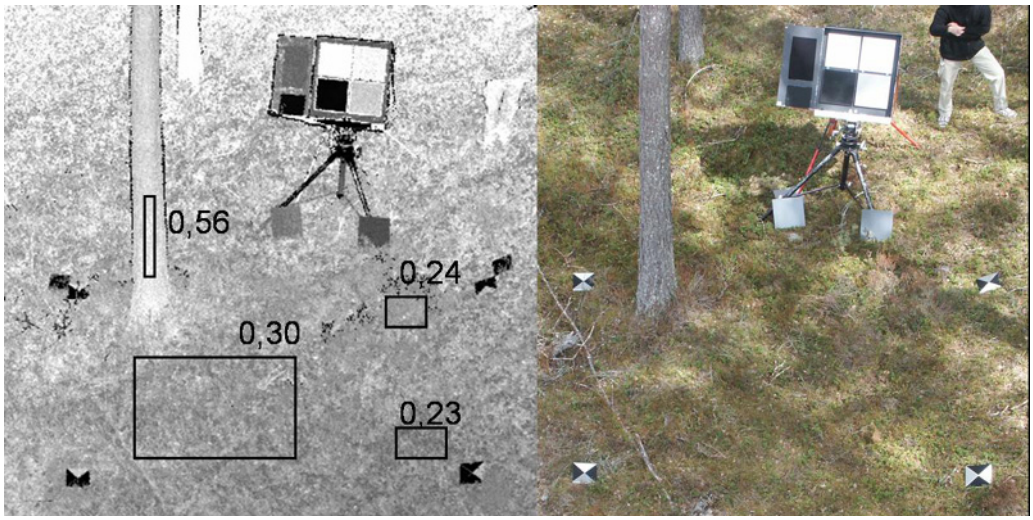

Figure 8-43. Backgrounds in test site 1.

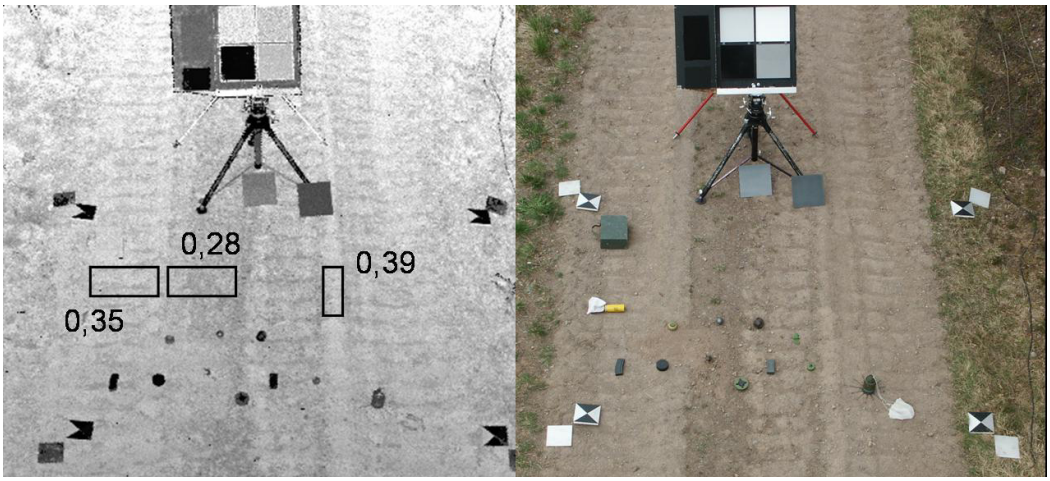

Figure 8-44. Backgrounds in test site 2.

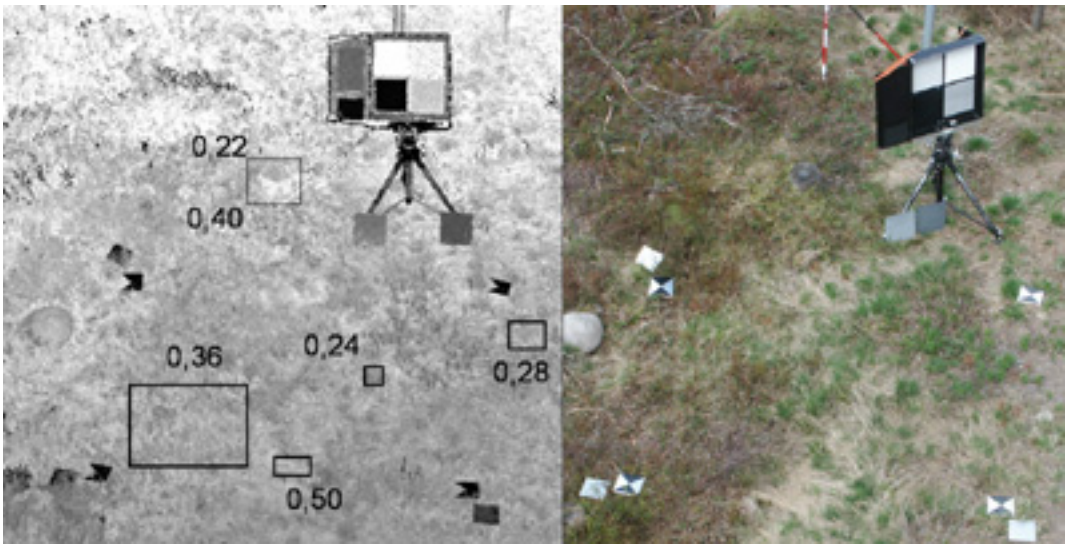

Figure 8-45. Backgrounds in test site 3.

8.2.2.6 UV sensor

Images from the UV sensor, extracted from DV-band, are shown in Figure 8-46.

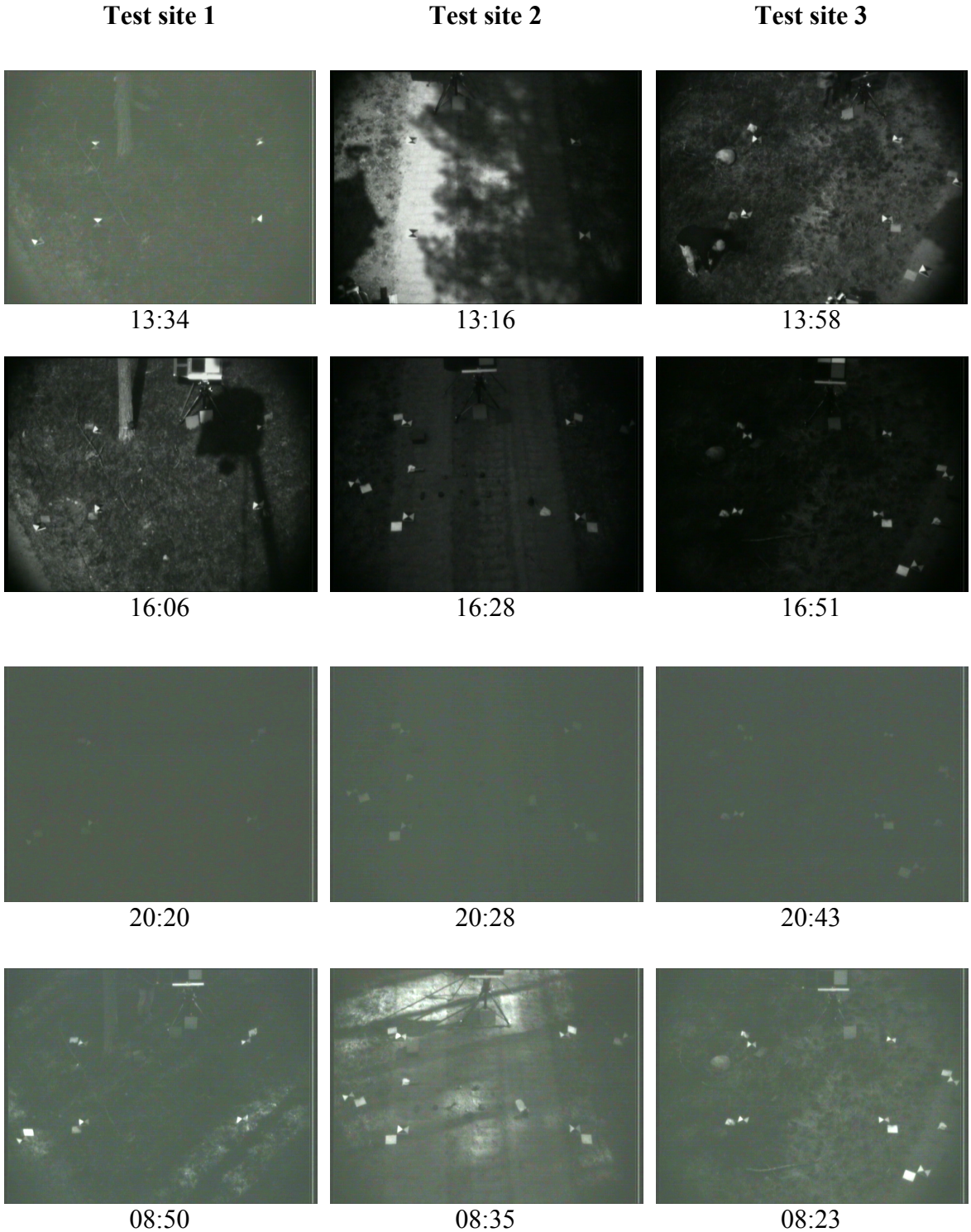

Figure 8-46. UV Images of the three test sites at different times of the day. The images are extracted from DV band.

8.2.2.7 VIS sensor

Images extracted from the DV-band are shown in Figure 8-47.

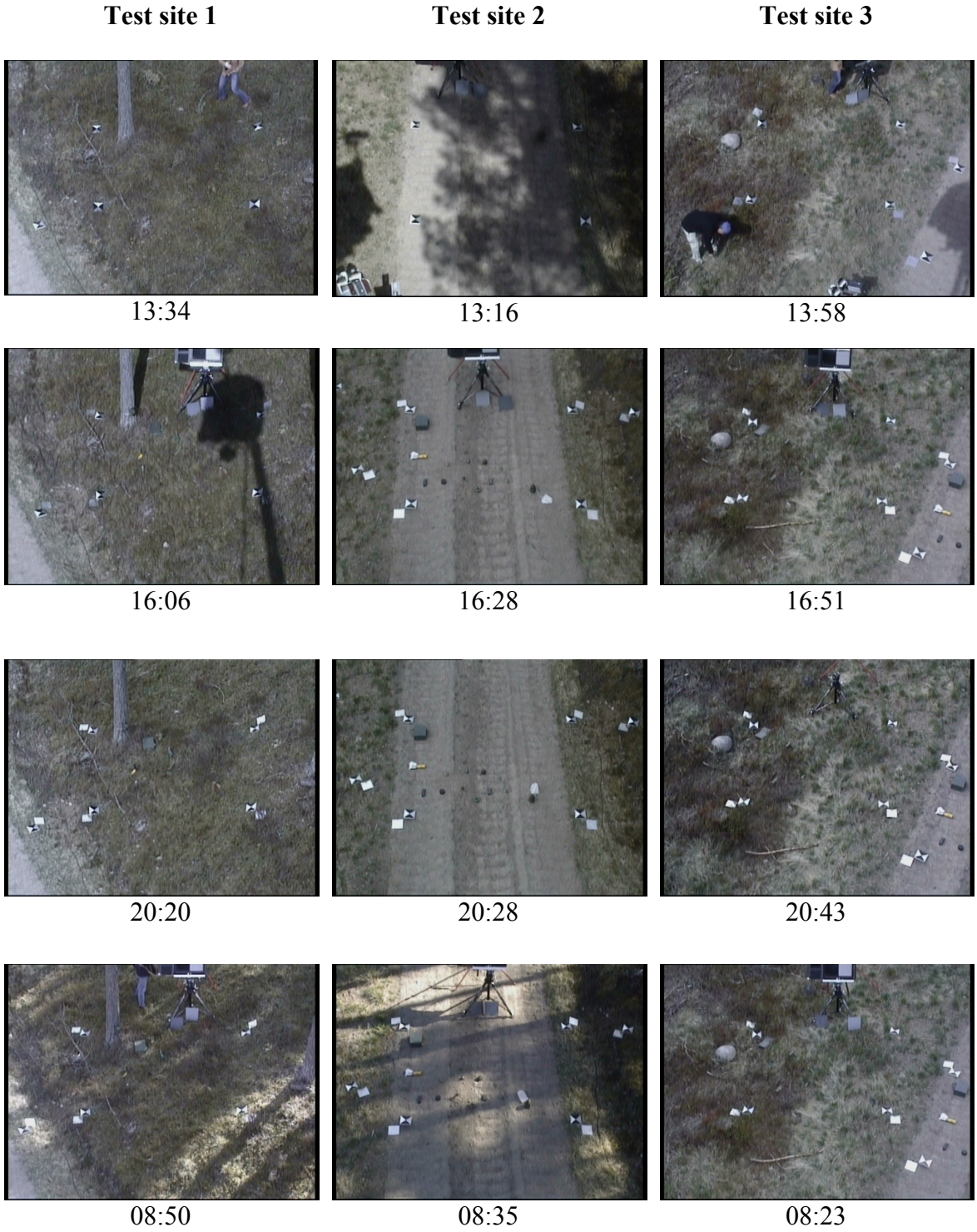

Figure 8-47. Colour images of the three test sites at different times of the day. The images are extracted from DV band.

8.2.2.8 NIR

Images extracted from DV-band are shown in Figure 8-48.

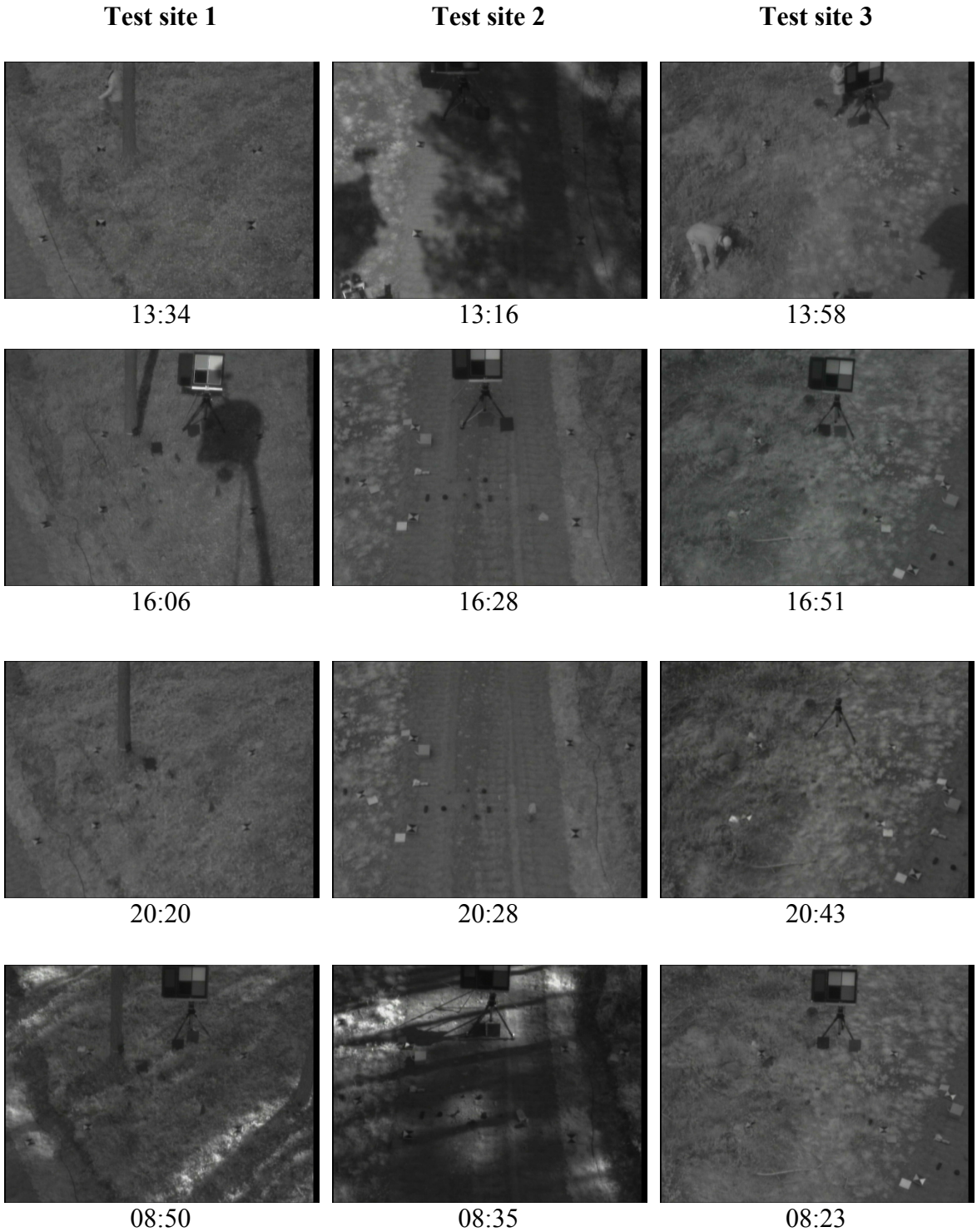

Figure 8-48. NIR images of the three test sites at different times of the day. The images are extracted from DV band.

8.2.2.9 TIR

In this section we show some initial results obtained by applying a number of image operators from Section 6.1.4 on infrared images acquired with the QWIP sensor. Figure 8-49 shows the input image and the operator responses and also an example of detection made using a simple threshold. In these examples the threshold is set manually but will later be determined adaptively. Other inputs are used in Figure 8-50 and Figure 8-44. Figure 8-51 is the same area as in Figure 8-50 but with reversed contrasts. As can be seen from these images, many mines may be detected. Also false alarms are present. To some extent the result may be better if more properties of the mines are used. Fusing with a different sensor may give even better results.

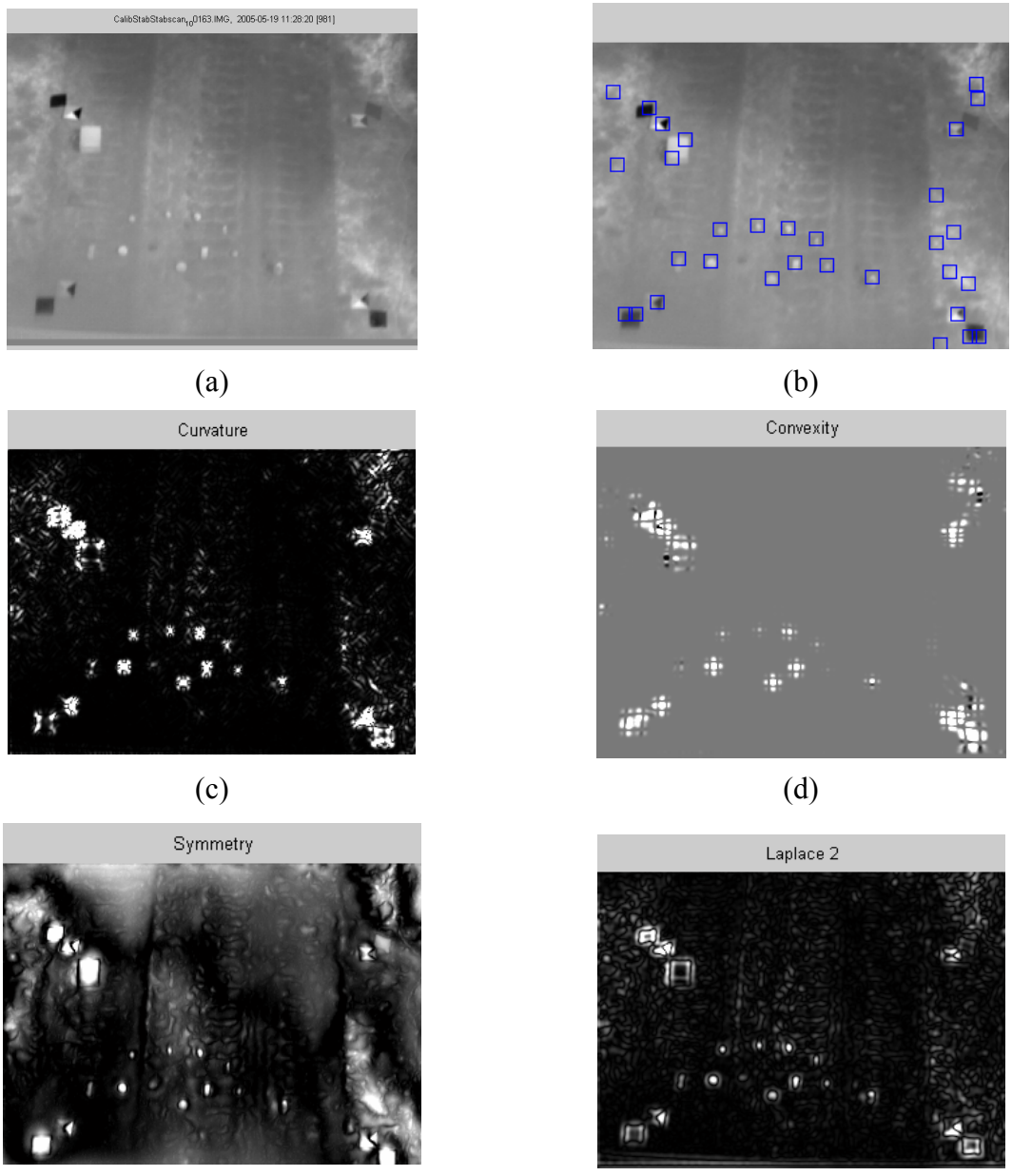

(a) (b) (c) (d) (e) (f)

Figure 8-49. Blob detection in frame 163 in the last sequence from Eksjö. (a) Original image, (b) blobs detected using curvature, (c) curvature operator output, (d) convexity operator output, (e) symmetry operator output and (f) Laplacian operator output.

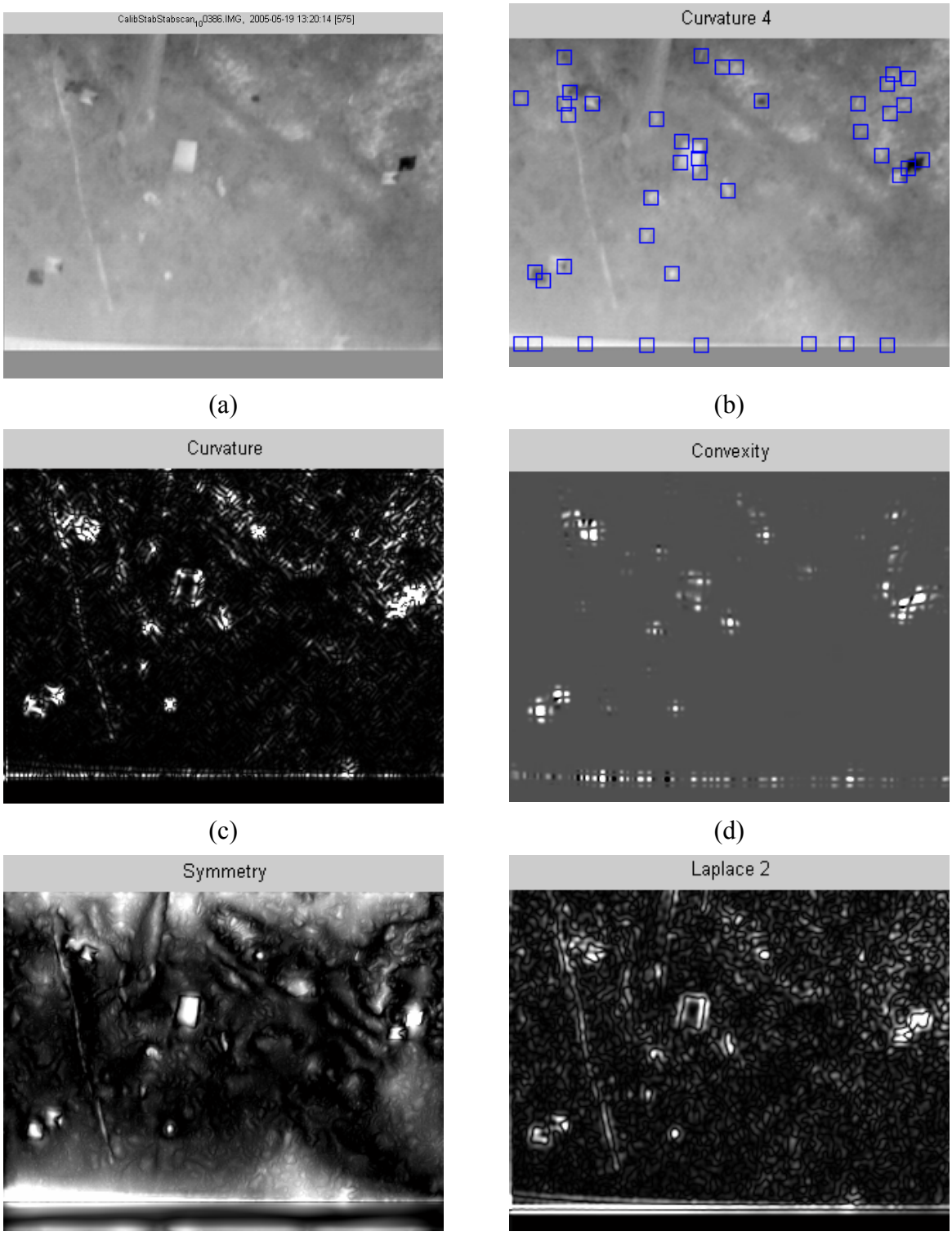

Figure 8-50. Blob detection in frame 386 in the last sequence from Eksjö. (a) Original image, (b) blobs detected using curvature, (c) curvature operator output, (d) convexity operator output, (e) symmetry operator output and (f) Laplacian operator output.

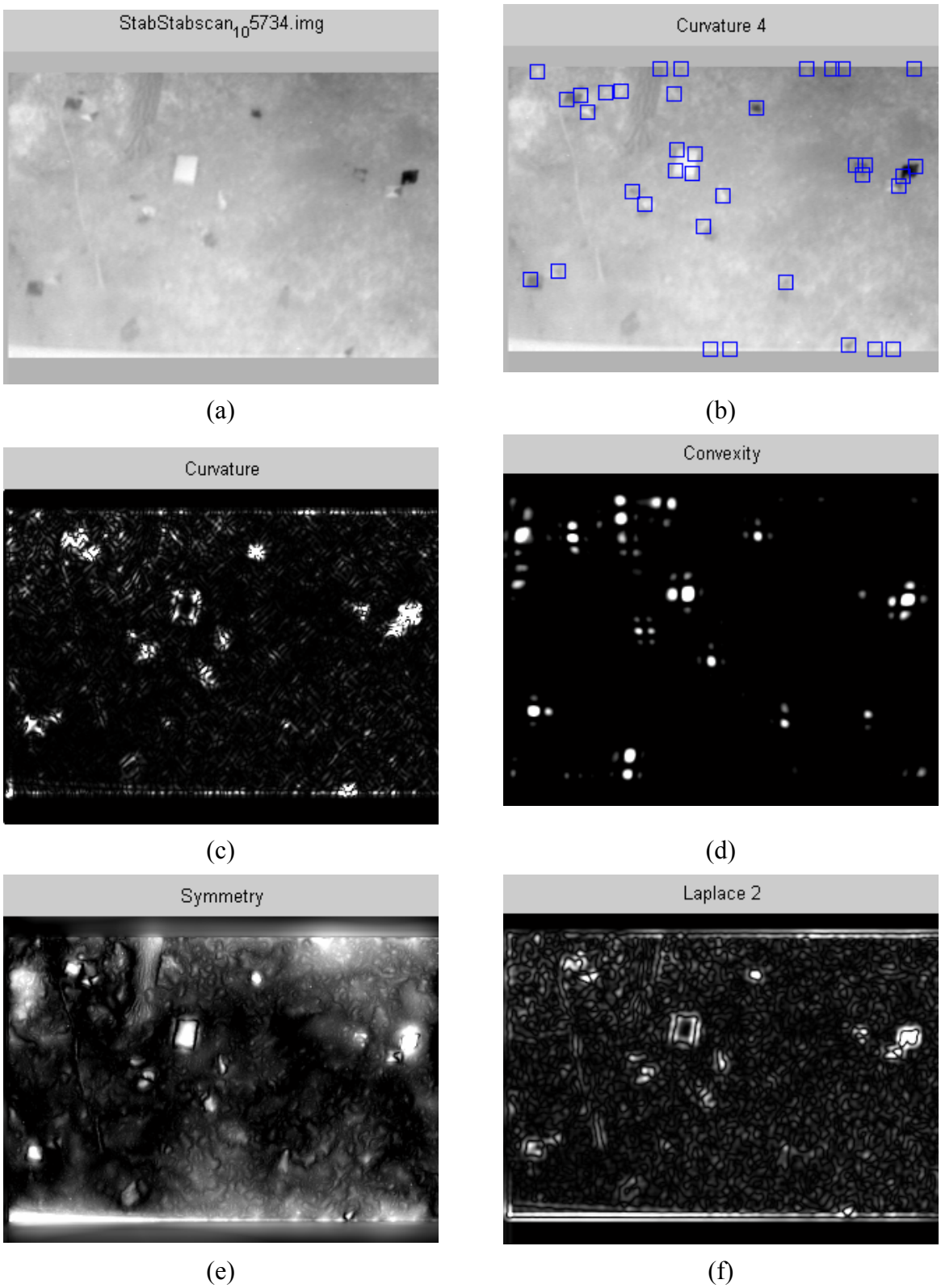

Figure 8-51. Blob detection in frame 5734 in the last sequence from Eksjö. (a) Original image, (b) blobs detected using curvature, (c) curvature operator output, (d) convexity operator output, (e) symmetry operator output and (f) Laplacian operator output.

8.2.2.10 Hyper-spectral sensor

In this section, we show some preliminary anomaly detection results on hyper-spectral data acquired at the FOI field trials. For more details, refer to section 6.2.1.

Anomaly detection

In the example in Figure 8-52, the dimension of the hyper-spectral image signal is reduced by coarse binning of the spectral dimension, Figure 8-52a, and the result of applying an anomaly detection is presented in Figure 8-52b.

a

b

Figure 8-52. Anomaly detection results for Test site 1 on hyper-spectral images.

Figure 8-53 illustrates the information theory based anomaly detection. Figure 8-53a shows the scene using only a few of the spectral bands. Figure 8-53b shows the result from information theoretic anomaly detection of the coarse binned spectral bands.

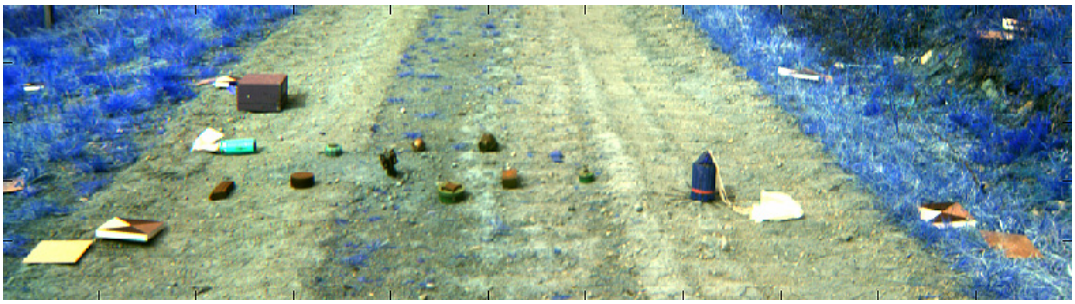

a

b

Figure 8-53. Anomaly detection results for Test site 1 obtained with an information theoretic approach.

8.3 Summary of the chapter

For some mines the emissivity is high in the 3-5 µm window and low in 8-12 µm window. For other mines the emissivity shows opposite behaviour. A careful investigation of the polarization signatures of mines and backgrounds would increase the certainty of the analysis.

The field trial in Eksjö has not yet been evaluated. Hence, the preliminary results and data from the imaging sensors that have been presented in this report should only be regarded as examples of the kind of information that can be obtained with the sensors. A reflectivity contrast between the mines and the background could be used for cueing other sensors, such as the 3-D laser radar. Some examples of processing algorithms have been presented, e.g., rectangle fitting and spin images. Some preliminary results from processing of the 3-D data have also been presented. With the TIR sensor, many of the mines could be detected.

9 Marketing and monitoring events

The members of the MOMS group have monitored the related work of other groups around the world by contributions, presentations, and personal contacts at conferences and meetings. This chapter describes the different activities during 2005.

9.1 Presentations

The project's scope and ambitions have been presented for:

- WEAG Panel 1 Countermine Equipment Group in April 2005.
- Meeting with the reference group in June 2005. This group includes representatives from FM/HKV, FM/SWEDEC, FMV and FOI.
- Swedish Armed Forces K3 UAVE in May 2005.
- Swedish Armed Forces school for engineering education (Försvarsmaktsingenjörsutbildning) June 2005.
- Swedish National Board (Nationella Samverkansgruppen) for research on mine/UXO related topics, September 2005.
- KCEM , Competence Centre for Energetic Materials, Symposium on security research in Sweden. September 2005.

9.2 Conference contributions

The MOMS group has presented 8 papers at mine related conferences during 2005

- Two conference papers and presentations at SPIE Orlando USA, March 2005.
- One presentation at ISPA-05, Special session on Airborne Remote Sensing and Remote Sensing for Humanitarian Demining, Zagreb, September 2005.
- One presentation at NATO Symposium Emerging Electro-Optic Phenomenology & Technology, Berlin, October 2005.

- Two presentations at (Nordic Demining Research Forum´s) NDRF (Nordic Demining Research Forum´s) Summer Conference -05, Karlberg, August 2005.

- Two conference papers and presentations at SPIE Brügge, Belgium, September 2005.

9.3 Other work

The already established contact network with the Humanitarian Demining community in Europe and America (Canada US) is alive through personal contacts, and especially with a joint application for EU project on TIRRS, Reinforcement of the research capacities for thermal infrared remote sensing in Croatia, EU FP6 ,WBC, Call title: FP6-2004-INCO-WBC-SSA-3.

The MOMS project has a continuous dialog with SWEDEC and FMV, and also close collaborations with the FOI projects OSA, MIRES, SNOD, and 3D-laser.

10 Future activities

A number of case studies will, in cooperation with SWEDEC, be extracted from scenarios defined by Swedish Armed Forces. Attention will be paid to future needs and demands in order to further develop and specify the MOMS concept. Methods and competence will be further developed with field trials and MoS as important sources of information. Attention will be paid to competence needs due to newly purchased sensor equipment. Platform solutions and system concepts will be considered in addition to continued work on evaluating different sensor solutions and combinations of sensors. A deeper understanding of phenomenologies is needed and initialisation of a signature database is planned as a method to achieve such knowledge. The work on signal processing will be directed against methods for detection of small targets when the speed of the sensor platform is high and results have to be presented with a minimum of delay. GIS will be considered as an instrument for data fusion. Participation in relevant national and international conferences will be performed. Cooperation opportunities will be investigated, internally with other projects as well as with national and international partners.

During the period October to December 2005 the project will also plan and make detailed road maps for the next coming years.

11 Summary

This report shows the first year of research and investigations carried out within the project "Multi Optical Mine Detection System", MOMS. Activities have mainly been focused on basic principles, phenomenons, acquisition of knowledge and literature studies. This report will serve as a common base for the evolution of the project.

Mines are classified in 3 categories: anti-tank mines, anti-personnel mines and blast antipersonnel mines. New mine types include multiple charge mines, and mines with new types of triggering mechanisms, such as acoustic, seismic and electro-optical sensors. Characteristic features of relevant mines and UXO have been investigated with respect to, e.g. geometry, size and colour.

An initial evaluation of sensor candidates was made based on requirements extracted from steering documents, phenomenology study giving base knowledge of detection and a review of different relevant sensor techniques. The phenomenologies considered are: 3-D shape, retro reflection, spectral characteristics, angular reflection characteristics, temporal characteristics, spatial characteristics, polarization and fluorescence. Sensor principles under consideration so far have been: laser illumination systems, 3-D imaging, retro reflection, passive multispectral sensing, active multispectral 3-D sensing and fluorescence. Also combinations of sensors are considered. For a deeper evaluation of sensor candidates there is a need to collect more data and to perform more modelling and signal processing tests. Due to the large variability of target background characteristics, an early assumption is that anomaly detection and change detection may be a more proper way for detection than direct feature evaluation. This needs to be further explored.

At this stage of the project, there is no support for excluding any candidate technique. Other candidate techniques might be added to the list, especially regarding different sensor solutions for exploiting phenomenologies. An approach for systematic evaluation of sensors and combinations of sensors remains. Statistical or mathematical evaluation of sensors and sensor combinations can only be made on a limited number of trials, scenarios and situations. Modelling and simulations can be used to extend the foundation for evaluation. The final recommendations regarding sensor systems will probably be made based on subjective expert reasoning, but with input from results and experiences achieved during the project life time.

Modelling and simulation (MoS) aspects concerning buried and surface laid objects are discussed regarding active as well as passive sensing. A conclusion of work done at FOI and from refereed work is that one need to emphasize the MoS work in order to achieve reliable outputs from simulations. MoS could be used as a bridge between analysis and experiments in order to decrease the need of expensive experiments. The validation and verification work of methods and codes used are important for reliable results.

From the signal processing point-of-view many techniques have been proposed, among which no single winner can be appointed at this time. A distinction between global and local techniques can be made, the difference being the assumptions made about the portion of the frame that is enough for characterizing the background and to detect regions that differ significantly from this. In order to be successful, both global and local information should preferably be taken into account – the former in order to acquire knowledge of some general terrain characteristics and the latter for (adaptive) object detection. From studying the literature it is also evident that a framework for combining, or *fusing*, different sources of

information – either acquired with different sensors or obtained with different algorithms is highly desirable.

System approaches to reach the goal of the MOMS system are discussed. Such a system roughly consists of a Platform, a combination of Sensors, and dedicated Signal processing and detection algorithms. Many of the technologies considered in this report have been demonstrated, both on ground based and airborne platforms. Many of the technologies have also been demonstrated with relevant stand-off capability. Examples are LAMD, COBRA and ARC. A useful discussion of overall system aspects is found in the RAND report and a report to the European Union. The US DoD also discusses system aspects of land mine detection. What has not been demonstrated is a sensor fused system with adequate overall performance although encouraging results have been obtained.

A field test with a large number of passive and active electro optical (EO) sensors was carried out in close cooperation with SWEDEC. The purpose was to collect data from surface laid mines, UXO, submunitions, IED's, and background with a variety of optical sensors. Laboratory experiments have also been made.

Several presentations of the project have been made during 2005: WEAG Panel 1 Countermine Equipment Group, meeting with the reference group for MOMS, Swedish Armed Forces K3 UAVE, Swedish Armed Forces school for engineering education, Swedish National Board for research on mine/UXO related topics, Competence Centre for Energetic Materials. Eight conference papers have been presented at international conferences during the year.

During the period October to December 2005 the project will also plan and make road maps for the next coming years.

References

[1] "Swedish Armed Forces Strategy for Research and Technology, English edition," Swedish Armed Forces 2002.

[2] Canadian Armed Forces Web page "http://ndmic-cidnm.forces.gc.ca/".

[3] http://www.maic.jmu.edu/ordata/Mission.asp.

[4] J. MacDonald, J. R. Lockwood, J. McFee, T. Altshuler, T. Broach, L. Carin, R. Harmon, C. Rappaport, W. Scott, and R. Weaver, "Alternatives for landmine detection," Rand Science and Technology Policy Institute 2003.

[5] http://www.onr.navy.mil/02/baa/expired/2002/baa%5F02%5F006/docs/.

[6] http://www.dtic.mil/doctrine/jel/doddict/.

[7] http://www.globalsecurity.org/military/intro/ied.htm.

[8] J. E. McFee, S.Achal, T. Ivanco, A.Tam, G. Baker, and C. Anger, "A proof-of-concept optical tripwire detector," presented at Detection and Remediation Technologies for Mines and Minelike Targets IX, Orlando, 2004.

[9] C. King, *Jane´s Mines and Mine Clearance 2000-2001*. Surrey, U.K.: Jane's Information Group Limited, 2000.

[10] C. Q. Cutshaw and L. Ness, *Jane´s Ammunition Handbook 2004-2005*. Surrey, U.K.: Jane´s Information Group Limited, 2004.

[11] T. Küchenmeister, T. O. Foundation, I. Doucet, and R. Lloyd, "Alternative anti-personnel mines: The next generations," Landmine Action, German Initiative to Ban Landmines 2001.

[12] http://www.dtic.mil/ndia/2002mines/risseeuw.pdf.

[13] http://www.photon.com, "Sensorvision," 1995.

[14] F. G. Wollenweber, "Thermal background modeling and its use in Science and Technology," presented at Characterization, Propagation, and Simulation of Sources and Backgrounds II, Orlando, USA, 1992.

[15] W. R. Reynolds, "Survey and analysis: the measurements and modelling of terrestrial thermal backgrounds," presented at Characterization and Propagation of Sources and Backgrounds, Orlando, USA, 1994.

[16] D. Clement and W. Jessen, "A Background Model in the Thermal Infrared: Status, Validation, and Applications," ForschungsgeseIIschaft für Angewandte Naturwissenschaften Forschungsinstitut für Optik (FGAN-FfO), Schloss Kressbach Tübingen Germany BETA-Tgb. -Nr. 1993/38, 1993.

[17] P. Jacobs, *Infrared Characterization of Targets and Background*, vol. TT26: Spie Optical Engineering Press, 1996.

[18] J. W. Deardorff, "Efficient prediction of ground surface temperature and moisture, with inclusion of a layer of vegetation," *Journal of Geophysical Research*, vol. 83, pp. 1889 - 1904, 1978.

[19] T. Miller, "Mathematical Model of Heat Conduction in Soil for Land Mine Detection," CSIRO, Division of Mathematics and Statistics, /Australia DMS-C95/95, 1996-01-23 1996.

[20] D. A. de Vries, "Simultaneous Transfer of Heat and Moisture in Porous Media," *Transactions American Geophysical Union*, vol. 39, pp. 909-916, 1958.

[21] M. Kaviany, *Principles of Heat Transfer in Porous Media*, 2 ed. Ann Arbour, Michigan: Springer Verlag, 1999.

[22] L. J. Carter, M. J. O'Sullivan, Y. J. Hung, and J. C.-C. Teng, "Thermal Imaging for land mine detection, ," presented at Second International Conference on the Detection of Abandoned Land Mines, Edinburgh, 1998.
[23] J. S. Accetta and D. L.Shumaker, "The Infrared and Electro-Optical Systems Handbook," SPIE Optical Engineering Press, 1993.
[24] J. R. Ballard, "Towards a High Temporal Frequency Grass Canopy Thermal IR Model for Background Signatures," presented at Targets and Backgrounds X, Characterization and Representation, Orlando, USA, 2004.
[25] J. J. R. Ballard, "High-resolution spatial measurements of minefield vegetation density and modeled surface heat flux," presented at SPIE, Orlando, USA, 2005.
[26] J. P. Lhomme, A. Chehbouni, and B. Monteny, "Sensible Heat Flux-Radiometric Surface Temperature Relationship over Sparse Vegetation: Parameterizing B^{-1}," *Boundary-Layer Meteorology*, vol. 97, pp. 431-457, 2000.
[27] E. Agassi and N. Ben-Yossef, "Parameterization of Sparse Vegetation in Thermal Images of Natural Ground Landscapes," *optical Engineering*, vol. 36, pp. 2910-29-17, 1997.
[28] M. V. Centeno, "New Formulae for the Equivalent Night Sky Emissivity," *Solar Energy*, vol. 28, pp. 489-498, 1982.
[29] S. Sjökvist, A. Linderhed, S. Nyberg, M. Uppsall, and D. Loyd, "Land mine detection by IR temporal analysis: physical numerical modeling," presented at Detection and Remediation Technologies for Mines and Minelike Targets X Orlando Fl, 2005.
[30] T. Chevalier, T. Winzell, J. Ahlberg, T. Svensson, H. Larsson, I. Renhorn, O. Steinvall, and D. Letalick, "Optroniska system 2004 (in Swedish)," Swedish Defence Research Agency FOI FOI-R--1422--SE, Nov 2004.
[31] S. S. Jackson, M. J. Bishop, D. L. Leese, and E. M. Lord, "High-Resolution 3D laser imaging of various surfaces in minefields and implications for surface modeling," presented at SPIE, Orlando, USA, 2005.
[32] R. R. Rupp, Z. Derzko, and G. R. Ax, "Lightweight airborne standoff minefield detection laser prototype," presented at Proceedings of SPIE, The International Society for optical engineering, Orlando, USA, 2004.
[33] A. N. d. Jong, H. Winkel, and M. J. J. Roos, "Active multispectral Near-IR detection of small surface targets," presented at Proceedings of SPIE, The International Society for optical engineering, Orlando, USA, 2001.
[34] O. Steinvall, T. Carlsson, C. Grönwall, H. Larsson, P. Andersson, and L. Klasén, "Laser based 3-D imaging-New capabilities for optical sensing," FOI-R--0856--SE, 2003.
[35] R. Hague, "Ladar puts the puzzle together," in *SPIE OE magazine*, 2003.
[36] O. K. Steinvall, H. Larsson, F. Gustafsson, T. R. Chevalier, Å. Persson, and L. M. Klasen, "Characterizing targets and backgrounds for 3D laser radars," presented at Military Remote Sensing, London, UK, 2004.
[37] R. W. Cannata, W. Clifton, S. Blask, and R. M. Marino, "Obscuration measurements of tree canopy structure using a 3D imaging ladar system," presented at Laser Radar Technology and Applications IX, Orlando, FL, USA, 2003.
[38] O. Steinvall and T. Chevalier, "Range accuracy and resolution for laserradars," Brygge, 2005.
[39] J. A. Coath and M. A. Richardson, "Regions of high contrast for the detection of scatterable land mines," presented at Detection and Remediation Technologies for Mines and Minelike Targets V, Orlando, FL, USA, 2000.

[40] A. N. d. Jong, H. Winkel, and M. J. J. Roos, "Active multi-spectral Near-IR detection of small surface targets," presented at Detection and Remediation Technologies for Mines and Minelike Targets VI, 2001.
[41] H. T. Hasketta, R. Ruppa, and T. Moore, "Quantitative performance of buried mine hyperspectral reflectance signatures (.35=2Spm) in various soils," presented at Detection and Remediation Technologies for Mines and Minelike Targets V, 2000.
[42] H. T. Hasketta, D. A. Reagoa, and R. R. Ruppa, "Detectability of buried mines in 3-5 and 8-12 μm regions for various soils using hyperspectral signatures " presented at Detection and Remediation Technologies for Mines and Minelike Targets VI, 2001.
[43] L. B. Wolff, D. A. Socolinsky, C. K. Eveland, J. Yalcin, and J. H. Holloway.
[44] F. J. Crosby and H. Suiter, "Background Adaptive Band Selection in a Fixed Filter System," presented at Detection and Remediation Technologies for Mines and Minelike Targets VII,, 2002.
[45] F. Crosby, J. John Holloway, D. Petee, S. Stetson, H. Suiter, and K. Tinsley, "Airborne testing of the joint mine detection technology's tunable filter multi-spectral camera," presented at Detection and Remediation Technologies for Mines and Minelike Targets VII, 2002.
[46] *The infrared and electro-optical handbook, Vol.1, Sources of Radiation, page 272-278*, vol. 1: SPIE Optical Engineering Press, 1993.
[47] H. Larsson, O. Steinvall, T. Chevalier, F. Gustafsson, Å. Persson, and P. Andersson, "Characterizing laser radar snow reflection for the wavelengths 0.9 and 1.5 mm," 2005.
[48] O. Steinvall and K. Koppari, *Depth sounding lidar – An overview of Swedish activities and with future prospects*, vol. 2964: SPIE, 1996.
[49] M. Tulldahl, " Detection and depth sounding of small targets with airborne laser bathymetry," in *Laboratory of Applied Optics*, vol. Ph.D. Linköping Linköping University, 2003, pp. 55.
[50] M.P. Strand, N. H. Witherspoon, J. J.H. Holloway, K. R. Tinsley, D. A. Petee, J. J.S. Taylor, E. A. Branham, and J. A. Thomas, "Environmental factors impacting the performance of airborne LIDAR sensors in the surf zone," presented at Detection and Remediation Technologies for Mines and Minelike Targets VIII, 2003.
[51] J. C. Stover, *Optical Scattering-Measurements and Analysis*: McGraw-Hill, 1990.
[52] J. M. Bennett and L. M. Mattsson, *Introduction to surface roughness and scattering*: Optical Society of America, 1989.
[53] O. Steinvall, " Theory for military laser systems performance modelling," FOI, Linköping, Scientific report FOA-R--97-00599-612--SE, 1997.
[54] O. Steinvall, "Effects of target shape and reflection on laser radar cross sections," FOI, Linköping, Scientific report FOA-R--99-01201-408,612--SE, 1999.
[55] Z. Derzko and D. Barr, "Polarized Reflectometry of Landmines at 814 Nanometers," presented at Detection and Remediation Technologies for Mines and Minelike Targets VII, 2002.
[56] T. H. Allik, D. Dawkin, J.Habersat, J. Nettleton, T. Writer, C. E. Buckingham, H. C. Schoeberlein, C. V. Nelson, and K. Sherbondy, "Eyesafe Laser Illuminated Tripwire (ELIT) Detector," presented at Detection and Remediation Technologies for Mines and Minelike Targets VI, 2001.
[57] M. Uppsäll, L. M. Pettersson, M. Georgson, and S. Sjökvist, "Temporal IR contrast variation of buried land mines," presented at Detection and Remediation Technologies for Mines and Minelike targets V, Orlando USA, 2000.

[58] A. Linderhed, S. Nyberg, S. Sjökvist, and M. Uppsäll, "Optical Methods for Detections of Minefields," FOI Sensor Technology, Linköping, Base data report FOI-R--1331--SE, 2004.
[59] A. Linderhed, S. Sjökvist, S. Nyberg, and M. Uppsall, "Land mine detection by IR temporal analysis: detection methods," presented at Detection and Remediation Technologies for Mines and Minelike Targets X Orlando Fl, 2005.
[60] S. Sjökvist, A. Linderhed, M. Uppsäll, S. Nyberg, and D. Loyd, "Land mine detection by IR temporal analysis: Physical numerical modeling," presented at Detection and Remediation Technologies for Mines and Minelike Targets X, Orlando, 2005.
[61] G. Boreman, "Infrared Systems Design," Lecture notes FOI, 2004, pp. 182.
[62] J. Johnson, "Analysis of Imaging Forming Systems," in *Selected Papers on Infrared Design, Reprint*, vol. 513: SPIE Milestone Series, 1985.
[63] S. Breugnote and P. Clemenceau, "Modeling and performance of an polarisation active imager at λ=806 nm," presented at Laser Radar Technology and Applications IV, Orlando, FL, USA, 1999.
[64] J. E. Karlshoven, M. R. Tierney, S. Craig, S. T. Daughtry, and J. E. McMurtrey, "Remote sensing of crop parameters with a polarised, frequency-doubled Nd:YAG laser," *Appl. Opt.*, vol. 34, pp. 2745-2749, 1995.
[65] J. Zallat and M. P. Stoll, "Simple model of a polarised bidirectional scattering cross section at 10.6 μm: application to SiO_2 sand," *Appl. Opt.*, vol. 36, pp. 1376-1385, 1997.
[66] H. T. Haskett and R. R. Rupp, "Landmine performance bounds in various background using airborne 808 nm laser imagery," presented at Detection and Remediation Technologies for Mines and Minelike Targets VI, 2002.
[67] Y. X. I. Reed, "Comparative Performance Analysis of Adaptive Multispectral Detector," *IEEE Transaction on Signal Processing*, vol. 41, 1993.
[68] H. T. Haskett and R. R. Rupp, "Statistical analysis of polarization responses for landmines in various solar angles and backgrounds using airborne laser imagery," presented at Detection and Remediation Technologies for Mines and Minelike Targets VII, 2002.
[69] W. d. Jong, F. Cremer, K. Schuttea, and J. Stormd, "Usage of polarisation features of landmines for improved automatic detection," presented at Detection and Remediation Technologies for Mines and Minelike Targets V, 2000.
[70] F. Cremer, W. d. Jong, and K. Shutter, "Analysis of Polarimetric IR Phenomena for Detection of Surface," presented at Detection and Remediation Technologies for Mines and Minelike Targets VI, 2001.
[71] I. K. Sendur, J. T. Johnson, and B. A. Baertlein, "Analysis of Polarimetric IR Phenomena for Detection of Surface," presented at Detection and Remediation Technologies for Mines and Minelike Targets VI, 2001.
[72] B. A. Baertlein and J. T. Johnson, "Physically Based Simulation of Passive Polarimetric IR Mine Signatures," presented at Detection and Remediation Technologies for Mines and Minelike Targets VII, 2002.
[73] J. W. Williams, H. S. Teeb, and M. A. Poulterb, "Image processing and classification for the UK Remote Minefield Detection System infrared polarimetric camera," presented at Detection and Remediation Technologies for Mines and Minelike Targets VI, 2001.
[74] G. Forssell, "Passive IR polarization measurements applied to covered surface landmines," presented at Detection and Remediation Technologies for Mines and Minelike Targets VIII, 2003.

[75] G. Forssell, "Test and analysis of the detectability of personnel mines in a realistic minefield by polarization in the infrared LW region," presented at Detection and Remediation Technologies for Mines and Minelike Targets IX, 2004.
[76] D. Daniels, S. Jennings, R. Amin, M. Gaskell, and N. Playle, "Use of COTS technology in tripwire detection," presented at Detection and Remediation Technologies for Mines and Minelike Targets IX, 2004.
[77] N. Playle, M. Gaskell, R. Deas, and R. Rutherford, "Feasibility of tripwire detection using infrared polarimetric sensor," presented at Detection and Remediation Technologies for Mines and Minelike Targets IX, 2004.
[78] R. Luke, J. Keller, P. Gader, M. Skubic, and T. Wang, "Experiments in tripwire detection using visible and near-IR imagery," presented at Detection and Remediation Technologies for Mines and Minelike Targets IX, 2004.
[79] M. G. Gore, "Spectrophotometry & Spectrofluorimetry," Oxford University Press, 2000, pp. 368.
[80] http://www.life.uiuc.edu/govindjee/movkautsky.html.
[81] http://www.vcu.edu/remotesensing/SPEC_S.htm.
[82] G. C. Papageorgiou and Govindjee, "Chlorophyll a Fluorescence A Signature of Photosynthesis," Springer, 2004, pp. 818.
[83] T. Tjärnhage, M. Strömqvist, G. Olofsson, D. Squirrell, J. Burke, J. Ho, and M. Spence, "Multivariate Data Analysis of Fluorescence Signals from Biological Aerosols," FOI, Reprint FOI-S--0128--SE, 2001.
[84] T. Carlsson, M. Norrefeldt, M. Elfsberg, and S. Wallin, "High Speed Combustion-activities during 2004," FOI FOI-R—1378—SE, 2004.
[85] P. Brzezinski, I. Smirnova, and L. Sarholm, "Detektion av landminor med bakteriella biosensorer," FOI FOI-R—1258—SE, 2003.
[86] M. Bengtsson, R. Grönlund, M. Sjöholm, C. Abrahamsson, A. D. Dernfalk, S. Wallström, A. Larsson, P. Weibring, S. Karlsson, S. M. Gubanski, S. Kröll, and S. Svanberg, "Fluorescence lidar imaging of fungal growth on high-voltage outdoor composite insulators," FOI, Reprint FOI-S—1679—SE, 2004.
[87] P. Jonsson, F. Kullander, M. Nordstrand, T. Tjärnhage, P. Wästerby, and M. Lindgren, "Development of fluorescence-based point detector for biological sensing," presented at Optically Based Biological and Chemical Sensing for Defence, 2004.
[88] R. M. Measures, *Laser Remote Sensing*. New York: Wiley Interscience, 1984.
[89] H. Edner, J. Johansson, S. Svanberg, and E. Wallinder, "Fluorescence lidar multicolor imaging of vegetation," *Appl. Opt.*, vol. 33, 1994.
[90] F. E. Hoge, R. N. Swift, and J. K. Yungel, "Feasibility of airborne detection of laser induced fluorescence emissions from green terrestrial plants," *Appl. Optics*, vol. 22, 1983.
[91] K. Smorenburg, G. B. Courrèges-Lacoste, M. Berger, C. Buschmann, A. Court, U. D. Bello, G. Langsdorf, H. K. Lichtenthaler, C. Sioris, M. P. Stoll, and H. Visser, "Remote sensing of solar induced fluorescence of vegetation," presented at Remote Sensing for Agriculture, Ecosystems, and Hydrology III, 2002.
[92] Y. Saito, M. Kanoh, K. Hatake, T. Kawahara, and A. Nomura, "Investigation of laser-induced fluorescence of several natural leaves for application to lidar vegetation monitoring," *Appl. Optics*, vol. 37, 1998.
[93] M. Sowinska, B. Cunin, F. Heisel, and J. A. Miehe, "New UV-A laser-induced fluorescence imaging system for near-field remote sensing of vegetation: characteristics and performance," 1999.
[94] 1999.

[95] J.-R. Simard, P. Mathieu, V. Larochelle, J.-M. Theriault, G. Roy, J. McFee, and J. Ho, "Active range-gated spectrometric standoff detection and characterisation of bioaerosols," 1999.
[96] R. M. Balanchandran and N. W. Lawandy, "Interface reflection effects in photonic paint," *Opt. Letters*, vol. 20, pp. 1271-1273, 1995.
[97] C. T. Field and P. S. Miller, "Laser remote sensing system analysis for search and rescue," *Appl. Optics*, vol. 38, 1999.
[98] R. S. Burlage, K. Everman, and D. Patek. USA, 1999.
[99] M. P. Strand, B. W. Coles, A. J. Nevis, and R. Regan, "Laser Line Scan Fluorescence and Multi-Spectral Imaging of Coral Reef Environments," 1996.
[100] http://www.eudem.vub.ac.be/projects/.
[101] M. Khalili and M. Eisl, "ARC Final Public Report," FOI, Reprint FOI-S--1282--SE, 2004.
[102] O. Steinvall, D. Letalick, U. Söderman, L. Ulander, and A. Gustavsson, " Laser radar for terrain and vegetation mapping," FOI FOI-R--0232--SE, 2001.
[103] F. Crosby, J. H. Jr., D. Petee, S. Stetson, H. Suiter, and K. Tinsley, "Laser Diode Arrays for Expanded Mine Detection Capability," 2002.
[104] J. John Holloway, F. Crosby, D. Petee, H. Suiter, and N. Witherspoon, "Laser Diode Arrays for Naval Reconnaissance," 2003.
[105] R. R. Rupp, Z. Derzko, and J. George R. Ax, "Lightweight airborne standoff minefield detection laser prototype," 2004.
[106] C. S. Wood, I. McKinnie, M. Hinckley, J. Koroshetz, T. Nichols, J. R. Unternahrer, G. Bennett, and J. H. Holloway, "Analysis of a high-energy, multispectral laser for surf zone mine countermeasures," 2004.
[107] O. Steinvall and D. Letalick, "Laser sensor concepts as part of a multi-sensor remote mine detection system – ”Concepts, technology and measurement needs”," FOI, 2005.
[108] C. Smithpeter, R. Nellums, S. Lebien, and G. Studor, "Miniature high-resolution laser radar operating at video rates," presented at Laser Radar Technologies and applications V, Orlando, FL, USA, 2000.
[109] S. W. McKnight, C. A. DiMarzio, W. Li, and J. Stott, "Laser-Induced Acoustic Imaging of Buried Objects," *Subsurface Sensing and Imaging Systems*, vol. 2, pp. 119-126, 2001.
[110] P. Gao and L. M. Collins, "A two-dimensional generalized likelihood ratio test for landmine and small unexploded ordnance detection," *Signal Processing*, vol. 80, pp. 1669-1686, 2000.
[111] D. Fäldt and J. Ohlsson, "Improved infrared object signature calculations for SensorVision by the use of RadTherm," FOI-R--0574--SE 2001.
[112] J. C. Savage, J. K. O'Neal, R. A. Brown, and J. E. Keeler, "Powered Low Cost Autonomous Attack System: cooperative, autonomous, wide-area-search munitions with capability to serve as non-traditional ISR assets in a network-centric environment," 2005.
[113] C. Andressen, "LADAR: The Emergence of an EO Technology to Defend Against Future Threats," in *raytheon Technology today*, vol. 2005, 2005.
[114] B. Humbert: EI/IR section, AFRL Eglin AFB, 2005.
[115] J. P. Donnelly, K. A. McIntosh, D. C. Oakley, A. Napoleone, S. H. Groves, S. Vernon, L. J.Mahoney, K. Molvar, J. Mahan, J. C. Aversa, E. K. Duerr, Z. L. Liau, B. F. Aull, and D. C. Shaver, "1-µm Geiger-Mode Detector Development," 2005.
[116] R. Stettner, H.Bailey, and R. Richmond, "Eye-safe laser radar 3-D imaging," 2004.
[117] R. Stettner, H. Bailey, and S. Silverman, "Large format time-of-flight focal plane detector development," 2005.

[118] I. Baker, S. Duncan, and J. Copley, "A Low Noise, Laser-Gated Imaging System for Long Range Target Identification ", 2004.
[119] L. Klasén, O. Steinvall, G. Bolander, and M. Elmqvist, "Gated Viewing in the Atmosphere – A Study of Performance Limits," presented at Laser Radar Technology and Applications VII, 2002.
[120] O. Steinvall, L. Klasen, P. Andersson, H. Larsson, T. Chevalier, and M. Henriksson, "Gated viewing - deepened study," FOI FOI-R--0991--SE, 2003.
[121] W. P. Elkins, B. L. Ulich, J. G. Lawrence, and H. E. Linton, "A 3D Lidar Sensor for Volumetric Imaging in Highly Backscattering Media," 2005.
[122] J. Busck, "Optical identification of sea-mines using Gated viewing three-dimensional laser radar," in *Ørsted DTU*, vol. Ph.D.: Technical University of Denmark, 2005.
[123] J. W. McLean and J. M. Murray, "Streak tube lidar allows ocean surveillance," in *Laser Focus World*, vol. January, 1998, pp. 171-176.
[124] A. D. Gleckler, "Multiple-Slit Streak Tube Imaging Lidar (MS-STIL) Applications," presented at Laser Radar Technology and Applications V, 2000.
[125] A. Gelbart, B. C. Redman, R. S. Light, C. A. Schwartzlow, and A. J. Griffis, "Flash lidar based on multiple-slit streak tube imaging lidar," presented at Laser Radar Technology and Applications VII, Orlando, FL, USA, 2002.
[126] A. D. Gleckler, A. Gelbart, and J. M. Bowden, "Multispectral and hyperspectral 3D imaging lidar based upon the multiple slit streak tube imaging lidar," presented at Laser Radar Technology and Applications VI.
[127] S. Poger and E. Angelopolou, "Multispectral Sensors in Computer Vision," Stevens Institute of Technology, Castle Point of Hudson, Department of Computer Science, Hoboken NJ 07030 USA, Technical Report CS-2001-3, 2001.
[128] A. D. Gleckler and A. Gebhart, "Three dimensional imaging polarimetry," 2001.
[129] Y. Wang, Y. Wang, and H. Q. Lea, "Multi-spectral mid-infrared laser stand-off imaging," *Optics Express*, vol. 13, 20095.
[130] B. Brusmark, A.-L. Christiansen, and A. Lauberts, "Preliminary concept study of a multisensor system for mine detection," FOI FOA-R--97-00489-310--SE, 1997.
[131] B. Haugstad, "Combined Detection." Fredrikshavn: Nordic Demining Research Forum, 2004.
[132] O. Dullum, "Correlation between different demining and detection methods." Fredrikshavn: Nordic Demining Research Forum, 2004.
[133] S. Sjökvist, "Heat Transfer Modelling and Simulation in Order to Predict Thermal Signatures -The Case of Buried Land Mine," in *Applied Thermodynamics and Fluid Mechanics*. Linköping: Linköping University, Institute of Technology, 1999, pp. 86.
[134] O. Balci, "Verification, Validation, and Accreditation," presented at Winter Simulation Conference, USA, 1998.
[135] K. R. Johnson and a. R. Curran, "Present State and Future of Infrared Signature Models," presented at 3rd Annual Ground Target Modeling and Validation Conference, Houghton, Michigan, 1992.
[136] M. L. B. Rodgers, "The Development and Application of Diurnal Thermal Modeling for Camouflage, Concealment and Deception," presented at SPIE Taget and Backgrounds, Orlando, 2000.
[137] L. S. Balfour, "A simple thermal model for natural background elements," presented at SPIE, Israel, 1995.
[138] A. W. Haynes, M. A. Gilmore, D. R. Filbee, and C. Stroud, "Accurate scene modeling using synthetic imagery," presented at Proceedings of SPIE, Orlando, 2003.
[139] M.A. Gilmore et al, "Assessments of synthetic image fidelity," presented at Proceedings of SPIE, Orlando, 2002.

[140] S. Newman et al, "Validation of the use of synthetic imagery for camouflage effectiveness assessment," presented at Proceedings of SPIE, Orlando, 2002.
[141] Paradigm Simulation Inc, "Validation of Sensor Vision," 1998.
[142] E. Bernardsson, "Initial Validation of SensorVision – A Program for Real-Time IR Simulations," IR system FOI-R--0083--SE, 2001.
[143] C. Nelsson, P. Hermansson, T. Winzell, and S. Sjökvist, "Benchmarking and Validation of IR Signature Programs: SensorVision, CAMEO-SIM and RadThermIR," presented at NATO RTO-M-SCI-145 Symposium on Sensors and Sensor Denial by Camouflage, Concealment and Deception, Brüssel, 2004.
[144] C. Nelsson, E. Andersson, D. Börjesson, P. Hermansson, S. Nyberg, S. Sjökvist, and T. Winzell, "Methods for validation of optical signature models," presented at SPIE, Orlando, 2005.
[145] D. Loyd and G. Andersson, "THAFEM - a finite element program for heat transfer analysis," in *Finite Element Systems - A Handbook*, C. A. Brebbia, Ed., 3 ed: Springer - Verlag, 1985, pp. 721-732.
[146] Comsol AB, *Femlab Users Guide*, 2004.
[147] V. Vavilov, D. Burleig, and A. Klimov, "Advanced Modeling of Thermal NDT Problems: From Buried Mines to Defects in Composites," *SPIE Thermosense XXIV*, vol. 4710, pp. 507-521, 2002.
[148] K. Khanafer, K. Vafai, and B. A. Baertlein, "Effects on Thin Metal Outer Case and Top Air Gap on Thermal IR Images of Buried Antitank and Antipersonnel Land Mines," *IEEE Transactions on Geosciense and Remote Sensing*, vol. 41, pp. 123-135, 2003.
[149] P. L. Martinez, L. v. Kempen, H. Sahli, and D. C. Ferrer, "Improved Thermal Analysis of Buried Landmines," *IEEE Transactions on Geosciense and Remote Sensing*, vol. 42, pp. 1965-1975, 2004.
[150] A. Muscio and M. A. Corticelli, "Land Mine Detection by Infrared Thermography: Reduction of Size and Duration of the Experiments," *IEEE Transactions on Geosciense and Remote Sensing*, vol. 42, pp. 1955-1964, 2004.
[151] A. Mahmoodi, A. Nabavi, and M. N. Fesharaki, "Thermal modeling of desert backgrounds in the far-infrared spectral region," *Optical Engineering*, vol. 39, pp. 2545 - 2554, 2000.
[152] P. Pregowski, "Buried mine and soil temperature prediction by numerical model," presented at 15th World Conference on Nondestructive Testing, Roma, 2000.
[153] J. McFee, Y. Das, and A. Faust, "Canadian landmine detection research program," presented at Detection and Remediation Technologies for Mines and Minelike Targets VIII, Orlando, USA, 2003.
[154] I. K. Sendur and B. A. B. Baertlein, "The Role of Environmental Factors and Mine Geometry in Thermal IR Mine Signatures," presented at Detection and Remediation Technologies for Mines and Minelike Targets V, Orlando, USA, 2001.
[155] J. M. Cathcart, R. Campbell, R. Bock, M. Karlowatz, B. Mizaikoff, and T. Orlando, "Impact of shallow buried objects on the spectral properties of terrain features," presented at SPIE Detection and Remediation Technologies for Mines and Minelike Targets VIII, Orlando, 2003.
[156] B. A. Baertlein and I. K. Sendur, "The Role of Environmental Factors and Mine Geometry in Thermal IR Mine Signatures," presented at SPIE Detection and Remediation Technologies for Mines and Minelike Targets VI, Orlando, 2001.
[157] S. Sjökvist, R. Garcia-Padron, and D. Loyd, "Heat Transfer Modelling Of Solar Radiated Soil, Including Moisture Transfer," presented at Third Baltic Heat Transfer Conference, Gdansk, Poland, 1999.

[158] S. Sjökvist, M. Georgson, S. Ringberg, and D. Loyd, "Simulation of thermal contrast on solar radiated sand surfaces containing buried minelike objects," presented at Second International Conference on The Detection of Abandoned Land Mines, Edinburgh, UK, 1998.
[159] S. Sjökvist, M. Georgson, S. Ringberg, M. Uppsäll, A.-L. Christiansen, and D. Loyd, "Modelling of thermal heat-transfer of landmines - a heat transfer analysis," presented at 1st international disposal conference, Lund, 1997.
[160] S. Sjökvist, M. Georgson, S. Ringberg, M. Uppsäll, and D. Loyd, "Thermal Effects on Solar Radiated Sand Surfaces Containing Land Mines, -A Heat Transfer Analysis," presented at Fifth International Conference on Advanced Computational Methods in Heat Transfer, Cracow, Poland, 1998.
[161] S. Sjökvist, A. Linderhed, S. Nyberg, and M. Uppsäll, "Temporal method for IR minefield feature detection," presented at Detection and Remediation Technologies for Mines and Minelike Targets IX, Orlando, USA, 2004.
[162] S. Sjökvist, A. Linderhed, S. Nyberg, M. Uppsäll, and D. Loyd, "Minefield temporal feature extraction supported by heat transfer modelling," presented at EUDEM2-SCOT 2003,
International Conference on Requirements and Technologies for the Detection, Removal and Neutralization of Landmines and UXO, Brüssel, 2003.
[163] S. Sjökvist, M. Lundberg, I. Gu, and M. Ulvklo, "Aspects of an airborne system for detection of landmines using multispectral imaging," presented at SSAB symp. on image analysis, Gothenburg, Sweden, 1999.
[164] S. Sjökvist, M. Uppsäll, S. Nyberg, A. Linderhed, and M. Lundberg, "Optical detection of land mines at FOI," presented at Subsurface and Surface Sensing Technologies and Applications III, San Diego, USA, 2001.
[165] J. G. Hartley, "Coupled Heat and Moisture Transfer in Soils -A Review," in *Advances in Drying*, vol. 4: Hemisphere Publishing Corporation, 1987.
[166] T. S. Chevalier, O.; Letalick, D., "Signature simulation and signal analysis for 3-D laser radar," FOI, Sensor Technology FOI-R--0163--SE, July 2001.
[167] Nicholas M. Short Sr., "NASA, Solar Irradiation as a Heating Mechanism, http://rst.gsfc.nasa.gov/Sect9/Sect9_3.html," 2005.
[168] M. R. Sanjeev Agarwal, Richard Hall, Thomas Woodhard, John Brown and Anh Trang, "Evaluating operator performance in aided airborne mine detection," presented at SPIE, Orlando, 2005.
[169] I. S. Reed and X. Yu, "Adaptive multiple-band CFAR detection of an optical pattern with unknown spectral distribution," *IEEE Trans. Acoust., Speech Signal Processing*, vol. 38, pp. 1760-1770, October 1990.
[170] H. Kwon and N. M. Nasrabadi, "Kernel RX-Algorithm: A Nonlinear Anomaly Detector for Hyperspectral Imagery," *IEEE Trans. Geoscience and Remote Sensing*, vol. 43, pp. 388-397, 2005.
[171] E. A. Ashton, "Detection of Subpixel Anomalies in Multispectral Infrared Imagery Using an Adaptive Bayesian Classifier," *IEEE Trans. Geoscience and Remote Sensing*, vol. 36, pp. 506-517, 1998.
[172] M. J. Carlotto, "A Cluster-Based Approach for Detection Man-Made Objects and Changes in Imagery," *IEEE Trans. Geoscience and Remote Sensing*, vol. 43, pp. 374-387, 2005.
[173] G. G. Hazel, "Multivariate Gaussian MRF for Multispectral Scene Segmentation and Anomaly Detection," *IEEE Trans. Geoscience and Remote Sensing*, vol. 38, pp. 1199-1211, 2000.

[174] C.-I. Chang and C. M. Brumbley, "A Kalman Filtering Approach to Multispectral Image Classification and Detection of Changes in Signature Abundance," *IEEE Trans. Geoscience and Remote Sensing*, vol. 37, pp. 257-268, 1999.
[175] J. C. Harsanyi and C.-I. Chang, "Hyperspectral Image Classification and Dimensionality Reduction: An Orthogonal Subspace Projection Approach," *IEEE Trans. Geoscience and Remote Sensing*, vol. 32, pp. 779-785, July 1994.
[176] F. Cremer, T. Nguyen, L. Yang, and H. Sahli, "Stand-off thermal IR minefield survey: System concept and experimental results," presented at SPIE, Orlando, 2005.
[177] L. Bruzzone and D. F. Prieto, "Automatic Analysis of the Difference Image for Unsupervised Change Detection," *IEEE Trans. Geoscience and Remote Sensing*, vol. 38, pp. 1171-1182, 2000.
[178] T. Yamamoto, H. Hanaizumi, and S. Chino, "A Change Detection Method for Remotely Sensed Multispectral and Multitemporal Images Using 3-D Segmentation," *IEEE Trans. Geoscience and Remote Sensing*, vol. 39, pp. 976-985, 2001.
[179] T. P. Donzelli, L. Jackson, M. Yeshnik, and T. Petty, "An airborne change detection system for the detection of route mines," presented at SPIE, Orlando, 2003.
[180] R. L. Kitchen and A, "Gray-level corner detection," *Pattern Recognition Letters*, vol. 1, pp. 95--102, 1982.
[181] A. Tankus, Y. Yeshurun, and N. Intrator, "Face detection by direct convexity estimation," *Pattern Recognition Letters*, vol. 18, pp. 913-922, 1997.
[182] P. Kovesi, "Image features from phase congruency," *Videre: A journal of computer vision research*, vol. 1, 1999.
[183] T. Lindeberg, *Scale space theory in computer vision*: Kluwer Academic Publishers, 1994.
[184] E. Gelenbe and T. Koçak, "Area-Based Results for Mine Detection," *IEEE Trans. Geoscience and Remote Sensing*, vol. 38, pp. 12-24, 2000.
[185] P. L. Martínez, L. v. Kempen, H. Sahli, and D.C.Ferrer, "Improved Thermal Analysis of Buried Landmines," *IEEE Trans. Geoscience and Remote Sensing*, vol. 42, pp. 1965-1975, 2004.
[186] P. Lopez, M. Balsi, D. L. Vilarino, and D. Cabello, "Design and training of multilayer discrete time cellular neural networks for antipersonnel mine detection using genetic algorithms," presented at 6th IEEE Internat. Workshop on Cellular Neural Networks and Their Applications (CNNA 2000), 2000.
[187] P. L. Martínez, M. Balsi, D. L. Vilarino, and D. Cabello, "Design and training of multilayer discrete time cellular neural networks for antipersonnel mine detection using genetic algorithms," presented at 6th IEEE Internat. Workshop on Cellular Neural Networks and Their Applications (CNNA 2000), 2000.
[188] A. P. W. Bowman, E.M.; Stocker, A.D.; Lucey, P.G.,, "Hyperspectral infrared techniques for buried landmine detection," presented at Detection of Abandoned Land Mines, 1998. Second International Conference on the, 1998.
[189] G. A. S. Clark, S.K.; Aimonetti, W.D.; Roeske, F.; Donetti, J.G., "Multispectral image feature selection for land mine detection," *IEEE Transactions on Geoscience and Remote Sensing*, vol. 38, pp. 304-311, 2000.
[190] N. Shimoi, Y. Takita, K. Nonami, and K. Wasaki, "Smart sensing for mine detection studies with IR cameras," presented at IEEE International Symposium on Computational Intelligence in Robotics and Automation, 2001.
[191] T. T. Nguyen, D. N. Hao, P. Lopez, F. Cremer, and H. Sahli, "Thermal infrared identification of buried landmines," presented at SPIE, Orlando, 2005.
[192] J. E. McFee, S. Achal, T. Ivanco, and C. Anger, "A short wave infrared hyperspectral imager for landmine detection," presented at SPIE, Orlando, 2005.

[193] M. Bajic, "Fusing Aerial Multispectral Imagery and High-Resolution Photography," *Journal of Mine Action*, pp. 97-100, 2004.
[194] L. B. Wolff, D. A. Socolinsky, and J. H. Holloway, "Image fusion of shortwave infrared (SWIR) and visible for detection of mines, obstacles and camouflage," presented at SPIE, Orlando, 2003.
[195] M. Lundberg, "Land Mine Detection using Dual-Band Electro-Optical Sensing," in *Department of Signals and Systems*. Gothenburg, Sweden: Chalmers University of Technology, 2003, pp. 182.
[196] J. McElroy, C. Hawkins, P. D. Gader, J. M. Keller, and R. Luke, "Side attack mine detection using near infra-red imagery," presented at SPIE, Orlando, 2005.
[197] A. H. a. B. Gunatilaka, B.A., "Feature-level and decision-level fusion of noncoincidently sampled sensors for land mine detection," *IEEE Trans. PAMI*, vol. 23, pp. 577-589, 2001.
[198] S. Auephanwiriyakul, J. M. Keller, and P. D. Gader, "Generalized Choquet fuzzy integral fusion," *Information Fusion*, vol. 3, pp. 69-85, 2002.
[199] N. Milisavljevic, I. Bloch, S. v. d. Broek, and M. Acheroy, "Improving mine recognition through processing and Dempster-Shafer fusion of ground-penetrating radar data," *Pattern Recognition*, vol. 36, pp. 1233-1250, 2003.
[200] D. W. J. Stein, S. G. Beaven, L. E. Hoff, E. M. Winter, A. P. Schaum, and A. D. Stocker, "Anomaly Detection from Hyperspectral Imagery," in *IEEE Signal Processing Magazine*, 2002, pp. 58-69.
[201] T. Meitzler, D. Bryk, E. J. Sohn, K. Lane, J. Raj, and H. Singh, "Fuzzy logic based sensor fusion for mine and concealed weapon detection," presented at SPIE, Orlando, 2003.
[202] A. Johnson and M. Hebert, "Using Spin Images for Efficient Object Recognition in Cluttered 3D Scenes," *IEEE Transactions on Pattern Analysis and Machine Intelligence*, vol. 21, pp. 433-449, 1999.
[203] Q. Zheng, S. Z. Der, and H. I. Mahmoud, "Model-Based Target Recognition in Pulsed Ladar Imagery," *IEEE Transactions on Image Processing*, vol. 10, pp. 565-572, 2001.
[204] A. E. Johnson, "Spin-Images: A Representation for 3-D Surface Matching," in *Robotics Institute*. Pittsburgh, Pennsylvania: Carnegie Mellon University, 1998.
[205] A. Vasile and R. M. Marino, "Pose-Independent Automatic Target Detection and Recognition using 3-D Ladar Data," presented at SPIE, Orlando, USA, 2004.
[206] S. Ruiz-Correa, L. G. Shapiro, and M. Meila, "A New Paradigm for Recognizing 3-D Object Shapes from Range Data," presented at Ninth IEEE International Conference on Computer Vision (ICCV 2003), Nice, France, 2003.
[207] J. Ahlberg and I. Renhorn, "Multi- and Hyperspectral Target and Anomaly Detection," FOI Sensorteknik, Linköping, Scientiffic Report FOI-R--1526--SE, decembre 2004 2004.
[208] J. Ahlberg and I. Renhorn, "An information-theoretic approach to band selection," presented at TARGETS AND BACKGROUNDS XI: CHARACTERIZATION AND REPRESENTATION, Orlando Fl, 2005.
[209] A. Linderhed, S. Sjökvist, M. Uppsäll, and S. Nyberg, "Land mine detection by IR temporal analysis: detection methods," presented at Detection and Remediation Technologies for Mines and Minelike Targets X Orlando Fl, 2005.
[210] A. Linderhed, M. Lundberg, S. Nyberg, S. Sjökvist, and M. Uppsäll, "Analysis of Optical Measurements on Real Minefields," presented at 16th International symposium on Aerospace/Defense Sensing, Simulation and Controls, 2002.

[211] A. Linderhed, S. Nyberg, S. Sjökvist, and M. Uppsäll, "Optical Methods for Detections of Minefields," Sensor Technology, IR-System, Linköping, Sweden, Base Data report FOI-R---1331--SE, September 2004.
[212] http://www.dtic.mil/mctl/DSTL/Sec17.pdf.
[213] http://www.janes.com/.
[214] http://www.dtic.mil/ndia/night/Rupp.pdf.
[215] http://www.fas.org/spp/military/docops/defense/97_jwstp/jw4g.htm.
[216] G. Forssell, "Surface landmine and trip wire detection using calibrated polarization measurements in the LWIR and SWIR," presented at Subsurface and Surface Sensing Technologies and Applications III, San Diego, 2001.
[217] S. Sjökvist, "Provprogram för MOMS verksamhet på SWEDEC:s sensorbana vecka 520, 2005-05-16 – 2005-05-20," 2005.
[218] G. Forssell and T. Hallberg, "Calibrated sensitive polarization measurement methods in the regions 3-5 μm and 8-12 μm, corrected for contributions to the detector signal from the polarizer," presented at Polarization Analysis and Measurement IV, San Diego, 2002.
[219] "Measurement equipment at the department of IR Systems," FOA-R--99-01111-615--SE, 1999.
[220] G. Forssell and E. Hedborg-Karlsson, "Passive IR polarization measurements applied to rough surfaces consisting of cenosphere particles covered with gold," presented at Polarization Measurement, Analysis, and Applications V, Seattle, 2002.
[221] C. Grönwall, F. Gustafsson, and P. Andersson, "Least-squares fitting of articulated objects," presented at Workshop on advanced 3D imaging for safety and security, San Diego, CA, USA, 2005.

Errata for references in MOMS report FOI-R--1721—SE

Chapter	Page	Erroneous reference	Correct Reference
2.1.3	21	[5]	http://www.onr.navy.mil/02/baa/expired/2002/baa_02_006/docs/assault_lane.ppt
2.1.3	22	[5]	http://www.onr.navy.mil/02/baa/expired/2002/baa_02_006/docs/assault_lane.ppt
4.1.2	61	[15]	http://www.dtic.mil/doctrine/jel/doddict/data/r/04424.html
4.2.8	82	[92-94]	[92,93,95]
4.2.8	83	[65]	[88]
4.2.8	83	[95,96]	[87,96]
4.2.8	83	[4,98]	[98]
4.3.1	87	[68]	[68], Note: Detection and Remediation Technologies for Mines and Minelike Targets VII, Proceedings of SPIE Vol. 4742, 2002
4.3.2	89	[109]	http://www.canesta.com/
4.3.2.1	89	[44]	http://www.riegl.com/
4.3.2.1	89	[110]	http://www.zf-laser.com/
4.3.2.1	89	[111]	http://www.leica-geosystems.com/corporate/en/lgs_405.htm
4.3.2.1	89	[44]	http://www.riegl.com/
4.3.2.1	89	[10]	http://www.topeye.com/
4.3.2.1	89	[76]	http://www.leica-geosystems.com
4.3.2.1	89	[18]	http://www.globalsecurity.org/military/systems/munitions/net-fires.htm
4.3.2.1	89	[113]	http://www.fbodaily.com/cbd/archive/2001/06(June)/19-Jun-2001/aawd006.htm
4.3.4	100	[2]	Remote Sensing Tutorial, NASA Goddard Training Manual on the Role of Space Science and Technology for Using Remote Sensing to Monitor Earth and Distant Objects; http://rst.gsfc.nasa.gov/Homepage/Homepage.html
4.3.4	103	[2]	Remote Sensing Tutorial, NASA Goddard Training Manual on the Role of Space Science and Technology for Using Remote Sensing to Monitor Earth and Distant Objects; http://rst.gsfc.nasa.gov/Homepage/Homepage.html
4.3.6	105	[62]	B. Johnson, R. Joseph, M. Nischan, A. Newbury, J. Kerekes, H. Barclay, B. Willard, J. J. Zayhowski, "A compact, active hyperspectral imaging system for the detection of concealed targets", in Detection and Remediation Technologies for Mines and Minelike Targets IV, SPIE Vol. 3710, 1999.
4.3.6	106	[45]	B. Johnson, R. Joseph, M. Nischan, A. Newbury, J. Kerekes, H. Barclay, B. Willard, J. J. Zayhowski, "A compact, active hyperspectral imaging system for the detection of concealed targets", in Detection and Remediation Technologies for Mines and Minelike Targets IV, SPIE Vol. 3710, 1999.
4.3.6	106	[26]	[107]
8.2.1.1.1	162	[44]	http://www.optech.ca/
8.2.1.1.2	163	[27]	http://www.riegl.com/